UNIVERSITY OF LONDON THESIS

Degree PhD Year 2007 Name of Author HUTCHINS, Peter Thomas

In Situ Synthesis Studies of Silicon Clathrates

Peter Thomas Hutchins

Thesis submitted to the University of London for the Degree of Doctor of Philosophy

University College London

ProQuest LLC
789 East Eisenhower Parkway
P.O. Box 1346
Ann Arbor, MI 48106-1346

Declaration

This is to certify that the work presented in this thesis in entirely my own, unless stated otherwise.

Peter Thomas Hutchins (September 2007)

Abstract

Solid state clathrates have shown considerable potential as a new class of materials over the past 30 years. Experimental and theoretical studies have shown that precise tuning and synthetic control of these materials, may lead to desirable properties. Very little is known about the mechanism of formation of the clathrates and so the desire to have accurate synthetic control was, until now, unrealistic. This thesis address the problem using in situ synchrotron x-ray techniques.

In this study, experiments were designed to utilise time-resolved *in situ* diffraction techniques and high temperature ^{23}Na NMR, in efforts to understand the mechanism of formation for this class of expanded framework materials. A complex high vacuum capillary synthesis cell was designed for loading under inert conditions and operation under high vacuum at station 6.2 of the SRS Daresbury. The cell was designed to operate in conjunction with a custom made furnace capable of temperatures in excess of 1000°C, as well as a vacuum system capable of 10^{-5} bar.

The clathrate system was studied *in situ*, using rapid data collection to elucidate the mechanism of formation. The data were analysed using Rietveld methods and showed a structural link between the monoclinic, *C2/c*, Zintl precursors and the cubic, *Pm3n*, clathrate I phase. The phases were found to be linked by relation of the sodium planes in the silicide and the sodium atoms resident at cages centres in the clathrate system. This evidence suggests the guest species is instrumental in formation of the clathrate structure by templating the formation of the cages in the structure.

Solid state ^{23}Na NMR was utilised to complete specially design experiments, similar to those complete *in situ* using synchrotron x-ray techniques. The experiments showed increased spherical symmetry of the alkali metal sites and suggested increased mobility of the guest atoms during heating. In addition, cyclic heating experiments using *in situ* diffraction showed reversible reintroduction of the guest species on heating and cooling, during formation and subsequent dissipation of the clathrate structure.

The realisation of the synthesis of a guest free type II clathrate and the theoretical prediction of negative thermal expansion behaviour at low temperature prompted the use of laboratory x-ray diffraction and a liquid helium cryostat to test the prediction. Careful study of the region from 20 to 200 K showed a region of zero or negative thermal expansion in the predicted region; the effect observed showed good agreement with theory.

Dedication

I would like to dedicate this work to my parents Kathryn and Jeffery, who gave me my love for the natural world and science. Their hard work over the years has provided opportunities for which I am eternally grateful. I would also like to dedicate it to my brothers and sister, who have done a great deal to help me throughout my education.

I would like to dedicate this work also to my partner, Trisha, who has tirelessly stood by me through thick and thin and has always been there to keep me going, while I complete my education.

Acknowledgements

I would to thank my supervisor Professor Paul McMillan whose incredible enthusiasm, patience, knowledge, guidance, suggestions and ideas have been invaluable throughout my PhD. I'd also like to thank my second supervisor Professor Paul Barnes, who has offered a great deal of support and guidance and showed a great deal of faith in me throughout my work. Dr. Olivier Leynaud has been a great source of help, advice, ideas and general moral support throughout my PhD, for which I am very grateful. I would also like to thank our collaborator Dr. J. J. Dong at Auburn State University. I would especially like to thank Dr. Jan Gryko at Jacksonville State University Alabama, whose help, suggestions, boundless knowledge and enthusiasm helped me a great deal.

I would like to thank all my colleagues in the materials chemistry centre at UCL for their support, help and guidance, these include: Dr. Jeremy Cockcroft, Dr. Andrea Sellar, Dr. Simon Jacques, Dr. Olga Shebanova, Dr. Ed Bailey, Dr. Agnieszka Wlodarczyk, Dr. Oleg Barkalov, Dr. Steve Firth, Dr. Dmitry Strusevich, Martin Vickers, Dominic Daisenberger, Will Bisson, Victoria Lees, Raul Quesada, Ashkan Salamat, Stuart Turner, Olivier Lazzari, Vesna Middlekoop and Sandra Saborido.

A great deal of my work required specialist equipment to be made, without which I would not have been able to complete the research. For this I am very grateful for the hard work of Paul Stukas at Birkbeck, the Staff of the UCL workshop and Glass blowing facility.

I would like to extend my gratitude to the staff at the SRS Daresbury for their constant help, guidance and often beyond the call of duty effort on my behalf, these include; Dr. Chris Martin, Dr. Graham Clark at station 6.2 and Alfie Nield of the mechanical workshop for his hard work, help, enthusiasm and constant good nature and wit.

I have to take a moment to acknowledge the EPSRC for financial support and making the study a reality.

Finally, I would like to thank my friends and family for boundless support and understanding over the past few years.

Men fear thought as they fear nothing else on earth -- more than ruin -- more even than death.... Thought is subversive and revolutionary, destructive and terrible, thought is merciless to privilege, established institutions, and comfortable habit. Thought looks into the pit of hell and is not afraid. Thought is great and swift and free, the light of the world, and the chief glory of man.

Bertrand Russell

Some assorted quotes:

"It is necessary for someone to do this, and to jog the remarkably selective memories of pessimists. The speed with which those who once claimed "It's impossible" can switch to "I said it could be done all the time" is really astounding. (There is sometimes a third stage "I thought of it first").

Arthur C Clarke, Profiles of the Future.

The most beautiful thing we can experience is the mysterious. It is the source of all true art and science. He to whom this emotion is a stranger, who can no longer pause to wonder and stand wrapt in awe, is as good as dead.

Albert Einstein.

Imagination is more important than knowledge.
Albert Einstein.

Judge of a man by his questions rather than by his answers
Voltaire

Love truth, and pardon error.
Voltaire

The opposite of a correct statement is a false statement. But the opposite of a profound truth may well be another profound truth.
Niels Bohr

Science may set limits to knowledge, but should not set limits to imagination.
Bertrand Russell

The greatest challenge to any thinker is stating the problem in a way that will allow a solution.
Bertrand Russell

Index

Index of Figures

Chapter 1:

Chapter 2:

Chapter 3:

Chapter 4:

Chapter 5:

Chapter 6:

Chapter 7:

Chapter 1

Introduction

1.1: The History of Clathrates:

The story of clathrates began in 1811 at the Royal Institution of Great Britain. In his paper; "*On a combination of oxymuriatic gas and oxygene gas*" [1], Humphry Davy noted that under specific conditions chlorine gas reacted with water to form a new compound.

$$Cl_{2(g)} + H_2O = Cl_{2\cdot x}H_2O$$

This discovery was made during studies of compression of gases in efforts to liquefy them; the experiment yielded an odd "scum" in the reaction apparatus, which Davy could not account for. Davy considered the compound a lab curiosity, the structure of which was unknown until in 1823[2], when Michael Faraday performed a successful elucidation of the composition of this hydrate of chlorine, later known as the clathrate hydrates.

$$Cl_{2(g)} + H_2O = (Cl_2)(H_2O)_{10}$$

The nature of this compound was to elude science for 130 years, until the advent of X-ray diffraction methods became widely available in the laboratory for structural determination. At this time, independently of each other, Claussen[3] and Pauling & Marsh[4] determined the structure to be a hydrogen-bonded network structure, in which the water molecules form an expanded framework system, naturally isomorphic to melanophlogite and dodecasil-3C. The chlorine atoms however, experience a host-guest relationship as *endohedrally* positioned occupants of the cages in these structures, and are often described as "guest impurities". It was also found at this time, that the correct stoichiometry for this compound was in fact not as Faraday had shown it but was $(Cl_2(H_2O)_{5.75})$.

In the ensuing years, several examples of these hydrogen-bonded water based structures with guest solvent species in the cages, were demonstrated in the literature[5, 6]. It was found that there was a great diversity of guest species that could reside in the cages in nature; from methane and propane through to synthetic examples containing argon, krypton, xenon, hydrogen disulfide, methane etc. These formed two distinct groups for which the compositions were $G_8(H_2O)_{46}$ and $G_{24}(H_2O)_{136}$ or $G_{16}G_8(H_2O)_{136}$, where G is the guest species and is fundamental in promoting one composition versus the other.

In 1961, Klemm and Schäfer[7], [8], completed studies on the thermal behaviour of Zintl compounds of silicon and germanium under vacuum conditions. While conducting thermogravimetric analysis (TGA) on various Zintl phases, they observed a plateau region in the TGA data, which could not readily be explained. Further study found that heating of the zintl phases resulted in metastable intermediate compounds of a cubic nature, based on silicon and germanium but with a considerably reduced alkali metal composition. It was also found that higher temperatures resulted in lower metal contents of the alkali metal. These new materials were studied using thermogravimetric analysis methods, to determine stoichiometry of the phase. On degradation of KSi the resultant product was of the form KSi_6 where for RbSi, $RbSi_6$ resulted. For CsSi and NaSi the results differed however; CsSi produced a phase of stoichiometry of $CsSi_8$ with no intermediate step. However, NaSi was found to decompose completely to the pure elements. Decomposition was observed for all of the silicide phases examined in the study, where the application of temperatures above 550-600°C was employed.

In 1965, Cros *et al*[9],[10] - spurred on by the work of Klemm and Schäfer – repeated the studies in the same manner as Klemm had done, four years earlier. However, upon restudying the thermal decomposition of NaSi, Cros did not observe degradation to pure elements as Klemm had. Instead, the system was found to decompose to a mixed product of two phases; most significantly, $NaSi_{5.75}$ was one of the phases present in the product – this was of the same form as that seen by Klemm on decomposition of KSi. The phases were studied using x-ray diffraction techniques but Cros was unable to identify them until, by chance, the materials were identified as being isostructural with the clathrate hydrates by Kasper, while visiting Cros's laboratory. These new structures were comprised of silicon as the framework material – in comparison to water in the hydrate clathrate – and the alkali metal as the encapsulated guest species. Two structures for the clathrates were determined in the synthetic solid state systems; the first composed of 46 framework atoms and 8 guest atoms resident at cage centres; the second, composed of 136 framework atoms and 24 guest atoms in the stoichiometrically fully occupied state.

The work of Cros was to truly define the study of a new area of materials; that of the synthetic solid state clathrates composed of group 14 elements as framework constituents, in contrast to the hydrogen bonded H_2O structures found in nature. This was the birth of the study of a new class of clathrates structured materials based around tetrahedrally coordinated silicon – the semiconductor clathrates.

By 1969[11], the field of clathrate research had refocused around attempts to synthesis materials with germanium, tin, lead and carbon as framework elements; Ge (K_8Ge_{46}) and Ti (K_8Ti_{46}) type I clathrates had been demonstrated by direct fusion of pure elements. Such intense activity led to 5 binary and 17 ternary phases of clathrate I structure and 3-non stoichiometric clathrate II structures by 1991[11]. Today there are approximately 100-150 solid state clathrate structured materials, most of which are type I. Clathrate structures have been realised with a modest number of elements as the constituent framework component thus far; these include: silicon, germanium, gallium, tin and very recently phosphorous. Carbon has been widely predicted and discussed as a potential framework candidate for electronic materials with promising electronic properties, but as yet, has not been realised synthetically[12].

It is also noteworthy that in the last few years a synthetic clathrate III structure, *isostructural* with the natural hydrate form $A_{30}T_{172}$ (where A = alkali metal, T = Tetrahedral coordinated framework atom Si, Ge, Sn for the synthetic) has been shown[13]. Though found to exist in nature, this phase was synthetically elusive until 2001 when $Cs_{30}Na_{(1.33x-10)}Sn_{(172-x)}$ and $Cs_{13.8(1)}Rb_{16.2(1)}Na_{(1.33x-10)}Sn_{(172-x)}$ (where x is approximately 9.62) were both synthesised. At the same time, $Ba_{24}Si_{100}$ was synthesised independently by Yamanaka *et al*[14] and was also found to exhibit the clathrate III structure.

A wide breadth of theoretical research was undertaken during this time, much of which was a force to bolster the fevered activity in the field. The main driving force for the increased interest in solid state clathrates was a theoretical prediction [15], [16], [17], [18] that the clathrates may have 0.05-0.01 eV less cohesive energy per atom than the *d*-Si phase, while having larger, more attractive and accessible bandgaps for electronics applications. This prediction suggested a good marriage with existing silicon electronics technologies. This was further supported[19], [20], [21] by *ab initio* DFT planewave pseudopotential techniques that showed the same values for the pure bulk materials.

The semiconductor clathrates have now been shown and predicted to exhibit a wide array of properties, which include: insulators, semiconductors, metals, superconductors, magnetic and ferromagnetic and thermoelectric among many. This array of properties gives the semiconductor clathrates a good diversity of potential

application and thus has lead to wide coverage in the literature, in attempts to control the composition and properties of these materials.

1.2: The Zintl Phases[22], [23], [24], [25]:

Production of the synthetic solid state clathrates by thermal degradation is completed using Zintl phases as precursors. Zintl phases are a class of compounds produced in the reactions of alkali or alkaline earth metals, with post transition metals or metalloids of groups 13, 14, 15 and 16. The first work on such phases was done in 1929[22], by the German chemist Eduard Zintl, after whom they were eventually named. Zintl phases can be formed by reduction of the group 13, 14, 15, 16 elements in liquid ammonia but are also commonly produced by reaction of the elements at high temperature under inert conditions, as is the case in this study (*see Chapter 2, Section 2*). The bonding in these materials is generally considered to be ionic, where electron donation occurs completely and in the favour of the more electropositive metal. In the occurrence of zintl clusters (such as is the case for NaSi) bonding of a more covalent nature is exhibited within the polyhedral clusters. The evidence of zintl clusters for some systems explains the propensity of the zintl phases to have variable stoichiometries. Zintl phases are generally brittle, diamagnetic, poor conductors and bare no comparison with more traditional alloys, being in fact, more salt-like in nature.

The zintl phase used in this study is NaSi, and consists of $(Si_4)^{4-}$ tetrahedral anions in a matrix of sodium cations and is similar to the P_4 white phosphorous structure. The crystal structure is monoclinic C2/c and is of relatively low symmetry in comparison to the clathrate it can be induced to form (*see Figure 1.2.1*). Bonding within the system is complex, in that Si-Si bonds exhibit more covalent bonding nature and thus reside in the form of tetrahedra but have a largely ionic bonding interaction with Na^+. The resultant electronic configurations are:

Si		**Si^{1-}**		**4Si ~ in the tetrahedra**
$1s^2 2s^2 2p^6 3s^2 3p^2$	→	$1s^2 2s^2 2p^6 3s^2 3p^3$	~	$1s^2 2s^2 2p^6 3s^2 3p^6$ (delocalised)

Na		**Na^{1+}**
$1s^2 2s^2 2p^6 3s^1$	→	$1s^2 2s^2 2p^6$

Variation of the proportion of sodium in the initial preparation, has been shown to induce the formation of an amorphous matrix-like compound with variable stoichiometry, in the range Na_XSi (X = 1~4); this product appears as a silver/black semi-solid material (*see Chapter 2, section 2.3*). NaSi is highly reactive with O_2 and H_2O and therefore must be handled in inert atmosphere at all times to avoid oxidation.

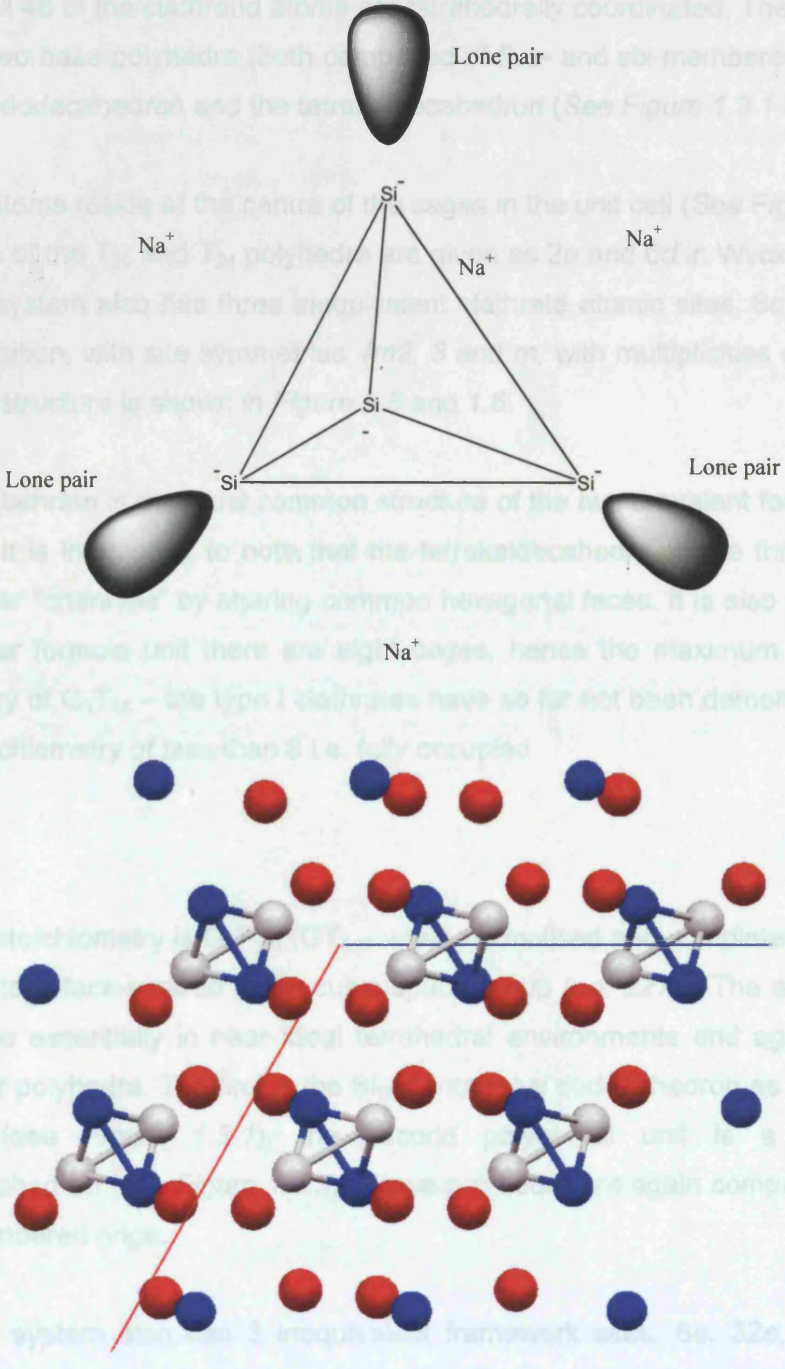

Figure 1.2.1: (Top): The nature of the silicon tetrahedra in NaSi; (Bottom): C2/c unit cell of NaSi viewed along the b axis. Red denotes sodium, blue denotes Si1 crystallographic position, white Si2 crystallographic position.

1.3: The Clathrate Structure:

Type I

The type I clathrate phase has the stoichiometry G_xT_{46} ($GT_{5.75}$ when normalised and completely filled) and crystallizes with a primitive cubic lattice, space group $Pm\bar{3}n$ (no. 223). All 46 of the clathrand atoms are tetrahedrally coordinated. The structure is built up of two base polyhedra (both composed of five- and six-membered rings); the pentagonal dodecahedron and the tetrakaidecahedron (*See Figure 1.3.1 and 1. 3.2).*

The guest atoms reside at the centre of the cages in the unit cell (*See Figure: 1. 3.4).* The centres of the T_{20} and T_{24} polyhedra are given as 2*a* and 6*d* in Wyckoff notation. The type I system also has three inequivalent clathrate atomic sites, 6*c*, 16*i*, 24*k* in Wyckoff notation, with site symmetries *4m2, 3* and *m,* with multiplicities of 6, 16, 24. The overall structure is shown in *Figure 1.5* and *1.6.*

The type I clathrate is the most common structure of the two prevalent forms (I and II of I, II, III). It is interesting to note that the tetrakaidecahedra create three mutually perpendicular "channels" by sharing common hexagonal faces. It is also important to note that per formula unit there are eight cages, hence the maximum guest atom stoichiometry of G_8T_{46} – the type I clathrates have so far not been demonstrated with a guest stoichiometry of less than 8 i.e. fully occupied.

Type II

The type II stoichiometry is G_xT_{136} ($GT_{5.67}$ when normalised and completely filled) and crystallizes to a face-centred $Fd\bar{3}m$ cubic space group (no. 227). The atoms in this structure are essentially in near ideal tetrahedral environments and again exist as two different polyhedra. The first is the Si_{20} pentagonal dodecahedron as in the type I structures (see *Figure 1.3.1*), the second polyhedral unit is a larger T_{28} hexakaidecahedron (see *Figure 1.3.3*). These polyhedra are again composed of five- and six-membered rings.

The type II system also has 3 inequivalent framework sites, 8*a*, 32*e*, 96*g* in the Wyckoff notation for which the symmetries are $\bar{4}3m$, *3m, m*, with multiplicities of 8, 32, 96.

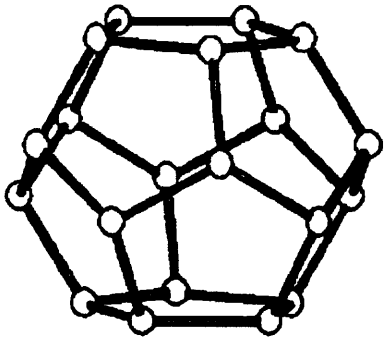

Dodecahedron

Figure 1.3.1: T_{20} pentagonal dodecahedron [5^{12}] containing 12 pentagonal faces (Redrawn from Ramachandran[26]).

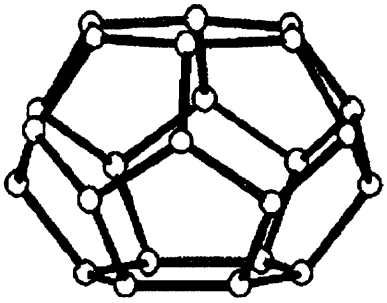

Tetrakaidecahedron

Figure 1.3.2: T_{24} tetrakaidecahedron [$5^{12}6^{2}$] which is composed of 12 pentagonal faces and 2 hexagonal faces(Redrawn from Ramachandran[26]).

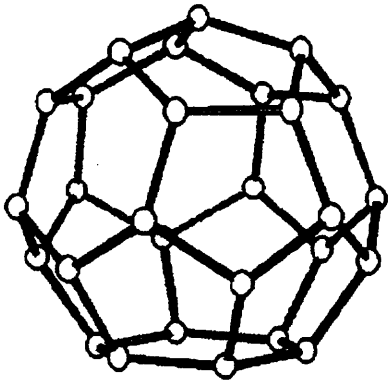

Hexakaidecahedron

Figure 1.3.3: T_{28} hexakaidecahedron [$5^{12}6^{4}$] with 12 pentagonal faces and 4 non-adjacent hexagonal faces (Redrawn from Ramachandran[26]).

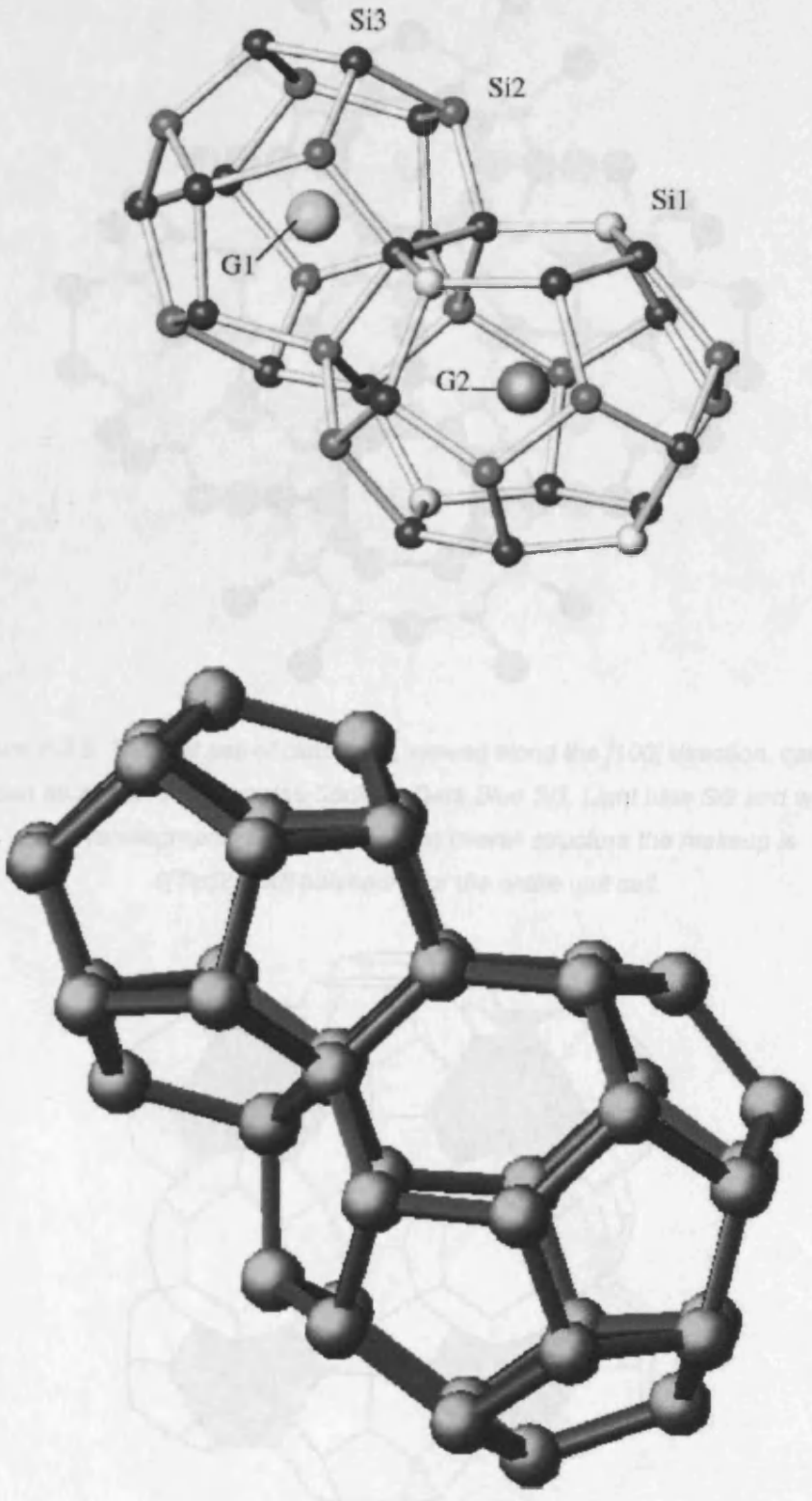

Figure 1.3.4: This shows a dodecahedron and a tetrakaidecahedron on combination in the clathrate I system with guest atoms residing in the cages (top) and without guest atoms (bottom) [11], [27].

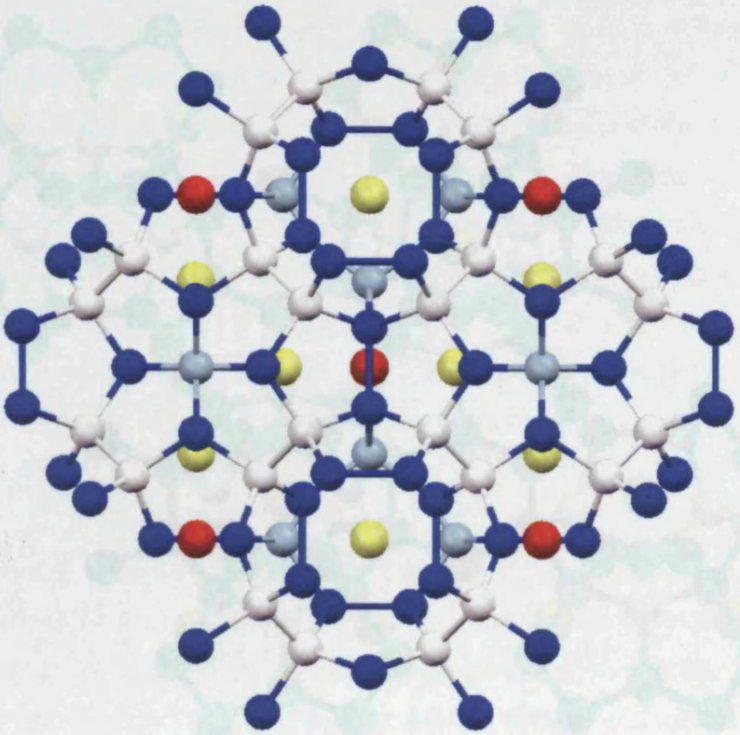

Figure 1.3.5: The unit cell of clathrate I, viewed along the [100] direction, can be shown as above. Red denotes Sodium, Dark Blue Si3, Light blue Si2 and white Si1 crystallographic positions. For the overall structure the makeup is 6[Tet]2[Dod] polyhedra for the entire unit cell.

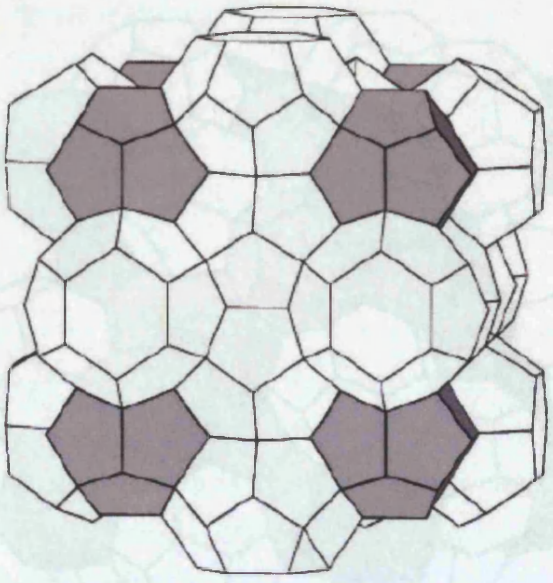

Figure 1.3.6: This shows the structure highlighting the two polyhedra in there positions in the unit cell (pentagonal dodecahedra are shown in dark grey) [11].

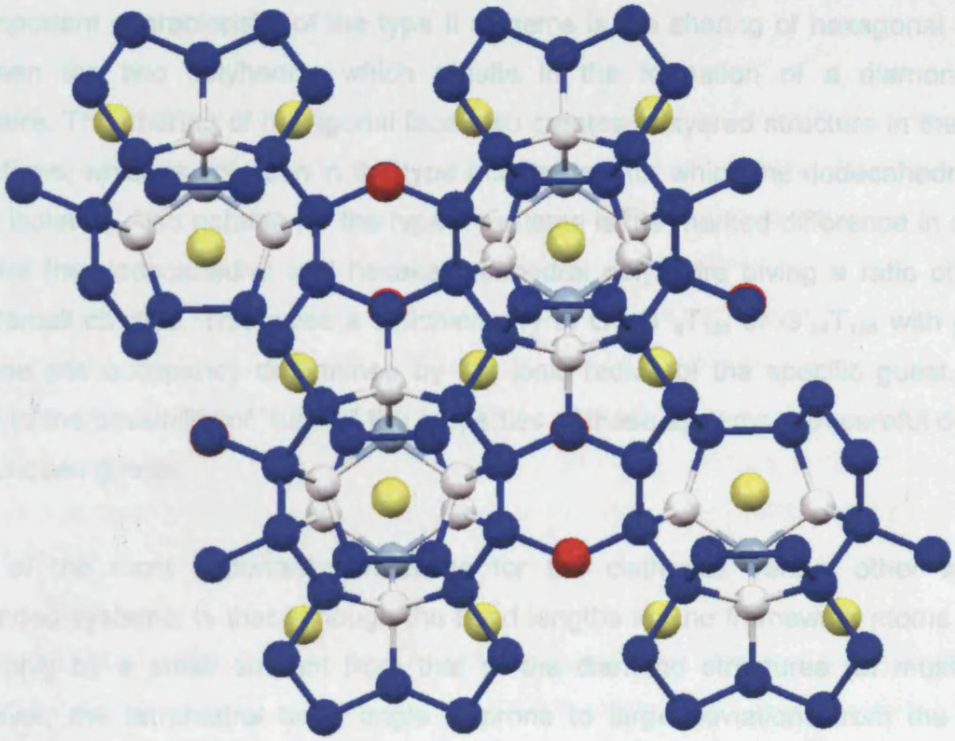

Figure 1.3.7: This shows the type II system along the [100] direction. Red denotes Sodium, Dark Blue Si3, Light blue Si2 and white Si1 crystallographic positions. The final unit cell makeup for the type II systems is 16[Dod]8[Hex].

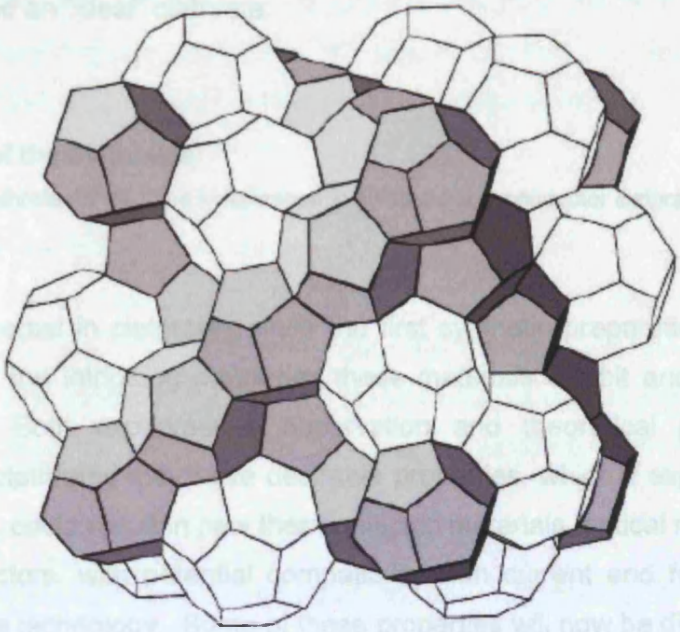

Figure 1.3.8: This shows the structure highlighting the two polyhedra in there final positions in the unit cell (pentagonal dodecahedra are shown in dark grey) [11].

An important characteristic of the type II systems is the sharing of hexagonal faces between the two polyhedra, which results in the formation of a diamond-like structure. The sharing of hexagonal face also creates a layered structure in the type II systems, which is not seen in the type I clathrates, for which the dodecahedra are more isolated. Also notable for the type II systems is the marked difference in cavity size for the dodecahedral and hexakaidecahedral polyhedra giving a ratio of 16:8 large:small cavities. This gives a stoichiometry of $G'_{16}G''_{8}T_{136}$ or $G'_{24}T_{136}$ with guest species site occupancy determined by the ionic radius of the specific guest. This leads to the possibility of "tuning" the properties of these systems with careful doping with chosen guests.

One of the most important differences for the clathrates versus other similar expanded systems, is that although the bond lengths for the framework atoms (T-T) vary only by a small amount from that of the diamond structures (at most 1%) However, the tetrahedral bond angle is prone to large deviations from the ideal 109.4°. It has been observed that in the six membered rings the angle can be as large as 125° for the A-T/G-T bonds. It is these distorted bond angles to which the large band gaps have been attributed[11]. In addition there are four defined bond lengths and eight defined bond angles in the type I and type II systems. Models have been demonstrated[28] where T-T bond lengths are constrained to be equal, resulting in what is termed an "ideal" clathrate.

1.4: Properties of the Clathrates:

(Note: The term clathrate will be used in reference to synthetic semiconductor clathrates, not clathrate hydrates).

Much of the interest in clathrates since the first synthetic preparation in 1965, has been driven by the intriguing properties these materials exhibit and there possible industrial use. Both experimental observation and theoretical prediction have suggested the clathrates may have desirable properties, which if exploited to create novel materials, could result in new thermoelectric materials, optical materials as well as superconductors, with potential compatibility with current and future micro and nano electronics technology. Some of these properties will now be discussed.

Electronic:

The electronic properties of clathrates make them very appealing subjects for scientific research as they are both tuneable and wide ranging. By modification of both framework sites and the guest atoms, solid state clathrates have been made that exhibit insulating[29], semiconducting and superconducting[30], [31], [32], [33], [34], [35], properties and hence are often described as "intermetallides". Bulk Si and Ge have small indirect bandgaps, across which optical transitions are unfavourable. This results in reducing the light emitting efficiency and limits large-scale use in optical roles. As discussed earlier clathrates (specifically the guest-free forms) have been predicted to have marginally less stable than *d*-Si, while possessing wider bandgaps, of around 0.7 eV wider than the sp^3 *d*-Si, as a result of the expanded structure[11].

It has also been predicted[20], [36], [37] that the nature of the bandgap and subsequent properties of the material, are the result of the stoichiometric level of dopant guest atom and its type. Specifically, it was shown theoretically that Na_xSi_{136} undergoes a semiconductor to metal transition as x increases from 0 to approximately 8.

Interestingly, the case of silicon germanium alloys has recently[38], [39] been considered theoretically in the literature. It was found that for these systems the stability of the phase would again not be greatly less than that of the pure clathrate phases. The interesting result of this study was the finding that the bandgap exists between 1.2~2.0 eV and is direct, with part in the visible region.

Superconductivity in clathrates has attracted a large amount of attention over the past few years. All reported incidence of superconductivity in clathrates systems contain barium as the intercalated guest species. Systems of this nature have been shown for both silicon[30]-[35], [40], [41] and germanium[42], [43] and in all cases type I clathrate structures were observed. Thus far all materials containing barium with the clathrate II structure have shown no evidence of superconductivity [44], [14], despite it being predicted.

Though the mechanism of superconductivity in these compounds is unknown at this time, it has been suggested for the Si systems at least, that it is an intrinsic property of the framework and that the role of barium is to provide electron density via hybridisation[27], of the Ba 5d and Si 3p orbitals in the conduction band.

The first example of superconductivity in clathrates was reported by Yamanaka *et al*[30]-[35]. Two compounds were reported to be superconducting $Na_xBa_ySi_{46}$ and Ba_8Si_{46} with T_c of approximately 4K and 8K respectively. It was found that for these compounds the bandgap was very narrow around the Fermi level at around 0.3 eV[40].

Recently three germanium systems were shown[45], [46] to be superconducting. The first two are close in nature to the silicon based systems being of the form Ba_6Ge_{25}, $Ba_4Na_2Ge_{25}$ and showed T_c at approximately 0.24K and 0.84K respectively, at ambient pressure. Interestingly, the value of T_c increases drastically to 3.85K at the critical pressure $p_c \approx 2.8$GPa[47]. The third example for germanium is for the compound $Ba_8Ga_{16}Ge_{30}$ with T_c approximately 7.5K. The search for superconductivity in systems not containing Ba as guest has been investigated in the literature but has so far yielded no positive results[48].

Thermoelectric:

In 1995 G. A. Slack [49], [50] suggested that materials with large unit cells that contained atoms encapsulated into the structure, would have low thermal conductivity due to a propensity for the encapsulated atoms to "rattle", and cause scattering of the acoustic-mode heat-carrying phonons. He also suggested that the electrical conductivity would not be affected by the "rattling" activity of the guest species as the electronic charge carriers are believed to propagate through the host framework and will be unaffected. Slack called these hypothetical materials "phonon-glass electron-crystals" or PGEC materials.

The figure of merit of thermoelectric materials is given by the dimensionless quantity ZT, where Z is given by the equation;

$$Z = S^2\sigma/\kappa$$

Where: S = Seebeck coefficient, σ = electrical conductivity, κ = Thermal conductivity, T = temperature.

The larger the value of ZT the more useful a material is for thermoelectric applications. If a material can be found for which the ratio is 3 or 4, thermoelectric

cooling could replace conventional refrigeration. Materials that are thought to be good candidates for thermoelectric materials will have glass-like thermal conductivity but high electrical conductivity, hence the term PGEC. Current thermoelectric materials, such as bismuth telluride, exhibit figures of merit of around 1 and have an array of applications including; refrigeration, heat exchange/transfer and thermogenerators among others.

There has been much discussion over whether the clathrates are good candidates for thermoelectric materials based around their nature as electron-crystals and/or phonon glasses. The electron-crystal nature has only been sparsely studied in the form of charge-carrier mobilities for Ge based type I systems[51], [52], [53], [54]. In general, the mobilities were found to be low but it was conceded that the samples were non-stoichiometric. It was also conceded that it was unknown as to whether stoichiometric clathrate materials would increase the mobilities or whether the mobilities are intrinsically low for clathrates.

Phonons in the clathrates have been studied by various techniques. Inelastic neutron scattering has been used on Na_8Si_{46} and K_8Si_{46} revealing sharp low-energy peaks in the phonon density of states corresponding to Einstein-like vibrations of Na and K[55]. Similar results where found in the Raman spectra of $Cs_8Ga_{16}Sn_{30}$ where low frequency modes where identified as "rattling" of Cs atoms[56].

There are a number of promising examples of clathrate structured materials currently being studied and modified for optimal thermoelectric properties. The most promising and most extensively studied of these is Ba_6Ge_{25}. Ba_6Ge_{25} was found to have both high electrical conductivity but also low thermal conductivity[57] this was found to change below room temperature and hence ruin the thermoelectric characteristics. As such modifying the system along the lines $Ba_4Na_2Ge_{25}$ are now being considered to counter this problem[58]. The research into the thermoelectric properties of clathrates has only really picked up speed over the last few years and continues to be a vibrant field of interest.

Thermal Properties of $Na_{x=0}Si_{136}$:

The clathrate $Na_{x=0}Si_{136}$ has been predicted[59] to have a region of negative thermal expansion at very low temperatures, specifically in the range 40~120K (See *Figure*

1.4.1). This is novel for two reasons; the first is due to the relatively low number of negative thermal expansion materials; the second reason is that the effect is predicted to result from a negative sign to the lattice phonon-phonon interaction. This effect is only known, thus far, for diamond like silicon. (See Chapter 6 for further detail).

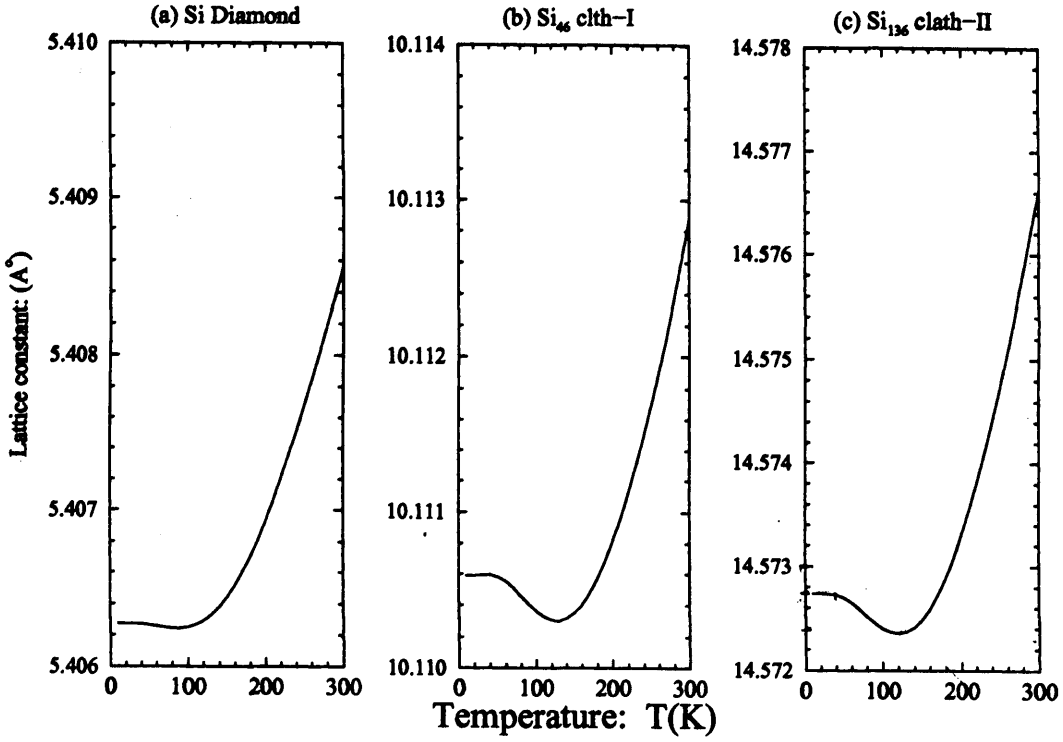

Figure 1.4.1: Graph shows the trend of predicted variation of lattice constant with increasing temperature for (a) Si Diamond, (b) Si_{46} clathrates, (c) Si_{136} clathrates.

Magnetic:

Very recent developments in the field have brought attention to new magnetic characteristics in clathrates. This is the result of successful inclusion of lanthanides into the systems resulting in long range magnetic ordering due to the intrinsic magnetic nature of f-electron systems. It has been suggested[60] that the *f*-electrons of lanthanides would strongly hybridize with the conduction electrons in the silicon/germanium framework. Additionally, the magnetic *f*-electrons have been suggested to cause spontaneous spin ordering at 6.5K in the system $Ba_6Ce_2Au_4Si_{42}$[61]. Further interesting magnetic properties were reported for another

cerium system 2003[62]. $Ce_3Pd_{20}Ge_6$ was found to exhibit both ferroquadropole ordering and antiferromagnetic order at low temperature.

Thus far only systems containing cerium and europium have been synthesised from the lanthanides. Two closely related europium compounds have been reported and well studied. $Eu_4Ga_8Ge_{16}$ has been synthesised[63], [64] as a by product of the $Eu_8Ga_{16}Ge_{30}$ preparation. This compound was found to exhibit anitferromagnetic ordering at 8K with ferromagnetic chains parallel to the a axis[65] and that the Eu atoms exist in the Eu^{2+} state in the cages versus Eu^{3+} [66].

$Eu_8Ga_{16}Ge_{30}$ is a closely related material for which Eu is again found to be in the +2 state and is observed to ferromagnetically order below 35K[67]. It is also a semiconductor and has been evaluated for its thermoelectric properties[52].

Two further examples of europium systems can be found in the literature, both of which have been less stringently studied. $Eu_2Ba_6Al_8Si_{36}$ and $Eu_2Ba_6Ga_8Si_{36}$ have been synthesised and shown to have long-range magnetic ordering[68]. These systems are both metals with poor electrical conductivity and have negative Seebeck coefficients suggesting that the transport processes for these species are electron based.

Other Systems:

While the systems already discussed cover the main properties of the clathrates, there are many other compounds that have been synthesised and studied in the literature with clathrate structures. Though detailed discussion of their properties is not warranted there are a number of noteworthy systems in the literature, which are examples of interesting substitutions for both guest atoms and onto framework sites. Such examples convey the diverse nature of the materials that represent the clathrate structures.

Some of the more unique examples among these include the iodine doped clathrates of the form $I_8Si_{44}I_2$[18] and $I_8Ge_{46-x}I_x$[69]. In both cases iodine is found to occupy both the cages (the stoichiometric majority) and some silicon sites in the framework. Theory has predicted[63] a high level of hybridisation between the iodine and the Si network orbitals creating a large opening of the bandgap. The result is the compounds are found to be electrical insulators, as was the case for $I_8Si_{44}I_2$[18].

Further examples have been synthesised containing transition metals such as copper, gold and silver, but there are few examples in the literature that are not d^{10} or d^0 thus far.

Also clathrates containing tellurium have been synthesised and studied but have shown no remarkable properties. Strontium, gallium and indium have also been introduced into the structures and studied for superconductivity and thermoelectric properties. There are recent reports of clathrates for which the framework is composed entirely of phosphorous. These are the first examples of group 15 clathrates[70].

Aims of the project:

As discussed in this chapter, the clathrates have a large number of potential compositions and properties and have good potential for compatibility and integration with current silicon electronics. However, little is known or has been discussed in the literature about the mechanism of formation of these materials. It is known that in synthesis by thermal degradation, the guest atoms are lost such as to reduce the Zintl phase stoichiometry so the clathrate may form. Given the need for precise control of the synthesis, to "tune" the materials for desired properties, a detailed understanding of the mechanism of formation would seemingly give access to a considerable increase in synthetic control.

Advances in the field of rapid x-ray diffraction using synchrotron sources has made the study of mechanism in the solid state far more feasible in the past 10 years. Time-resolved, rapid *in situ* diffraction is a powerful technique for studying structural changes and transformations and is thus a suitable choice of technique to attempt to study the formation of clathrates. The aim of this study is to use these methods to develop an experiment to synthesise clathrate I and II *in situ,* under the standard laboratory conditions for their formation. For the purposes of this study, NaSi will be used in the reaction *in situ*, given its propensity to selectively form type I and II clathrates with careful modification of the reaction conditions. The scope of an *in situ* synthesis study would encompass the study of the effect of the variation in; heating ramp-rate, level of vacuum applied, synthesis temperature, duration of heating and the effect of flash heating.

1.5: Synchrotron Radiation and Powder Diffraction[71]:

Synchrotron radiation is emitted when the path of an electron travelling at relativistic speed is bent by a magnetic field. It was termed *synchrotron radiation* as a consequence of its initial observation at the laboratories of General Electric using a 70 MeV synchrotron, in 1947. The useful properties of synchrotron radiation were finally recognised after several decades of overcoming technological issues associated with the technique and were, at first, not seen as a particularly eventful discovery. Many years passed until the realisation of the worlds first dedicated synchrotron x-ray source was commissioned at the SRS Daresbury in 1981. The speed and acceleration of electrons commonly utilised in most synchrotrons is such that they produce a wide spectrum of electromagnetic radiation, from radio-frequency range through to infra-red, visible, ultra-violet and x-ray portion of the electromagnetic spectrum.

1.5.1: The Modern Synchrotron:

Synchrotrons today are composed of a number of core components, which are commonly shared between the various different facilities around the world (*see Figure 1.5.1.1*). These are:

- Linear Accelerator.
- Booster ring.
- Storage ring.
- Insertion devices.

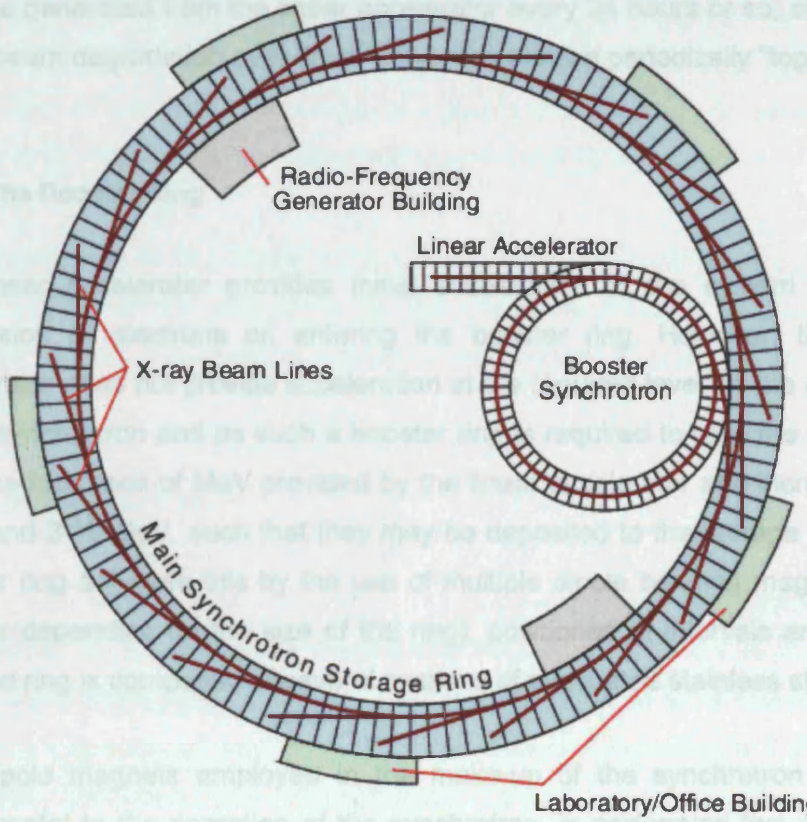

Figure 1.5.1.1: A schematic representation of a synchrotron[72].

1.5.2: Linear Accelerator:

Current linear accelerators are composed of a linear array of accelerating cells, powdered by a voltage plate source. The voltage plate source is operated in the megawatt power range and with the frequency range in gigahertz. In this fashion, a linear accelerator produces discrete pulses of electrons, such that at any one time 100-200 bunches of electrons will be processing around the ring at any one time. The frequency of processing bunches is essential in the operation of the radio frequency generator/cavity, which are seated at a number of intervals around the ring. The voltage plate generators purpose is to synchronously inject energy into the electrons bunches as they process, to compensate the energy loss that occurs in the emission of radiation from the system. Despite the use of ultra-high vacuum (10^{-10} mbar) within the storage ring system, the energy of the electron bunches will decay as a result of collision with any residual molecules left in the storage ring; typically the beam

must be generated from the linear accelerator every 24 hours or so, as a result of the beam degradation over time[72] and may also be periodically "topped-up".

1.5.3: The Booster Ring

The linear accelerator provides initial acceleration to the system to begin procession of electrons on entering the booster ring. However, the linear accelerator does not provide acceleration at the required level for the operation of the synchrotron and as such a booster ring is required to take the electrons from the hundreds of MeV provided by the linear accelerator and increase that to around 2-10 GeV, such that they may be deposited to the storage ring. The booster ring achieves this by the use of multiple dipole bending magnets (the number depending on the size of the ring), positioned at intervals around the ring; the ring is composed of several sections of evacuated stainless steel tube.

The dipole magnets employed in the make-up of the synchrotron ring are fundamental to the operation of the synchrotron, in performing two vital roles (*see Figure 1.5.3.1*).

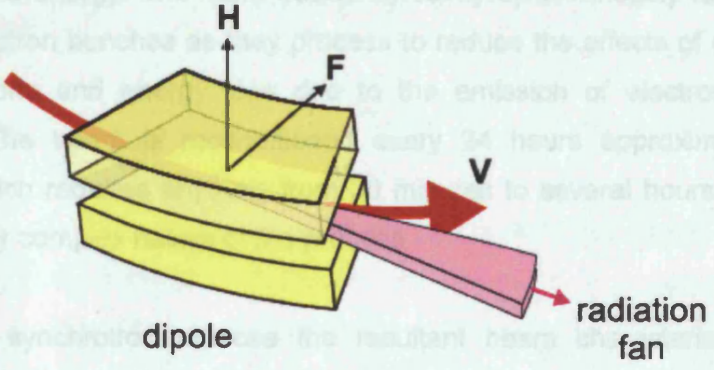

Figure 1.5.3.1: A dipole bending magnet, such as is utilised in a synchrotron[72].

Electrons have a number of fundamental properties that are utilised in the operation of a synchrotron source; electrons possesses negative charge and velocity, v. Electrons will travel in a straight line with a velocity, v, until an external magnetic field is applied to cause a deviation from this path. Since the desired path of electrons in a synchrotron is circular, a magnetic field, H, is applied perpendicular to the direction of the travel such that the electrons experience the so called *Lorentz force*, F. The *Lorentz force*, acts in a direction

perpendicular to the velocity of the electrons, v, and the magnetic field, H (*see Figure 1.5.3.1*). Since the electron travels with a velocity, v, the Lorentz force, F, induces a centripetal acceleration causing the electron to process in a circular orbit. This is the first role of the dipole bending magnets.

The second role of the dipole magnet is inducing the centripetal acceleration within system which will result in the electrons emitting electromagnetic radiation; this is a fundamental property of accelerated subatomic particles.

1.5.4: The Storage Ring

The storage ring of a synchrotron is the main apparatus for provision of an environment upon which user beams may be built. It is similar to the booster ring in being composed of several sections of evacuated steel tubing, a radio frequency generator(s) and multiple dipole magnets (*see Figure 1.5.4.1*). For the SRS Daresbury the storage ring consist of 16 dipole magnets, interconnected with the straight sections of the ring. Daresbury contains 4 radio frequency cavity but larger synchrotrons require more to maintain beam condition and energy. The radio frequency cavity synchronously feeds energy into the electron bunches as they process to reduce the effects of energy loss from collisions and energy loss due to the emission of electron magnetic radiation. The beam is reconditioned every 24 hours approximately, in a process which requires anything from 30 minutes to several hours due to the considerably complex nature of the process.

In modern synchrotron sources the resultant beam characteristics of the emitted electromagnetic radiation can be specifically tuned for end user purposes. This is achieved both at beamline level, by means of optics and monochromators and is also crucial affected by the use of insertion devices such as wigglers and undulators, which are positioned at specific points in the storage ring.

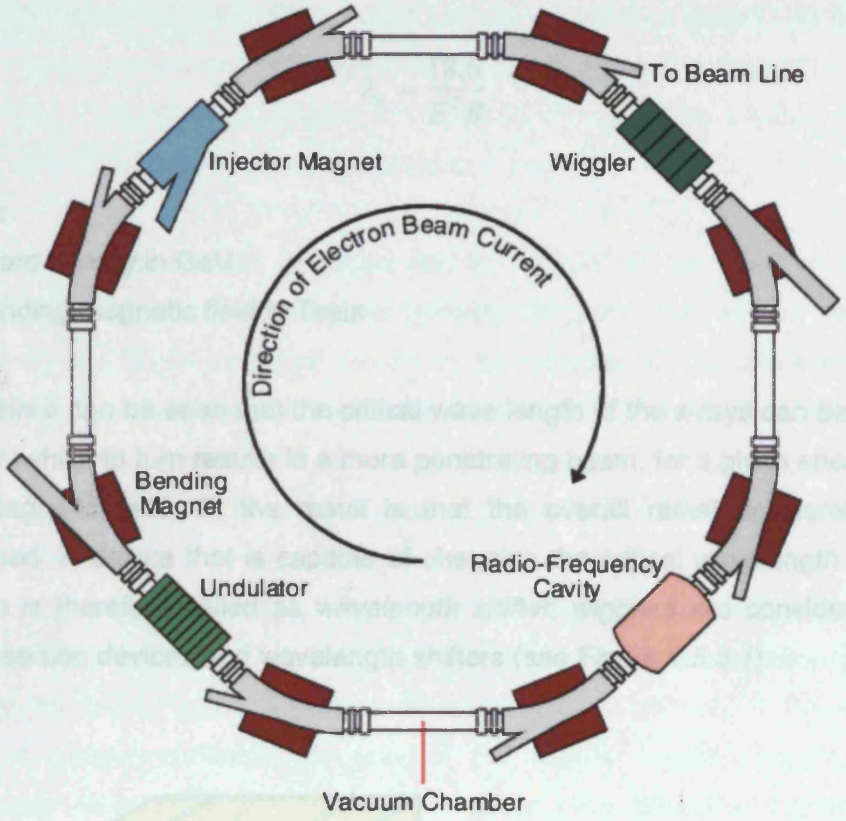

Figure 1.5.4.1: The diagram shows a schematic of the storage ring, dipole magnets, insertion devices and radio frequency devices employed in a synchrotron[72].

1.5.5: Insertion Devices

Insertion devices are specifically designed and positioned arrays of powerful (superconducting) magnets, commonly employed in the storage ring of synchrotron sources to tune the electromagnetic radiation emission, in certain regions of the storage ring. Insertion devices are designed such that they accept and return electrons bunches in the same direction and operation of the dipole magnets is not affected, and ultimately, the processing electrons are not impeded.

Wigglers:

The radiative emission caused by the action of a dipole bending magnet can be characterised by the parameter, λ_c, known as the critical wavelength, by which the total power spectrum reaches 50%. λ_c, is given by the formula;

$$\lambda_c = \frac{18.6}{E^2 B}$$

Where:

E = beam energy in GeV

B = bending magnetic field in Tesla

From this it can be seen that the critical wave length of the x-rays can be made shorter, which in turn results in a more penetrating beam, for a given energy, E, and magnetic field, B; the result is that the overall radial acceleration is increased. A device that is capable of changing the critical wavelength in this fashion is therefore called as *wavelength shifter*, wigglers are considered as both insertion devices and wavelength shifters (*see Figure 1.5.5.1*).

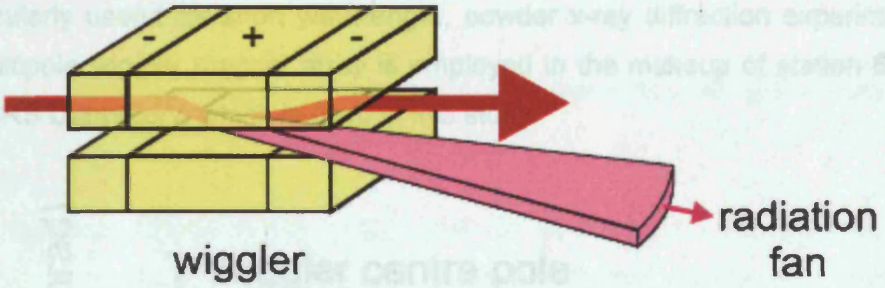

Figure 1.5.5.1: A schematic representation of a wiggler magnet array[72].

Wiggler magnet arrays are composed of a complex make-up of componentry, but they are in general, composed of multiple magnets (the simplest forming being three), with the outer two being of opposed polarity to the central magnet. A wiggler operates thus:

1. The first magnet is chosen such that it bends the electron beam in the opposite direction to the curvature caused by the storage rings dipole magnets.
2. The second magnet is chosen such that it over compensates for this and bends the beam sharply back towards the original direction of motion and the centre of the synchrotron ring. The central magnet

requires a very strong magnetic field of the order of magnitude of 5-6T. This is usually performed by a strong superconducting magnet.

3. The third and final magnet is employed to correct the trajectory of the electrons, back to their original path.

The resultant motion can be observed as "wiggle" in the electron beams motion, and thus the magnets are termed, *Wigglers*. The strong deviation caused by the central magnet results in an increase in radial acceleration, which in turn leads to "harder" x-rays being emitted to the user beamline. The overall affect of a wiggler is a very similar wavelength and intensity profile to the standard dipole magnets (*see Figure 1.5.5.2*) but for the wiggler, a shorter wavelength of around a few tenths of an angstrom shorter and for comparative regions an intensity increase of an order of magnitude or more, versus the standard dipole magnet. The result then is a beam of characteristically shorter wavelength, harder x-rays with a non trivial increase in intensity of the beam in terms of photons delivered per second; this makes wiggler magnet arrays particularly useful for short wavelength, powder x-ray diffraction experiments. A multipole wiggler magnet array is employed in the makeup of station 6.2 at the SRS Daresbury, which is used in this study.

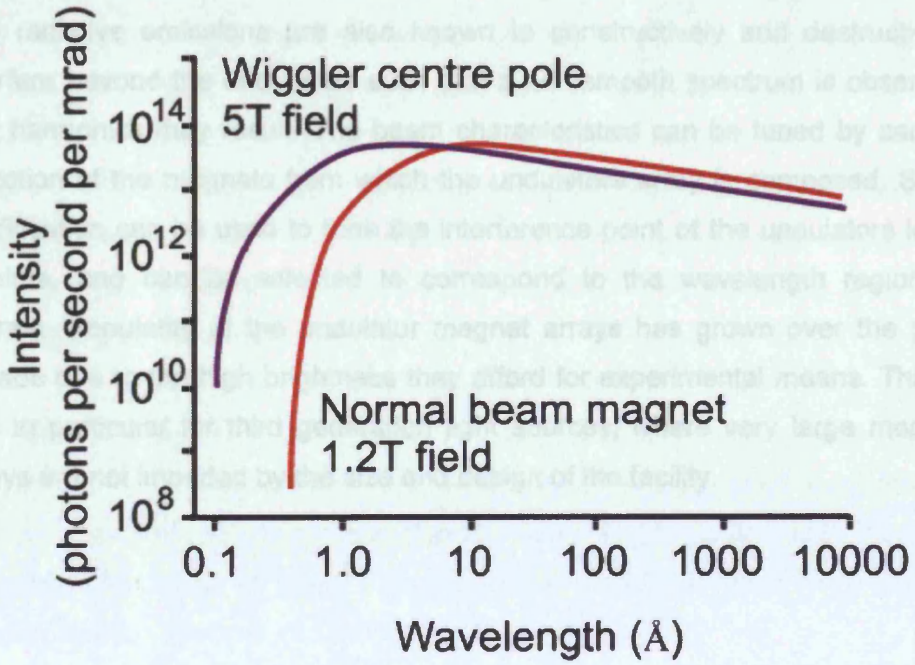

Figure 1.5.5.2: The diagram shows the comparison of the wavelength and intensity profile of a wiggler magnet (purple) versus a dipole magnet (red)[72].

Undulators:

In contrast to wigglers, undulators are composed of many (20+) alternating, low field magnetic poles, arrayed such as to cause continued undulation of the electron beam, hence the name *undulators (See Figure 1.5.5.3)*. This undulation is characterised by a series of opposed radial accelerations for the electrons beam, sequentially towards and away from the rings centre; the result is each acceleration event has its own radiative emission from the electron system.

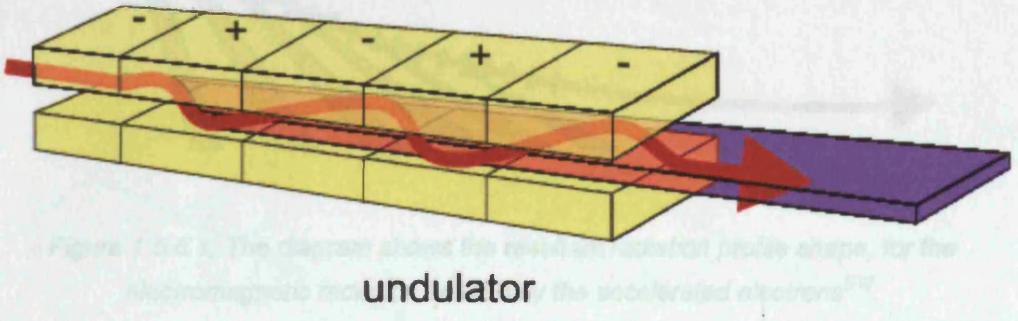

Figure 1.5.5.3: The diagram shows a schematic representation of a typical undulator magnet array[72].

The radiative emissions are also known to constructively and destructively interfere beyond the undulators such that a non-smooth spectrum is observed and harmonics may result. The beam characteristics can be tuned by careful selection of the magnets from which the undulators array is composed. Such modification can be used to tune the interference point of the undulators local maxima, and can be selected to correspond to the wavelength region of interest. Popularity of the undulator magnet arrays has grown over the past decade due to the high brightness they afford for experimental means. This is true in particular for third generation light sources, where very large magnet arrays are not impeded by the size and design of the facility.

1.5.6: Properties and Characteristics of Synchrotron radiation

The radiation emitted in a synchrotron as a result of the radial acceleration, is contained with a narrow fan-like shape (*See Figure 1.5.6.1*).

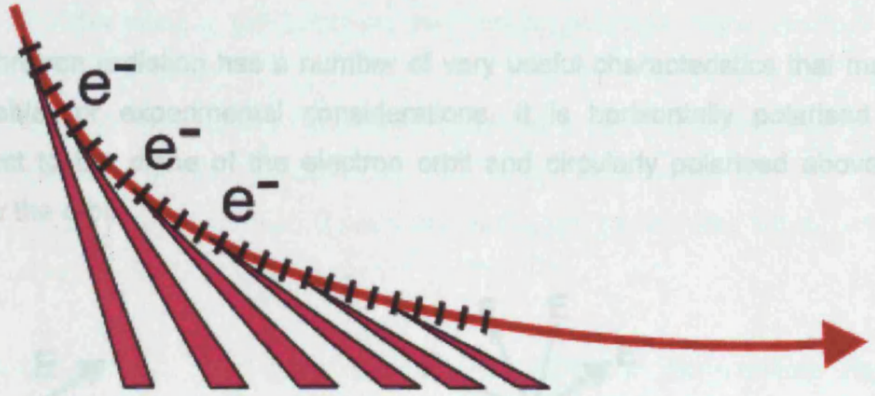

Figure 1.5.6.1: The diagram shows the resultant radiation profile shape, for the electromagnetic radiation emitted by the accelerated electrons[72].

The fan-like shape of the radiative emission is a characteristic result of electrons travelling at relativistic velocities. At energies of around 2GeV, the electrons processing within the synchrotron system will be travelling at around 99% the speed of light and with a mass 4000 times that of the rest mass of an electron. This results in the narrow spatial array of radiation and fanned shape, emitted in the direction of the electron procession; the beam is typically around 0.3mrad in the vertical plane. The presence of multiple processing bunches of electrons leads to a continuum of radiation fans, which spread over an arc. The resulting fan shape is wider horizontally than it is vertically due to the plane and direction of the electrons motion.

The consequences of relativistic velocities on the spatial characteristics of the emitted radiative beam, present a considerable advantage over the laboratory experiments. For synchrotron radiation the resultant fan gives a high intensity and collimation, something not observed in the laboratory where the radiation fan is considerably wider and more diffuse.

Synchrotrons have an available spectrum that ranges broadly across the electromagnetic spectrum and includes x-ray; this is a result of the extreme

conditions under which emission occurs. This wide spectrum is often referred to as a white beam. The use of appropriate insertion devices can be employed to select specific beam characteristics for the white beam or individual wave lengths, for user applications. For many purposes, the x-ray portion is specifically chosen and conditioned in very specialist, user focused stations.

Synchrotron radiation has a number of very useful characteristics that make it desirable for experimental considerations. It is horizontally polarised with respect to the plane of the electron orbit and circularly polarised above and below the orbit.

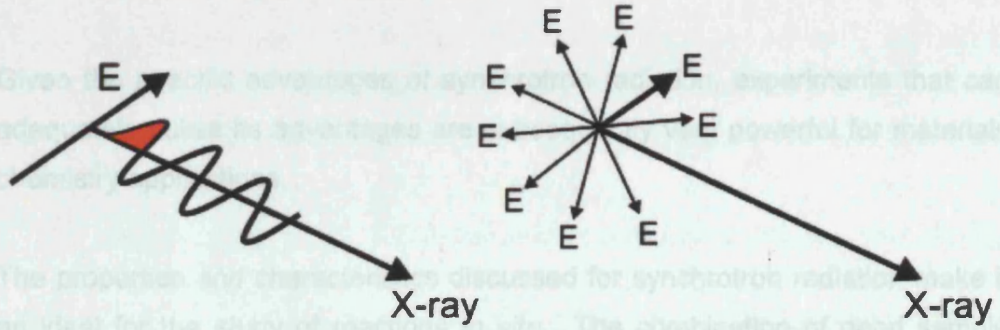

Figure 1.5.6.2: The diagram shows the differences in the electric field polarisation characteristics of synchrotron radiation, (left), against conventional laboratory x-ray sources, (right)[72].

For laboratory x-ray sources, the x-ray electric vector vibrates in all directions perpendicular to the propagation of the x-rays; for synchrotron sources the resultant x-rays have a horizontally polarised electric vector vibration.

An additional feature of synchrotron radiation comes as a consequences of the uses of electron bunches in the propagation of radiation; the result is that the synchrotrons output has a precise flashing time structure. Depending on variables such as density, size and speed of procession of the electron bunches, the times intervals for radiative emission can be of the order of 100ps per flash and a repeat interval of around 1-300ns. Such rapid flashing time sequences lend themselves well to specialist experiments for the study of chemical reaction and physical processes occurring on these timescales.

The benefits of synchrotron radiation for use in materials based chemistry experiments, can therefore be summarised as follows:

- **High intensity:** Superior statistics and high speed measurements.
- **Highly collimated:** Low radiation wastage in transition through the optical array of the beamline and greater eventual resolution due to its spatial precision.
- **Smooth continuous spectrum:** Facilitates experiments with either white radiation or a single wavelength by using monochromators.
- **Circularlarly polarised:** Above and below the plane of the orbit.
- **Precise flashing time structure:**

Given the specific advantages of synchrotron radiation, experiments that can adequately utilise its advantages are subsequently very powerful for materials chemistry applications.

The properties and characteristics discussed for synchrotron radiation make it an ideal for the study of reactions *in situ*. The combination of good sample penetration, rapid detection time-resolved techniques and good structural resolution are vital in a study of this nature.

1. 6: References

1. Davy, H., *On a Combination of Oxymuriatic Gas and Oxygen Gas.* Philosophical Transactions of the Royal Society, 1811. **101**: p. 155.
2. Faraday, M., Quarterly journal of science, 1823. **15**: p. 17.
3. Claussen, W., F, J. Chem. Phys, 1951. **19**: p. 1425.
4. Pauling, L. and R. March, E,, Acad. Sci. USA, 1952. **36**: p. 112.
5. Chatti, I., et al., *Benefits and drawbacks of clathrate hydrates: A review of their areas of interest.* Energy Conservation and management, 2004. **46**(9-10): p. 1333-1343.
6. Sloan, E., D and C. Koh, *Clathrate Hydrates of Natural Gases, Third Edition.* Chemical Industries Series. 2007: CRC. 752.
7. Schafer, R. and W. Klemm, *Wietere beitrage zur kenntnis der silicide und germanide der alkalimetalle.* Z. Anorg. Allg. Chem., 1961. **312**: p. 214-220.
8. Klemm, W., *Metalloids and their compounds with the alkali metals.* Proc. Chem. Soc. London, 1958: p. 329-341
9. Kasper, J., S, et al., *Clathrate structure of silicon Na_8Si_{46} and Na_xSi_{136} (x < 11).* . Science, 1965. **150**.
10. Cros, C., M. Pouchard, and P. Hagenmuller, Compt. Rend, 1965. **260**.
11. Bobev, S. and S. Sevov, C, J. Solid State Chem, 2000. **153**.
12. Yamanaka, S., et al., Physica B, 2006. **383**.
13. Bobev, S. and S. Sevov, C, J. Am. Chem. Soc, 2001. **123**.
14. Fukuoka, H., K. Ueno, and S. Yamanaka, J. Organomet. Chem, 2000. **611**.
15. Nesper, R., K. Vogel, and P. Blochl, E, Agnew. Chem. Int. ed. Egnl, 1993. **32**.
16. O'keffe, M., G. Adams, B, and O. Sankey, F, Phys. Rev. Lett, 1992. **68**.
17. Shimizu, H., et al., Phys. Rev. B, 2003. **68**.
18. Reny, E., et al., Chem. Commun, 2000. **2000**.
19. Demkov, A., A, O. Sankey, F, and W. Windl, Phys. Rev. B, 1996. **53**.
20. Demkov, A., A, et al., Phys. Rev. B, 1994. **50**.
21. O'keffe, M., G. Adams, B, and O. Sankey, F, Philos. Mag. Lett, 1998. **78**.
22. Various, *Chemistry, Structure and Bonding of Zintl Phases and Ions,* . 1996: VCH Publishers.
23. Zintl, E., *Salt-like compounds of Sodium and their Transition to Intermetallic Phases.* Naturwiss, 1929. **17**.
24. Gallmeier, J., H. Schafer, and A. Weiss, Naturforsch, 1996. **246**.
25. Villars, P. and L. Calvers, D, *Pearson's Handbook of crystallographic data for intermetallic phases.* 1991: ASM International: Materials Park, OH.

26. Ramachandran, G., et al., J. Solid State Chem, 1999. **145**.
27. Connetable, D. and X. Blase, App. Surface Science, 2004. **226**.
28. Saito, S. and A. Shiyama, Phys. Rev. B, 1995. **51**.
29. Schaujman, S., B, et al., J. Appl. Phys, 2000. **87**.
30. Kawaji, H., et al., Phys. Rev. Lett, 1995. **74**.
31. Kawaji, H., et al., Solid State Commun., 1996. **100**.
32. Yahiro, H., et al., Phys. Rev. Lett, 1995. **246**.
33. Shimizu, F., et al., Phys. Rev. B, 1996. **54**.
34. Fang, S., L, et al., Phys. Rev. B, 1998. **57**.
35. Kahn, D. and J. Lu, P, Phys. Rev. B, 1997.
36. Mott, N., F, J. Solid State Chem, 1973. **6**.
37. Smelyansky, V., I and J. Tse, S, Chem. Phys. Lett, 1997. **264**.
38. Moriguchi, K., S. Munetoh, and A. Shintani, Phys. Rev. B, 2000. **62**.
39. Zhao, J., et al., Phys. Rev. B, 1999. **60**.
40. Koyoa, T., et al., Phys. Rev. B, 2001. **64**.
41. Connetable, D., et al., Phys. Rev. Lett, 2003. **91**.
42. Carrillo-Cabrera, W., et al., Z. Kristostallogr; NCS, 2001. **216**.
43. Paschen, S., et al., *Proc. 19th ICT*. 2000: Babrow Press, Wales, UK.
44. Fukuoka, H., et al., J. Solid State Chem, 2000. **151**.
45. Grosche, F., M, et al., Phys. Rev. Lett, 2001. **81**.
46. Bryan, J., D, et al., Phys. Rev. B, 1999. **60**.
47. Yaun, H., Q, et al., High Pressure Research, 2002. **22**.
48. Roy, S., B, K. Sim, E, and A. Caplin, D, Phys. Mag. B, 1991. **64**.
49. Slack, G., A, *CRC Handbook of Thermoelectrics*, ed. D. Rowe, M. 1995: CRC Press, Boca Raton, FL.
50. Slack, G., A, Mater. Res. Symp. Proc, 1997. **478**.
51. Nolas, G., S, et al., Appl. Phys. Lett, 1999. **73**.
52. Paschen, S., et al., Phys. Rev. B, 2001. **64**.
53. Uher, C., J. Yang, and S. Hu, Mater. Res. Soc. Symp. Proc., 1999. **545**.
54. Sales, B., C, et al., Phys. Rev. B, 2001. **64**.
55. Melinon, P., et al., Phys. Rev. B, 1999. **59**.
56. Myles, C., W, et al., Phys. Rev. B, 1999. **65**.
57. Petkov, V. and T. Vogt, Solid State Commun., 2003. **127**.
58. Zerec, I., et al., Phys. Rev. B, 2002. **66**.
59. Tang, X., et al., Phys. Rev. B, 2006. **74**.
60. Hermann, R., F, W, et al., Phys. Rev. B, 1999. **60**.
61. Kawaguchi, T., K. Tanigaki, and M. Yusakawa, Phys. Rev. Lett, 2000. **85**.

62. Nemoto, Y., et al., Phys. Rev. B, 2003. **68**.
63. Bryan, J., D and G. Stucky, D, Chem. Mater., 2001. **13**.
64. Carrillo-Cabrera, W., S. Paschen, and Y. Grin, J. Alloys. Compd., 2002. **333**.
65. Christensen, M., et al., *Crystal and magnetic structure of $Eu_4Ga_8Ge_{16}$.* Phys. Rev. B, 2003. **68**.
66. Bryan, J., D, et al., Phys. Rev. B, 2003. **68**.
67. Chakoumakos, B., C, B. Sales, C, and D. Mandrus, J. Alloys. Compd., 2001. **322**.
68. Mudryk, Y., et al., Physica B, 2003. **328**.
69. Nesper, R., J. Curda, and H. Von Schnering, G, Angew. Chem. Int. Edn. Engl, 1986. **25**.
70. Kovnir, K., A, et al., Novel compounds $Sn_{20}Zn_4P_{22}$–vI_8 (v = 1.2), $Sn_{17}Zn_7P_{22}I_8$, and $Sn_{17}Zn_7P_{22}Br_8$: Synthesis, properties, and special features of their clathrate-like crystal structures Solid State Sciences, 2005. **7**.
71. Robinson, A., L, *X-Ray Data Booklet.* 2001: Lawrence Berkeley National Laboratory.
72. Barnes, P., et al., *Powder Diffraction on the web; Industrial Materials group.* 2004.

Chapter 2

Experimental Methods and Techniques

Synthesis of Solid State Clathrates:

2.1: Introduction:

Since the original report in 1965[1], various approaches have been employed to synthesize the solid state clathrates. For binary clathrates of silicon and germanium, e.g. Na_8Si_{46} and $Na_{24}Si_{136}$, the thermal degradation from Zintl intermediates synthetic route is most commonly employed. Systems with framework substitutions, such as $Ba_8Ga_{16}Sn_{30}$, $Ba_8Ga_{16}Ge_{30}$ and $Eu_4Ga_8Ge_{16}$, a more common approach is direct melting of pure elements or flux growth techniques[2],[3],[4],[5]. In September 2006, a new route to synthesize guest-free germanium clathrates of the composition $\square_{24}Ge_{136}$, was reported by Guloy *et al*[6]. This novel approach employed the use of low temperature, ionic liquid synthesis to create germanium type II clathrates; to date it is the only "wet chemistry" approach to the synthesis of the solid state clathrates.

In the present work, it was chosen to study the synthesis of Si-bearing clathrates by partial thermal decomposition of zintl phases, such as NaSi.

2.2: Synthesis and Characterisation of the Zintl Phases of Group 14 Elements:

The process of thermal degradation of Zintl phases is undertaken using high vacuum and high temperatures to reduce the stoichiometric content of the guest species, in a given system. In these reactions, the starting material is of the composition A_1T_{1-4}; for T =1, the product is a black powdered crystalline solid, for T = 4, a metallic semi-solid of amorphous nature; between 1 and 4 is a discreet range of compositions for which the products physical appearance varies accordingly between the crystalline and the semi-solid.

$$1.15 \sim 1.3\ A_{(s)} + T_{(s)} \xrightarrow[24\ Hrs]{600\text{-}650^\circ C} AT_{(s)}$$

The Zintl phases are prepared by direct mixing of the elements under dry-box conditions; typically less than 5ppm H_2O and O_2. For low melting alkali metals, an excess of the metal is often employed to counteract the issues of evaporation and

coating of the inner reaction vessel. The correct proportions are placed into an inert crucible. Many materials are suitable for this including tantalum, corundum, niobium, platinum and tungsten, among others. These crucibles are often subject to sealing by spot or arc-welding which to some extent reduces issues associated with evaporation of low-melting metals. It is, however, also acceptable to use a crucible with a lid that is not attached firmly and still achieve favourable results.

The inert crucible was then placed into a steel autoclave and sealed using a polished copper plate. The autoclave was sealed firmly and placed into a furnace for 24 to 48 hours at temperatures from 600°C – 650°C. At the higher end of this range, residual clathrate and group14 elements can occur as impurities with some regularity. When the reaction was complete, the product was recovered in a dry-box due to the highly air and moisture sensitive nature of the Zintl phases of the group 14 elements.

In some circumstances, the product will contain a degree of non-stoichiometric guest species, for example a stoichiometry Na_1Si_1 is desired but $Na_{1.4}Si_1$ has resulted. In such cases, the sample can be placed into an inert metal boat under vacuum at a temperature below that at which clathrate formation occurs - typically in the range 200°C to 250°C - until the desired, stoichiometrically balanced Zintl phase crystallises.

In terms of considerations of Zintl phases produced here, phase quality and composition were ascertained using x-ray powder diffraction. Samples were prepared in dry-box conditions by moderate grinding of the solid, then sieving through a 38 micron sieve. The finely sieved powder was then carefully loaded into a 0.5 mm borosilicate glass capillary for study via diffraction techniques. The capillary was mounted into a brass goniometer stub, sealed with wax in the dry-box and then super-glue upon exiting, to ensure good protection from atmospheric H_2O/O_2.

Phase quality was determined by comparison of *hkl* reflections against those reported in the literature in previous studies. For many of the silicides used in this study, the samples were appraised *in situ* using the synchrotron station in use for the studies, as a result of limited sample volume for pre beam-time analysis. The greater part of the work for this study focused on NaSi and the mechanism of clathrate formation and as such, much of the data shown here will pertain to that phase. The reason for the choice of NaSi as the main candidate for the *in situ* experiments is its propensity to form both clathrate phases under varying conditions.

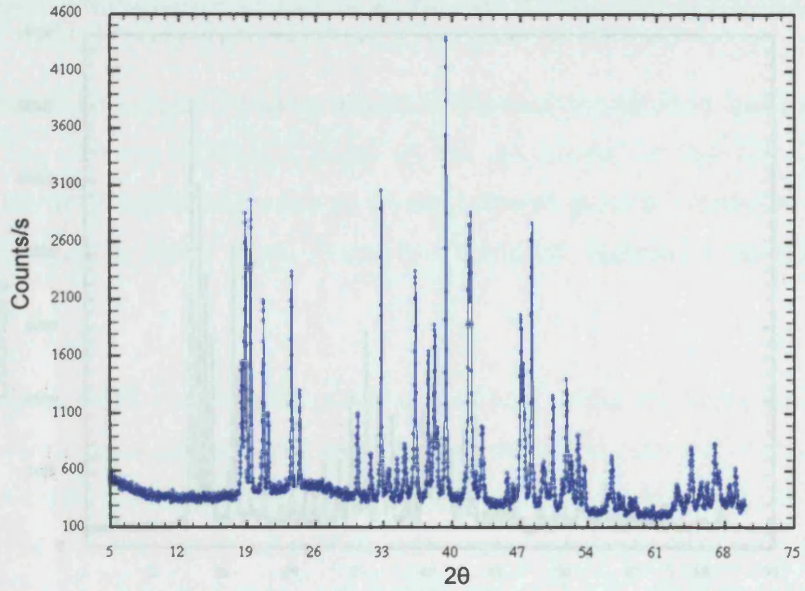

Figure 2.2.1: Laboratory x-ray powder diffraction pattern for NaSi (C2/c). The amorphous bump seen from 19-30° 2θ represents the SiO_2 capillary.

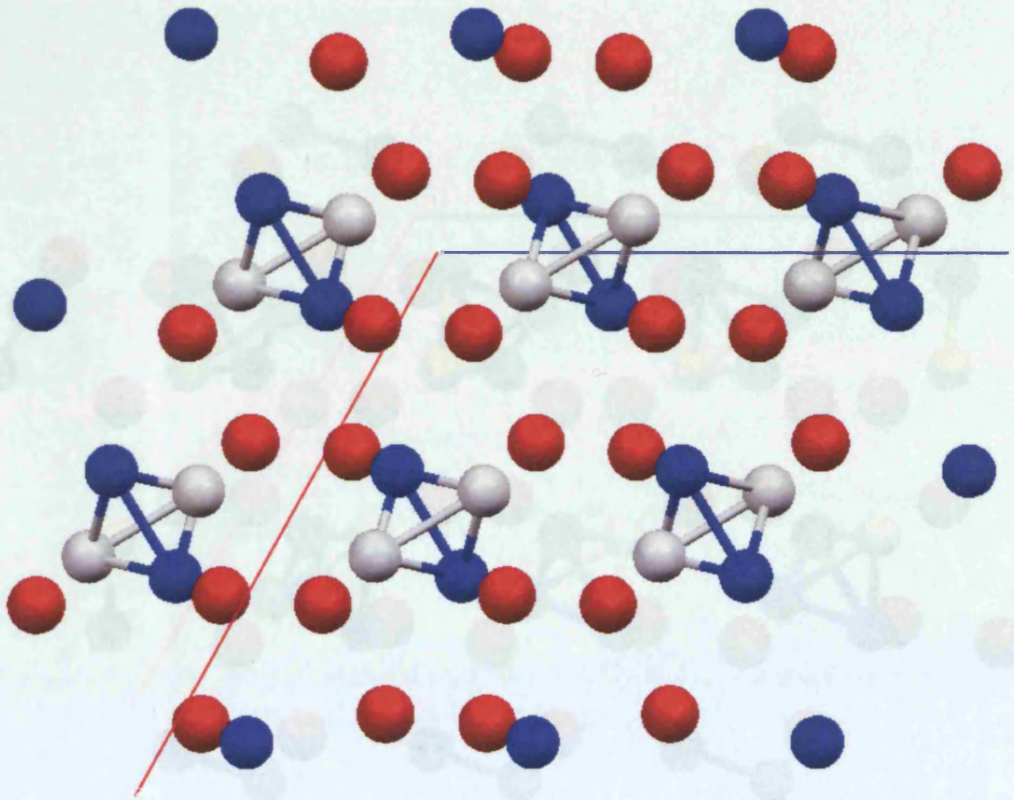

Figure 2.2.2: C2/c unit cell of NaSi viewed along the b axis. Red denotes sodium, blue denotes Si1 position, white Si2 position.

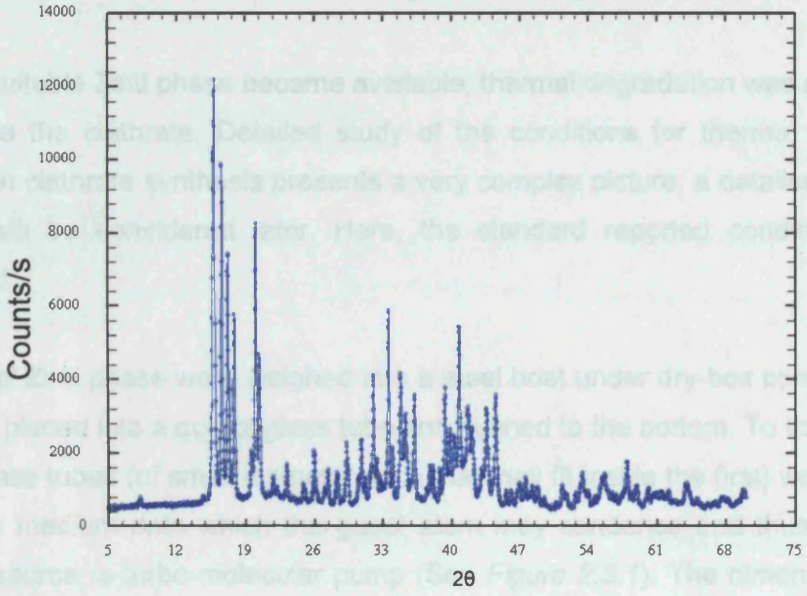

Figure 2.2.3 Laboratory x-ray powder diffraction pattern for NaGe ($P2_1/c$).

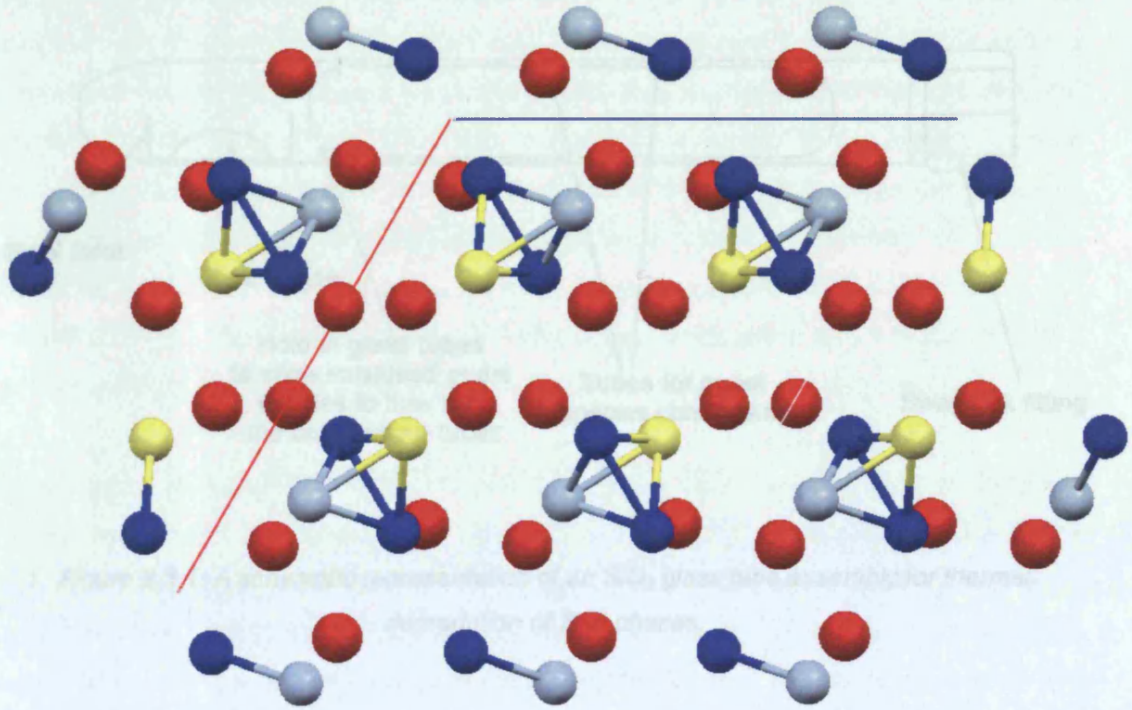

Figure 2.2.4: $P2_1/c$ unit cell of NaGe viewed along the b axis. Red denotes sodium, blue denotes Ge3 position, yellow Ge2 position and white Ge1 position.

2.3: Preparation of Solid State Clathrates by Thermal Degradation of Zintl Phases:

When a suitable Zintl phase became available, thermal degradation was attempted to synthesise the clathrate. Detailed study of the conditions for thermal degradation required in clathrate synthesis presents a very complex picture; a detailed discussion on this will be considered later. Here, the standard reported conditions will be discussed.

Aliquots of Zintl phase were weighed into a steel boat under dry-box conditions. This was then placed into a quartz glass tube and pushed to the bottom. To this, a second pair of glass tubes (of small diameter such that they fit inside the first) were added to provide a medium onto which the guest atom may condense and thus protect the vacuum source, a turbo molecular pump (See *Figure 2.3.1*). The dimensions of this assembly may be varied to any proportion, assuming the chosen dimension allow high vacuum to be applied inside the sample chamber. This was then connected to a modified Swagelok fitting, attached to a high vacuum tap and then to a Schlenk line (See *Figure 2.3.2*). The turbo molecular pump was protected from the out-gassing guest species by a liquid nitrogen trap.

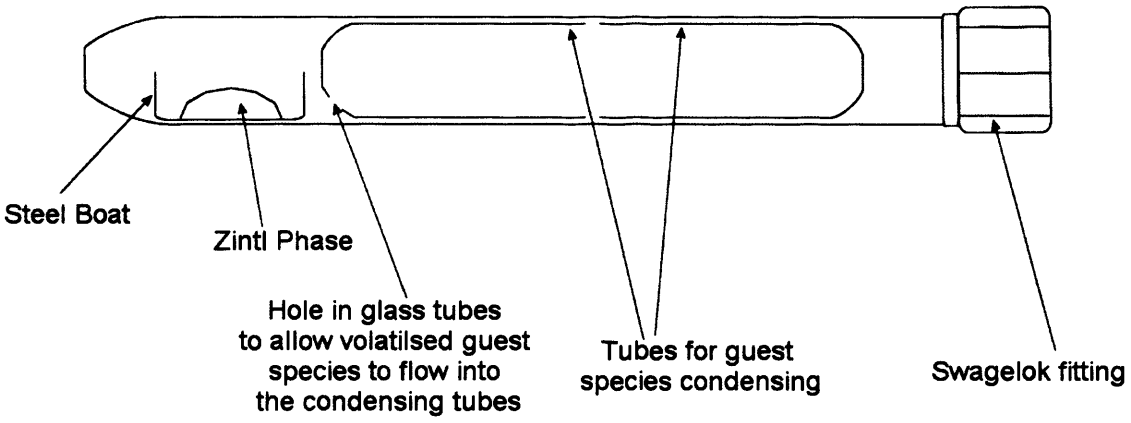

Figure 2.3.1: A schematic representation of an SiO_2 glass tube assembly for thermal degradation of Zintl phases.

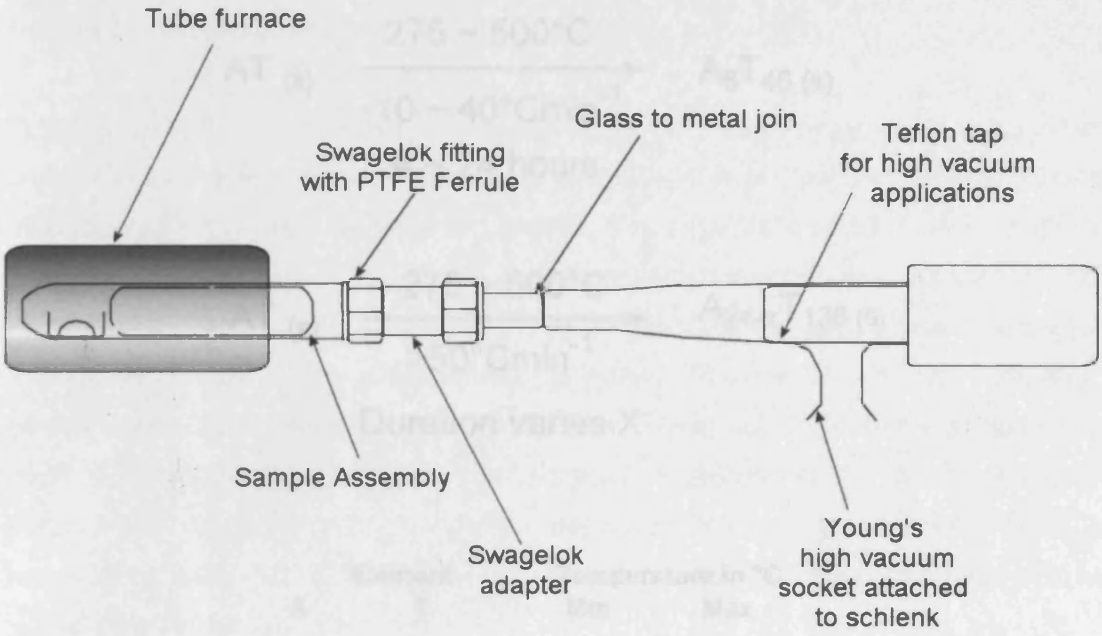

Figure 2.3.2: Vacuum assembly for thermal degradation of Zintl phases. Diagram shows the sample assembly (Figure 2.3.1) connected to a swagelok vacuum assembly for loading in a dry-box and thermal degradation studies.

The sample was then mounted into a pre-calibrated tube furnace and held in place by use of retort stands. It was then connected to the vacuum line and vacuum was applied with the sample isolated from vacuum by the taps at the Schlenk line and the Swagelok assembly; this was necessary such that the powdered sample was not sucked into the turbo pump. The vacuum was slowly applied to the sample using a two tap system as a kind of "air lock" or antechamber, such that vacuum could be slowly equalised using the isolated chamber as a mid point between sample and vacuum line. When the sample reaches a suitable vacuum, 10^{-5} bar, heating can begin. Choice of temperature ramp rate and target temperature has a profound effect on the product gained from this reaction, if NaSi is used as a starting material.

It has been reported[7] that the use of slow heating rates (2-10°Cmin^{-1}) of the NaSi under vacuum, in the temperature range 275°C to 500°C, produces Na_8Si_{46} as the predominant phase; rapid heating rates (>50°Cmin^{-1}) in the same temperature range promotes the formation of the $Na_{24}Si_{136}$ clathrate phase. There are considerations associated with the sample assembly and stoichiometry of the starting material that will be discussed in greater detail later in this chapter. The basic reaction schemes are shown below.

$$AT_{(s)} \xrightarrow[10 \sim 40°C min^{-1}]{275 \sim 500°C} A_8T_{46\,(s)}$$

4 ~ 24 hours

$$AT_{(s)} \xrightarrow[>50°C min^{-1}]{275 \sim 500°C} A_{24-x}T_{136\,(S)}$$

Duration varies X

	Element	Temperature in °C	
A	T	Min	Max
Na	Si	375	400
K	Si	420	440
Rb	Si	400	420
Cs	Si	400	430
Na	Ge	370	400
K	Ge	350	380
Rb	Ge	360	375
Cs	Ge	325	350

Figure 2.3.3: Table of reported temperature ranges for the synthesis of type I clathrates of the group 14 elements[8].

In the synthesis of a mixed phase sample separation may be achieved using a standard swim-sink differential solvolysis separation methodology, in addition to fractionation via gravimetric chromatographic methods[7]. Though such methods are possible and provide adequate means of differentiation of phase, such procedures are more time consuming than alternative methods and often wasteful of material, thus it is sensible to enlist a direct synthesis with accurate denomination of phase.

As discussed in the previous paragraph the synthetic procedure of clathrate preparation can be a complex issue and requires detailed explanation. The course of much of this study is focused on NaSi as a starting material, due to its tendency to form type I and II clathrates. The procedure for a preparation that differentiates between the two predominant clathrate forms is therefore demonstrated by the use of this starting material; as such it will be the focus of the discussion.

Preparation of Na_8Si_{46} and $Na_{24-x}Si_{136}$ from Na_1Si_1:

Preparation of type I clathrates is by far the more simple synthesis to complete when compared to the synthesis of clathrate II using NaSi. A stoichiometric NaSi starting material can very easily be used to create a type I clathrate under a wide range of conditions. During the course of this work, it was noted that unless a sufficiently high vacuum and ramp rate were achieved in the preparation, the type I phase was almost exclusively formed as the product, with typically <5% of *d*-Si as the only impurity. Where temperature ramp rates above 50°Cmin^{-1} were achieved in the presence of good vacuum (10^{-5} bar), the type II phase predominates with <5% *d*-Si. Where a poor vacuum was present (<10^{-4}) the type II clathrate could still be formed but with much higher ramp rates (100-200°Cmin^{-1}) and was often present as a mixed phase product with variable Na_8Si_{46} content.

In addition, it appears that the preparation environment plays a key factor in determining the composition of the products. It has become apparent that the diameter of tubing used for the sample environment (*Figure 2.3.1*) can be a factor in determining composition. It was seen[9] that using a 10mm diameter of glassware or lower, has a tendency to result in a mixed product, if the type II clathrate synthesis is attempted. If a diameter of 20mm or greater was used in the same preparation - assuming the same conditions of vacuum and temperature - a pure phase with only *d*-Si as an impurity was seen. The reason for this must be related to the rate of loss of sodium from the system and therefore the effect of confinement of the sample environment on local vapour pressure under vacuum (and additionally the quality and effectiveness of vacuum applied). This has two consequences; the first is the importance of choosing appropriate glassware for pure synthesis; the second is that the rate of loss of sodium is important in a formation that differentiates between the forms. These results clearly demonstrate the metastable nature of these reactions.

Preparation of Na_8Si_{46} and $Na_{24-x}Si_{136}$ from Na_xSi_1 (X=2-4) (Amorphous Na rich alloy):

In the preparation of sodium silicide, it is possible to use a three to one stoichiometry of sodium to silicon and produce a semi-solid, metallic, amorphous alloy of NaSi that appears silver/black in colour. This was prepared in much the same way as previously discussed and its sodium content is readily identified via elemental analysis.

$$3.0 \sim 3.5\ A_{(s)} + T_{(s)} \xrightarrow[24\ Hrs]{600\text{-}650^{\circ}C} A_3T_{(s)}$$

The use of this product for the synthesis of clathrates is interesting in that though it has a considerably higher stoichiometric excess of sodium than NaSi, it forms $Na_{24}Si_{136}$ far more readily. In the previous section it was discussed that rapid heating and high vacuum is required to produce the clathrate II structure. However, in this instance it appears the presence of a high stoichiometric content of sodium stabilises the formation of the type II phase. In addition to this, it is interesting to note that in the use of Na_3Si, if the above conditions are used and higher temperatures are applied in the synthesis, a mixed phase product again persists (see *Figure 2.3.7*). It appears, in the case of Na_3Si, the clathrate II phase becomes the thermodynamically favourable product relative to Na_8Si_{46}, where Na_8Si_{46} is the kinetically favourable product; this is a complete reverse of the reaction with NaSi.

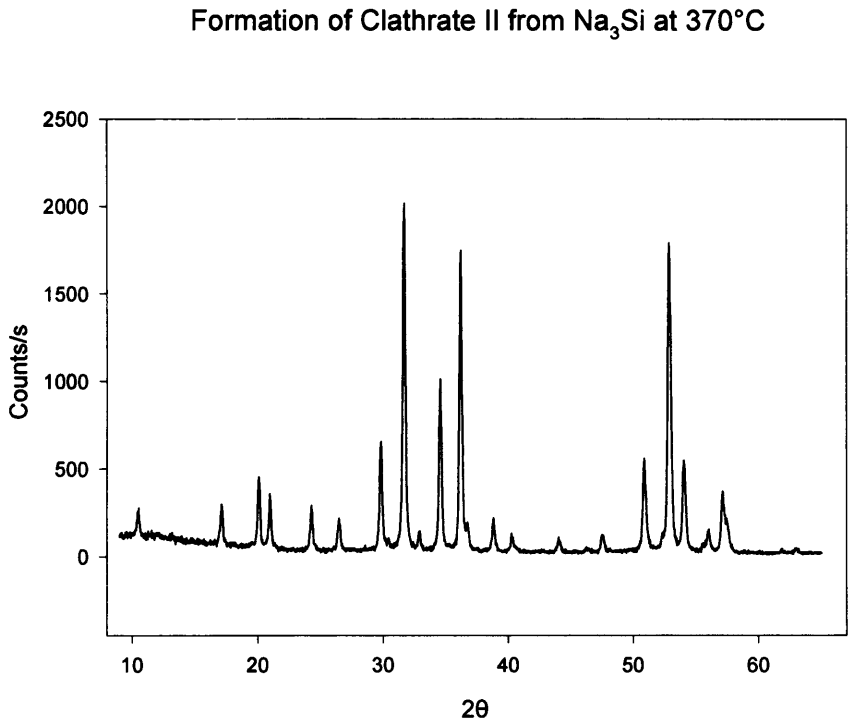

Figure 2.3.4: X-ray data set for clathrate II prepared at 370°C for 8 hours.

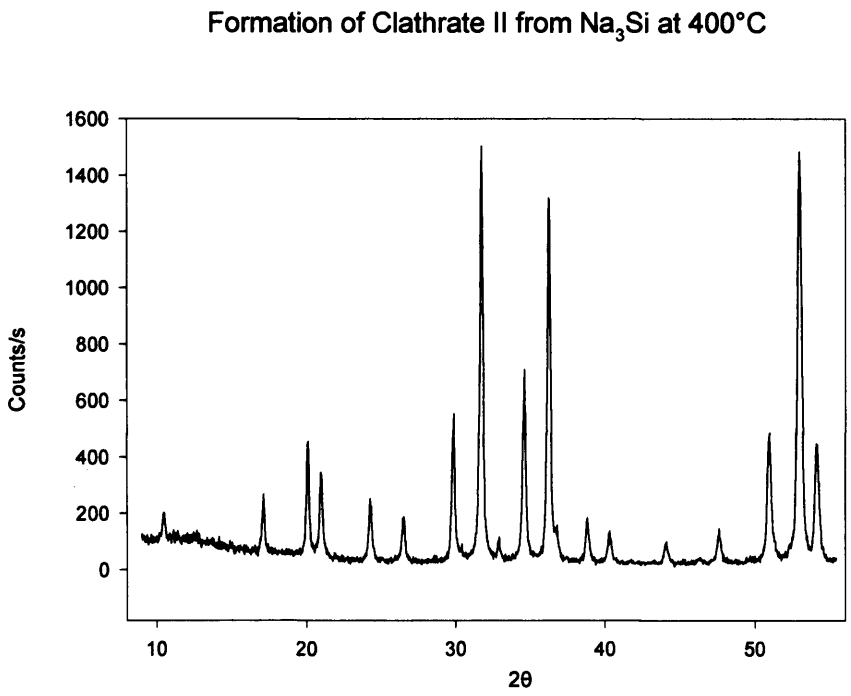

Figure 2.3.5: X-ray data set for clathrate II prepared at 400°C for 8 hours.

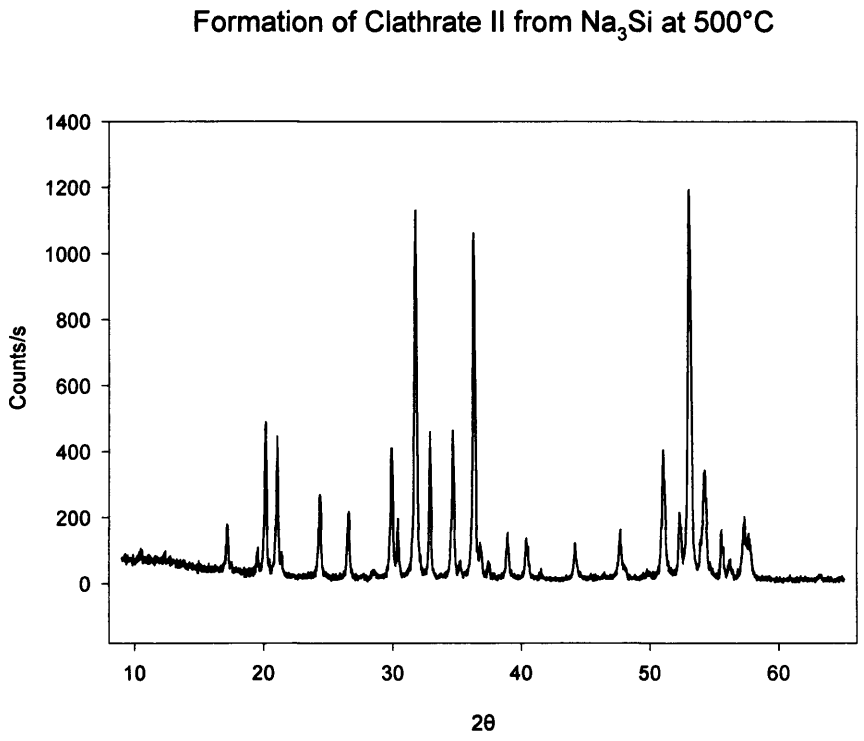

Figure 2.3.6: X-ray data set for clathrate II prepared at 500°C for 8 hours.

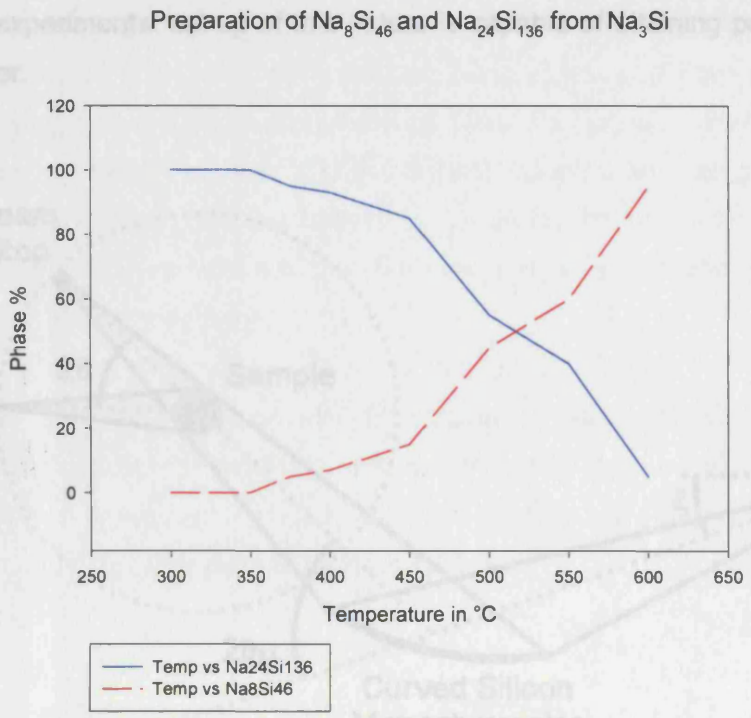

Figure 2.3.7: Graph shows the trends of phase percentage of clathrate I vs. clathrate II as a result of variation of synthesis temperature when using sodium rich alloy as th precursor material.

2.4 Laboratory X-Ray Power Diffraction:

As previously discussed, the reaction environment for the preparation of Zintl phases and the subsequent formation of clathrates must be highly inert i.e. environments with sub-ppm O_2 and H_2O levels. As much of the work was carried out in dry-box conditions, it was necessary to utilise diffraction techniques that allow for highly reactive samples to be used without contamination from the atmosphere. Given these restrictions, the use of quartz or borosilicate glass capillaries – which can be easily sealed and secured from the atmosphere – was the most practical solution.

Transmission diffractometry was utilised in this experiment (*see Figure 2.4.1*) using the Debye-Scherrer set-up; this utilises a pre-sample narrow-band pass silicon monochromator to achieve high resolution data. This curved monochromator focuses the divergent beam, not onto the sample environment, but past the 2θ acquisition circle of the detector. The Bragg angle of the monochromator is determined using the *d* spacing of a given lattice plane for a standard, such as the [111] plane for

silicon; an experimental set-up of this nature is capable of attaining peaks widths of 0.1° or better.

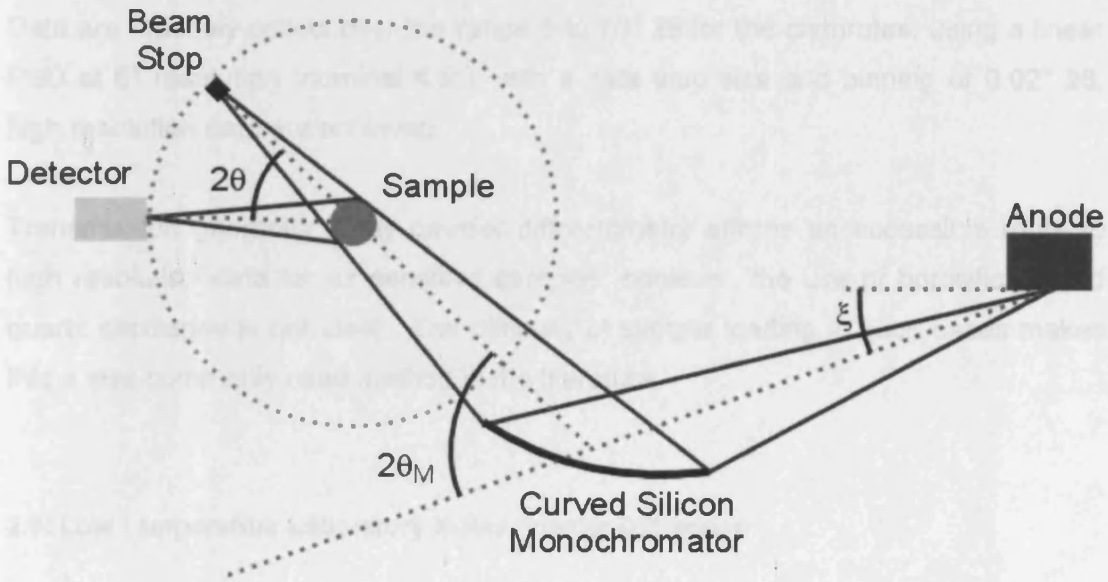

Figure 2.4.1: A Schematic of the geometry associated with transmission geometry or Debye-Scherrer x-ray diffraction techniques[10].

The diffractometer used was a Stoe StadiP, transmission geometry, capillary, powder diffractometer with a 30mA, 4KW (40 KeV) Spellmann X-ray generator. The X-ray source is a twin copper $K\alpha_1$ radiation source (though other sources are readily interchangeable) and uses a silicon pre-sample monochromator. The sample was prepared by grinding in agate and sieved using a 38 micron sieve to assure a good homogeneity of the crystallites. The capillary used was most commonly borosilicate (SiO_2 for high temperature work) of 0.5 mm diameter and wall thickness 0.01 mm. When a well-sieved, homogenous sample was achieved, it was loaded by careful application of vibration to the capillary. This is most commonly done using a sonic bath but for such high reactivity intermediates as the zintl phases, it is necessary to do this by hand inside the dry-box, using a finely serrated surface and a great deal of care. The sample holder was mounted into a brass stub and sealed into position using wax. Upon exiting the dry-box, the sample was further secured using fast-drying super-glue.

The sample was mounted and fastened into the goniometer using the brass stub and aligned accurately such that it spins with no evident deviation from the origin; this was done using a microscope with graticule. Data are collected from 1 hour up to anything over several days, with data quality and statistics improving with duration. Data are routinely collect over the range 5 to 70° 2θ for the clathrates, using a linear PSD at 6° resolution (nominal 4.5°); with a data step size and binning of 0.02° 2θ, high resolution data are achieved.

Transmission geometry X-ray powder diffractometry affords an accessible route to high resolution data for air sensitive samples; however, the use of borosilicate and quartz capillaries is not ideal. The difficulty of sample loading in such cases makes this a less commonly used method in the literature.

2.5: Low Temperature Laboratory X-Ray Powder Diffraction:

The Stoe StadiP diffractometer described in the previous section can be equipped with a liquid helium cryostat, akin in design to those of ILL "orange" design used at ILL Grenoble. The basic design of the laboratory cryostat is the same as the large instrument conformer, yet has a modified "tail" such that it may be mounted onto the laboratory diffraction apparatus (*see Figure 2.5.1*). In addition, the cryostat has been modified to take into account the small sample size used in the laboratory environments and the weaker X-ray source used.

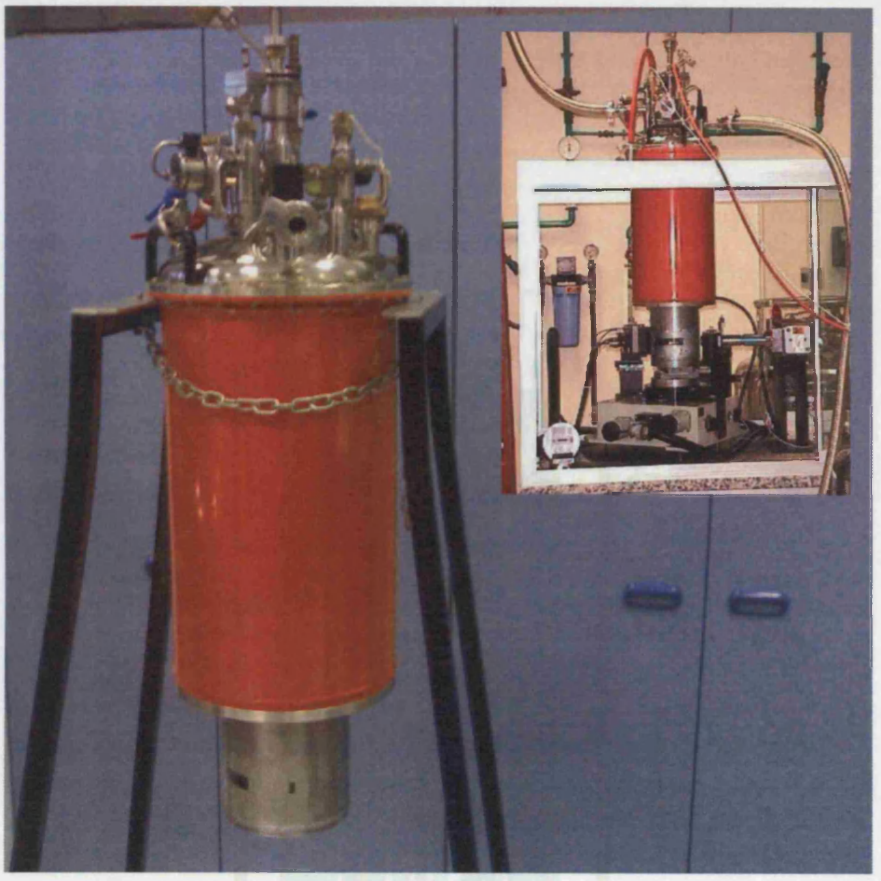

Figure 2.5.1: Modified ILL design "Orange" cryostat (main) and shown in position, mounted onto the Stoe StadiP diffractometer (insert).

The cryostat is composed of two jackets, the first an outer liquid nitrogen jacket, the second an inner liquid helium jacket whose volumes are approximately 25 and 10 litres respectively (Figure 2.5.2). The helium is applied to the sample via a needle valve to the heat exchange which connects to the sample holder. The sample is mounted into a long rotating rod, comprised of a series of thermal radiation baffles, and is situated via the top of the cryostat (Figure 2.5.3). Samples are again mounted into glass capillaries as they provide a suitable secure sample environment to which very low temperatures may be administered. The sample is accessed via a Mylar™ window that provides adequate contact to the sample with minimal absorption of intensity. The cryostat is capable of temperatures as low as around 3 to 4 K; at these temperatures the cryostat suffers the affects of photon heating through the Mylar™ window and thus requires considerable volumes of liquid helium to maintain these temperatures. For temperatures above 20 K, equilibration is achieved within 20 to 30 minutes of reaching the temperature and may be maintained at a constant for many hours.

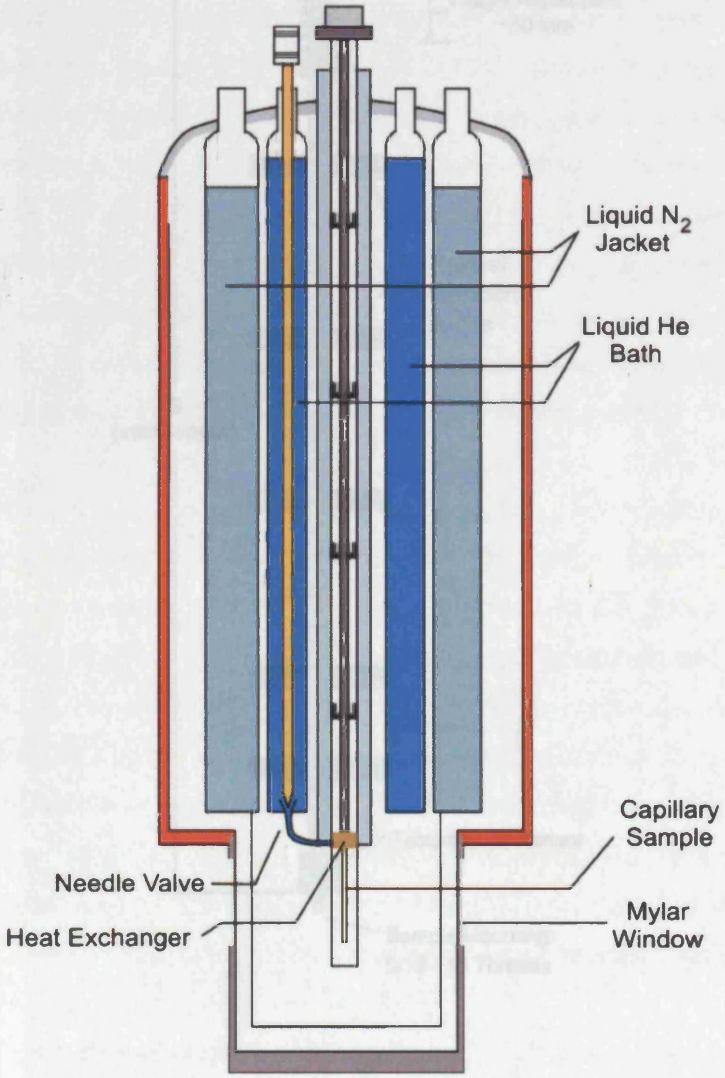

Figure 2.5.2: The internal design of the modified ILL "Orange" design liquid helium cryostat [10].

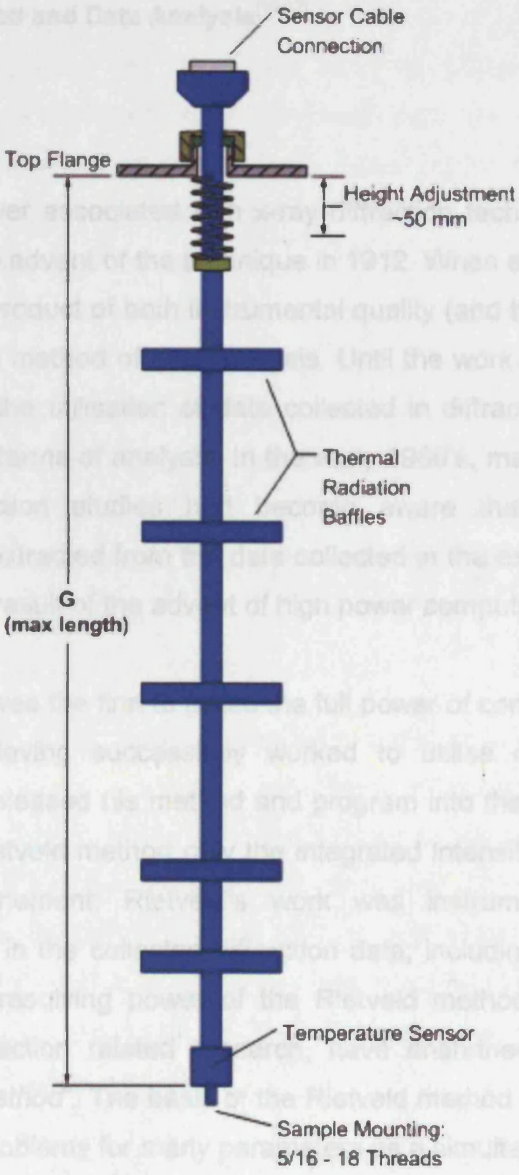

Figure 2.5.3: Diagram shows the rotating central sample mount with radiation baffles, temperature sensor positioning and the sample mounting socket[10]. The capillary mounted sample is attached into the end of this mounting rod.

2.6: The Rietveld Method and Data Analysis[10-12]:

Introduction:

The considerable power associated with x-ray diffraction techniques has increased considerably since the advent of the technique in 1912. When employed, the success of the technique is a product of both instrumental quality (and thus data collection) in addition to quality and method of data analysis. Until the work of Rietveld in the mid to late 1960's[13, 14], the utilisation of data collected in diffraction experiments was relatively simplistic in terms of analysis. In the early 1960's, many researchers in the field of x-ray diffraction studies had become aware that considerably more information could be extracted from the data collected in the experiments; this would only be possible as a result of the advent of high power computing.

The work of Rietveld was the first to utilise the full power of computers, for powder x-ray data analysis. Having successfully worked to utilise diffraction data more thoroughly, Rietveld released his method and program into the public domain[13, 14]. Until the advent of Rietveld method only the integrated intensities of resolved peaks were utilised in refinement; Rietveld's work was instrumental in utilising all information contained in the collected diffraction data, including complex composite peaks. The inherent resolving power of the Rietveld method and the associated revolution within diffraction related research, have enshrined technique with the name the "*Rietveld method*". The basis of the Rietveld method is the solution of non-linear least squares problems for many parameters as a simultaneous calculation.

In the field of materials chemistry it is considerably difficult experimentally to grow crystals of many compounds and thus much diffraction must be completed on powdered samples. The advantage of the Rietveld method is that it provides treatment for diffraction data collected from powdered sample. Given the complex problems associated with single crystal growth, it is clear why the advent of the Rietveld method is both so desirable and important. The initial application of the Rietveld method was in the area of neutron diffraction experiments, utilising a single wave length but has since be modified for the use in a wide range of related techniques. The technique is applicable to both fixed wave length problems and recently energy dispersive data sets and requires modification, only, in the instrumental parameters associated with the experiments and not the overall methodology.

The Rietveld method functions by use of least squares refinements, until a best fit is achieved between the entire observed (experimental) powder diffraction pattern and the entire calculated pattern. This calculation is based on the simultaneously refined model for the crystals structure, diffraction optics, instrumental factors and other associated characteristics (lattice parameters etc) as may be desired and suitable modeled[15]. One considerably significant draw back to the Rietveld method is the requirement of a model upon which the calculations may be based; the Rietveld method itself, is not a structural refinement solution method. The obvious issue associated with this requirement of the method is that it is not suitable for the resolution of unknown structures but in addition, may find considerable difficulty resolving a structure which deviates too greatly from the initial suggested model.

Rietveld Method:

The data collected in an x-ray powder diffraction experiment is essentially a collection of numerical intensity values, y_i, where, *i,* represents all increments for the collected pattern. The Rietveld method attempts to find solution to y_i's simultaneously by least squares methods, such that the observed and calculated profiles approach a match. Optimisation of the parameters within the solution and model is reached when the differences between the intensities calculated from the structural model, $y_i(calc)$, and the observed intensities collected in the diffraction experiment, $y_i(obs)$, are minimised. The relationship is expressed:

$$\Delta = \sum_i w_i \{y_i(obs) - y_i(calc)\}^2$$

Where:

- Δ = the least squares residual that is to be minimised,
- w_i = weight factor which takes into account the precision with which each intensity measurement is acquired. If the errors are purely found within the counting statistics, the weight factor is simply $1/y_i$. The summation is over all of the data points for both patterns,
- $y_i(obs)$ = intensity of the observed diffraction pattern at the i^{th} step,
- $y_i(calc)$ = intensity of the calculated pattern at the point $2\theta_i$,

The calculation of the value $y_i(calc)$ in itself is a complex problem and is fundamental to the Rietveld method and thus solution of powder diffraction problem:

$$y_i(calc) = s\sum_{hkl} L_{hkl} P_{hkl} M_{hkl} |F_{hkl}|^2 \phi(2\theta_i - 2\theta_{hkl}) P_k A M E + y_i(back)$$

Where:

- L_{hkl} is the Lorentz factor;
- P_{hkl} is the polarization factor;
- M_{hkl} is the multiplicity factor;
- F_{hkl} is the structure factor of the hkl^{th} Bragg reflection;
- is $(2\theta_i - 2\theta_{hkl})$ the reflection profile function;
- P_k is the preferred orientation function;
- A is an absorption factor;
- M is a correction for multiple scattering;
- E is used to model extinction within the crystallites.
- y_i(back) is the background function.

It can thus be seen that the model requires a complex set of parameter, of which as many as possible must be refined to achieve minimisation. The complexity of the model and array of parameters is somewhat reduced by the introduction of constraints and restraints.

Taking these parameters and the experimental data the general least squares refinements for the minimized function can be written as:

$$S = \sum_{i}^{n} [y_i(obs) - y_i(calc)(P_1 ... P_m)]^2$$

In this case $P_1 ... P_m$ represent the parameters, for which there are m in total. The least squares residual is considered to be at a minimum when the partial derivatives with respect to each of the parameters, is zero. However the majority of parameters within the crystallographic model are non-linear and thus cannot be solved directly; as such an iterative approach is used in the solution.

The issue of non-linear functions is solved by using the Taylor expansions. This is utilised to calculate the difference between the two non-linear function, $y_i(calc)$ and $y_i(obs)$. Using this method terms of magnitude greater than $n > 1$ are ignored, since it

is considered that the model of the crystal structure is close to that of the real system. In this manor it becomes apparent that if the structure observed in the experiment is not a close match for the model, this means of solving the non-linear functions will fail to reach a true global minimum.

Parameters in the Rietveld Method:

The data collected in a powder diffraction experiment is strongly affected by the nature of both the diffractometer and the sample itself. It is for this reason that, in Rietveld refinement, many parameters that correspond to instrumental and sample consideration must be utilised, such that suitable global minima are achieved, and, ultimately, a good refinement. The parameters used to denote each of the experimental factors that affect the final outcome of the refinement can be of instrumental or structural origin. For some parameters, a combination of both denominations is apparent, as is the case for peak shape. Ultimately, the parameters associated with the structure are those with which experiment is concerned and aims to elucidate. The overriding requirement with the method is however, that all associated parameters are well modelled and refined, such that all factors altering the diffraction pattern are fully considered. In this way the best and most meaning full refinement of data is achieved.

As previously mentioned the parameters refined in the Rietveld refinement are essential of two overall groups. The summarised as a function of the origin or their contribution thus:

Instrumental:

- $2\theta_{zero}$ - Instrumental zero error
- A,B,C,D,E,F - Unit cell metric tensor
- U,V,W - Peak width parameters
- P, η, etc.- Peak shape parameters
- G - Preferred orientation parameter

Structural:

- c - Overall scale factor
- x_n,y_n,z_n - Fractional atomic coordinates

- B_n - Isotropic temperature factor
- β_{ij} - Anisotropic temperature factor
- N_n - Site occupation factor

When considering this specific ordering of parameters, it is of note that the parameters of instrumental origin most typically affect peak position and shape. Parameters for which the origin is structural are more typically related to reflection intensity and thus are related to the structure factors.

The background is one of the most vital parameters to address in any refinement of diffraction data. The background is generally approached using two methods; the first is linear interpolation between points of the background in the diffraction pattern. The main feature of this method is that the background will follow a straight line between each point of the dataset but only for area in which no peaks associated with the phase in question reside. The second approach is to use a mathematical function to model the background, the most popular being the *n*-order polynomial function. In such cases refinement of the background may be achieved if the polynomial describes well the background in the experiment. However, for many experiments the background will vary across the data set with 2θ and thus a radial distribution function is used.

Peak shape is one of the overriding and fundamental issues associated with refinement of diffraction data. Correct modelling of peak shape is pivotal to achieving a good refinement. For this purpose a number of peak shape functions are available for modelling peaks shape in various different experimental environments. As a result of different diffraction techniques, data collected may exhibit characteristic peak shapes in association with that technique. For the original neutron work of Rietveld the Gaussian shape was most apparent; in modern laboratory diffraction settings, peaks more often exhibit asymmetry and more close fit the Lorentzian peak shape functions. As a result of this most Rietveld packages offer an array of peak shape functions for the purposes of fitting peak shapes from many experimental methods these include; Gaussian, Lorentzian, Pearson VII and combination functions such a Voigt and pseudo Voigt.

The issue of fitting peak shape is further complicated by the fact that the peak width is known to vary as a function of 2θ across the data set and as such is modelled using the formula[16]:

$$H^2 = U\tan^2\theta + V\tan\theta + W$$

Where:

- H - The peak width at half the maximum intensity (FWHM).
- U, V, W - refineable peak width parameters.

Peak width may also be strongly affected by the nature of the sample. Effects such as sample strain, crystal size and others may be calculated and factored into the refinement to more closely model the peak shape.

The lattice parameters are fundamental in determining peak position also and as such are always refined. In the event that the observed and calculated peak positions are not a good match, it is probably that either the zero offset, $2\theta_{zero}$, or the lattice parameters are incorrect. Such errors are often corrected by the use of an internal standard which aides in accurate determination of the zero offset.

Of fundamental importance and influence in the Rietveld method, are the atomic coordinates, x, y, z, and provide powerful insight into the chemical system and nature of the chemical geometry. The atomic coordinates are taken from a model or determined using software and utilised as a starting point from which to refine; the complex nature of the atomic coordinate positions make use of a starting model vital. In x-ray experiments, the positions of heavy elements are refined first as they exhibit the largest effects on the system as a result of having larger form factors.

The last parameters to be refined are normally those whose nature is mostly non-linear, due to the propensity of the refinement to have problems dealing with these functions. Such parameters include both the thermal parameters and the site occupancies which both have contributions to the structure factor equations.

Preferred orientation is often a considerable issue with x-ray powder diffraction experiments. The solution to the issue is complex and can be approached in both experimental terms and in sample preparation and rotation of the sample to create an

averaged sampling of crystallite position; it may also be corrected and minimized within the Rietveld method. The problem is mostly commonly countered by consideration of the angle between the relevant face of the crystallite and the reciprocal of the *hkl* th *d* spacing.

Quality of refinement and the R-Factor, the Reliability factor:

The most practically useful means of judging the quality of fit, while completing a refinement, is visually inspecting the difference plot. The difference plot demonstrates the difference between the observed system and the calculation based on the model used. Issues associated with impurity phases and peak shape and position fitting issues are readily identified visually by this method, and so it provide an excellent means of following progress while the refinement is progressed.

Though the validity of a refinement and its quality of fit is well followed visually - by inspection of the difference plot associated with the difference between observed and calculated data – it is often helpful to provide a numerical value to denote the degree of convergence reached with in the refinement. This is achieved by calculation of *R*-factors for the system as a statistical tool to evaluate the match between the observed data and the calculations, based on the initial model.

Though there are several means of calculating the *R*-factor, many of which are quoted with the field of crystallography, the most physically meaningful of those quoted however, is the weighted profile *R*-factor, R_{wp}. It is physically most significant in that its numerator is the Rietveld residual that is minimized in the process of refinement. The weighted profile *R*-factor is given by the formula:

$$R_{wp} = \sqrt{\frac{\sum_i w_i [y_i(obs) - y_i(calc)]^2}{\sum_i w_i [y_i(obs)]^2}}$$

Though physically the most meaningful, this value is not without its limitations. The most significant limitation of this method is the propensity of the method to produce artificially low values when the back ground is included in the refinement, since it is considerably easier to refine a high flat background than to fully resolve Bragg peaks. In addition to the weighted profile R-factor, the goodness of fit, χ^2, is also commonly

used as an indicator of the quality of the refinement. It is a statistical value that relates to the weighted profile R-factor and the expected R-factor (which is a measure of the quality of data collection). A good refinement is one for which the goodness of fit approaches or is close to 1; it is common for values below 5 to be reached in good refinements. χ^2, is however, sensitive to the number of parameters being refined and is therefore subject to artificial lowering in some cases where large numbers of parameters are refined.

2.7: The Lebail Method:

Though the Rietveld method is a powerful tool for the analysis of x-ray powder diffraction data, is has a number of limitations that are considerably difficult to circumvent and it is for this reason that the Lebail method is such a good and routinely used compliment to the Rietveld technique. The two major limitations of the Rietveld technique are[10]; 1) its inability to be able to solve structures outside the presence of an initial model; 2) its inability to deal with closely related phases for which, overlapping exhibit close correlation of position and thus intensity. These problems are considerable for cases such as discerning impurity phases that are either unknown or closely correlated with the phase of interest. In addition, dual and multiphase refinements often exhibit reflection profiles that demonstrate considerable overlap between the two phases; this makes structural solution and refinement a considerably more complex problem[11].

Though other methods of solving such problems as encountered with the Rietveld method have been developed (Pawley for example[10]), the Lebail methodology enjoys considerable focus due to its close compatibility with the code of the Rietveld method. It is for this reasons that the Lebail method is now included in the vast majority of Rietveld structural refinement packages.

The Lebail method works on the assumption that no initial model is available and the structure under study is currently unknown. As such the method begins by considering that there is no calculated structure factor and that all integrated intensities are initially equal. As a consequence of the intensities no longer being treated as least squares parameters, matrices are relatively simple versus similar methods (e.g. Pawley) and thus refinement cycles are rapid. On completion of one refinement iteration, isolated peaks are assigned an observed intensity equal to the

area under the peak; overlapping peaks require more refinement cycles. The technique of the Lebail method utilises partitioning of the observed profile points, *y(obs)*, results in a set of observed intensity values.

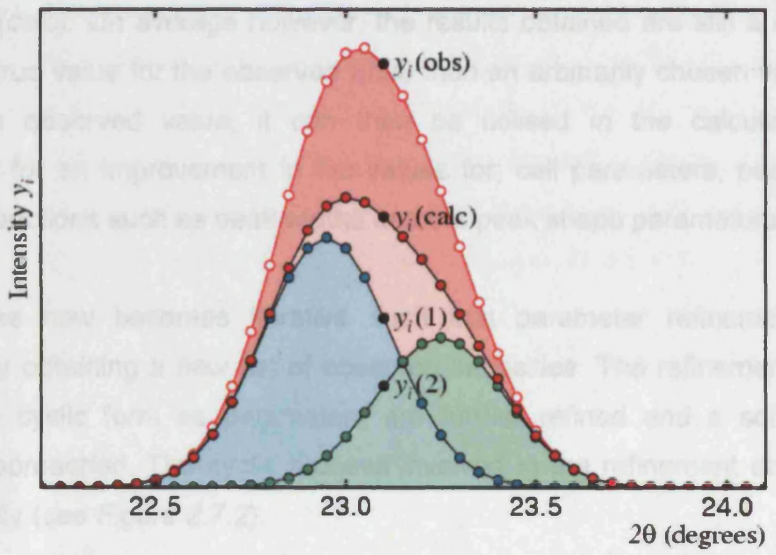

Figure 2.7.1: Relationship between the observed profile point, y(obs), and the calculated profile point, y(calc), and its components, $y_i(1)$ and $y_i(2)$[10].

Figure 2.7.1 demonstrates the relationships between the observed profile and the calculated profile. In addition the component parts the calculated profile points are shown with respect to it. The observed total intensity of peak 1 (shown in blue) is given by the expression:

$$I_{obs}(1) = \sum_i \frac{y_i(obs)y_i(1)}{y_i(calc)}$$

Similarly, the total intensity for peak 2 (shown in green) is given in:

$$I_{obs}(2) = \sum_i \frac{y_i(obs)y_i(2)}{y_i(calc)}$$

For both cases *y(calc)* is give by:

$$y(calc) = y_i(1) + y_i(2)$$

The summation is taken over all profile point, *i*, which contribute to the peak intensity. This method is the principle means of dealing with overlapping peaks and is capable

of doing so with any number of peaks that exhibit this problem; the method is often referred to profile intensity partitioning.

The result is that the observed intensity values are biased as a result of the starting values for *I(calc)*. On average however, the results obtained are still a considerably nearer the true value for the observed *I(hkl)* than an arbitrarily chosen value. Having attained an observed value, it can then be utilised in the calculation and is responsible for an improvement in the values for; cell parameters, peak positions, resolution functions such as peak widths and the peak shape parameters.

The process now becomes iterative such that parameter refinements can be improved by obtaining a new set of observed intensities. The refinement cycle thus takes on a cyclic form as parameters are further refined and a solution to the structure approached. The cyclic process involved in the refinement can be shown schematically (*see Figure 2.7.2*).

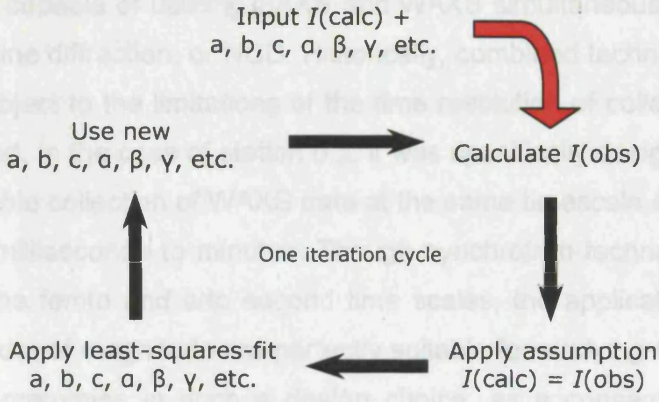

Figure 2.7.2: The cyclic process associated with the Lebail method of analysing diffraction data[10].

The convergence of the refinement is slow, as a result of the iterative nature of the process. Additionally, the avoidance of least squares determination of the value for *I(obs)* is also a factor that play a part in slowing the convergence. In such circumstances many cycles are required for convergence and often fall in the time scale of 10-100s seconds. During each cycle, *I(calc)* is set to equal *I(obs)* such that the intensity *R*-Factor will approach zero. In the process of refining data by the Lebail method, where correct determination of the background is achieved, it is not possible for the Lebail method to produce negative intensities.

2.8: Synchrotron Radiation Techniques and Station 6.2 at the SRS Daresbury:

Overview:

Station 6.2 at the SRS Daresbury represents the most recently commissioned beamline to have been introduced to the facility. It was developed in the late 90's based around the concept of using multipole wigglers to condition the electron beam to produce "hard" x-rays. The station uses state of the art technology for the purposes of studying materials processing and its associated effects. The station was designed to provide a number of complementary techniques that would be available with reconfigurations of the station; the techniques associated are:

- Time resolved, medium resolution diffraction (XRD) or wide-angle scattering (WAXS).
- Small-angle scattering (SAXS).

The station is capable of utilising SAXS and WAXS simultaneously for the purposes of non-crystalline diffraction, or NCD. Historically, combined techniques of this nature have been subject to the limitations of the time resolution of collection of the WAXS apparatus used. In the case of station 6.2, it was specifically designed to counter this issue and enable collection of WAXS data at the same timescale as that for SAXS, in the range of milliseconds to minutes. Though synchrotron technology is capable of operation in the femto and atto second time scales, the application of times in the millisecond order of magnitude are perfectly suitable for studying reaction in the solid state. The compromise in such a design choice, as a consequence of fast time resolutions, is seen in data quality; it is thus a considerable feat for a technique to present such time resolutions for combined techniques but retain data that is susceptible to treatment using the Rietveld method[17].

The physical make up of station 6.2 is composed of the commonly seen two hutch set-up, both of which are lead lined. The user facility is comprised of an inner, optics hutch which is off limits to facility users and an outer hutch where the diffractometer a situated and is designed for user experiments. The experimental hutch is home to the equipment and detectors that constitute the varying techniques available at the station; a θ=2θ powder diffractometer, EXAFS table, SAXS camera and environmental chambers. The WAXS and associated detector are a state-of-the-art technology, developed around the multi-wire, micro-gap technology. The

experiments detailed within this study exclusively used the WAXS methodology to study the changes within the clathrate systems.

As has been stated before, station 6.2 represents technology and was specifically design by Cernik *et al*[17], to push the bounds of experimental possibility within the materials fields. To make this goal a reality a new detector, the RAPID 2, was developed to provide time resolved, medium resolution WAXS collection performance[18], [19]. The detector is capable of a time resolution such that data may be collected over 60° 2θ range for 1 second and will provide refineable patterns, as was shown for silicon 640b in the work of Cernik *et al*. The quality of data collected at such short timescales is suggested to be refineable to a χ^2 of 2.4, with peaks refined most successfully using the Pearson VII function. Consistency across the range was assessed by comparing the peak halfwidths across the data range, and was found to be constant across a 2θ range from 0.06° to 120°, suggesting the instrument had successfully matched its originally stated resolution function. The overall quoted specification of station 6.2 is shown below[20].

- **X-ray Delivery:** 10-pole wiggler installed in the straight section of beamline 6, at the SRS Daresbury.
- **Focussing optics:** 2 plane Si/Rh mirrors for vertical focussing. A 2-crystal, double-bounce, saggitally-bent Si (111) monochromator for energy selection and horizontal focussing.
- **Collimation:** 5 pairs of horizontal and vertical slits, the final pair being just before the sample position.
- **Bandpass (monochromatisation):** $\Delta E/E \sim 10^{-4}$. Photon flux ~ e^{12} photons/s/0.01% bandpass at 200mA stored beam current. Photon flux is energy-dependent and is peaked at 8-9 keV.
- **Beamsize at focus:** ~1.3 x 0.3 mm^2 (H x V).
- **Energy range:** 5 – 18 keV.
- **X-ray detection system:** 2 1-dimensional WAXS and SAXS detectors based on RAPID2 technology (gas microgap, multi-wire). Efficiency is energy-dependent and is peaked at 8-9 keV. The WAXS detector has an acceptance angle of 60° 2θ and a resolution of ~0.06°. Minimum SAXS camera tube length is 1.3 m, maximum is 4.0 m with a maximum resolution of ~800 Å at λ = 1.40 Å.

- **Experimental configurations:** Medium-high resolution powder diffraction based on a 2-circle diffractometer OR simultaneous SAXS and WAXS.

Station 6.2 enjoys a particularly high flux as a result of the utilisation of a multipole wiggler array. This is a particularly good demonstration of the relevance of the optics arrays at synchrotron beamlines and the effects of variation. A detailed discussion of the optics array at station 6.2 is beyond the scope of this study, however certain aspects are worthy of note with respect to the type of experiments completed in this study.

The beamline is composed of a complex array of mirrors, slits, beryllium windows and a sagittal monochromator (*See Figure 2.8.1*).

Component	Distance (m)
1st Be window	13.215
Slits 1	13.480
Mirror 1	14.425
Monochromator (1st crystal)	15.980
Slits 2	16.910
Mirror 2	17.965
Slits 3	19.000
Slits 4	20.460
2nd Be window	20.665
Sample position (min)	21.000

Figure 2.8.1: Beamline component makeup of station 6.2 and the position from the incident source[18].

The optics array is position with considerable accuracy at pre-determined positions from the source that sits in the centre of the wiggler magnet array. The focusing optics are tasked with performing a number of vital operations on the beam, that condition it in terms of the desired user configuration. The main roles of the focusing optics are; 1) The collection of all available photons into the beamline, 2) Selection of wavelength, 3) Collimation of the beam to prepare it for delivery to the user in the experimental hutch. It is by these means that the delivered beam may be tuned as required for specific user application.

Focusing of the beam is achieved using multiple slit arrangements along the beamline (*see Figure 2.8.2*). Water-cooled, motor driven slits and florescence screens may be driven into the beam remotely by computer with high accuracy, and thus fine control of the beam may be achieved from the control hutch.

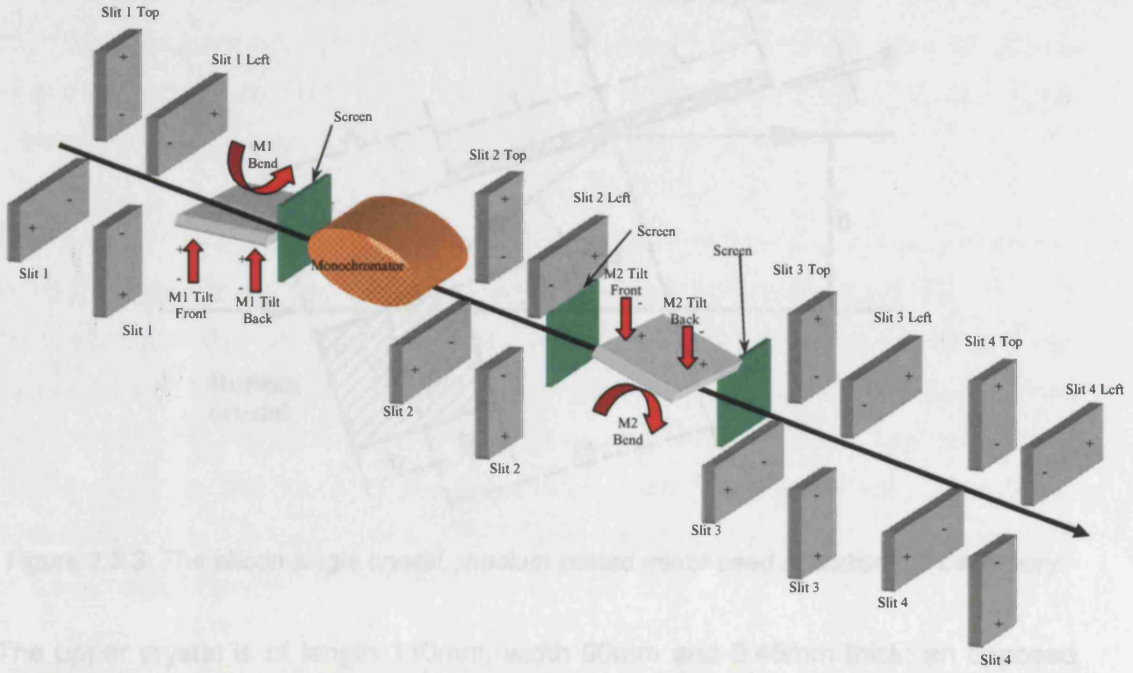

Figure 2.8.2: The optics configuration of Station 6.2 at the SRS Daresbury.

The array utilises two identical silicon single crystal mirrors with a 50nm rhodium coating, the result of which is a critical energy, E_c, as quoted previously, of ~20keV. Precise tilting and angling of these mirrors ensures delivery of the full photon beam from the monochromator.

The sagittal monochromator utilises double bounce geometry in the use of two silicon single crystals, specifically machined such that the (111) plane is normal to the reflection surface (*see Figure 2.8.3*). It is by rotation of the Bragg angle, θ_B, that the desired wavelength is selected for experimental purposes; at 1.4λ and 8.8keV the photon flux and detector efficiencies are found to be at a maximum[20] and thus this is the commonly used configuration. The lower crystal (*see Figure 2.8.3*) is water cooled to 288.15K and has dimensions of 45mm (b+b) in length and is 100mm wide at the surface facing the incident beam. The wide face is required to receive the full flux and therefore heat load of the incident white beam, such that a monochromatic beam may be produced.

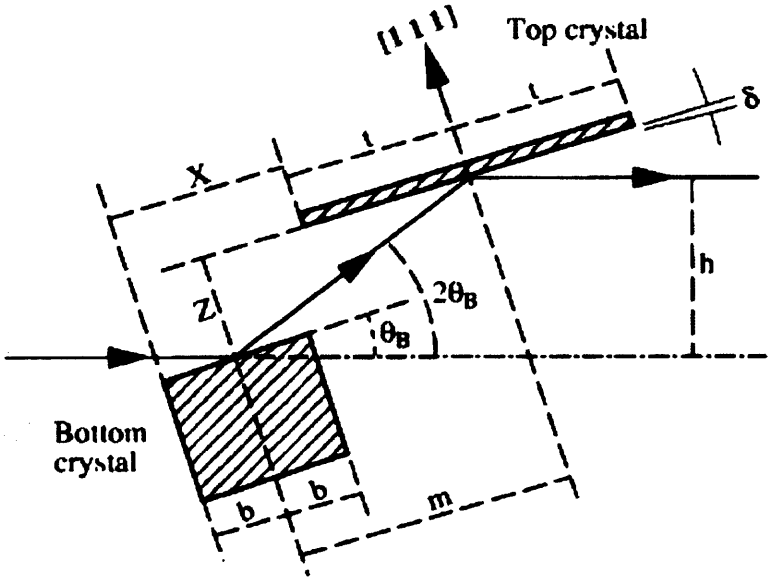

Figure 2.8.3: The silicon single crystal, rhodium coated mirror used at station 6.2 Daresbury.

The upper crystal is of length 110mm, width 90mm and 0.45mm thick; an opposed long face is required for the second crystal such that the wide horizontal fan may be received and then bent sagittally, such that the beam may be horizontally focused.

Detector:

The feasibility of this study was entirely a product of the availability of data quality that could be collected within the order of magnitude of seconds, but still retaining suitable resolution for Rietveld refinement. The study of the discrete reordering of crystal structures in the solid state, is considerably less illuminating of mechanism, in instances where atomic coordinates and occupancy cannot be found. Thus the RAPID2 detector technology was fundamental to the success of the study.

The RAPID 2 detector is curved and specifically designed for the purpose of use in simultaneous SAXS/WAXS experiments (*see Figure 2.8.4*). The development of the RAPID2 detector technology was achieved within a curved environment and utilises the wire micro-gap detector methodology of the RAPID1 area detector system[21]. The spatial resolution requirements associated with powder diffraction experiments require considerable resolution in the operation of the detector. This spatial resolution requirement results in the use of 4096 interpolated channels for such powder diffraction experiments.

The detector is comprised of 512 wires with an amplifier for every 4 wires. The associated signal is interpolated using an interpolation algorithm, such that 4096 intensity points are collected over the 60° 2θ range[19], [22]. The utilisation of such a wire area within the detector is the reason it is possible to rapidly collect time-resolved data while retaining relatively high resolution data.

The detector is controlled using a custom written software package called the Generic Data Acquisition software, or GDA. The software allows for x, y, z manipulation of the detector that is mounted on an electrically driven table and can be moved with an accuracy of millimetres. In addition, the detector circle position can be controlled by the same means but with greater accuracy. The GDA software is also used to control much of the apparatus in the optics hutch, such that beam optimisation may be undertaken during experiments with minimal disruption to the beamline infrastructure.

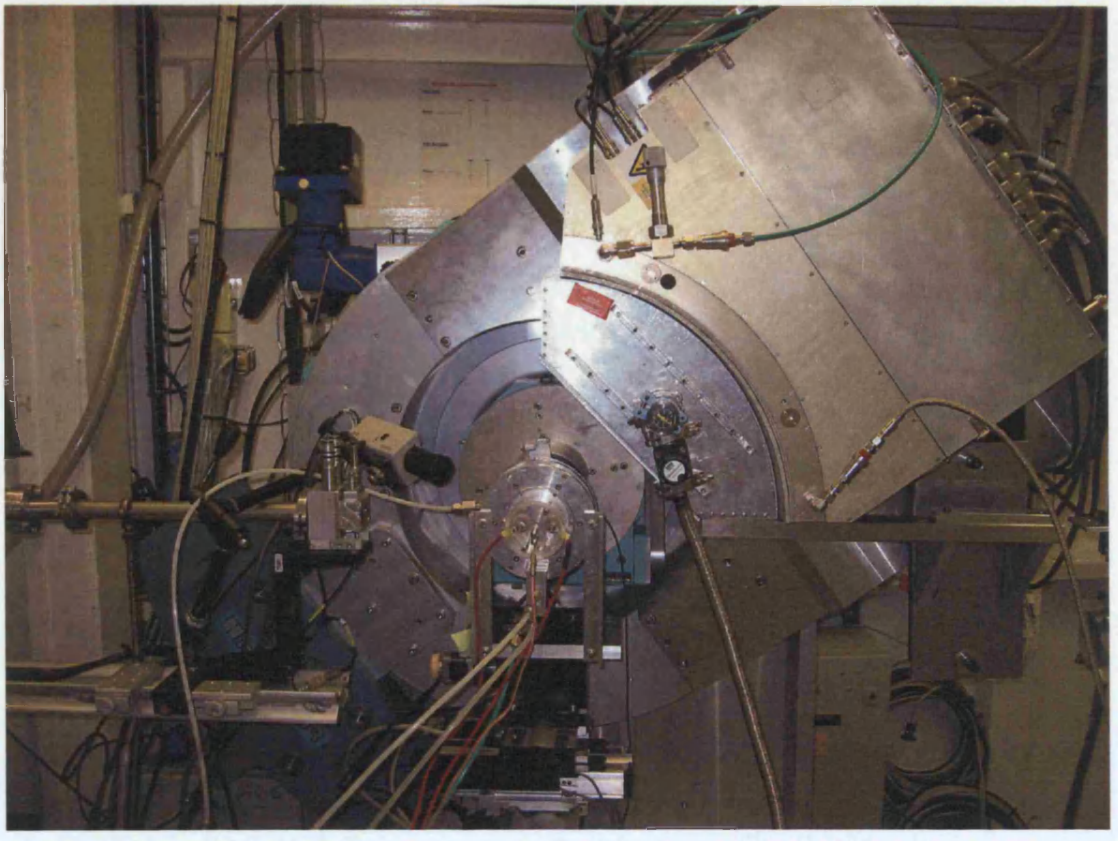

Figure 2.8.4: The RAPID 2 detector in position in the user hutch at the SRS Daresbury.

User Functionality:

The user functionality of the station is enhanced by considerably versatile sample working area. The sample region, between the detector and the beam is essentially entirely customizable with respect to the experiments being undertaken. For the purposes of this study, an x, y, z stage was utilised for mounting a custom designed capillary furnace. The x, y, z stage is again controlled using the GDA software suite and is highly accurate in motion around the sample, allowing complete sample environment control while the hutch is interlocked. This versatility of sample set up and experimental apparatus design allows for incredibly complex experiments to be completed at the station.

The station also offers several furnace set-ups and equipment assemblies to meet experimental needs. For the chosen assembly for these studies, the main limitation of the station was the beam penetration characteristics with respect to the sample and sample holder. However, the diverse nature of the experimental environment caters very satisfactorily for experiments of this kind and complexity.

2.9: References

1. Cros, C., M. Pouchard, and P. Hagenmuller, *Sur deux nouvelles phases du système silicium-sodium.* C.R. Acad. Sc, 1965. **260**.
2. Bryan, J., D and G. Stucky, D, Chem. Mater., 2001. **13**.
3. Hou, D., et al., *Structural, transport and thermal properties of the single-crystalline type-VIII clathrate $Ba_8Ga_{16}Sn_{30}$.* Phys. Rev. B, 2005. **71**.
4. Bryan, J., D, et al., Phys. Rev. B, 1999. **60**.
5. Christensen, M., et al., *Crystal and magnetic structure of $Eu_4Ga_8Ge_{16}$.* Phys. Rev. B, 2003. **68**.
6. Guloy, A., M, et al., *A guest-free germanium clathrate.* Nature Letters, 2006. **204**.
7. Ramachandran, G., et al., J. Solid State Chem, 1999. **145**.
8. Ramachandran, G., *PhD Thesis.* Arizona State University, 2003.
9. Gryko, J., P. Hutchins, T, and P. McMillan, F, Unpublished Results, 2006.
10. Barnes, P., et al., *Powder Diffraction on the web; Industrial Materials group.* 2004.
11. Evans, J.S. and I.R. Evans, *Beyond Classical Applications of Powder Diffraction.* Royal Society of Chemistry: Tutorial Review, 2004. **33**: p. 539-547.
12. Walton, R., I and D. O'Hare, *Watching solids crystallise using in situ powder diffraction.* Chem. Commun, 2000. **2000**: p. 2283-2291.
13. Rietveld, H., M, Acta Crystallographica, 1967. **22**.
14. Rietveld, H., M, Journal of Applied Crystallography, 1969. **2**.
15. Young, R., A, *The Rietveld Method.* 1993: Oxford Press.
16. Caglioti, G., A. Paoletti, and F. Ricci, P, Nuclear instruments, 1958. **2**: p. 223-228.
17. Cernk, R., J, et al., *The New Materials Processing Beamline at the SRS Daresbury, MPW6.2.* Journal of Synchrotron Radiation, 2004. **11**: p. 163-170.
18. Helsby, W., et al., *The RAPID2 Interpolating System.* Nuclear Instruments & Methods in Physics Research A, 2003. **510**: p. 138-144.
19. Berry, A., et al., Nuclear Instruments & Methods in Physics Research A, 2003. **513**: p. 260-263.
20. website, S.b.u. *Station 6.2.* 2007 [cited; Available from: http://www.srs.ac.uk/srs/stations/station6.2.htm.

21. Tang, C., C, et al., *X-ray Beam Characteristics on MPW6.2 at the SRS.* Nuclear Instruments & Methods in Physics Research B, 2004. **222**: p. 659-666.

22. Lewis, R., A, et al., *The RAPID Detector System – First User Data.* Nuclear Instruments & Methods in Physics Research A, 2000. **454**: p. 165-172.

Chapter 3

Negative thermal expansion of guest-free type II silicon clathrate

3.1: Negative Thermal Expansion in the Clathrates

In the year 2000, Gryko *et al*[1], reported the synthesis of a guest-free silicon clathrate II structure, that represents a new allotrope of silicon. Given the nature of the material with respect to silicon, its properties were of great interest in comparison to those of *d*-Si. Around the time of the first synthesis of the material, Dong *et al*[2], predicted that the guest-free clathrate II would exhibit a region of negative thermal expansion in the range 40-140 K, comparable to that exhibited by *d*-Si. This prediction suggested the guest-free clathrate would be an interesting candidate for study using low temperature, laboratory x-ray diffraction studies, to ascertain if negative thermal expansion did, in fact, occur in this region.

3.2: Background: Extended Deintercalation and Guest-Free Clathrate II

As far back as the earliest clathrate experiments by Klemm[3], [4], it was observed that on formation of clathrates (at the time the structure was unknown) from metalloids or specifically NaSi or KSi, the system underwent weight loss, observed by thermogravimetric analysis methods. The affect of this mass loss on the structure or stoichiometry was not known at the time of Klemm's work but was the first observation of the systems predilection to loose the metallic species to form the clathrate. The consequences of this on thermal degradation were not discussed or studied, until Cros *et al*[5] demonstrated the nature of clathrate II and its propensity to de-intercalate to form clathrates of lower guest stoichiometry, with vacant cages centres.

Cros's work[5] demonstrated that type II clathrates of the form Na_XSi_{136} (X = 1 or 2) were possible by standard synthetic means. This result and the implication for the potential applications for the material were to lead to the obvious question; is it possible to synthesise guest-free clathrates and if so, what would its properties be? If synthetically possible, this guest-free material would be a new allotrope of silicon and thus exhibit silicon-like properties but potentially, modified by the pronounced structural differences.

Efforts began in the field to synthesize the guest-free material, and at the same time simulation work was undertaken to see how the material properties would vary versus *d*-Si. In structural terms the clathrate differs in both subtle and drastic

proportions; *d*-Si has the 5 atom square based pyramid as its main structural unit, the clathrate contains the 4 atom tetrahedra. *d*-Si and clathrate II share the same cubic space group, $Fd\bar{3}m$, yet the lattice constant for *d*-Si is around 5.29 Å at room temperature, where the clathrate shows around 14.6 Å at room temperature depending on the stoichiometry of the guest species. The clathrate system is composed of complex multi-atom polyhedra built from tetrahedra which are arranged such that hexagonal faces are shared, leading to a diamond-like array within the structure. The overall picture is one of a material with some similarities to *d*-Si but overall a relatively expanded structure with a considerable increase in structural complexity. A comparison of the electronic properties is not simple due to the nature of the clathrate materials; it is possible to consider particular stoichiometries versus *d*-Si. In general the higher guest atom stoichiometry clathrates – where the guest is an alkali metal – tend to exhibit comparable stability but more desirable band gaps and electronic properties than *d*-Si. This is the main reason for the interest in the solid state clathrate materials and their diverse compositions.

One of the less noted properties of *d*-Si is the negative thermal expansion it undergoes at very low temperatures[6]. In 1958 at Bell laboratories, silicon crystals were prepared by 3 differing methods and subject to cooling under liquid helium. The crystals exhibited negative thermal expansion (or zero thermal expansion if considered in terms of the experimental error of the diffractometer) at 119.5 K; it was noted that the means of preparation of the crystals induced no change in the observed effect. In the ensuing years the problem was studied theoretically and the origin of the effect was discussed in terms of the ratio of Grüneisen parameters and effects associated with the phonon dispersion[2]; detailed discussions of these effects and the associated theory are beyond the scope of this study.

The realisation that total, or near total, deintercalation was possible with the type II clathrate structures, resulted in much focus on theoretical studies of the properties of the guest free materials. In the late 1990's Dong *et al*[2], undertook theoretical studies on the properties of the guest free silicon clathrate II material, and predicted a negative thermal expansion in the region 40-140 K (see *Figure: 3.2.1*).

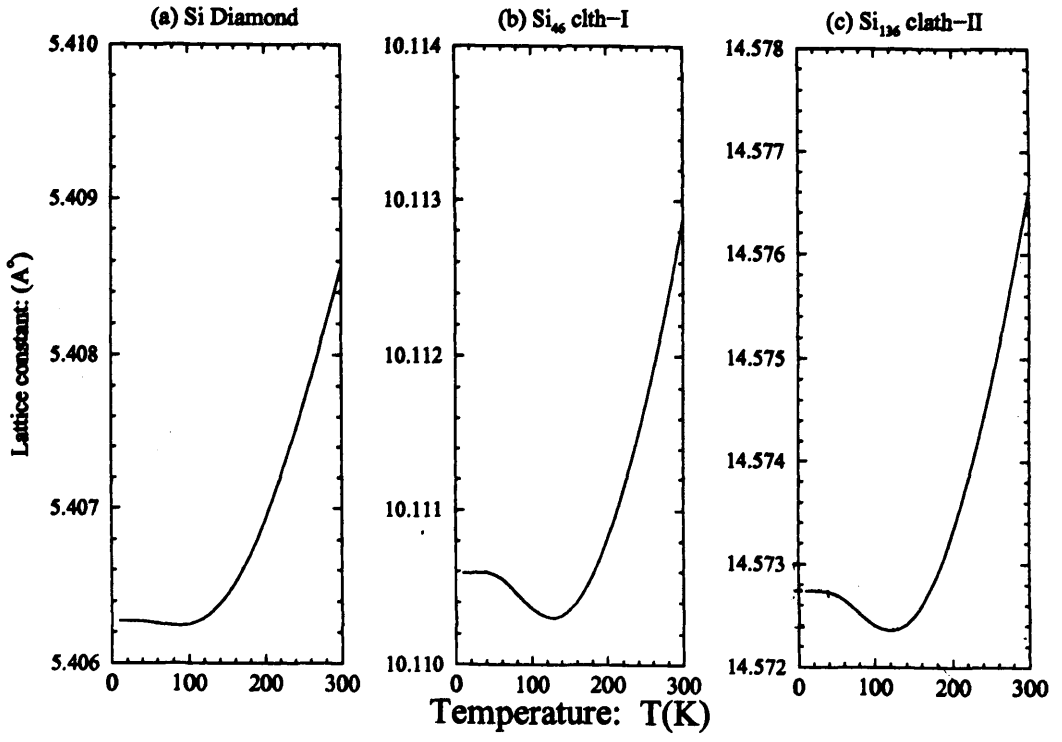

Figure 3.2.1: Graph shows theoretically calculated lattice constant for the region 0-300 K for (a) d-Si, (b) Si_{46} Clathrates, (c) Si_{136} Clathrates[7].

3.3: Synthesis of Guest Free Type II Silicon Clathrates:

During the 1990's Ramachandran *et al*[8] did a great deal of work based on that of Cros in the 1970's[5], on the properties and synthesis by thermal degradation of $Na_{24-x}Si_{136}$. As discuss earlier, it was found to be possible to deintercalate the type II system to produce a Na stoichiometry of 1 or 2, by continued heating under high vacuum. This posed the obvious question, is it possible to reach Na = 0 by means of thermal degradation, or direct chemical reaction, to remove the last stoichiometric percent of sodium.

In 2000 Gryko *et al*[1] gave the first reports of the guest free type II material, essentially a new allotrope of silicon. The material was claimed to possess less than 600 ppm sodium within the structure and was prepared by thermal degradation methods. The sample was prepared by taking a suitable aliquot of NaSi and subjecting it to vacuum (10^{-5} bar) and heating in the temperature range 350-375°C to form Na_XSi_{136} with X > 10. The product was then subjected repeated cycles of long heating under vacuum followed by density separation of phases, such that sodium

content was reduced with each successive cycle. When the sample reached $X < 4$ the product was washed in concentrated HCl and dried in vacuo then degassed at 430°C under vacuum (10^{-5} Torr) for several days. Continued applications of this process resulted in decreasing sodium content in the product fraction. The final fraction was isolated by centrifugation in a dibromomethane-methanol solution. Sodium content was estimated using chemical elemental analysis.

3.4: Laboratory X-Ray Studies of Negative Thermal Expansion in Type II Clathrates:

To study the thermal expansion properties of this material at very low temperatures i.e. down to 5K, it was necessary to use a liquid helium cryostat in conjunction with a laboratory diffractometer (see Chapter 2).

For all such powder diffraction experiments, a Stoe StadiP powder diffractometer (Small, moving, linear PSD at 6° 2θ resolution, nominal 4.5° 2θ) using transmission geometry was employed. The x-ray source was a copper $K\alpha_1$ radiation source running at 30mA and 40KeV, with a germanium pre-sample monochromator. A liquid helium cryostat was used based on an ILL design orange liquid helium cryostat, modified as a result of small capillary size and relatively weak laboratory X-ray source, with Mylar windows and anti-scatter components. Borosilicate capillaries (0.3 mm) were used as sample holder. This choice of sample holder allows easy cooling under rotation; the rotation ability to rotate the sample improves counting statistics and reduces texture effects. The sample was ground using an agate pestle and mortar and then sieved using a 38 micron sieve.

The data were collected for three high angle peaks. High angle was chosen to reduce zero offset effects; three peaks were utilised to improve counting statistics as long, high resolution scans were possible due to the cubic unit cell. Such experiments would have been too time consuming over the full data range of 5-65 2θ, for high resolution data to be possible; the issue of collection time strongly affects the temperature stability as retention of liquid helium becomes harder over time, due to evaporation loss. The detector step size for data collection was 0.02° 2θ and the collect duration per cycle was 112.0 seconds. The data bin size was also 0.02° 2θ.

The data were collected from 5K to 295K at 5K intervals. The sample was left for 30 minutes to equilibrate at each temperature and data sets were collected for one hour

per temperature. For each temperature 2 or 3 collections was completed, this was undertaken by completing the full temperature scale transition for each collection cycle, as opposed to multiple collections during a single cryostat temperature cycle. Operations below 20 K were considerably more challenging in terms of equilibration and temperature retention during scans, due to photon heating through the Mylar window. This was to some extent combated by instigation of dark room like conditions in the reaction environment.

Lebail refinements were completed versus Rietveld as the aim of the experiment was to find unit cell variations as opposed to structural change. The data were analysed using Chekcell and Rietica for comparative refinements.

3.5: Results:

As discussed in section 3.4, three high angle peaks were selected for data collection in this study (see *Figure: 3.5.1*). This allows for collection of high resolution data with a small 2θ range PSD in a fashion that would not be possible, for time reasons and the effect of long collection times on temperature stability due to liquid helium evaporation, if using the full 2θ range. The peaks were selected from full 2θ range (see *Figure: 3.5.2*) and high angle chosen to counteract zero offset. The advantage of this choice was high resolution data with the loss of more detailed structural information presented by a full 2θ range. However, this does allow for excellent resolution data in terms of unit cell volume, which is required if we consider the size of the predicted effect i.e. in the 10^{-3} Å order of magnitude (*see Figure 3.2.1*).

On examination of the stacked high angle data (see *Figure: 3.5.2*) for the extreme of temperature in the experimental range, it can be seen that there is no visibly detectable change in the peak position, shape or width which is to be expected in terms of the predicted effect. This alone is worthy of note in such that it suggests that the clathrate posses a very low coefficient of thermal expansion. It has been shown in the literature[9] that this material possesses the lowest coefficient of thermal expansion for any known crystalline solid.

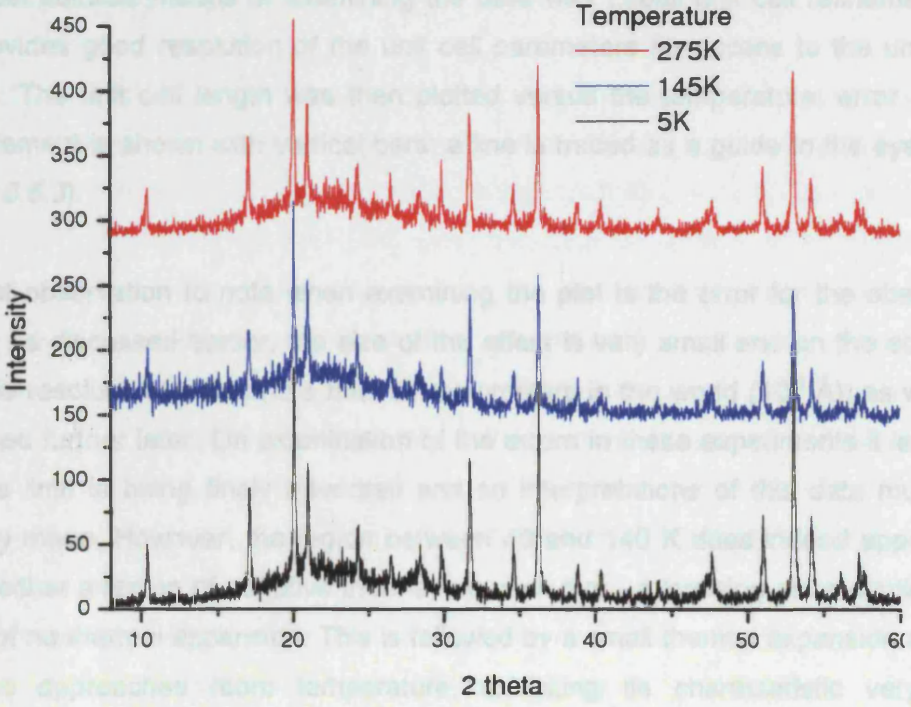

Figure 3.5.1: The lowest (black), median (blue) and highest (red) temperatures are shown for the full 2θ range of data collection. The three peaks between 50-55° 2θ were the peaks chosen for high resolution data collection.

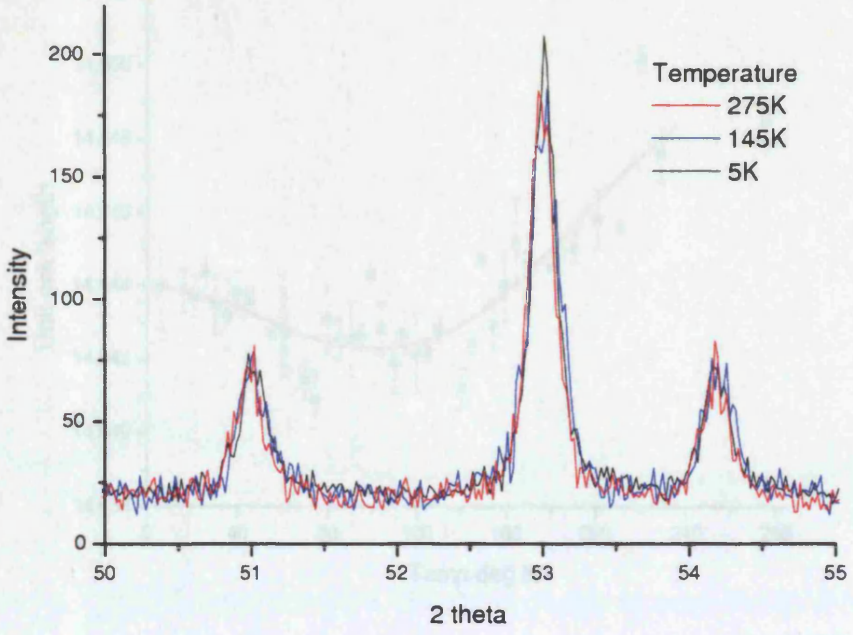

Figure 3.5.2: The three high angle peaks chosen for data collection at lower temperature. The peaks represent the [337], [066] and [715] reflections from respectively, starting from lowest to highest 2θ angles.

The most suitable means of examining the data was Lebail unit cell refinement as this provides good resolution of the unit cell parameters for access to the unit cell volume. The unit cell length was then plotted versus the temperature; error in the measurement is shown with vertical bars; a line is traced as a guide to the eye (*see Figure: 3.5.3*).

The first observation to note when examining the plot is the error for the observed values. As discussed earlier, the size of the effect is very small and on the edge of operable resolution for even the best diffractometers in the world (10^{-3} Á), as will be discussed further later. On examination of the errors in these experiments it is clear that this limit is being finely traversed and so interpretations of this data must be carefully made. However, the region between 40 and 140 K does indeed appear to exhibit either a region of negative thermal expansion or - exercising more caution - a region of no thermal expansion. This is followed by a small thermal expansion as the clathrate approaches room temperature, exhibiting its characteristic very low coefficient of thermal expansion of 3.4×10^{-6} K^{-1} for the region 145K to 295K, which shows good agreement with the literature. This trend was observed in each of the successive temperature cycles used during operation of the cryostat.

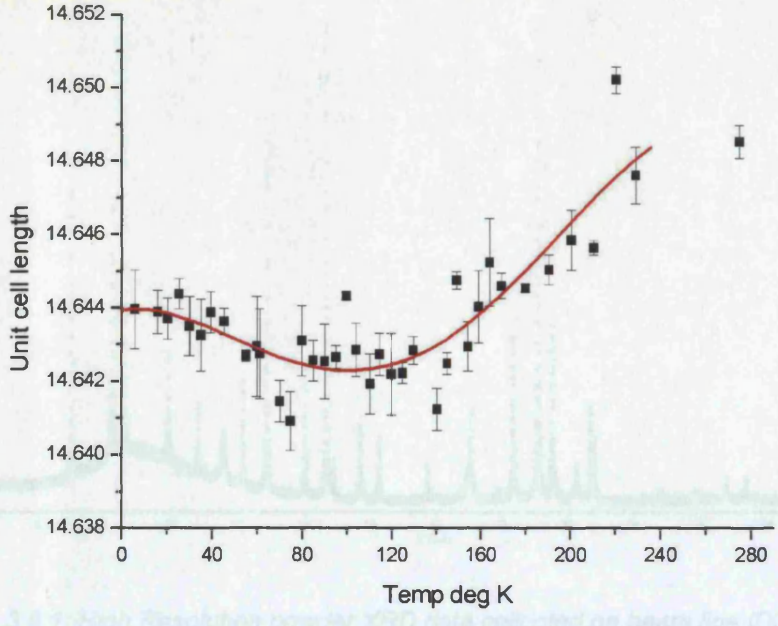

Figure 3.5.3: The Lebail refined data for the three high angle peaks showing and area of zero or no thermal expansion in the region 40-140 K. The line shown through the data is a guide to the eye.

3.6: Discussion and Conclusions:

Having completed the laboratory studies and seen what appeared to be a positive example of the predicted effect, it was decided that attempting the experiment on a high resolution diffractometer may provide more conclusive results. To this end the sample was taken to ID31 at the ESRF Grenoble, for a short series of experiments at room temperature. The main aim of this was to examine the affect sample broadening may have on the system and thus to ascertain if a low temperature experiment at ID31 would be beneficial. Several long scans were completed at ID31 (*see Figure: 3.6.1*) and each compared against a room temperature powder XRD pattern from the laboratory apparatus. On examination and comparison of the full width half maxima it was found that ID31 provided on average a 15% peak width reduction versus the laboratory equipment. This was deemed to be small enough to not pursue a synchrotron experiment, in that this provided clear evidence the large broadening effect for this system was predominantly due to the sample.

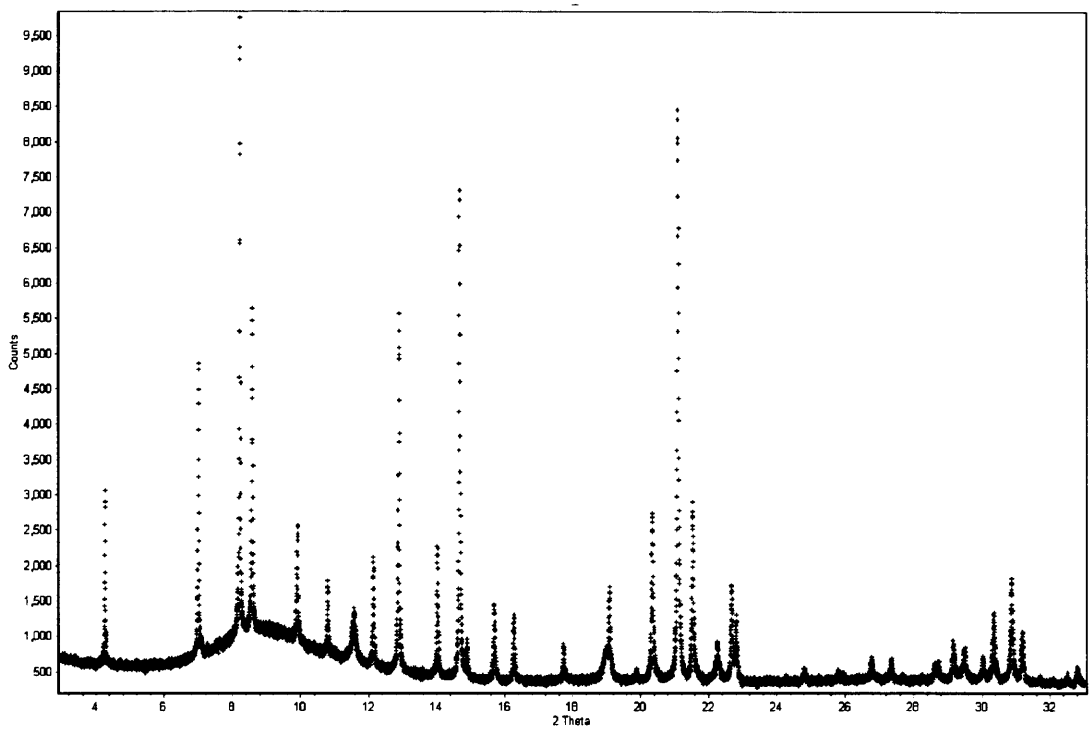

Figure 3.6.1: High Resolution powder XRD data collected on beam line ID31 for the $Na_{X=0}Si_{136}$ sample used in the low temperature experiment. The shows only a 15% full width half maxima reduction over the laboratory, denoting that considerable peak broadening is evident due to the sample.

The strong sample related peak broadening effect for this material makes further study by PXRD difficult. When considering the results of these experiments we cannot ignore the issue of error, size of effect and the limitations of the diffractometer. However, the good agreement with the theoretical work of Dong *et al*[2] gives weight to the suggestion that a negative thermal expansion was indeed exhibited in this experiment.

3.7: References

1. Gryko, J., et al., *Low-density framework form of crystalline silicon with a wide optical band gap.* Phys. Rev. B, 2000. **62**.
2. Tang, X., et al., Phys. Rev. B, 2006. **74**.
3. Schafer, R. and W. Klemm, *Wietere beitrage zur kenntnis der silicide und germanide der alkalimetalle.* Z. Anorg. Allg. Chem., 1961. **312**: p. 214-220.
4. Klemm, W., *Metalloids and their compounds with the alkali metals.* Proc. Chem. Soc. London, 1958: p. 329-341
5. Cros, C., *Phd Thesis No. 229.* University of Bordeaux, 1970.
6. Gibbons, D., F, *Thermal Expansion of some crystals with the diamond structure.* Phys. Rev, 1958. **112**.
7. Dong, J., J, *Unpublished Results.* Auburn State University, 2002.
8. Ramachandran, G., et al., J. Solid State Chem, 1999. **145**.
9. Nolas, G., S, et al., Appl. Phys. Lett, 2003. **82**.

Chapter 4

Experimental equipment design for *in situ* synthesis studies

4.1: Autoclave Design for Zintl Phase Preparation at High Temperature and Under Inert Atmosphere

Preparation of Zintl phase in a laboratory would appear to be trivial on consideration of the synthesis conditions. A typical synthesis of sodium silicide is done at 650 °C (923.15 K) for 18 to 24 hours. Given these relatively standard conditions one could be forgiven for thinking the synthesis to be free from complexity. The problems arise in the highly reactive nature of the Zintl phases and reagents used to create them (where alkali metals are used). Starting reagents such as the alkali metals result in the necessity to have an inert atmosphere environment, such as provided by a nitrogen or argon glove box. In addition, any reaction vessel chosen must be totally sealed from atmosphere to avoid contact of atmospheric H_2O and O_2 from reacting with the starting materials or Zintl phases produced.

To complete such a synthesis, a suitable container must be devised that can fulfil the following requirements:

1. Must be able to withstand temperatures of 600 °C and higher for sustained periods.
2. Must be robust enough to withstand pressure increases associated with fixed volume and temperature increase of this magnitude.
3. Must be of a material inert to reaction with volatilised alkali metals and other reactive materials.
4. Must be easily sealed from atmosphere in a glove box.
5. Must be made of easily accessible materials that can be machined in a conventional fashion.
6. Must be large enough to house suitable sized crucibles selected of metalos and materials inert (platinum, tantalum etc) to extremely volatile metals such as Rb and Cs.
7. Must be easy to work with in a glove box environment and as such contain no sharp edges, points or potential hazards, which may result in a breach of the environment by rupturing of the gloves.

Key Considerations:

Pressure:

On heating any sealed reaction vessel of fixed volume, there will be an associated pressure change as governed by:

$$Pv = nRT$$

Where:

P = Pressure in Pa or atmospheres
V = Volume in M^3
n = 1
R = Gas constant = $8.314JK^{-1}mol^{-1}$
T = Temperature in Kelvin

For which n = 1 and R is the gas constant and so

$$P_1V_1=T_1$$

V is a fixed in this case and so can be dismissed giving:

$$P_1/T_1 = P_2/T_2$$

Rearranging to get:

$$P_2 = T_2/T_1 \times P_1$$

Where:

P_1 = 101325 Pa = 1 atm
T_1 = 25 °C = 298.15 K
T_2 = 650 °C = 923.15 K

P2 = 313728 Pa = 3 atm

So the pressure consideration for a non calorimetric autoclave environment is trivial (Note: The environment during heating i.e. nitrogen/argon and volatilised sodium is far from an ideal gas yet for the purposes of this consideration, such assumptions are not wildly inaccurate). As a result, pressure release systems and thick-bodied autoclaves are not necessary in this case. A wall thickness of stainless steel can be within 0.5-1 cm thickness.

Temperature:

Target temperature is important in consideration of the material used in crafting the autoclave. There are various grades of steel available and a varying range of properties from chemically resistant to heat treated etc. For the synthesis of NaSi temperatures in excess of 650°C are needed and as such machineable grade steels should be sufficient, despite issues of carbide precipitation observed in this temperature range.

Chemical resistance:

Given the extreme reactivity of the alkali metals and the Zintl phases they produce, the material used to hold the reaction must be inert. If the reaction was done in steel there is a high chance of forming Iron silicide as a reaction impurity. As such the materials commonly used in such situations include tantalum, tungsten, niobium and platinum in crucible or foil form. These elements come with inherent problems in themselves; for tungsten the problem of machining a material of such inherent hardness, where for tantalum and platinum it is sheer the prohibitive cost that reduces the appeal. In terms of cost, ease of manipulation and reactivity considerations, niobium and tantalum stand out among these. The use of tantalum in surgical implants and many areas of the chemical and nuclear industries is widespread, due to its low toxicity and reactivity and so is a perfect choice for synthesis using very reactive alkali metals such as rubidium and caesium. Niobium is similar in nature to tantalum though some what less expensive.

Another solution is to take a metal that will easily coat with either oxide or react to create a Zintl phase layer on its surface. After an initial coating, such materials will

then behave as though inert and present no further impurity issues. Materials such as Nickel and chromium can be used to these ends. Though more chemically reactive and hence demonstrate reduced longevity in such uses, they are considerably less expensive to purchase as ready made crucibles of an appropriate size and shape.

Sealing using metals:

As a result of the use of air and moisture sensitive materials, it is necessary to use some method to seal the reaction chamber from atmospheric contact. Due to the temperature and pressure required, metal to metal seals must be achieved. The most efficient way to do this is choose a different metal, to the metal chosen for the main body of the autoclave and so utilise the difference in coefficient of thermal expansion for the two metals. It is also beneficial to use a metal with a high malleability such that on sealing the metal may deform and hence form a better seal.

Given these considerations copper is most commonly used to achieve a reliable seal. Copper is ideal in that it is malleable and has a coefficient of thermal expansion of 16.5 $10^{6}K^{-1}$ versus that of standard, machineable 303 steel of 0.297 $10^{6}K^{-1}$. The result is that it will not only deform to the shape of the reaction chamber on screwing the autoclave shut but also on heating, it will expand more than steel and hence guarantee that the seal will not be compromised.

Materials:

The issue of materials consideration is vital in the design of such a reaction environment. There are several suitable materials and within that several grades that have varying properties, uses and machineability ratings that must be considered when before selection. The most obvious choice of material is steel, given the temperature range needed, desire for moderate machineability and moderate chemical resistance with low percentages of metals likely to form Zintl phases. Given the number of grades available for a wide range of applications, choosing the correct grade is important.

It is also important to consider cooling rate associated with any given target temperature. The issues of Austenite formation and the Martensite transformation are important considerations for the chosen material if any longevity of use is desired.

Austenite:

Austenite is a metallic, non-magnetic solid solution of Carbon and Iron that exists metastably in steel at the critical temperature of around 725°C. The Austenite phase is an FCC cubic system that results in a larger volume of carbon to remain in solution in the steel. The problem associated with Austenite is that when it cools a mixture of ferrite (α-fe) and cementite (iron carbide, Fe_3C) form as the dissolved carbon falls from solution. If the cooling rate is high the martensite transformation may occur, which results in the alloy undergoing a slight lattice distortion and hence reduces the longevity of the material. Cooling rate directly determines the proportions of these products and thus the properties of the steel. High cooling rates promote the martensite transformation and thus quenching may be utilised to induce it. Upon cooling, carbide formation will occur at the steels surface and results in a sooty appearance. Austenite can be stabilised by the addition of metals such as nickel and manganese to the steel.

As a result of these affects, slow cooling is desirable when using Austenitic steels. It is important to note that Austenite is a vital factor in the hardness of these steels. Austenitic steels are also difficult to weld and form poorly, due to the inclusion of sulphur to facilitate machining. Lack of sulphur improves the welding and forming attributes but makes the steel considerably harder to machine.

Martensite:

Martensite is an allotrope of Austenite and as a result of the identical chemical nature, a metastable phase transition (see: *Figure 4.1.1*) between the two structural forms has very low thermal activation energy and occurs readily.

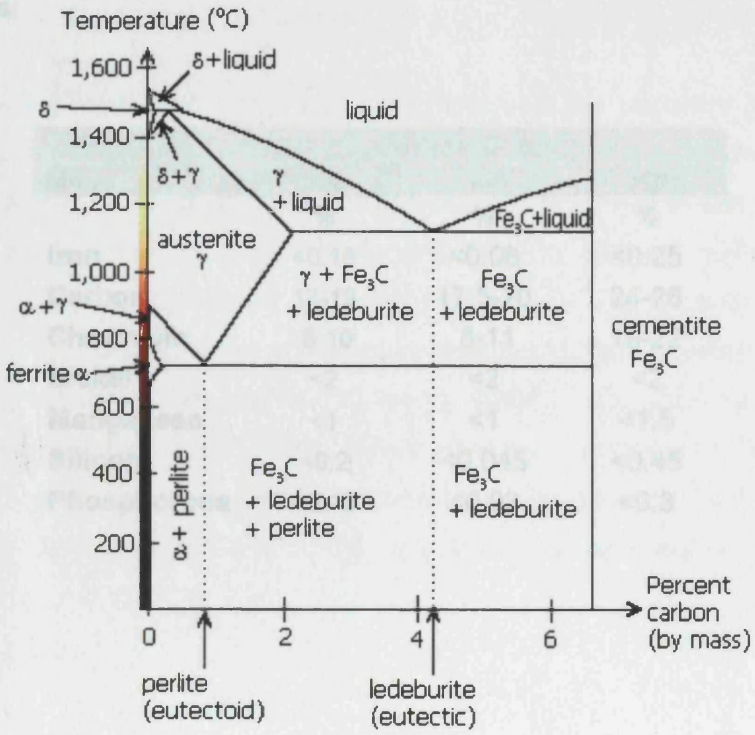

Figure 4.1.1: Phase diagram for Iron-Carbon at Atmospheric Pressure[1].

On formation of martensite, plate like crystals form in the steel that appear like striations on examination (see: *figure 4.1.2*). High levels of Martensite result in steel with a brittle nature, hence the concerns associated with cooling rates for any reaction occurring, too little Martensite results in soft steels. In summary, martensite can be viewed most appropriately as a metastable intermediate in the diffusion and nucleation processes necessary to form ferrite and cementite.

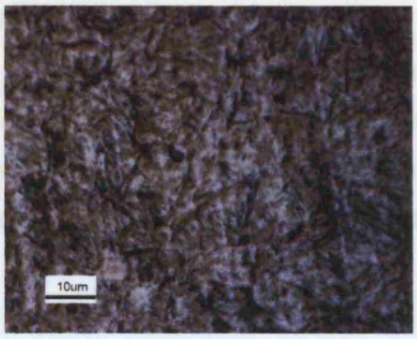

Figure 4.1.2: Martensite Crystals in Steel[2].

Steel Grades:

	Steel Grade		
Metal	**303**	**304**	**310**
	%	%	%
Iron	<0.15	<0.08	<0.25
Carbon	17-19	17.5-20	24-26
Chromium	8-10	8-11	19-22
Nickel	<2	<2	<2
Manganese	<1	<1	<1.5
Silicon	<0.2	<0.045	<0.45
Phosphorous	>0.15	<0.03	<0.3

303[3]:

303 steel is among the most commonly used grades and is employed in a wide range of applications. It is a reasonably good all round steel that has best machineability of the austenitic steels, good temperature performance and retains low levels of iron which may result in problems with Zintl phase formation.

303 steels do suffer from the issue of austenite, martensite and carbide formation. However, they maintain reasonable temperature performance up to 800°C, though they are not recommended for constant use in the range 400-700°C, due to high carbon composition and the problem of carbide precipitation.

303 steels have very good machineability as mentioned before but perform only averagely in welding and are not recommended for use in such cases. For better temperature resistances 303se may be utilized. 303se is similar to 303 in composition but contains more selenium to improve hot and cold performance of the steel and slightly improve finishing in machining. 303 steels have reasonable chemical resistance in mild environments but perform poorly in water.

304[3]:

304 steel is the most commonly used and most versatile stainless steel. Its good forming and welding characteristics make it a favored choice for many applications. 304 has a good and wide ranging resistance to many chemical environments and corrosives. Its temperature performance is similar to 303 but with a little more tolerance of higher temperature. For high temperature applications 304L exhibits better temperature performance and is more resistant to carbide precipitation and so find easier operation in the 400-800°C range. 304H is also very suitable for high temperature applications but exhibits higher strength than 304 and 304L and so is often used for structural and pressure containing applications. 304 is noticeably harder to machine than 303 due to the lack of Sulphur as a chipping agent in the alloy.

310[3]:

310 steels are primarily for high temperature applications. They resist oxidation up to 1150°C and have good chemical resistance in the temperature range. 310S shows resistance to moist corrodents in the temperature range and thus has even more desirable chemical resistance. 310 steels show good performance in welding and forming applications but poor machineability. 310 is commonly used in the manufacture of components for furnaces.

4.2: Design iterations and early generations of autoclaves for Zintl phase preparation

Design One:

In the initial attempts at this synthesis, NaSi was the prime target for study. Early attempts use the standard solid state synthesis methodology employing Tantalum foil to create a rolled tube, crimped closed at the ends, which is then sealed into a quartz tube, evacuated and heated. The quartz tube is placed into an autoclave of special design for such applications (See: *figures 4.2.1 and 4.2.2*) and heated in a tube furnace. This iteration used 303 steel and 0.1mm thick Tantalum foil that is rolled by hand into a tube of suitable size. The ends are then crimped closed after filling using pliers.

The main problems with this design are lack of utility for a wide range of experiments. If the starting materials are high melting solids, the Tantalum foil approach is suitable. However, should the one or more of the starting materials be low melting i.e. the alkali metals, this approach becomes useless due to the issues of poor sealing using rolled and crimped Tantalum foil, in that alkali metals will tend to leak from the foil on heating and begin reacting with and destroying the quartz tubing. Upon opening, it is common to find a cracked or already broken quartz tube and unsuccessful reaction.

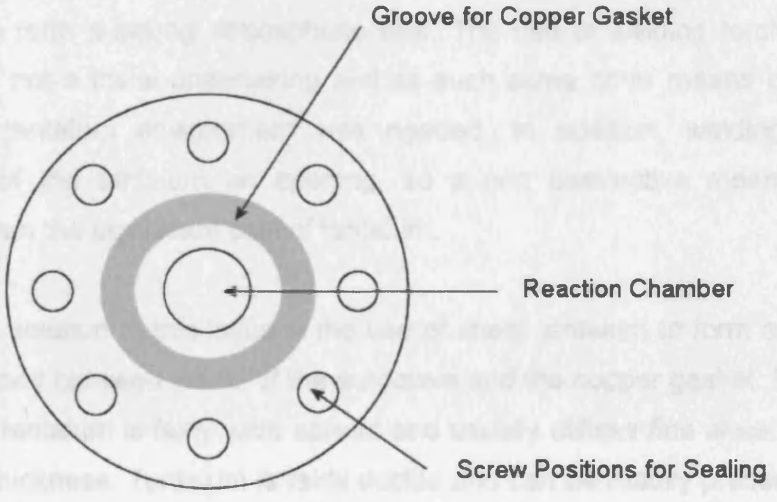

Figure 4.2.1: Top view down inside the quartz tube chamber of the autoclave.

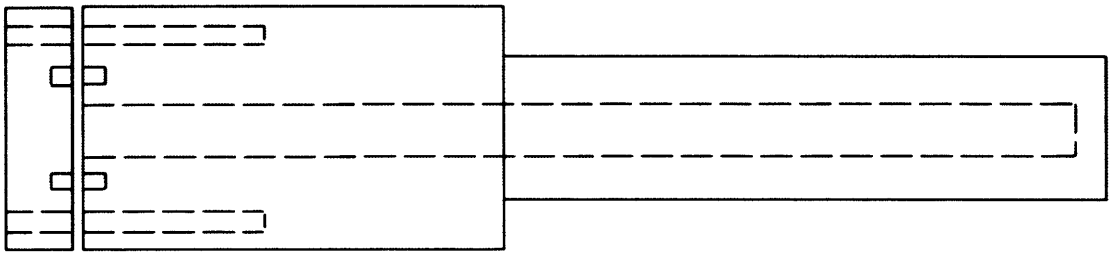

Figure 4.2.2: Side view showing positioning of gasket seal and screw thread.

After several attempts using this method with alkali metals it becomes clear that it is not suitable and will not yield the desired results.

Design Two:

As a result of the issues associated with standard solid state synthesis techniques, it is clear that a suitable reaction vessel must have a well sealed, inert, reaction vessel from which low melting solids cannot escape, as well as a robust holder for that inert environment.

Tantalum crucibles from non destructive means

Discussions of synthesis of such materials talks of arc-welding tantalum inside a glove box to form a strong atmospheric seal. The use of welding torches inside a glove box is not a trivial undertaking and as such some other means of creating a well-sealed tantalum environment was needed. In addition, welding results in destruction of the tantalum on opening, so a non destructive means was also desirable given the significant cost of tantalum.

The obvious solution to this issue is the use of sheet tantalum to form crucibles that can be clamped between the lid of the autoclave and the copper gasket. Forming and stamping of tantalum is fairly wide spread and usually utilises fine sheet up to a few millimetres thickness. Tantalum is fairly ductile and can be readily pressed, punched or formed in such sheets. However, the process becomes considerably easier if the metal is annealed. To anneal tantalum requires heating to approximately 1000 °C in a vacuum furnace and is then allow to cool. This is obviously not viable for most laboratories or metal work shops and so other means where needed.

It is a well known fact that galling, tearing and seizing in forming procedures can be lessened by using brass or aluminium in fabrication of any forming tool. It is also common to use suitable oils in the procedure to reduce such effects. As such a brass forming tool (see: *Figure 4.2.3*) was developed to facilitate cheaper, reusable crucibles. The idea was to make small crucibles, holding a reaction of around 0.5g, such that two full crucibles could be cut from each 50 x 50 mm tantalum sheet.

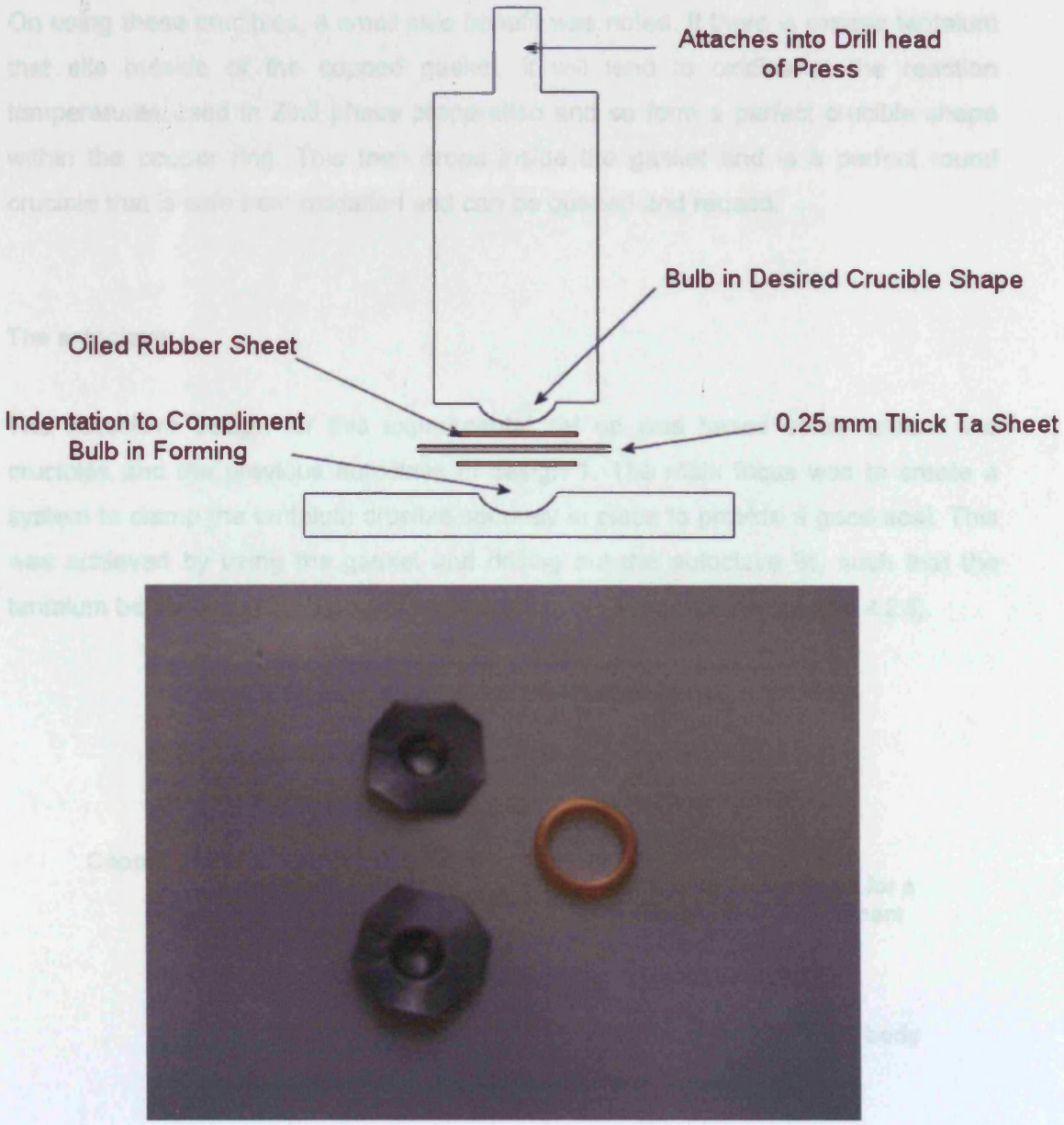

Figure 4.2.3: Forming tool for pressing tantalum crucibles from tantalum sheet (top) and the finished tantalum crucible and Copper gasket (below).

One further precaution utilised to avoid seizing and crimping is to use rubber sheets either side of the tantalum sheet. This, in addition to the oil, should reduce any issue of damage to the metal on forming. The result is a small saucer-shaped crucible that must be cleaned and oven dried before use. Placing two in opposition to each other creates a totally sealed crucible that can be clamped between lid and copper gasket and firmly sealed on screwing closed of the autoclave.

On using these crucibles, a small side benefit was noted. If there is excess tantalum that sits outside of the copped gasket, it will tend to oxidise at the reaction temperatures used in Zintl phase preparation and so form a perfect crucible shape within the copper ring. This then drops inside the gasket and is a perfect round crucible that is safe from oxidation and can be opened and reused.

The autoclave:

The autoclave design for this experimental set up was based solely around the crucibles and the previous autoclave in design 1. The main focus was to create a system to clamp the tantalum crucible securely in place to provide a good seal. This was achieved by using the gasket and drilling out the autoclave lid, such that the tantalum bends around the gasket and seals firmly (See: *Figure 4.2.4 and 4.2.5*).

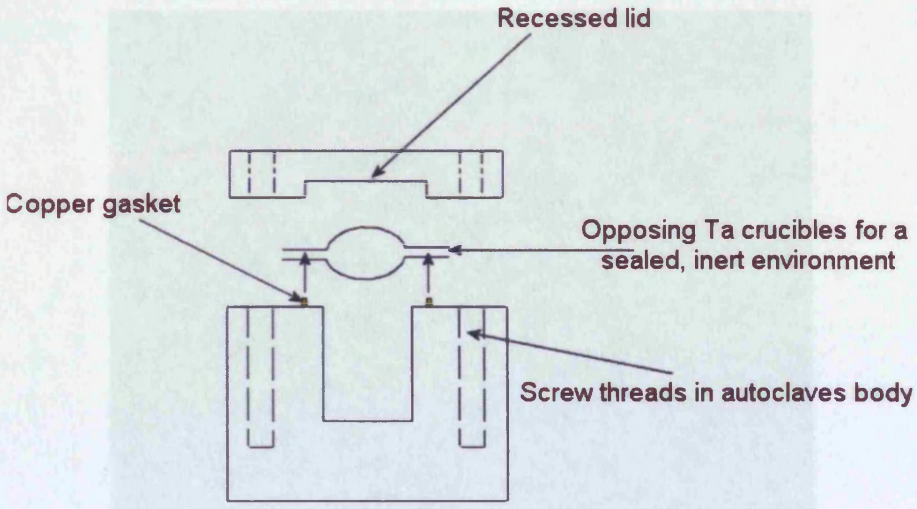

Figure 4.2.4: Side view of crucible clamping using a gasket and recessed autoclave lid.

Figure 4.2.5: The autoclave with gasket in place (top), with the crucibles ready for loading (middle) and Crucible closed before sealing shut with the lid (top).

As mentioned before, anything outside the gasket will oxidise and can be easily removed on opening of the autoclave. The crucible itself is usually easily opened with tweezers and the solid detaches with ease from the tantalum surface. As a design this works well for small sample sizes and results in good reproducible experiments.

There are a number of draw backs to this method of undertaking the synthesis. The first problem is the sample size possible. In capillary based *in-situ* experiments, small samples present no problem but large laboratory preparation of the Clathrates is considerable easier with samples in excess of 1g, especially given sodium loss and resultant sample size reduction. The second issue is that of using thin sheet in the crucibles. tantalum has a tendency to become brittle when heated, even when not exposed to air. The result can often be destruction of the crucible upon opening inside the glove box, which in turn results in powdered tantalum in the product. The third issue is on oxidising everything outside the copper gasket; it is very easy to contaminate the sample with tantalum oxide. The final problem with this design is the positioning of the M6 bolts used to seal the autoclave. Use of screw threads inside the body tends to result in the need to repeatedly re-tap the threads due to clogging by carbide and any coating (which tend to flake off) or oxide present on the bolts. Upon opening this tends to result in sheering the heads from bolts and having to re-drill the threads after each use.

Though the design is adequate for some purposes i.e. small samples, it is not the most efficient in terms of cost or purity of the products.

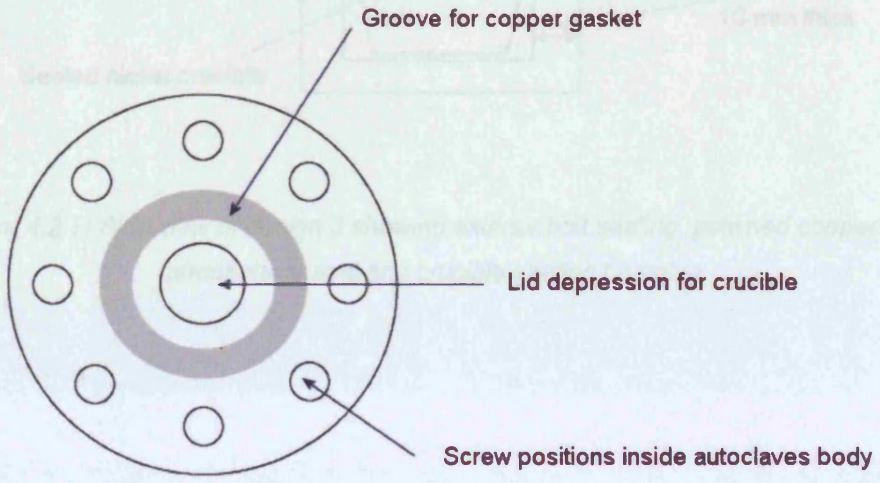

Figure 4.2.6: Autoclave lid showing depression and grove for copper gasket.

Design 3:

As a result of discussion with collaborators, it became clear that for the less reactive alkali metals, one could use metal crucibles such as nickel or chromium and rely on an initial coating of Zintl phase to keep subsequent preparations free from contamination. After a few trial attempts this was confirmed to be the case. Nickel crucibles from 10 mm to 100 mm are readily available for purchase and are considerably cheaper than similar tantalum or platinum counterparts. This knowledge allowed for a total redesign of the autoclave architecture to utilise much larger crucibles and hence undertake large Zintl phase preparations.

Using the knowledge gained from previous designs, a new set-up was developed to maximise the efficiency of the preparation (see: *Figure 4.2.7, 4.2.8, 4.2.9*). Several features present in previous designs were used in modified forms.

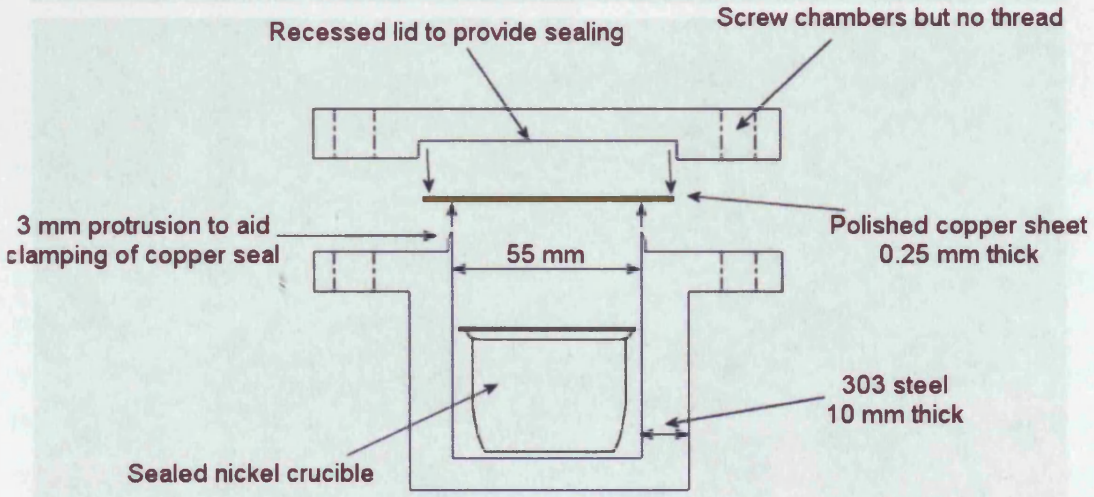

Figure 4.2.7: Side view of design 3 showing exterior bolt sealing, polished copper inert atmosphere seal and crucible seating chamber.

Figure 4.2.8: Photograph of design 3 showing the zinc bolts, nickel crucible and copper plate used in sealing (top) and a side view of design 3 showing protruding lip for sealing into the recessed lid (bottom).

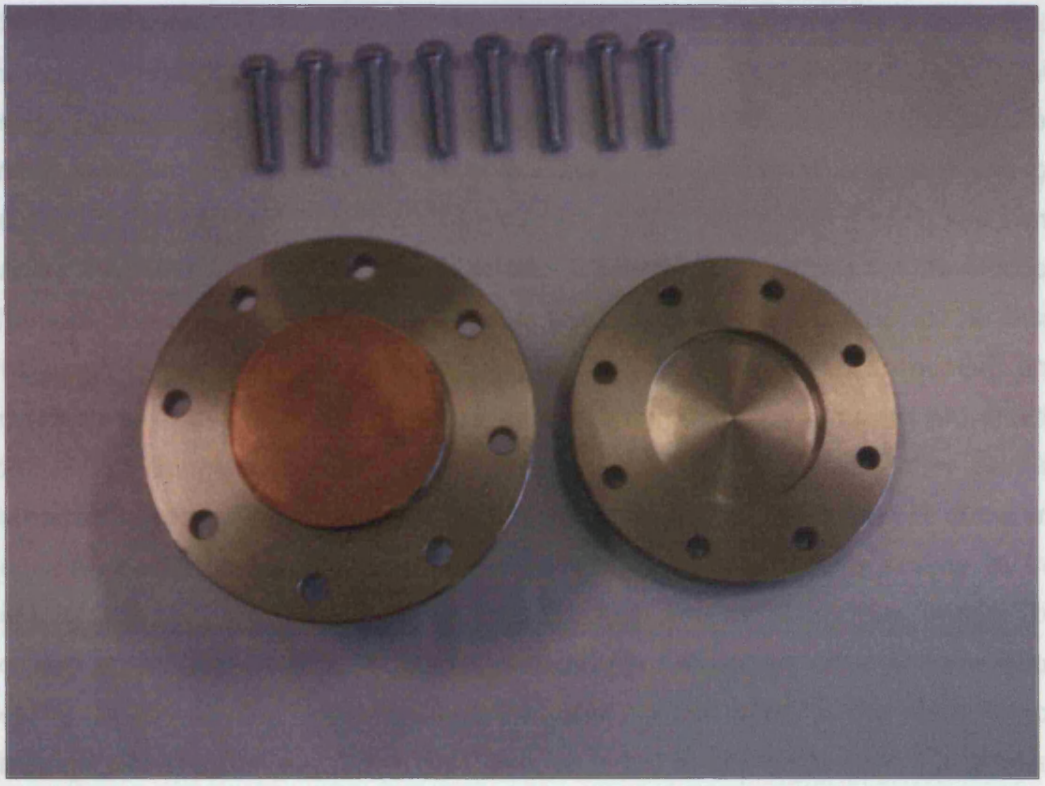

Figure 4.2.9: Shows copper plate seal in position on the autoclave before sealing.

The first major design change for the third design, was to move away from screw threads in the autoclaves body. In previous designs internal threads tended to result in many difficulties in opening due to the bolts almost welding into the threads and requiring drilling out to the constant need for thread re-tapping to provide adequate sealing. The overall result of previous designs was that internal threads – indeed threads at all – are a poor idea and generally result in multiple means by which the reaction environment can be compromised with atmosphere, in for example, the need to use a vice to almost completely open the autoclave outside the glove box and hence compromise atmosphere.

The solution to this was to use bolt chambers with no thread, outside the main autoclave body, such that bolts that can not be undone due to heating damage may be far more easily removed.

The other change is an obvious increase in size for the accommodation of the crucible into the autoclave. The chamber is large enough such that a relatively sizeable crucible can be used for mass preparations.

The final change was the metal to metal seal. In previous designs the small size of the reaction meant that using a relatively small copper washer was sufficient. In this design however, the much large reaction chamber and the crucible not being sealed firmly, result in the need for a more sturdy seal. The solution was to take a large copper disc of approximately 0.25-0.5 mm thick copper and polish it using wet sand paper. The autoclave was then designed with a 3 mm lip protruding from the reaction chamber to aid in sealing and to present a good clamping point for the copper disc. The result is that the copper disc actually tends to bond to the lip on heating and provides a mild chemical seal. The copper disc often has to be removed with a little force which suggests a good seal is indeed achieved. In addition, after several successive preparations, the steel lip of the bomb opposing the copper plate will become heavily coated in carbide. Over time, this results in poor sealing of the sample such that the NaSi will react with the steal and air at the seal break. The solution is to file the opposing lip with a metal file before use. This ensures good sealing as the copper has a tendency to form a weak bond to the steel, hence chemically sealing the autoclave. This also leads to the conclusion that it is prudent to coat the inner lid of the autoclave in carbide, before use.

The steel chosen for this particular autoclave was 303. Despite 304 and 310 and various other grade being more suitable for the temperature requirements, the issue of machineability was the deciding factor in steel choice here. The result is a very sooty finish (see: *Figure 4.2.10*) after the first heating of the autoclave due to carbide precipitation. However, the lack of availability of specialist machining equipment makes the use of other grades limited and thus 303 was chosen.

The resulting autoclave is a considerable improvement on previous iterations. It is considerably easier to open and handle before and after heating in the glove box.

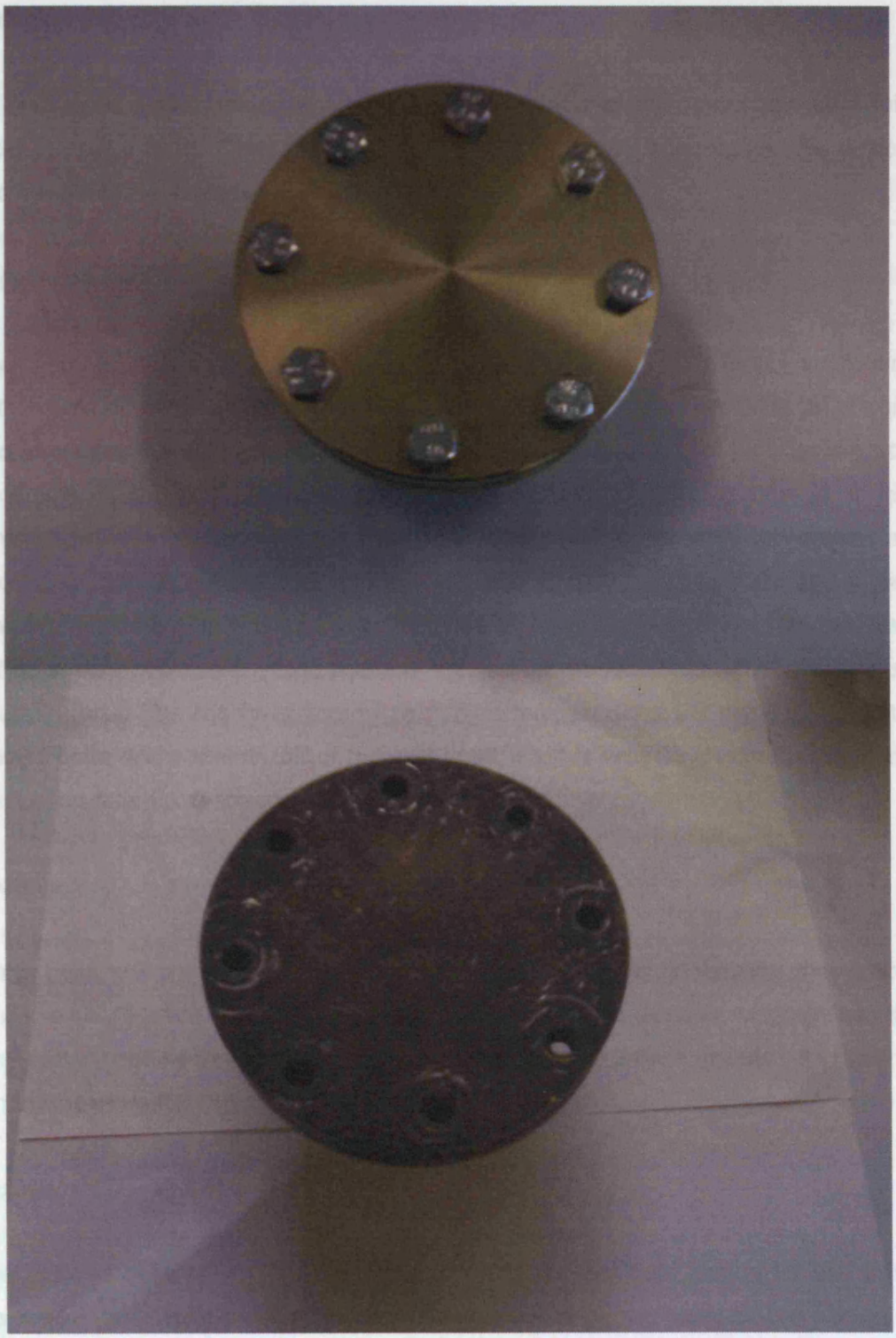

Figure 4.2.10: Photographs show before heating (top) and subsequent carbide precipitation post heating (bottom).

Fittings:

As discussed earlier, the means of sealing the autoclave using bolts can be a fairly tricky technical issue. Choice of bolts, screws etc can be as important as the position and nature of the threads/chambers they will occupy.

High Tensile vs. Low Tensile:

The dilemma that occurs in the choice of high vs. low tensile bolts in this application, is the trade off between the higher likelihood of low tensile bolts breaking on undoing and leaving the autoclave difficult to undo, versus the problem of high tensile bolts becoming stuck in the thread and then very hard to remove due to it high tensile/hardness nature. The issue really comes down to personal preference and access to tools to remove high tensile bolts should they become stuck and a hack saw be insufficient. In this particular instance high tensile bolts were routinely used yet often did not prove any less prone to the problems associated with the low tensile counter parts. The reality is, use of such high temperatures will inevitably result in lodged bolts and sheering off of the bolt head, so it is wise to choose a grade that can be confidently removed should this happen.

Coatings:

Many bolts will come with some form of coating on them. In heating this coating tends to disintegrate and often will result in clogging of the threads, lodging such that they cannot be unscrewed and other such difficulties. Any bolts or nuts with coatings tend to be more trouble than is worth entering into.

Hexagonal Wrench Bolts:

Hex headed bolts (Allen key bolts) would seem like an ideal choice for use in the glove box, since wrench location is simple when wearing the bulky gloves necessary in such apparatus. However, even high tensile bolts suffer some increase in brittleness on heating to such temperatures. The result of this is that the hex shaped fitting will often round, rendering the bolt impossible to remove without milling or drilling the heads out. As such hex bolts are not very suitable for this application.

Standard Spanner nuts and bolts:

Standard hexagonal-headed spanner nuts and bolts are usually the most appropriate fittings for high temperature uses. The temperatures required in the preparation result in considerable increase in brittleness of the steel surface due to carbide precipitation. As a result it is very easy to sheer or round most bolt types, upon application of any pressure or torque in undoing. As such hexagonal spanner nuts and bolts provide the lowest risk fittings, in that adjustable tools may be used to counteract any nut or bolt damage due to heating.

Bolts: Steel or other metals:

When choosing a means of sealing for an autoclave, the obvious choice is to take high-tensile steel bolts. This isn't always the best choice however. The inherent issues of carbide precipitation at high temperatures, for most common steel grades, can be a considerable problem for opening the autoclave post heating. The result is that post heating, carbide precipitation often makes opening the autoclave nearly impossible and as such hack sawing the bolts off is the only viable option, which again compromises the sealed atmosphere.

A useful solution to this situation is to use two different metals i.e. one for the bolts and another for the nuts. In doing so you can again utilise the inherent differences in coefficient of thermal expansion and thus aid sealing if a more readily expansive metal is used for the bolts. In such situations if a metal of higher coefficient of thermal expansion is chosen for the bolts, under heating they should expand more than the nuts and thus form a very good seal. The added bonus in this instance is on cooling, when the autoclaves inner region is very well sealed due to carbide precipitation, the nuts and bolts will have marginally loosened due to the expansion on heating and subsequent contraction. This in turn is very helpful in aiding opening on cooling and can often lead to opening inside the glove box with no vice being used.
The obvious fear in these instances would be that the seal is poor given that the bolts are slightly loosened. This is not the case as the carbide precipitation on the inner surfaces provides a more than adequate seal, which must often be forcibly prized open inside the gloves box. In addition, the polished copper plate will be bonded to the protruding lip of the autoclave and will also need to be prized free with some force. It's noteworthy that the effort required forcing these seals free inside the glove

box, is considerably easier and more reliable, than the issues associated with bolts that require hack-sawing outside of the glove box.

A good example of this in practise is to use zinc bolts and steel nuts. The result is that the bolts undergo a mild oxidation during the reaction (which is easily brushed off) but the nut and bolt assembly is always loose enough to be undone with only moderate force inside the glove box.

The use of brass in such applications is also commonly seen but the inherent malleability of brass results in similar problems as for steel and carbide precipitation i.e. they can be next to impossible to undo. As such brass is also not a suitable choice at these temperatures.

4.3: Equipment Design for the Preparation of clathrates *in situ* at a Synchrotron Radiation Source

The main focus of this project has been to examine formation of the clathrates by the use of time-resolved synchrotron radiation techniques. However, the nature of the formation step from Zintl phase to clathrate is such that an *in situ* preparation is, in practice, a complex technical problem.

$$NaSi \xrightarrow[\text{Ramp rate } 2°Cmin^{-1} \text{ to } 200°Cmin^{-1}]{275 \sim 600°C} Na_8Si_{46} + Na_{24}Si_{136}$$

$$\text{Vacuum} = 10^{-5} \text{ bar}$$

The reaction above notes the conditions necessary to provide *in situ* at the synchrotron source[4]. The two main issues evident are the need to provide temperatures up to 600°C, including fast temperature ramps as high as 200°C per minute[5]. The second issue is to provide a strong vacuum at the beam line during operation. Both these problems seem trivial on first examination, however, the sample holder requirements in this instance are such that these become difficult to achieve.

Synchrotron Radiation

Synchrotron radiation sources generally consist of many user beams or stations, tapped from around the main source. Each station is designed for a specific purpose or application within the realms of scientific research and is often limited in its usage and specifications, such that a given station may excel at its specific desired application, yet posses limitations in others. These limitations are often something that has to be overcome or worked around in experimental design, such that the inherent advantages of the station may be maximised in any given study. Such was the case in designing a means by which to study the clathrate formation *in situ* and so choice of station was a trade off of these considerations.

The main desirable features when attempting to study the clathrates formation using synchrotron radiation are:

1. ***Time-resolved:*** Following phase formation would require regular data collection in the order of minutes, such that any subtle structural or chemical changes may be followed.

2. ***Good structural resolution:*** Similar to above, a relatively high degree of resolution for the instrument is desired to follow complex phase changes and should be high enough such that Rietveld refinement of the data is possible.

3. ***Penetration:*** To enable the experiment to be undertaken, a relatively good sample penetration is desired to make experimental design easier.

SRS Daresbury Station 6.2

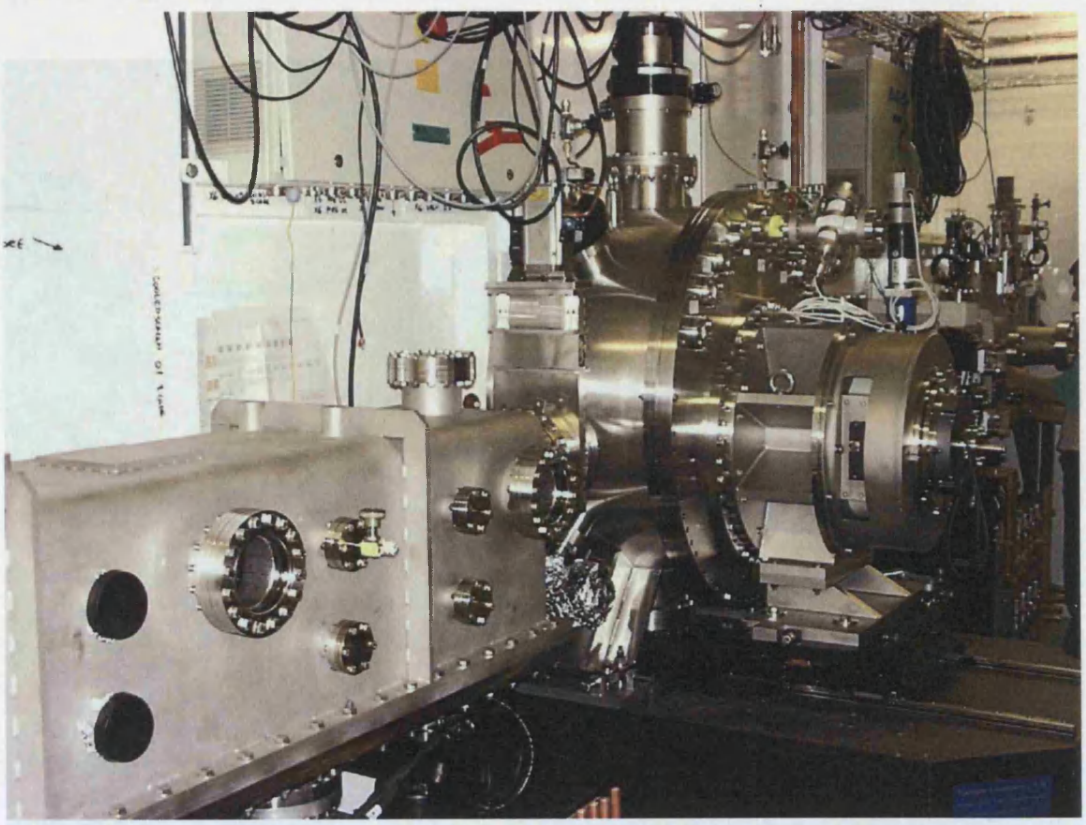

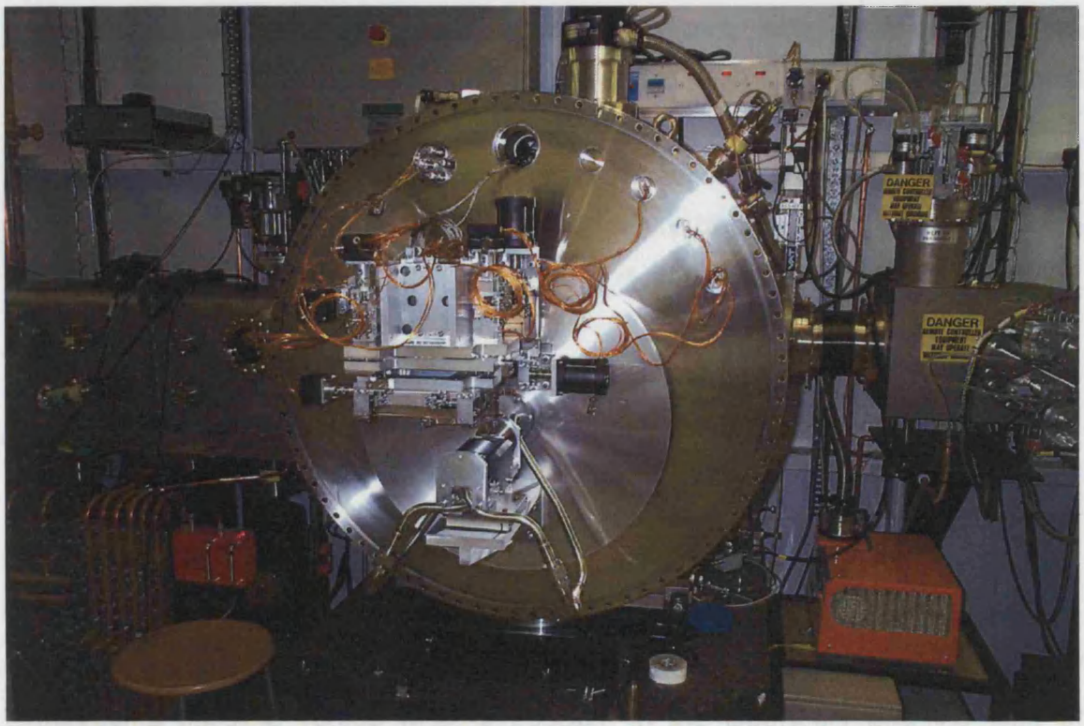

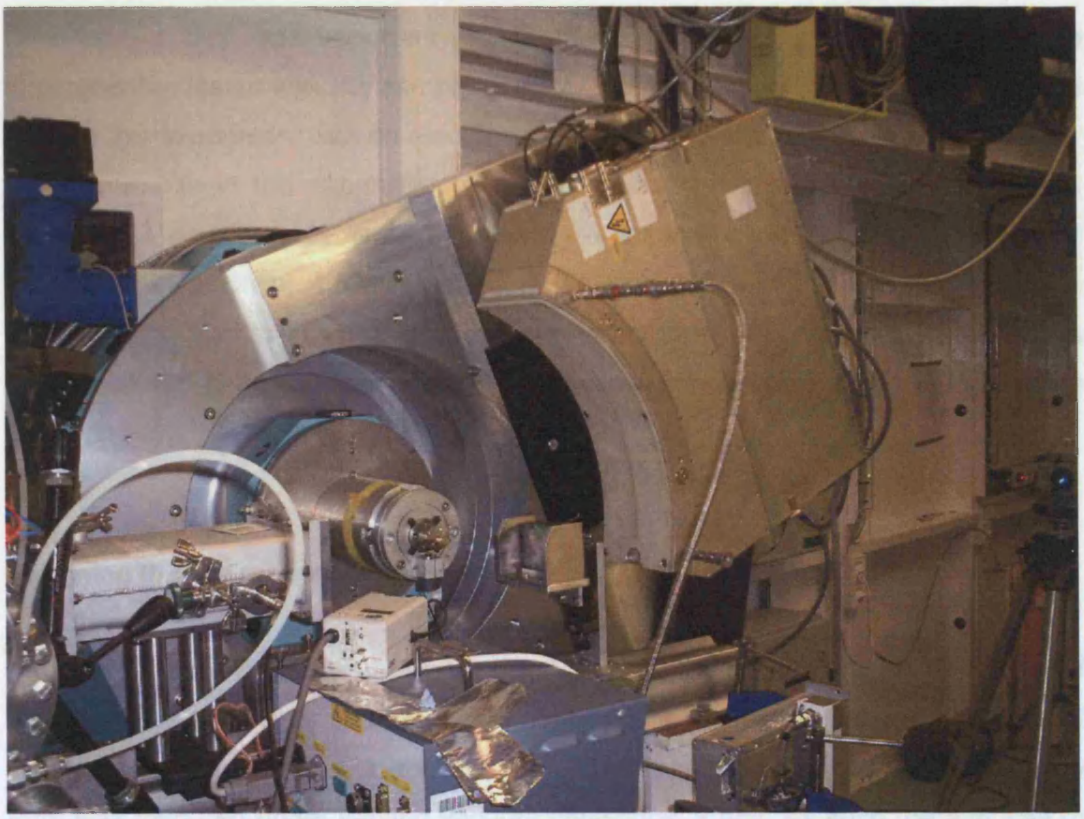

Figure 4.3.1: The apparatus inside the optics hutch (Previous page) and (Top), The Rapid2 detector and 2θ circle in the experimental hutch (bottom).

Station 6.2 at the SRS Daresbury is a materials science station dedicated to time-resolved study of short and/or long-range order variation in inorganic and organic materials. Station 6.2's source is a Multi-Pole wiggler insertion device that provides 5 to 18 KeV energy. The standard user beam for this application is 8.865 KeV, which is a wave length of 1.40 Å. The most desirable feature of station 6.2 is that it utilises Rapid 2 detector technology[6], [7], such that it is capable of time-resolution in the seconds and even milliseconds regime[8].

So the main desirable features for the completion of an *in situ* study were in place at station 6.2. However, a serious drawback came when sample penetration was considered. Station 6.2 has a penetration of about 2 mm of quartz and so any reaction that you wish to study must be carried out inside a fine glass capillary. This restriction results in a considerably more complex experimental set up than in the laboratory. In addition, it results in a certain level of restriction on the type of experiments possible versus what is possible in the laboratory and the type of starting materials.

One feature that was important in determining much of the geometry for the experimental design was the sample stage present at station 6.2. The sample stage used in this experiment was an electric xyz translation stage, controlled via computer for movements in the sub-millimetre range. This level of automation and control facilitates a considerable level of flexibility in apparatus design and experimental technique. In addition, it allows for some interesting use of the xyz stage to scan through regions of the sample environment for homogeneity, deposition and various other localised chemical and physical affects that may be occurring in the reaction environment.

Designing the *in situ* Vacuum System:

From experience it is obvious that a good vacuum is important in the synthesis of these materials. However, at the outset of the project it was not clear to what extent vacuum was important, how good of a vacuum was necessary or which clathrate form was favoured under varying vacuum conditions, if any. As such the aim was to attempt to apply a vacuum equivalent to that in the laboratory environment to the sample. This presents some technical issues: The system must:

1. Mount the capillary with either vertical or horizontal geometry.
2. Atmospherically seal, secure and rotate a 1 mm glass capillary.
3. Apply 10^{-5} bar vacuum to a capillary with an inside diameter of less than 1 mm and wall thickness of around 10 µm.
4. Apply dynamic vacuum using a turbo pump and protect the pump from any damage.
5. Use tubing and connections that adequately hold relatively high vacuum for several hours during exposure to volatilised sodium.
6. The vacuum must also be in monitored in such a system.

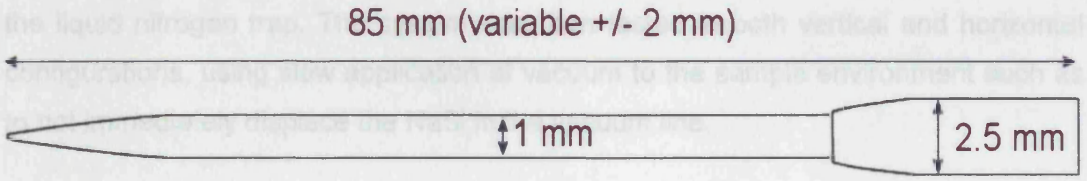

Figure 4.3.2: Dimensions for a 1 mm quartz or borosilicate glass capillary.

Testing and designing equipment for the *in situ* Experiment:

The nature of the experiment that was to be undertaken resulted in a great deal of development work and trial and error with various designs, set-ups and configurations of the apparatus. The work that resulted in a successful experiment in reality spanned over two years of the project and several weeks of SRS beam-time.

Capillary Mounting:

One of the first considerations was the geometry of the capillary mounting. The nature of the sample stage was such that both horizontal and vertical geometries were feasible, so some basic tests were necessary to ascertain the more appropriate of the two.

Some simple experiments were completed using 1.0 mm quartz-glass capillaries i.e. the upper end of the size and internal diameter range, such that the worse case scenarios associated with vacuum and powder samples could be tested. The NaSi

was ground using a 53 μm sieve and loaded into the capillary inside a glove box. It was noticeable on loading that the NaSi was prone to unload from the capillary on inversion (from sealed end down to sealed end up), irrespective of the density of fill or volume of material loaded.

The capillary was attached to hard plastic tubing using wax, super glue and silicon grease (the seal used was not a strong vacuum seal but merely enough to test the effect of geometry on the powder sample under vacuum). To this a standard ground-glass assembly was attached, which was connected to a vacuum system with a liquid nitrogen trap and a turbo molecular pump. Two vacuum gauges were placed in the system, one as close to the capillary as possible, the other between turbo pump and the liquid nitrogen trap. The system was then tested in both vertical and horizontal configurations, using slow application of vacuum to the sample environment such as to not immediately displace the NaSi in the vacuum line.

The test showed routinely that a mounting with the unsealed end down was – unsurprisingly – unreliable in retaining the sample for any duration under vacuum. A sample with the sealed end down is unfeasible in that the weight of the vacuum assembly and line would be on top of the sample, something undesirable with such a fragile sample environment and also would impede the diffracted signal trajectory from the sample to the detector.

This leaves the horizontal mounting as the most suitable candidate, as was seen in these tests. The issue of rapid unloading on fast vacuum application is still a feature of this geometry but with care becomes less problematic. The addition of this to the lack of unloading due to gravity as in the vertical configuration and lower equipment strain in the horizontal plane made it the obvious choice to design the system around.

Vacuum Sealing a Capillary under Rotation:

The biggest technical problem in the realisation of an *in situ* adaptation of the laboratory experiment was how to provide adequate vacuum to the sample and maintain an inert atmosphere after sealing inside a glove box. Due to the considerations associated with preferred orientation and texture affects in powder samples, a means of sample rotation was also an aim.

The initial idea was to take Swagelok fittings and modify them for holding a capillary under sealed conditions. This was done by taking a semi-soft plastic and machining it into the shape of a standard Swagelok ferrule, with a fine hole drilled through the centre. The capillary is easily super-glued into this assembly before loading inside the glove box. The metal ring counterpart to the Swagelok ferrule is then used in sealing the system; the soft nature of the plastic deforming around the metal fitting such that a strong seal is formed (*see: Figure 4.3.3*). The plastic capillary assembly was developed in conjunction with Strusevich *et al*[9].

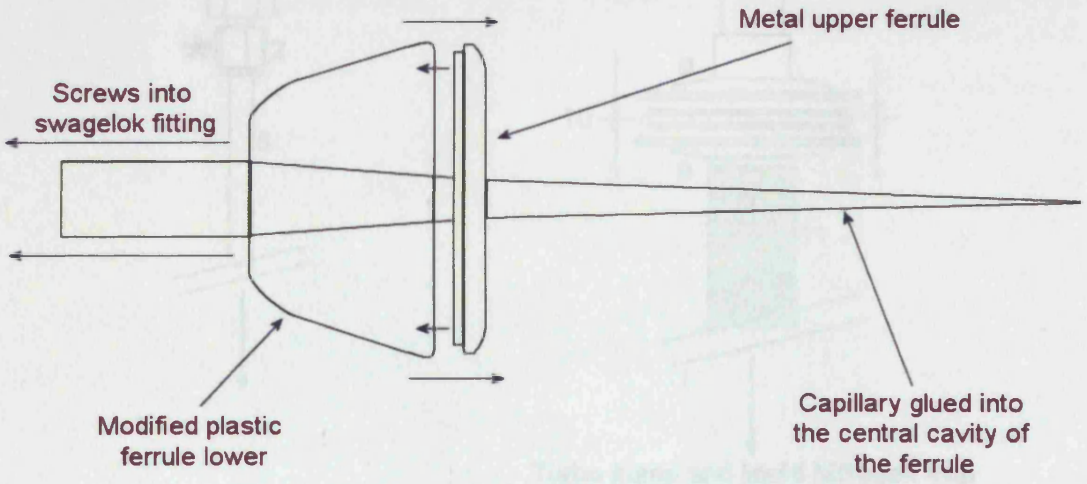

Figure 4.3.3: Custom plastic ferrule assembly for facilitating vacuum application to capillary-mounted samples in situ.

For the purposes of appropriate sealing inside the glove box and for transit to the station, a suitable holder assembly or "cell" was devised. It was initially designed such that it would sit in the goniometer and rotate using rotating seals under vacuum (*See: Figure 4.3.4*).

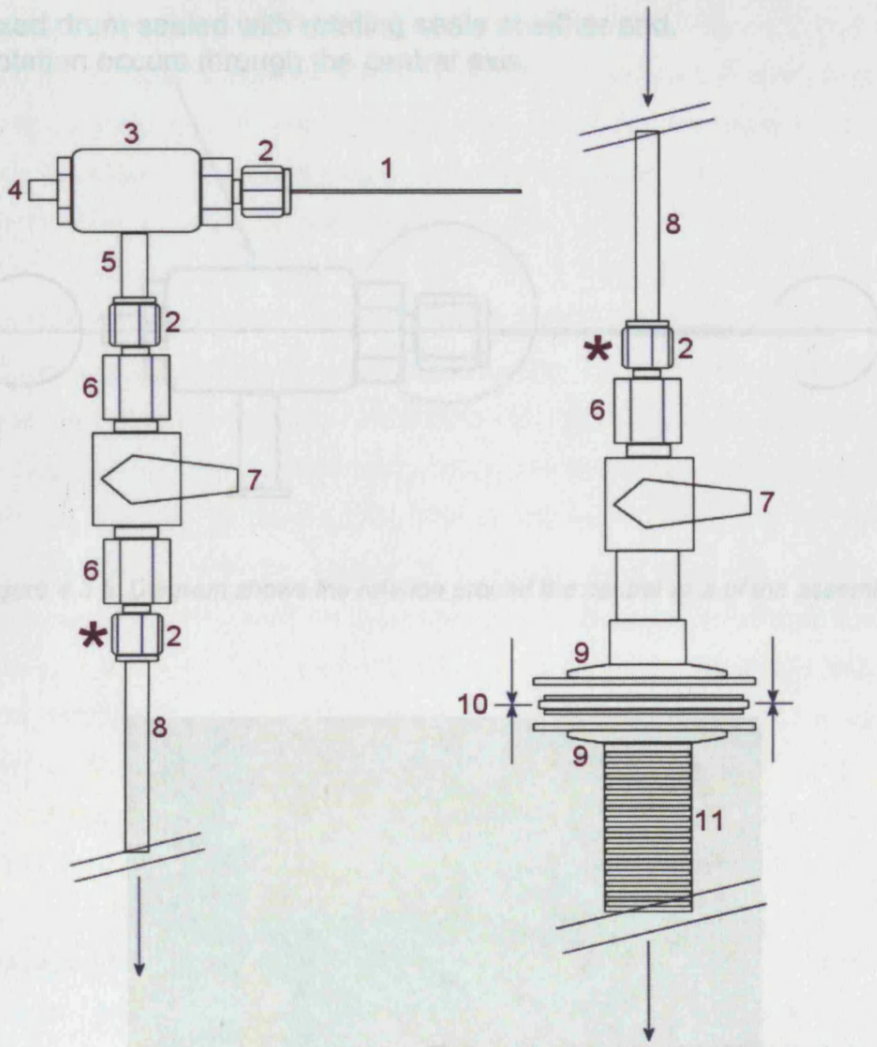

Figure 4.3.4: Diagram shows a schematic of the rotating seal vacuum assembly.

1: Loaded capillary

2: 1/2 inch Swagelok nuts sealed using metal ferrules

3: Chamber sealed at either end with rotating seals containing o-rings

4: Goniometer stub, 5: 5 mm diameter polished steel tube

6: 1/2 inch metric to imperial converter

7: Swagelok taps with o-ring and Teflon inners

8: 5 mm diameter hard plastic tubing

9: KF25 plate seal for high vacuum operation

10: Rubber/metal o-ring

11: Concertina high vacuum hose

**: Position at which vacuum is connected at the beam line after loading of the sample.*

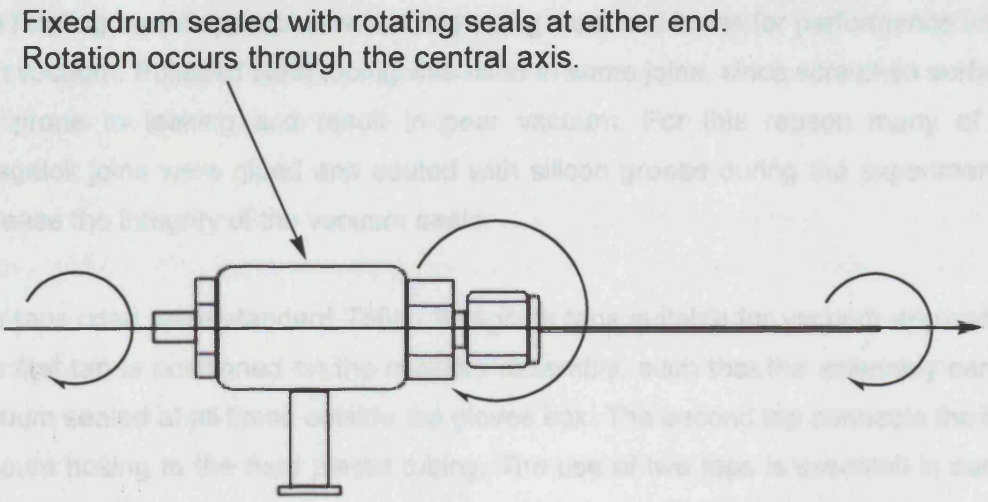

Figure 4.3.5: Diagram shows the rotation around the central axis of the assembly.

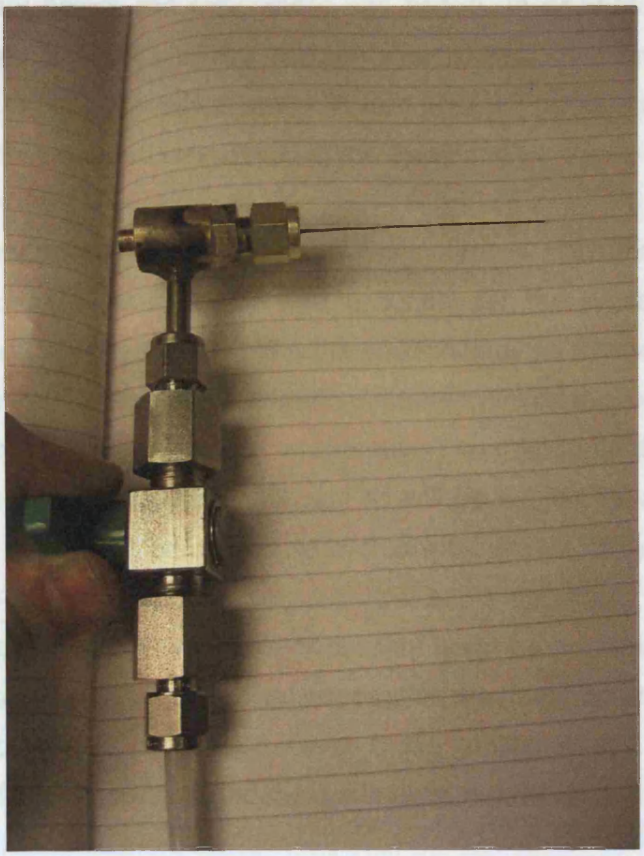

Figure 4.3.6: Photograph shows the assembly loaded, sealed and connected to the hard plastic tubing which completes the vacuum line.

The rotating barrel apparatus was made using steel and brass for performance under high vacuum. Polished steel tubing was used in some joins, since scratched surfaces are prone to leaking and result in poor vacuum. For this reason many of the Swagelok joins were glued and coated with silicon grease during the experiment to increase the integrity of the vacuum seals.

The taps used were standard Teflon Swagelok taps suitable for vacuum application. The first tap is positioned on the capillary assembly, such that the assembly can be vacuum sealed at all times outside the gloves box. The second tap connects the high vacuum hosing to the hard plastic tubing. The use of two taps is essential in careful application of vacuum to the sample. The two taps create a kind of "air lock" or pressure equalisation chamber (similar to a dry-box ante chamber), where vacuum application can be slowly built up between sample environment and the constantly active vacuum system. This is essential to avoid displacement of the NaSi powder out of the capillary before the experiment has begun. In addition, the second tap allows for constant operation of the vacuum system and isolation even when the sample environment is not present, which in turn ensures good vacuum at all times without the need for repeated evacuation of the system.

Where plastics had to be used, hard forms were applied such that collapse didn't occur under vacuum. Plastic tubing was essential for the pressure equalisation region since this region needed to be flexible enough to allow for manipulation during set-up and alignment. It was also an essential requirement as this region needs to be either washable or cheaply and easily replaceable. The reason for this is that it is the very close to the head of the assembly and so will be subject to volatilised sodium condensing onto its cold surface. This has two consequences; firstly it means a good vacuum can't be achieved successively with the same apparatus until it has been cleaned, as degassing of the region is necessary before a reasonable vacuum can established; secondly it can lead to total permeation such that no amount of cleaning will return the tubing to its initial state. Given these considerations, hard plastic was used and regularly replaced throughout experimental runs.

When the sample has been successfully mounted into the goniometer, the vacuum system is anchored in place using clamp stands and zip ties. This is vital such that the capillary is under no stress and will retain good alignment with the x-ray beam. Alignment is carried out with the furnace driven off in the first instance and then the furnace is driven on carefully and the capillary is checked for alignment. When the

capillary is aligned and the furnace is in place the vacuum can be carefully applied to the sample using the dual tap system for slow vacuum application. When the vacuum is stable in the system, heating and data collection may begin.

Use of the rotating vacuum seal assembly constituted the earliest set of experiments of this nature. The tests proved problematic for a number of reasons. Firstly, the nature of the assembly – i.e. its cumbersome nature - was such that rotation increases the likelihood of aligned problems overtime. The second issue was that over any prolonged exposure, the level of vacuum in the system reduces considerably as a result of the rotating seals leaking, despite attempts to prevent this i.e. greasing/gluing. The final problem is the high friction that results from the rotating seals, tends to lead to burning out of the motor driving rotation of the goniometer.

The selection of mechanical problems associated with the rotating chamber, were evaluated in light of these early experiments, versus the preferred orientation issues apparent for non-rotating systems. It was decided that the mechanical problems of the rotating system were such that abandoning a rotating sample environment for a static system was the most probably chance of success. The trade off in such a decision was to accept a more complex Rietveld refinement problem, for facilitating a more feasible and manageable experimental set-up.

In light of this design change (*See: Figure 4.3.7*) the cell-head and goniometer mount were changed to a simple fixed steel tube, with the goniometer mount in the same position as in the previous design. The advantage of this change was to reduce the weight of the assembly such that alignment of the sample in the beam became less difficult and hindered though still challenging.

Though there has been much work done on the development of novel in situ experimental apparatus[10-14], only one similar design for capillary based experiments - using a non-rotating sample - has been reported in the literature[15]. The reported apparatus used quick couplings for gas delivery through the sample of a kind totally unsuitable for this experiment. Additionally, the means by which the capillary was secured would be unsuitable for vacuum applications and so the cells developed in this study are a considerable departure from the reported apparatus. At the time of writing no other vacuum capillary cells were evident in the literature.

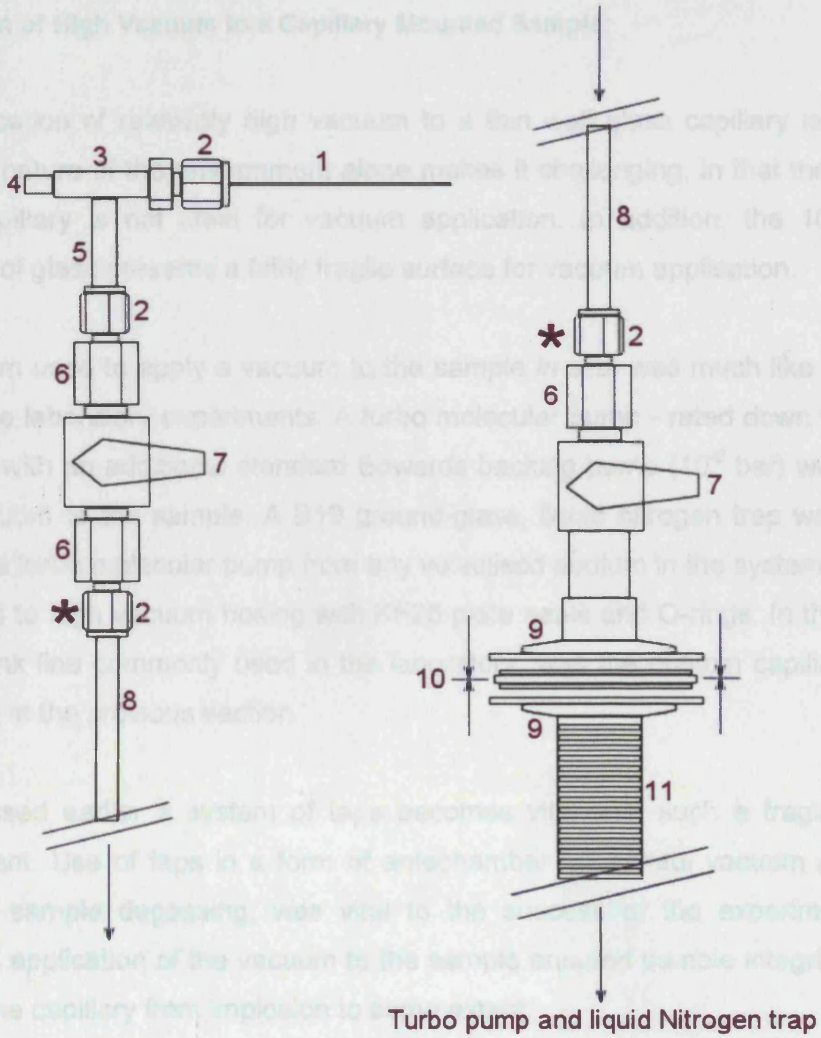

Figure 4.3.7: Diagram shows a schematic of the static vacuum capillary assembly.

1: Loaded capillary

2: 1/2 inch Swagelok nuts sealed using metal ferrules

3: Fixed non-rotating vacuum chamber

4: Goniometer stub

5: 5 mm diameter polished steel tube

6: 1/2 inch metric to imperial converter

7: Swagelok taps with o-ring and Teflon inners

8: 5 mm diameter hard plastic tubing

9: KF25 plate seal for high vacuum operation

10: Rubber/metal o-ring

11: Concertina high vacuum hose

**: Position at which vacuum is connected at the beam line after loading of the sample*

Application of High Vacuum to a Capillary Mounted Sample:

The application of relatively high vacuum to a thin wall glass capillary is a difficult task. The nature of the environment alone makes it challenging, in that the fine bore of the capillary is not ideal for vacuum application. In addition, the 10 μm wall thickness of glass presents a fairly fragile surface for vacuum application.

The system used to apply a vacuum to the sample *in situ*, was much like the set-up used in the laboratory experiments. A turbo molecular pump - rated down to 10^{-8} bar vacuum - with an additional standard Edwards backing pump (10^{-2} bar) was used to apply vacuum to the sample. A B19 ground-glass, liquid nitrogen trap was used to protect the turbo molecular pump from any volatilised sodium in the system. This was connected to high vacuum hosing with KF25 plate seals and O-rings. In the place of the Schlenk line commonly used in the laboratory, was the custom capillary design discussed in the previous section.

As discussed earlier a system of taps becomes vital with such a fragile working environment. Use of taps in a form of antechamber for careful vacuum application and slow sample degassing, was vital to the success of the experiment. Slow, measured application of the vacuum to the sample ensured sample integrity but also protects the capillary from implosion to some extent.

When considering the quality of the vacuum actually acting directly on the sample, the issue becomes somewhat uncertain. It is virtually impossible to measure the vacuum inside the capillary, so a measurement as close to the capillary head as possible is the only solution (*See: Figure 4.3.8*). The only measurable region being at the neck, results in only moderate certainty of the magnitude of the vacuum applied to the sample. Though at the neck of the capillary the vacuum is comparable to that seen in the laboratory i.e. 10^{-5} bar, it is entirely feasible that the sample is only subjected to a vacuum gradient across the boundary of the capillary head and the vacuum chamber that holds it. This in itself is probably sufficient for the reaction to occur - such a gradient will still provide a strong impetus for volatilised sodium to pass from the system - yet it is important to note the limitations of the *in situ* assembly versus the laboratory apparatus.

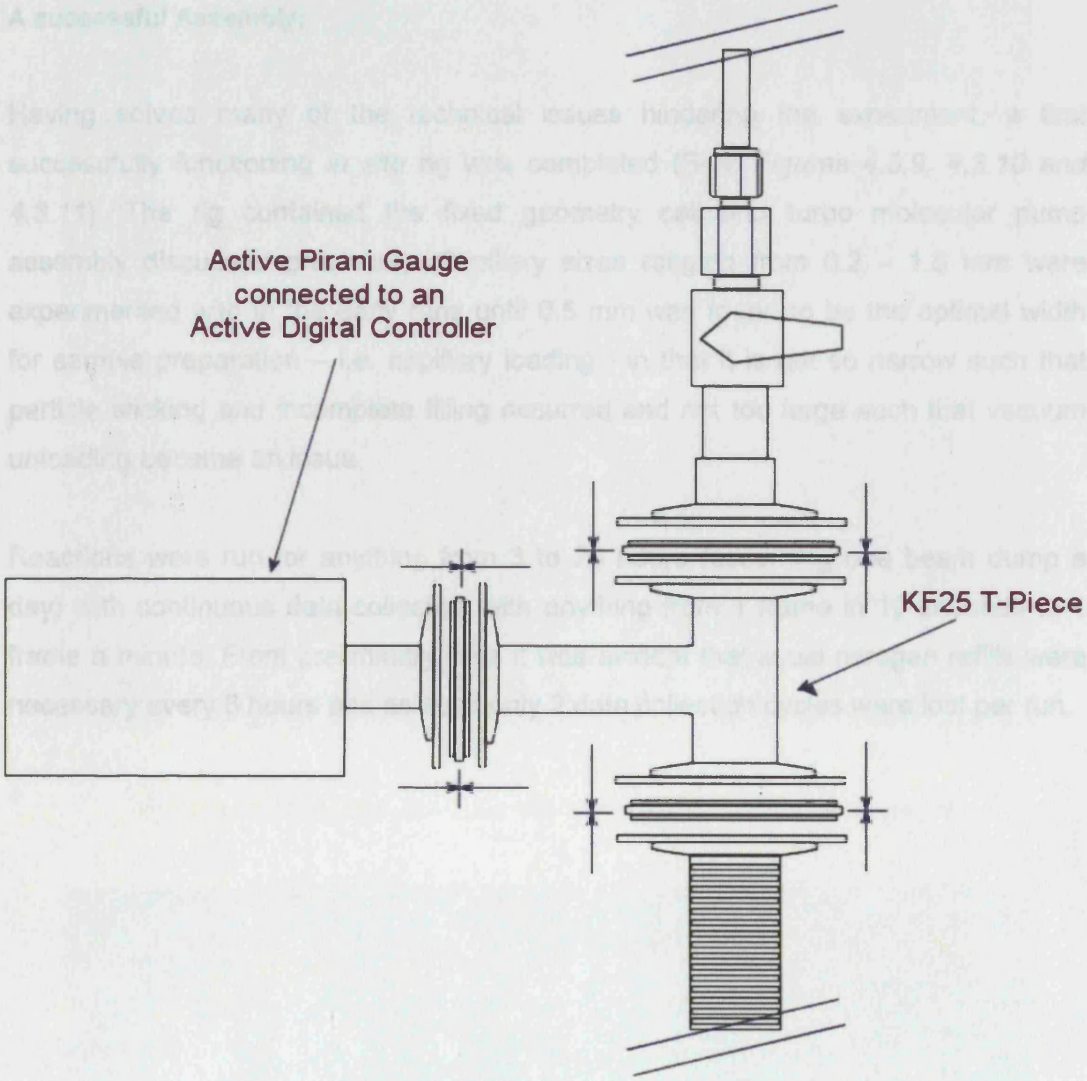

Figure 4.3.8: Diagram shows the connection from the sample environment pressure equalisation chamber to the high vacuum system. Note the positioning of an active Pirani gauge to monitor vacuum through out the experiment.

A successful Assembly:

Having solved many of the technical issues hindering the experiment, a first successfully functioning *in situ* rig was completed (See*: Figures 4.3.9, 4.3.10 and 4.3.11*). The rig contained the fixed geometry cell and turbo molecular pump assembly discussed previously. Capillary sizes ranging from 0.2 – 1.5 mm were experimented with in the early runs until 0.5 mm was found to be the optimal width for sample preparation – i.e. capillary loading - in that it is not so narrow such that particle sticking and incomplete filling occurred and not too large such that vacuum unloading became an issue.

Reactions were run for anything from 3 to 20 hours (assuming one beam dump a day) with continuous data collection with anything from 1 frame in 10 seconds to 1 frame a minute. From preliminary runs it was evident that liquid nitrogen refills were necessary every 6 hours and as such only 2 data collection cycles were lost per run.

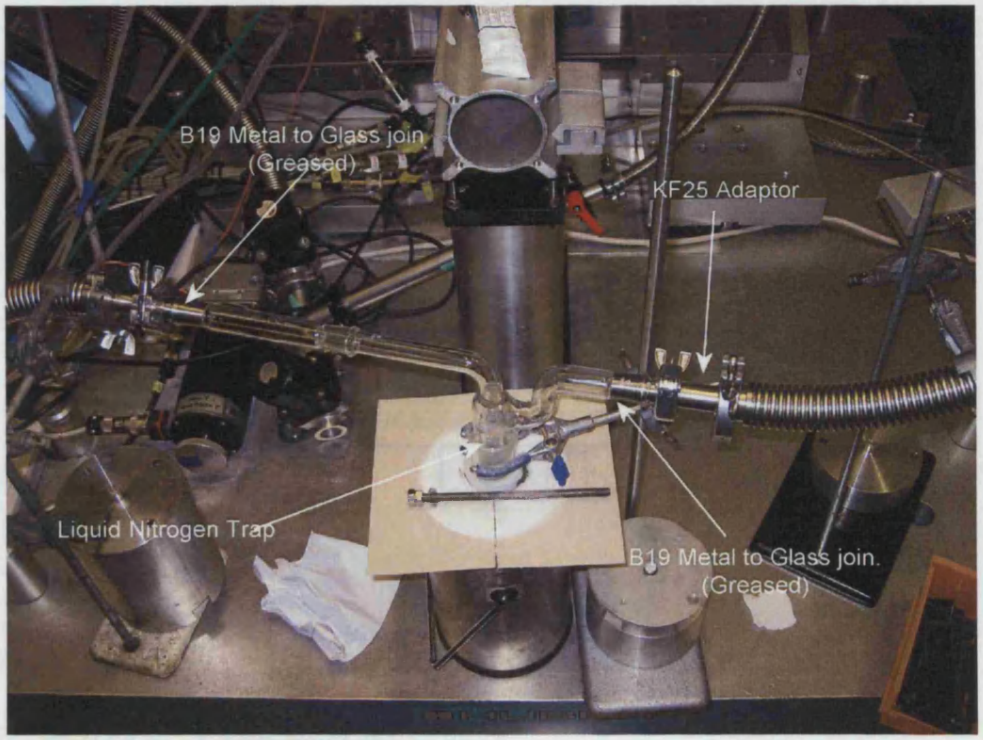

Figure 4.3.9: Diagram shows the elements of the in situ vacuum system.

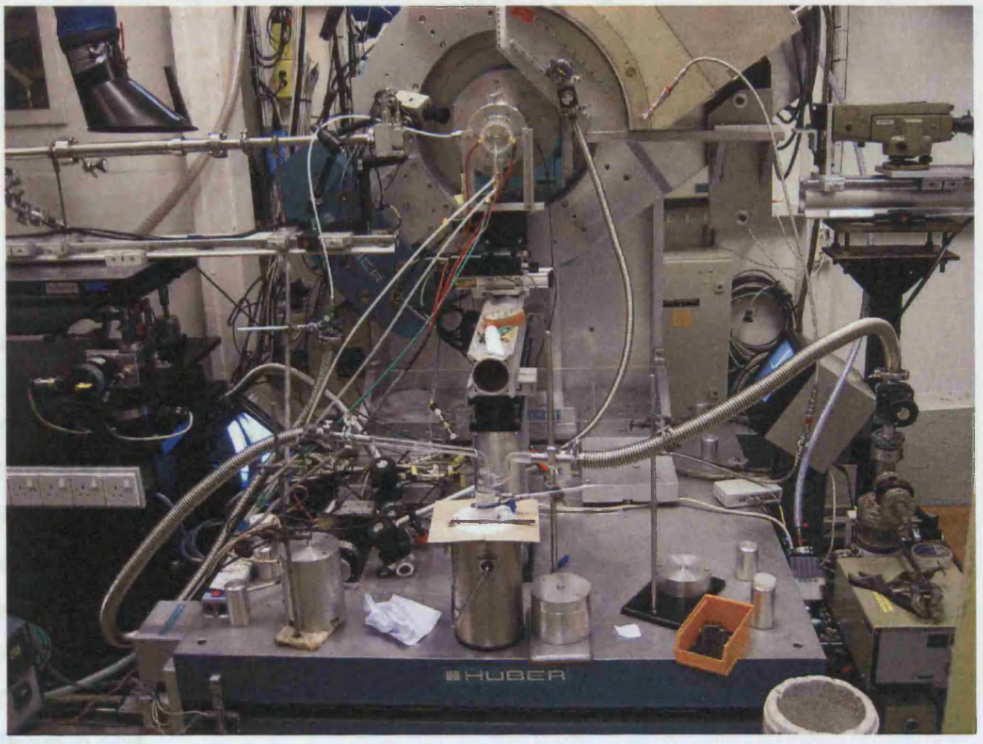

Figure 4.3.10: Diagram shows the full in situ assembly in operation at station 6.2 Daresbury.

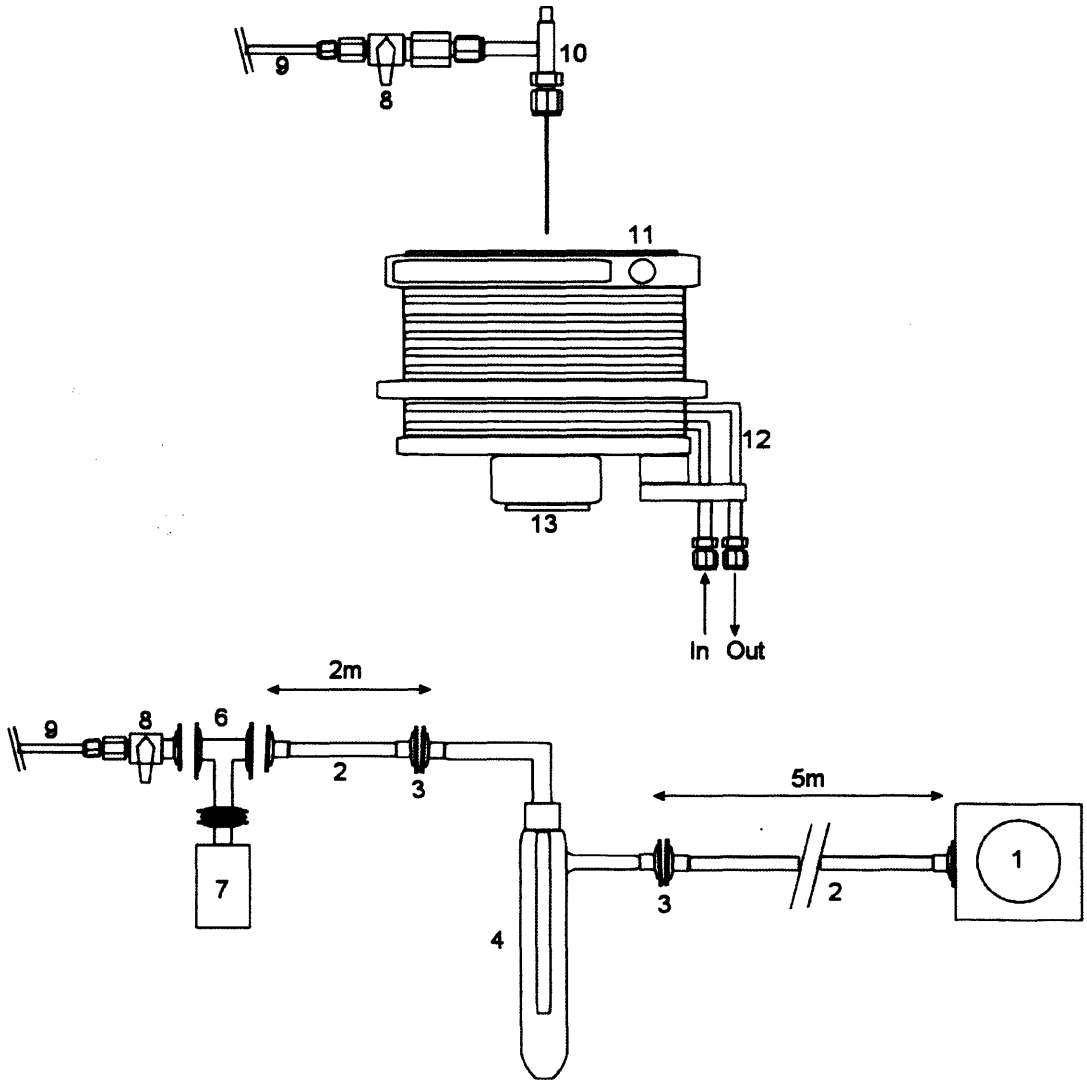

Figure 4.3.11: Diagram shows a schematic of the full in situ synthesis apparatus:

1: Turbo molecular pump

2: High vacuum metal hose

3: KF25 plate to a B19 polished metal to ground glass cone interface

4: Liquid nitrogen trap

6: KF25 T piece

7: Vacuum gauge connected to a monitoring controller

8: Teflon Swagelok taps

9: Hard plastic tubing, vacuum sealed using Swagelok ferrules

10: Capillary cell

11: Beam in port

12: Copper water cooling intake and outlet

13: Thermocouple connection point

4.4: The Furnace:

A vital feature of the experiment was the ability to deliver suitable temperature conditions to the system. The clathrate synthesis is sensitive to both reaction temperature and ramp rate at which the temperature is achieved. As such a capillary furnace was required that could be used with precise temperature control in the ranges 25°C to 700°C and ramp rates from 1°Cmin^{-1} to 200°Cmin^{-1}.

A custom capillary furnace was developed in conjunction with IMG Birkbeck[9], the Royal Institution and station 6.2 at the SRS Daresbury. The furnace was constructed from steel and brass and utilised copper-wound water cooling. It contains a central ceramic heating element that is monitored using a standard thermocouple. The beam input port utilises Kapton (polyimide) due to its flexible nature – i.e. easily attached and replaced in such custom applications – and general tensile strength versus many other thin film materials, despite its poor transmission characteristics. In addition, Kapton is relatively chemically resistant to many acids and chemical systems commonly used in solid state and autoclave based chemistries.

The furnace was controlled using a GUI interfaced Eurotherm controller, that could be accurately monitored and recorded remotely from outside the experimental hutch during the experiment. The most important feature of the system is the xyz stage onto which the furnace is mounted. This is connected to a computer in the control room of the station and so is capable of very accurate manipulation of the furnace position in relation to the mounted capillary assembly.

Figure 4.4.1: A side and bottom view of the custom built capillary furnace used at station 6.2 Daresbury.

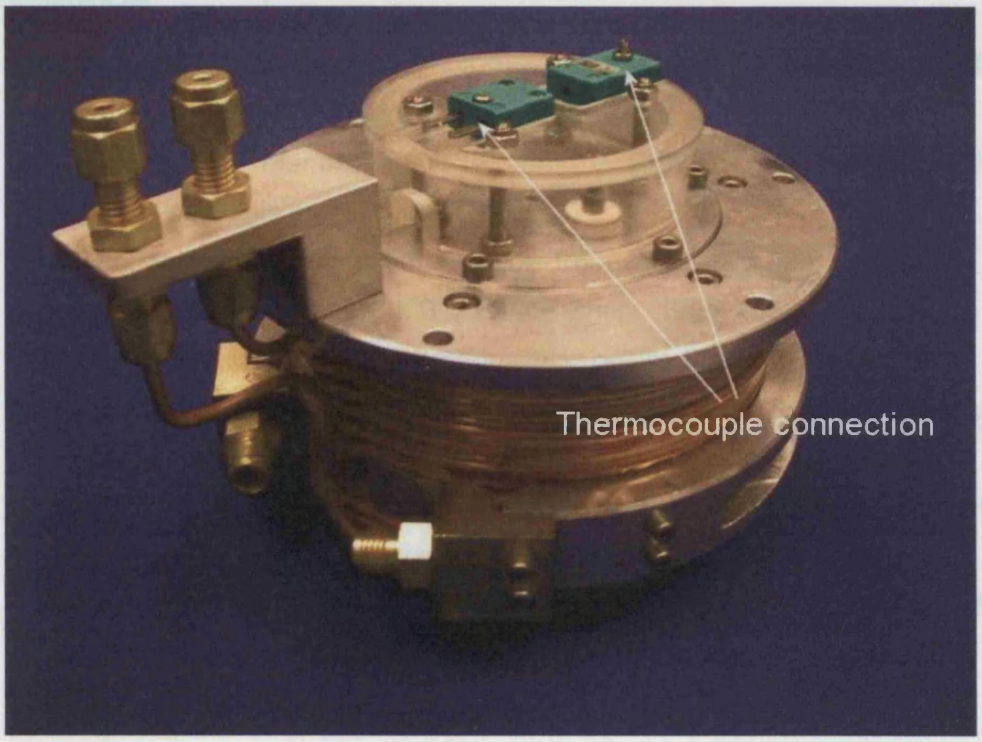

Figure 4.4.1: Side view of the custom built capillary furnace used at station 6.2 Daresbury.

4.5: References

1. Wikipedia. *Austenite*. [cited; Available from: http://en.wikipedia.org/wiki/Austenite.
2. Wikipedia. *Martensite*. [cited; Available from: http://en.wikipedia.org/wiki/Martensite.
3. AtoZofMaterials.com. [cited; Available from: http://www.azom.com/.
4. Ramachandran, G., et al., J. Solid State Chem, 1999. **145**.
5. Gryko, J., *Personal Communication*. Jacksonbille State University, 2006.
6. Berry, A., et al., Nuclear Instruments & Methods in Physics Research A, 2003. **513**: p. 260-263.
7. Helsby, W., et al., *The RAPID2 Interpolating System*. Nuclear Instruments & Methods in Physics Research A, 2003. **510**: p. 138-144.
8. website, S.b.u. *Station 6.2*. 2007 [cited; Available from: http://www.srs.ac.uk/srs/stations/station6.2.htm.
9. Strusevich, D., *PhD Thesis*. 2007.
10. H. Palancher, et al., *A cell for in situ dynamic X-ray diffraction studies: Application to the dehydration of zeolite SrX*. Journal of Applied Crystallography, 2005. **38**: p. 370-373.
11. Norby, P., et al., *A reaction cell for in situ studies of hydrothermal titration*. Journal of Applied Crystallography, 1998. **31**: p. 481-483.
12. Puxley, D.C., G.D. Squire, and D.R. Bates, *A New Cell for In Situ X-ray Diffraction Studies of Catalysts and Other Materials under Reactive Gas Atmospheres*. Journal of Applied Crystallography, 1994. **27**: p. 585-594.
13. Andreasen, J., W, et al., *An in situ cell for small-angle scattering experiments on nano-structured catalysts*. Journal of Applied Crystallography, 2003. **36**: p. 812-813.
14. Gray, E., D. Cookson, J, and T. Blach, P, *X-ray diffraction cell for studying solid-gas reactions under gas pressures to 100 bar*. Journal of Applied Crystallography, 2006. **39**: p. 850-855.
15. Brunelli, M. and A. Fitch, N, J, Synchrotron Rad., 2003. **10**: p. 337-339.

Chapter 5

Synthesis study of Na_8Si_{46} clathrate I using *in situ* synchrotron x-ray diffraction

5.1 Introduction

The clathrate family of solids have now been synthesised to exhibit a wide range of properties including; insulators, semiconductors, metals, superconductors, thermoelectrics among many others. In all of these cases the materials are strongly influenced by both stoichiometry of the framework and the guest species and its residency, but despite this there are no papers published in the literature on the mechanism of formation and growth of the solid state clathrates. The scant information that may be found is often in the form of anomalous facts about the materials, which suggest the relationship between framework and guest species during formation. The first information that may be gleaned is from Klemm's thermogravimetric analysis work, the suggestion that on heating of NaSi and NaGe, cubic materials result which contain a reduced guest species stoichiometry[1].

The work of Ramachandran and Gryko *et al*[2, 3] showed deintercalation of type II clathrates was possible down to low guest species compositions, where as the deintercalation of the type I clathrates was attempted but failed; these results bring some intriguing conclusions. On deintercalation of the type II systems it is found that the small polyhedra - the 20 atom pentagonal dodecahedron - are first to deintercalate[3]. There are a number of conclusions that can be arrived at in this instance; the first is that repulsive interactions may be more apparent in the smaller cage due to a closer approach between guest and framework, though this is somewhat refuted by the work of Bridges[4], that suggests that even for larger, more electron dense systems, *off-centre displacement* and weak guest to framework interactions may occur.

The second interpretation that may also be gleaned on consideration of the work of Bridges[4], is the possibility of the favourable interaction occurring between guest and framework in the large 28 atom hexakaidecahedra, possibly due to a lower stability resulting from the stronger deviation of the tetrahedral angles in the large polyhedra[4]. These two pieces of information pose interesting questions about the formation of clathrate if considered with the conclusions of Klemm's work.

Though the type II systems (Na_XSi_{136}, where X = 0~24) have been shown to exhibit deintercalation under vacuum heating[5-7], thus far the type I systems have not been shown to exhibit a stoichiometry of less than 8 for the guest species. In this instance, there are again a couple of conclusions that may be considered; the first is the

possibility that it is less energetically favourable for the guests to leave the system, due to higher electronic effects caused by the slightly higher structural density, that results from the presence of small polyhedra within the structure. The second possibility is that the guest species are evident in stabilisation of the system, by electronic means and thus loss is energetically unfavourable. If the second possibility was a reality, what might the implications be for the mechanism of formation for Na_8Si_{46} from NaSi?

The general lack of research on the mechanism of formation, and the questions posed by the results discussed here, provided the impetus for the desire to study these reactions *in situ*. The reality of the stoichiometries of both guest species and framework species, on the properties found in the clathrates, leads to the desire for accurate composition control in synthesis of these materials. The mechanism of formation being unknown, and thus the role of the guest atom loss being uninvestigated - in terms of formation - suggests in-depth study of these materials and elucidation of the mechanism of formation would be valuable in synthetic control.

5.2: Experimental Evaluation

The realisation of an *in situ* congener of the laboratory experiment was to be a complex engineering problem (*see Chapter 4*). The possibility of having an exact copy becomes low when you consider the make up of station 6.2 at Daresbury. As such, consideration of the data cannot reasonably be attempted without consideration of the limitations of the experiment versus the laboratory.

The main issues that were vital in recreating the laboratory experiment were; the vacuum supplied to the sample, ramp rate of heating, temperature, duration of heating versus data collection volume/regularity and sample environment.

In the *in situ* experiments the least problematic issues were the ramp rate and target temperature. The custom made furnace (*see Chapter 4*) was capable of heating at anything between $1°Cmin^{-1}$ and $200°Cmin^{-1}$, and was capable of temperatures up to 900°C, far beyond what is necessary in these experiments. The duration of heating was limited only by the number of frames of data taken per minute, since the station was only able to save 1024 patterns per experimental run. The result of this was to use variable collection of patterns i.e. such that the first hour was covered by two

patterns per minute but the reminder of the experiment i.e. crystallization of the phase not transformation, would be covered by one pattern per minute.

The sample environment used in the experiments was determined purely by beam penetration characteristics (i.e. λ dependent), given that the use of a wavelength of 1.4Å results in high absorption of the x-rays. The beam at station 6.2 is only capable of passing through around 1.5mm in diameter of SiO_2 glass and thus the experiment was limited to this dimension. In the laboratory, it is typical to use glass tubing of around 10-15 mm (up to 25mm) in diameter such that high vacuum is applied to the sample for removal of the guest species on heating. This limitation proves particularly troubling, in that it is very probable that the vacuum provided to the sample would be constituted only by a vacuum gradient across the capillary neck, and thus the sample would not receive full vacuum versus the laboratory set up. The issue of λ dependence in particular would provide considerable limitations on the scope of the experiment, which will be discussed later.

A further issue arises with such fine and fragile sample environments i.e. the use of both high vacuum and the volatilisation of sodium in the presence of 10μm thick SiO_2 glass. A common occurrence in the experiment - after several hours of exposure of volatised sodium - was for the capillary to break at the first cool region outside the furnace, as the sodium permeated and attacked the glass.

The vacuum also imposed other experimental limitations, the consideration of which, are vital in terms of data analysis. Rotating seals were found to be unsuitable for high vacuum application early on in the study, and so the assembly was modified for static use. This solution provided excellent vacuum in the system and the best chance of success for the experiments, however, increased the possibility of preferred orientation issues in the data, which would have been reduced by sample rotation. This trade-off was to make the experiment possible but would result in more problematic data analysis.

In conclusion, though there are a number of inconsistencies in comparison to the laboratory experiment, realisation of this complex experiment has been relatively successful in technical terms.

5.3: The Formation of Na_8Si_{46} from NaSi

For the *in situ* synthesis experiments NaSi was the precursor material of choice. The reason for this is that is can be induced to form both the clathrate I and II structures, by variation of the experimental conditions. In addition, the nature of the silicon clathrates containing sodium has been studied extensively in the literature[2, 3] making it an ideal candidate for mechanistic studies.

The reaction uses NaSi, a monoclinic structure of ionic nature that is composed of Si_4^{4-} Tetrahedra, which are essentially composed of three-coordinate silicon atoms each with a lone pair, residing in a matrix of Na^+ ions. The reaction forms the clathrate I, Na_8Si_{46}, a primitive cubic structure composed of four-coordinate silicon atoms arranged in tetrahedra which are covalently bonded. Sodium atoms reside in the structure within the tetrakaidecahedral and pentagonal dodecahedral cages, formed by connection of the silicon tetrahedra, and are neutral.

For the reaction to progress, the Na^+ ions must be reduced to Na^0 such that a stoichiometric change from NaSi ~ 1:1, to Na_8Si_{46} ~ 1:5.75 is possible. In this consideration, it becomes obvious that the oxidation of Si atoms and the loss of balancing Na^+ charges then facilitate the joining of silicon tetrahedra to dissipate growing charge imbalance in the system as sodium loss continues. The system undergoes transformation from an ionic, low symmetry solid to a high symmetry structure of predominantly covalent character.

On examination, it is hard to perceive that any structural relationship exists between these two materials, so evident are the differences in both structure and particularly chemistry. A mechanistic transformation between the two would conceivably be predicted to occur via loss of the NaSi structure into an amorphous melt or semi-melt, followed by the formation of the clathrate structure from this melt.

Some information about phase transformation in the solid state may be gleaned from Landau theory of displacive phase transitions. Landau predicts that the structure at high temperature will reside at the maximum possible volume and that any distortion or structural reordering will result in collapse and volume reduction that will be limited by short-range repulsive interactions[8]. Examples of structural transformations studied by means of the Landau theory have observed subtle reordering of structural units such as to balance excess charge and steric (geometrical) strain[8, 9], which

ultimately results in a displacive phase transition occurring, as the only means by which all structural units may achieve and balanced and ordered state.

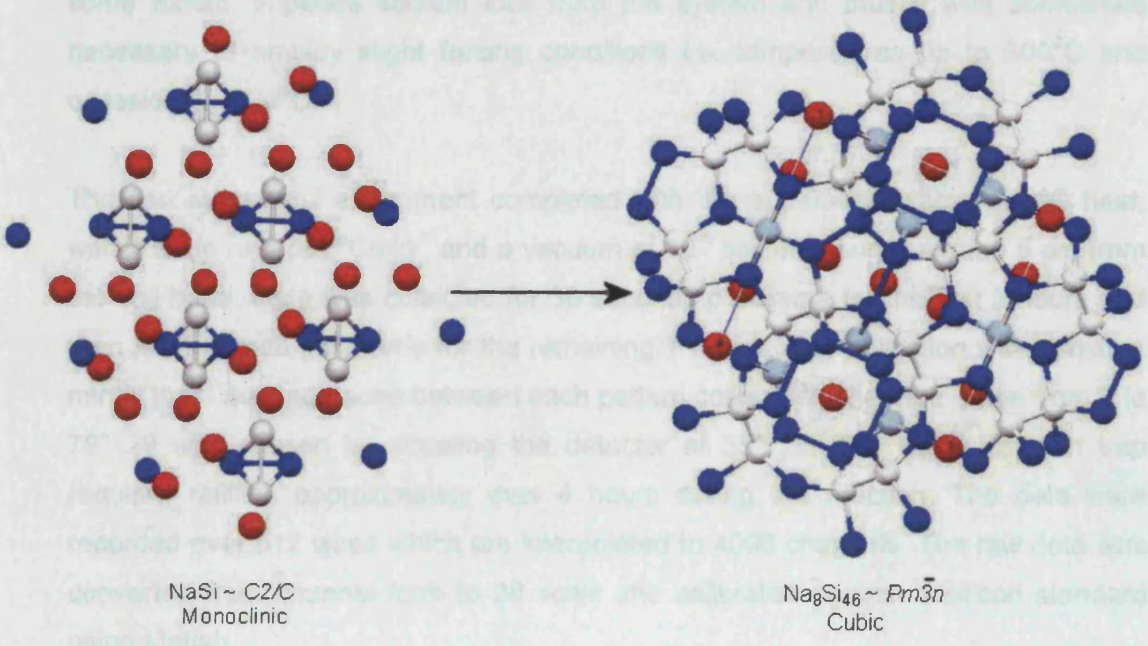

Figure 5.3.1: The structures of NaSi and Na_8Si_{46} showing the transformation occurring in the reaction.

5.4: Analysis of the Transition from NaSi to Na_8Si_{46}[10, 11]

In section 5.2, discussion of the limitations of the experimental set up made clear the issues associated with preferred orientation in these experiments. It is for this reason that many of the syntheses carried out during these studies produced data that was unusable or marred by the presence of periods of data that show strong preferred orientation issues. The most routinely exhibited problem was that of the occurrence of silicon crystallites. Silicon is an inevitable impurity of the reaction occurring in this experiment and as such, a pure starting material may develop a silicon impurity as the reaction proceeds. This causes very high intensity silicon peaks, which mask out the intensity of the reactant peaks thus rendering the data unusable. As such, with limited beam time it was difficult to produce with any certainty, an array of data sets with coverage across all reaction conditions.

In the initial experiments, low ramp rates (2-10°Cmin^{-1}) were used for the best possible chance of observing the reaction. In addition, low dwell temperatures were

also employed in the early experiments - again to give the best chance of slow reactions - however it became evident that the confined reaction environment to some extent, impedes sodium loss from the system and thus it was sometimes necessary to employ slight forcing conditions i.e. temperatures up to 500°C and occasionally 600°C.

The first successful experiment completed with the apparatus, was a 500°C heat, with a ramp rate of 8°Cmin^{-1} and a vacuum of 10^{-4} bar, measured around 5 cm from the cell head. Data was collected for 30 seconds per frame for the first 3 hours and then for 1 minute per frame for the remaining 7 hours; data collection was constant minus the 1 second pause between each pattern collection. The data range from 5 to 70° 2θ was chosen by situating the detector at 35° 2θ. The liquid nitrogen trap required refilling approximately ever 4 hours during the reaction. The data were recorded over 512 wires which are interpolated to 4096 channels. The raw data was converted from channel form to 2θ scale and calibrated against a silicon standard using Matlab.

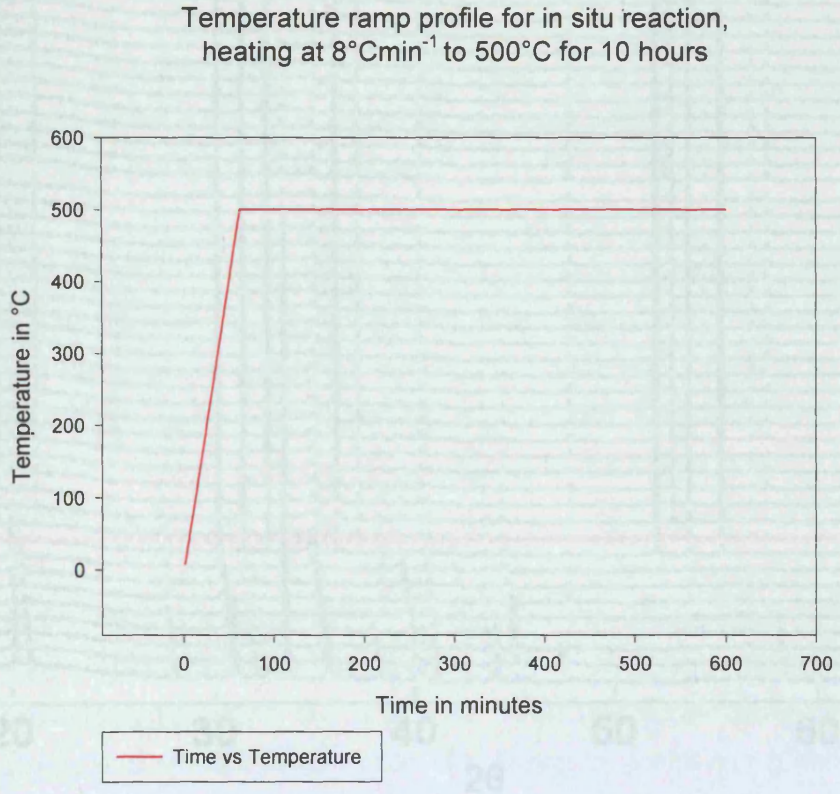

Figure 5.4.1: The diagram shows the temperature ramp profile used in the reaction.

The first examination of the data was most commonly done visually using Matlab to stack-plot multiple datasets (see *Figure 5.4.2*). The data shown in *Figure 5.4.2*

represent 7.5 minutes between each pattern i.e. every 15th pattern is shown; displaying the data in this fashion is a good visual tool to ascertain if a reaction has occurred. If the data are examined closely, it can be seen that the reaction begins with NaSi in crystalline form and as heating begins the silicide undergoes a strong thermal expansion ($4.54 \times 10^{-5}\ °C^{-1}$).

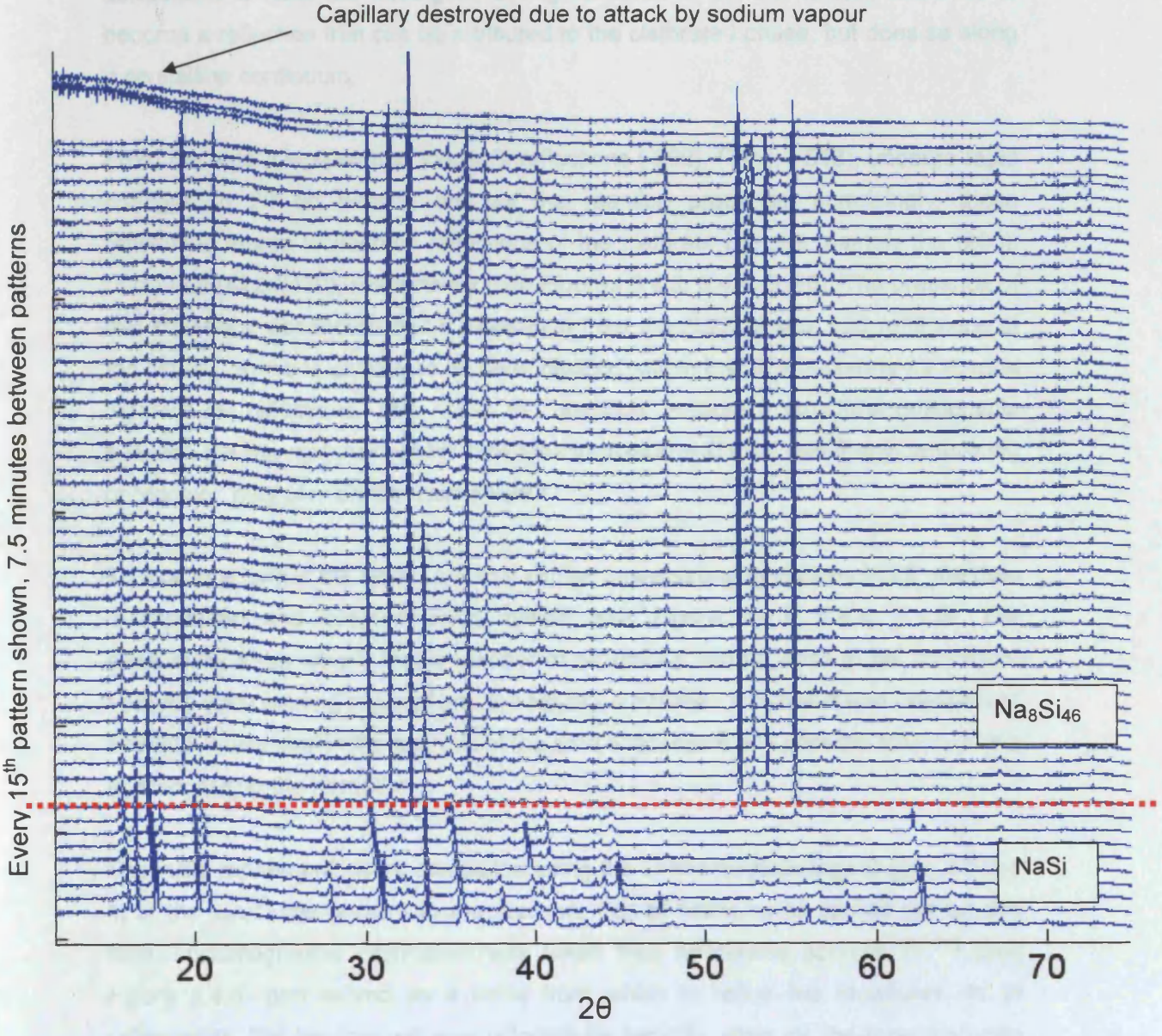

Figure 5.4.2: The diagram shows every 15th pattern in a stacked plot for NaSi to Na_8Si_{46} at 500°C, 8°Cmin^{-1} and 10^{-4} bar vacuum. Spacing between patterns represents 7.5 minutes.

NaSi continues to expand until around 60 to 68 minutes (marked by the dashed red line on *Figure 5.4.2*) into the reaction, during which time it becomes evident that clathrate is forming and is shortly becoming crystalline. The striking thing that is evident when viewing the data in this way is the absence of an amorphous region or loss of the monoclinic structure as heating occurs, such that the structure of NaSi is lost and clathrate formation can begin. Further more, on close examination some of the reflections appear to exhibit "lock-ins", in that a reflection begins as being attributable to NaSi but undergoes strong deviation of 2θ, and is then observed to become a reflection that can be attributed to the clathrate I phase, but does so along a crystalline continuum.

From the data it is seen that the NaSi reflections (-202), (311), (-513), undergo rapid changes in 2θ on heating and as the reaction proceeds, surprisingly, these reflections merge to become reflections of the clathrate I phase, namely the (200), (321) and (422)/(430), respectively (*see Figures 5.4.3, 5.4.4, 5.4.5*). The presence of this crystalline continuum of *hkl* reflections from the NaSi phase, into reflections of the Na_8Si_{46} phase is unlikely to be serendipitous, given that it is occurring for several different *hkl* reflections. This raises the question; is there a structural relationship between the two materials which facilitates formation and what role if any, templating or "epitaxy" may play on the mechanism?

To examine further the reflections that exhibit these strong deviations in 2θ, the data is expanded and zoomed using matlab (see *Figure 5.4.3, 5.4.4, 5.4.5*). The expansions show clearly that a number of reflections can be seen to be "locked-in" from the NaSi starting material and the Na_8Si_{46} clathrate. This result was unexpected and thus it was vital in the analysis of the data to assess if any possible structural link existed, during the formation.

The initial refinements were completed using the Lebail methodology to gain a basic fit of the structures present in the reaction. For all refinements carried out on this data, crystallographic information was taken from references sources [2], [12] (see *Figure 5.4.6*) and served as a basis from which to refine the structures. In all refinements, the background was selected by hand to allow for the most accurate refinement possible. Having ascertained the main parameters of the structure by Lebail refinement, the parameters were then used to create a ".pcr" file for use with Fullprof for a Rietveld refinement. The use of Rietveld methods is vital in this study

due to its ability to elucidate atomic position, which would be vital in understanding this reaction.

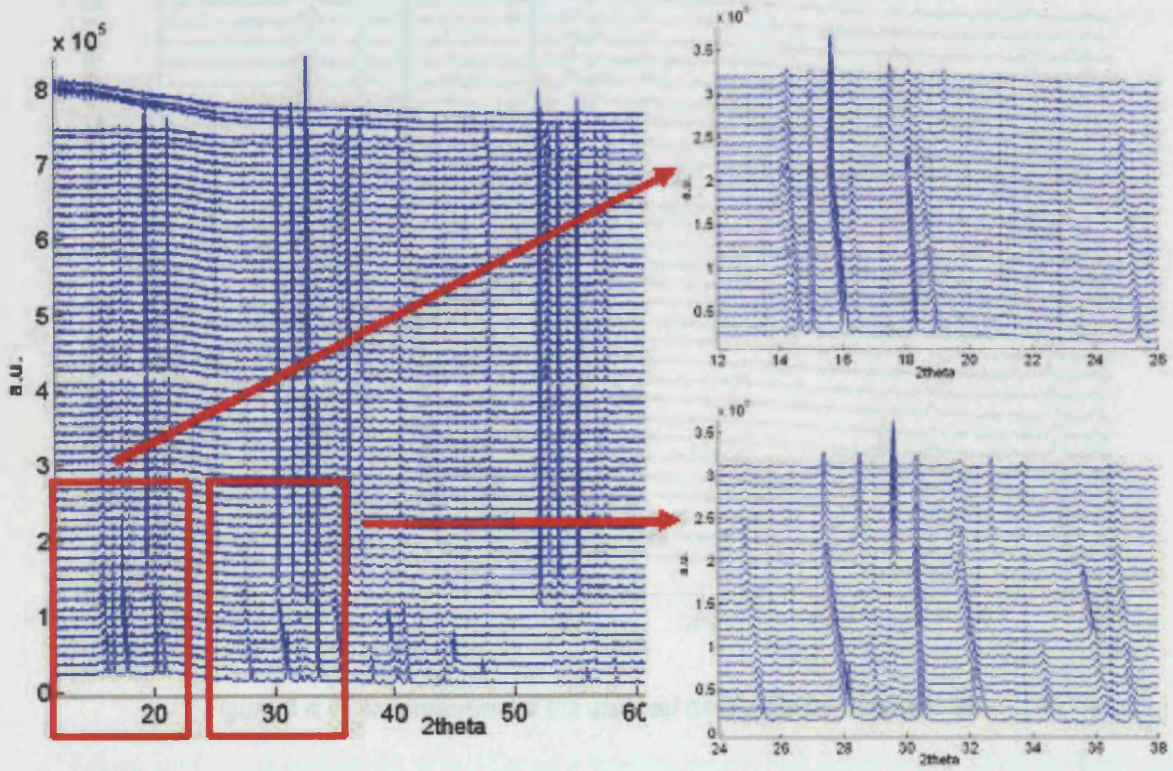

Figure 5.4.3: The diagram illustrates regions which exhibit related reflections for the reaction of NaSi to form Na_8Si_{46}. The expansion regions will be considered in detail later.

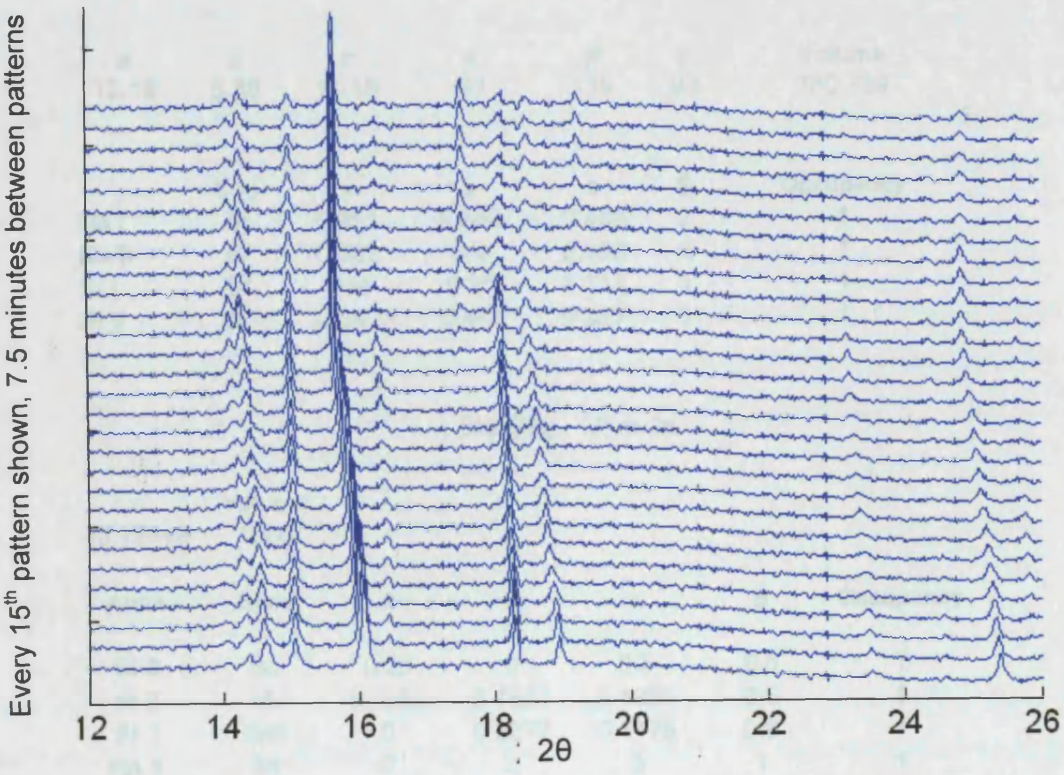

Figure 5.4.4: An expansion of the stacked data plots from 12-26° 2θ.

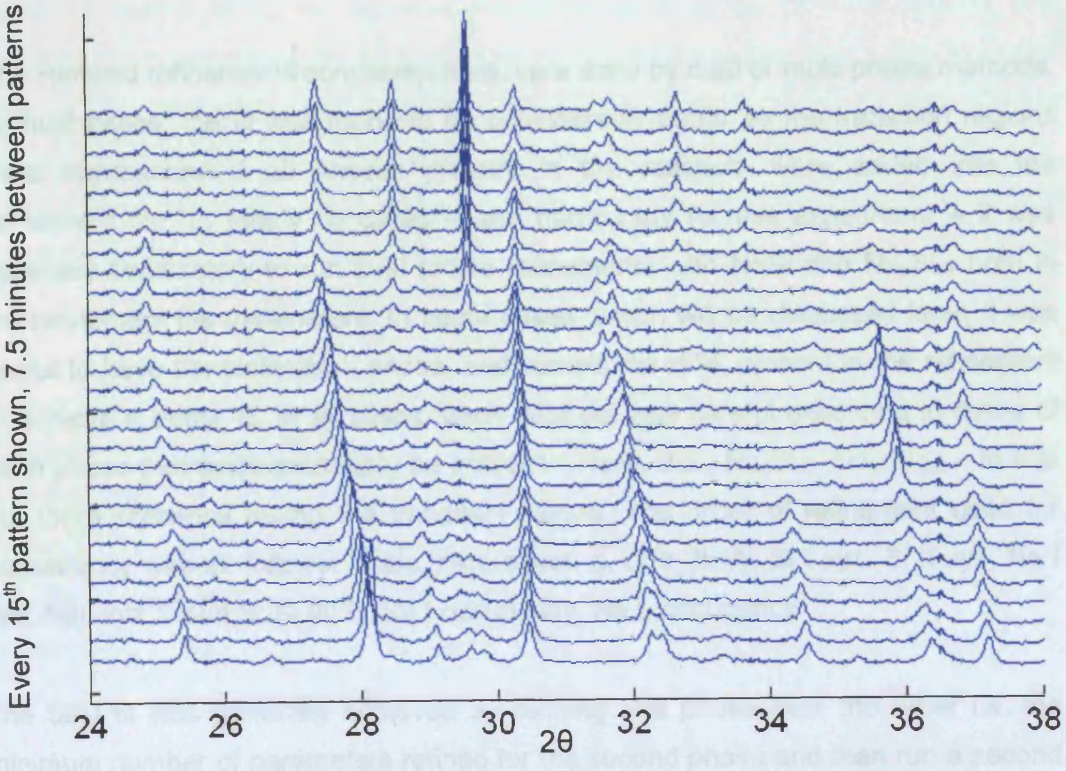

Figure 5.4.5: An expansion of the stacked data plots from 24-38° 2θ.

NaSi ~ C2/c

a	*b*	*c*	*α*	*β*	*γ*	Volume
12.19	6.55	11.18	90	119	90	780.739

	Site	x	y	z	B	Occupancy
Na I	8*f*	0.351	0.662	0.358	2	1
Na II	8*f*	0.632	0.9	0.455	2	1
Si I	8*f*	0.44	0.21	0.314	1	1
Si II	8*f*	0.597	0.463	0.357	1	1

Na_8Si_{46} $P\,m\,\bar{3}n$

a	Volume
10.19648	1060

Atom	Sites	*x*	*y*	*z*	B	Occupancy
Si 3	6*c*	0.25	0	0.5	0.6	1
Si 2	16*i*	0.1851	0.1851	0.1851	0.6	1
Si 1	24*k*	0	0.3077	0.1175	0.6	1
Na 1	2*a*	0	0	0	1	1
Na 2	6*d*	0.25	0.5	0	3	1

Figure 5.4.6: Crystallographic data used as a starting point for all refinements. (Top) Sodium silicide [12], (Bottom) Clathrate I [2].

The Rietveld refinements completed here were done by dual or multi phase methods. In most cases, the fit was found to be considerably better as the transition regions were approached if all phases present in the reaction, were added into the refinement file. In nearly all cases – and particularly for this experiment – it was generally satisfactory to run dual phase refinements with NaSi and Na_8Si_{46} both in the refinement file parameters. In some cases, which will be discussed later, it was useful to have the clathrate II phase, and sometimes *d*-Si, present in the refinement to achieve a better fit. In all cases, each data set was careful examined in terms of each phase that could potentially be present – NaSi, *d*-Si, Na_8Si_{46}, $Na_{24}Si_{136}$ – to rule out there presence during the transition stages. The order of refinement used for consistency was as follows: Scale, zero offset, a, b, c, β, W, Si I xyz, Si II xyz, Na I xyz, NaII xyz, NaI/II B, Si I/II B, Na I occupancy, Na 2 occupancy.

The best fit was generally achieved by refining one phase over the other i.e. the minimum number of parameters refined for the second phase and then run a second

refinement of the same data set, refining in favour of the second phase. This was necessary for these systems due to a degree of overlapping of peak positions – using such methods do however require considerable care to ensure the refinement is assigning the correct positions and intensities for overlapping peak positions. The practise of completing two refinements on each data set allowed for a far better fit and a considerably clearer picture of what is occurring in the reaction.

The dual refinement methodology has the consequences of splitting the reaction into two refinement regions that marginally overlap. The first stage during heating is the refinement for NaSi; the second is the refinement of Na_8Si_{46} during its formation and crystallisation (*see Figure 5.4.2*).

5.4.1: Sodium Silicide

The data region for NaSi spans from ambient until around pattern 170, which corresponds to 97.5 minutes. Full temperature is reached in the reaction at around 65 minutes given $8°Cmin^{-1}$ for the 500°C synthesis dwell temperature.

During the early stages of the experiment some peak distortion is evident for some sodium sensitive peaks, as non stoichiometric sodium is lost from the system. The result of this is that some low-angle sodium sensitive peaks start with a high intensity, and as heating commences this effect reduces as excess sodium is loss into the vacuum system; this effect can be seen for the 28° 2θ reflection (see *Figure 5.4.5*). The result of this effect was to make it more suitable to begin the refinement work at pattern 19 which falls 9.5 minutes into the heating phase and represents approximately 76°C (*see Figures 5.4.1.1 and 5.4.1.2*).

At this first data point it is important to note the difference plot and intensity issues present in the refinement. It is clear from pattern 19 that there are issues associated with fitting peak intensities, which are related to preferred orientation as a result of the lack of rotation of the sample. For all Rietveld refinements of the NaSi region of the synthesis, 24 parameters were refined between 9 and 68° 2θ and refined consistently in the same order (see *Figure 5.4.1.1*). (As stated previously the order of refinement used for consistency was as follows: Scale, zero offset, a, b, c, β, W, Si I xyz, Si II xyz, Na I xyz, NaII xyz, NaI/II B, Si I/II B, Na I occupancy, Na 2 occupancy).

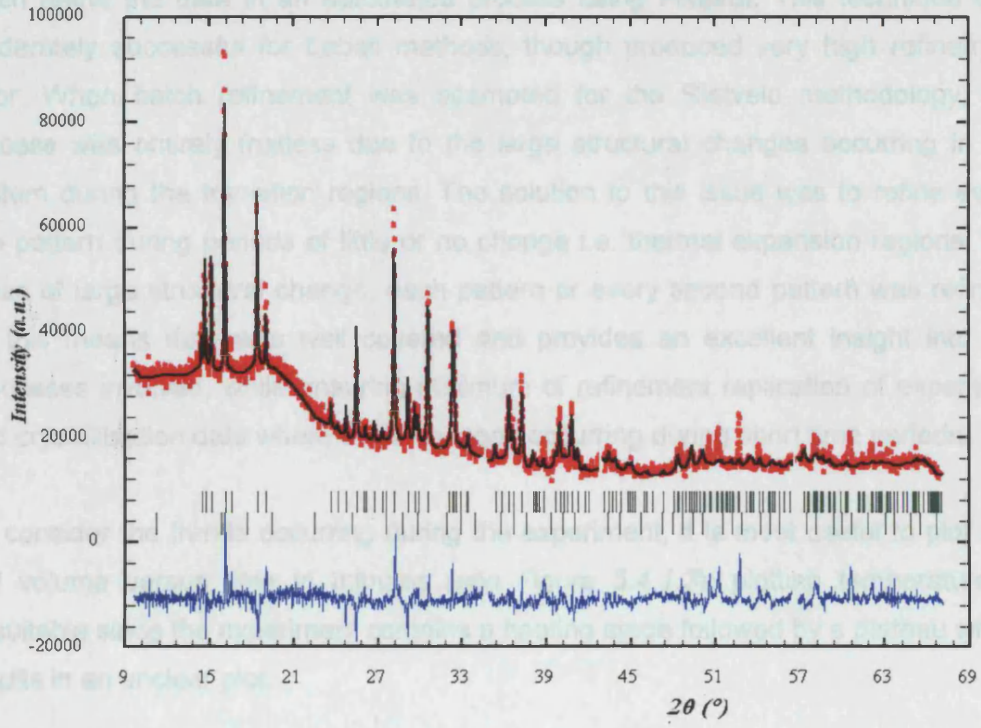

Figure 5.4.1.1: Rietveld refinement for pattern 19 for Sodium silicide, at around 9.5 minutes into the experiment at approximately 76°C (χ2: 79.0, Rwp: 41.3).

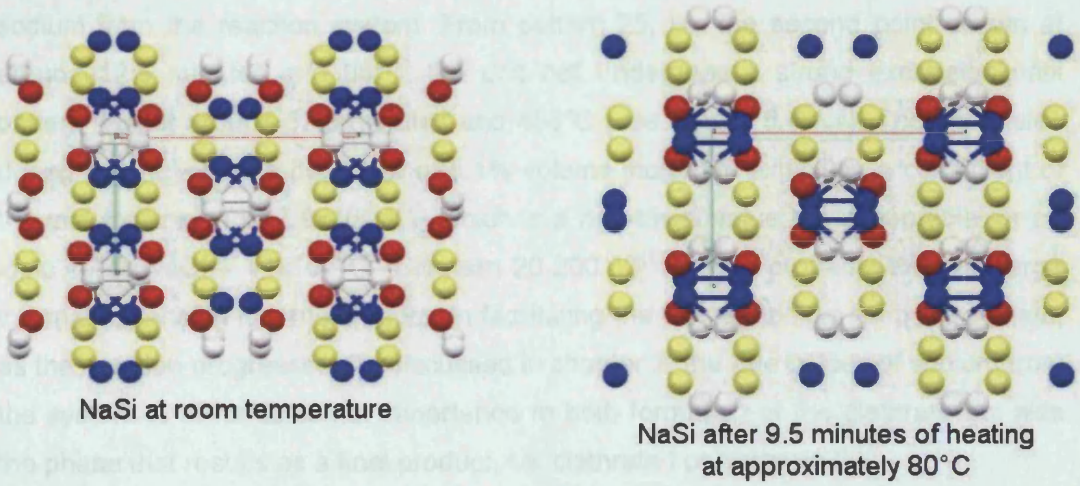

Figure 5.4.1.2: Structural comparison of sodium silicide at room temperature (left) and for pattern 19 at 76°C during heating (right). Thermal expansion is already evident in the structure even at low temperatures. (Si1 = white, Si2 = blue, Na1 = red, Na2 = yellow).

Due to the sheer volume of data collected in each experiment, it was desirable to batch refine the data in an automated process using Fullprof. This technique was moderately successful for Lebail methods, though produced very high refinement error. When batch refinement was attempted for the Rietveld methodology, the process was entirely fruitless due to the large structural changes occurring in the system during the transition regions. The solution to this issue was to refine every fifth pattern during periods of little or no change i.e. thermal expansion regions. For areas of large structural change, each pattern or every second pattern was refined. By this means data was well covered and provides an excellent insight into the processes involved, while ensuring minimum of refinement replication of expansion and crystallisation data where small changes occurring during short time periods.

To consider the trends occurring during the experiment, it is most useful to plot unit cell volume versus time in minutes (*see Figure 5.4.1.3*); plotting temperature is unsuitable since the experiment contains a heating stage followed by a plateau which results in an unclear plot.

The data shown in *Figure 5.4.1.3* starts at the previously discussed point around 9.5 minutes into heating, at approximately 76°C. The initial strong expansion between the first two points is the result of the final stages of the loss of non stoichiometric sodium from the reaction system. From pattern 25, i.e. the second point shown at around 12.5 minutes and 96°C, the unit cell undergoes a strong expansion until pattern 115 at around 57.5 minutes and 456°C (*see Figure 5.4.1.4*). The expansion during this region is in the order of 5.1% volume increase, exhibiting a coefficient of thermal expansion of 7.9×10^{-5} K^{-1}, which is a non-trivial value but acceptable for an ionic solid (NaCl = 44×10^{-6} $°C^{-1}$ between 20-200 °C[13]). It is probable that this large thermal expansion is a major factor in facilitating the loss of sodium from the system, as the reaction progresses. As discussed in chapter 2, the rate of loss of sodium from the system is of fundamental importance to both formation of the clathrate but also the phase that results as a final product, i.e. clathrate I or clathrate II.

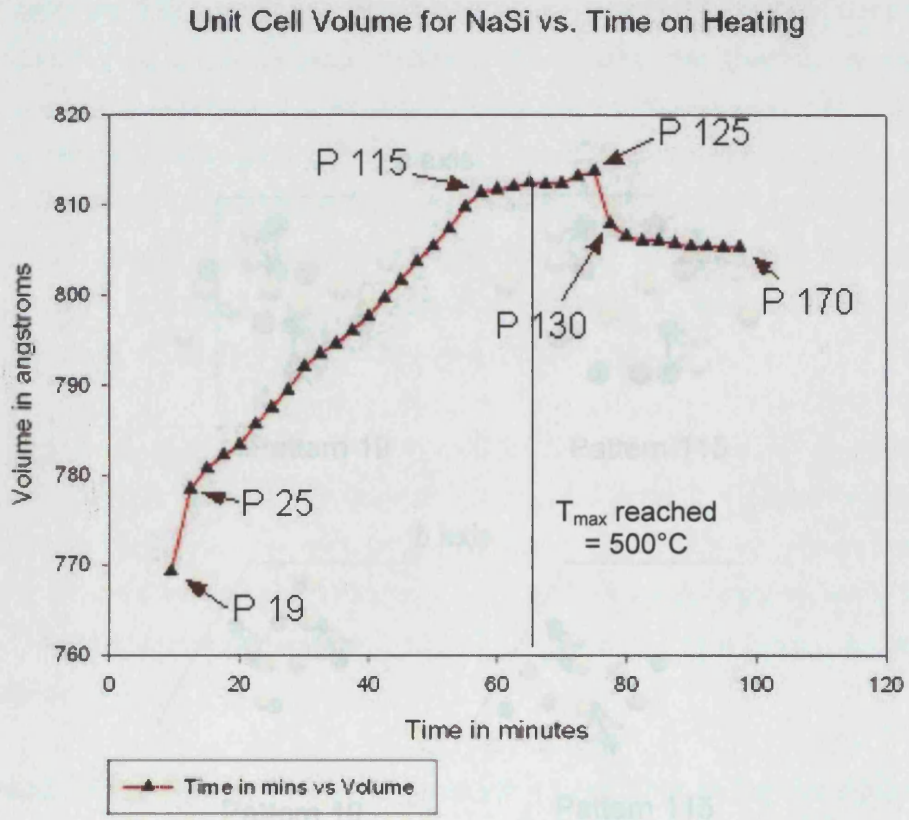

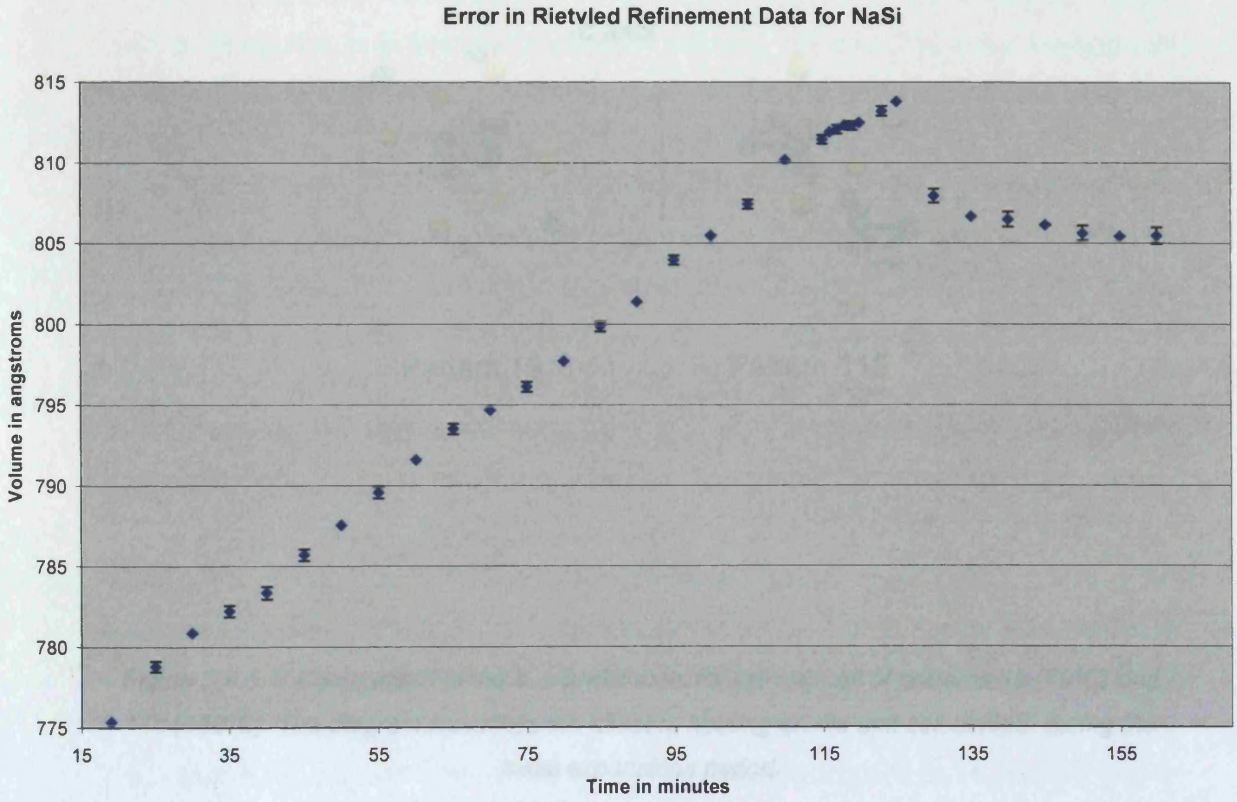

Figure 5.4.1.3: (Top) Unit cell volume in Å^3 for sodium silicide during heating and the reaction to form clathrate I. P19 = 76°C, P25 = 96°C, P115 = 456°C, P125 = 500°C, P130 = 500°C, P170 = 500°C. (bottom) Shows error in the NaSi Reitveld refinements.

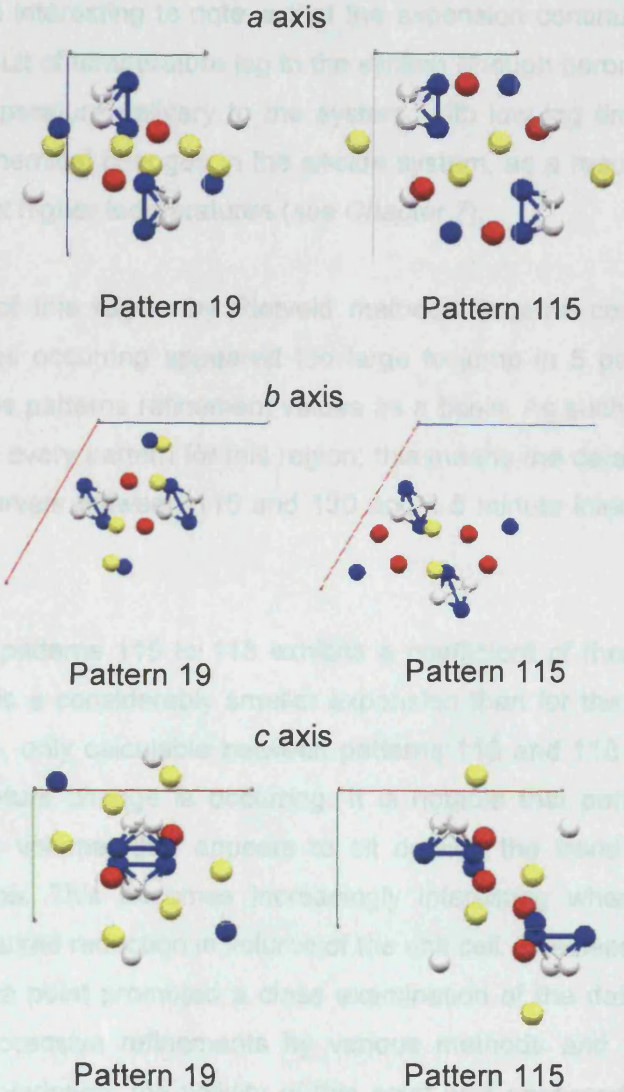

Figure 5.4.1.4: Comparison of the a, b and c axes for the unit cell of patterns 19 (76°C) and 115 (456°C). The diagram illustrates the affect of heating on the unit cell of NaSi during the initial expansions period.

From patterns 115 to 123 the expansion plateaus and the system continues to expanded but at a considerably reduced rate. During this heating region at 65 minutes into the experiment at pattern 118, the full reaction temperature of 500°C is reached. What is interesting to note is that the expansion continues past this point; this may be a result of temperature lag in the system (though boron nitride calibration shows rapid temperature delivery to the system, with low lag time); alternatively it may be due to chemical changes in the silicide system, as a result of the increased sodium mobility at higher temperatures (*see Chapter 7*).

The refinement of this region by Rietveld methods became complex, in that the structural changes occurring appeared too large to jump in 5 pattern steps, when using the previous patterns refinement values as a basis. As such, it was necessary to refine patterns every pattern for this region; this means the data region is covered in 30 second intervals between 115 and 120 and 1.5 minute intervals between 120 and 125.

The region from patterns 115 to 118 exhibits a coefficient of thermal expansion of 4.8×10^{-6} k^{-1}, this is a considerably smaller expansion than for the preceding region. This is, of course, only calculable between patterns 115 and 118 since beyond this point no temperature change is occurring. It is notable that pattern 125 shows a marginal jump in volume, that appears to sit outside the trend occurring for the preceding patterns. This becomes increasingly interesting when considering the following, very marked reduction in volume of the unit cell. The seemingly out of trend nature of this data point promoted a close examination of the data collected in this pattern. After successive refinements by various methods and careful parameter refinement order variation, the validity of this point was assessed and shows good agreement with the data points before and after it and therefore appears not to be in error.

The observations seen in this region are in good agreement with Landau theory for displacive phase transitions, in that the structure at temperature will reside at maximum volume. Landau theory also predicts that any distortion or reordering of the structure will result in lowering of the volume until short-range repulsive interactions halt volume reduction[8]. These observations do indeed appear to be evident in this reaction system for NaSi.

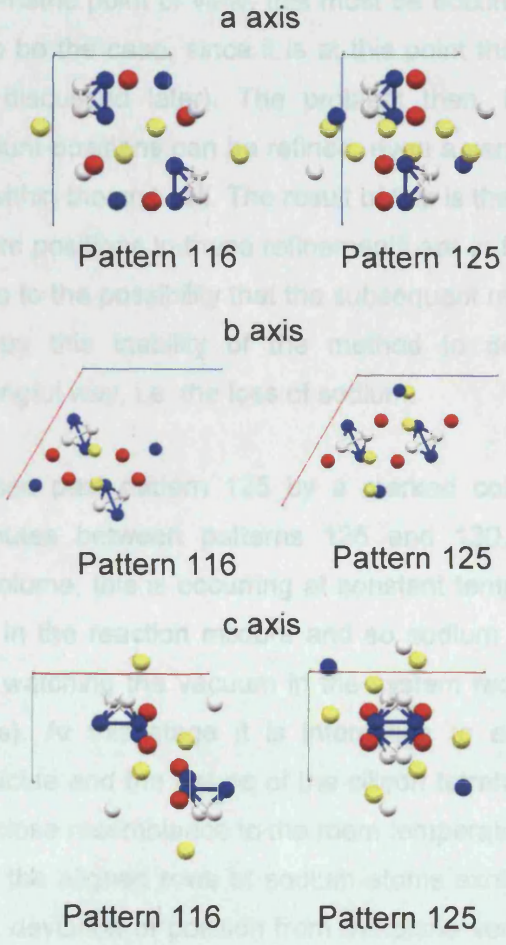

Figure 5.4.1.5: Comparison of the a, b and c axes for the unit cell of patterns 116 and 125. The diagram illustrates the affect of heating on the unit cell of NaSi during the initial expansions period.

However, there is an inherent problem in the analysis of this data as full temperature is approached and the reaction proceeds. As discussed previously, it is thought that the sodium atoms are lost from the system as a result of the application of vacuum. From a purely stoichiometric point of view, this must be occurring in the system and does indeed appear to be the case, since it is at this point that clathrate I becomes refinable (as will be discussed later). The problem then, becomes that though occupancy for the sodium positions can be refined, even a very small occupancy will register as a position within the unit cell. The result of this is that it is entirely probably that some of the sodium positions in these refinements are in fact vacant for the real system. This also leads to the possibility that the subsequent refinement of the silicon position, is affected by this inability of the method to deal with the reaction mechanism in a meaningful way, i.e. the loss of sodium.

The reaction progresses past pattern 125 by a marked collapse in the unit cell volume. The 2.5 minutes between patterns 125 and 130 represents a 0.71% reduction in unit cell volume; this is occurring at constant temperature. At this stage clathrate is refineable in the reaction mixture and so sodium loss is occurring (this can often be seen by watching the vacuum in the system reduce in quality, as the sodium loss increases). At this stage it is interesting to examine the structural environment for the silicide and the nature of the silicon tetrahedra. The structure at pattern 130 still has a close resemblance to the room temperature silicide but exhibits subtle differences, i.e. the aligned rows of sodium atoms exhibit a less symmetrical appearance with more deviation of position from the plane versus those seen in the initial silicide structure (*see Figure 5.4.1.6*).

A further important change in the structure can be seen on examination of the tetrahedra for the silicide at room temperature, versus those for pattern 130 (*see Figures 5.4.1.7a, b, c,*). It is clear that for pattern 130 the tetrahedra have undergone considerable distortion. In *Figure 5.4.1.7a, b, c,* the white positions represent the sodium 1 crystallographic position, blue marks the sodium 2 crystallographic positions. From the diagrams it is clear that the blue positions (sodium 2) have undergone an elongation of their shared bond, and the angle relating to the sodium 1 position that connects them has opened up. In addition, the white (sodium 1 positions) have had their shared bond distance reduced and the related angle has narrowed. It is also apparent that the tetrahedra for pattern 130 have undergone slight rotation as a result of this elongation and thermal expansion (*see Figure 5.4.1.8a and b*).

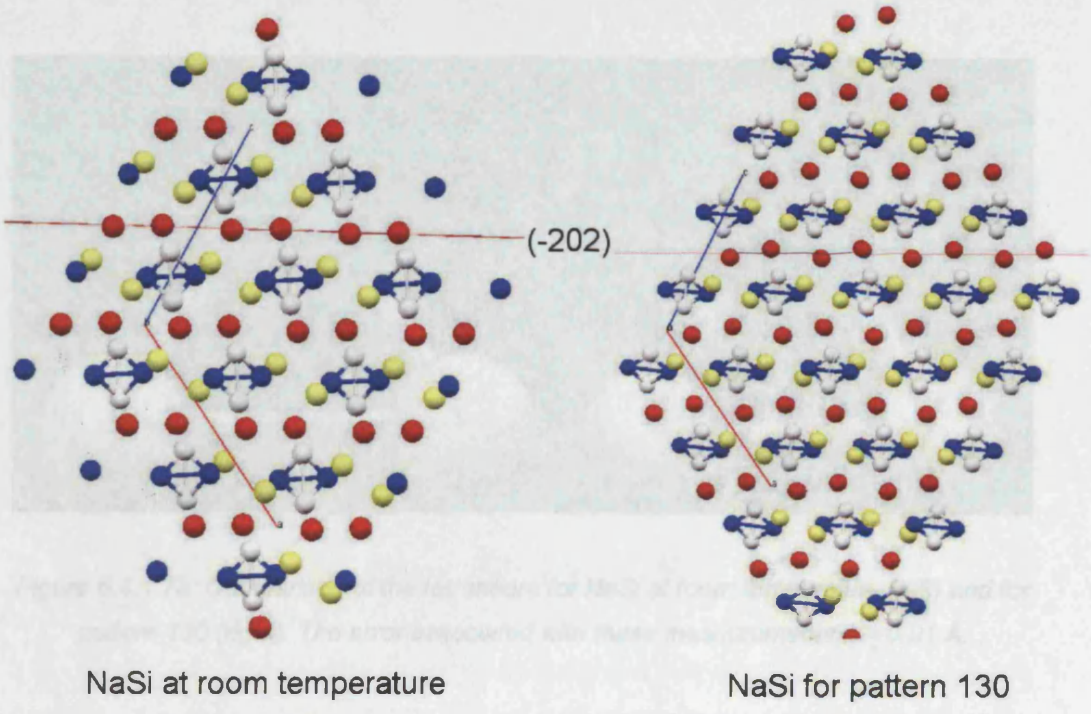

Figure 5.4.1.6: Comparison of the (-202) plane for the room temperature NaSi versus that for pattern 130. The diagram illustrates the deviation from the plane of sodium in the structure of pattern 130. Diagram represents a packing scheme to show additional sodium positions for clarity.

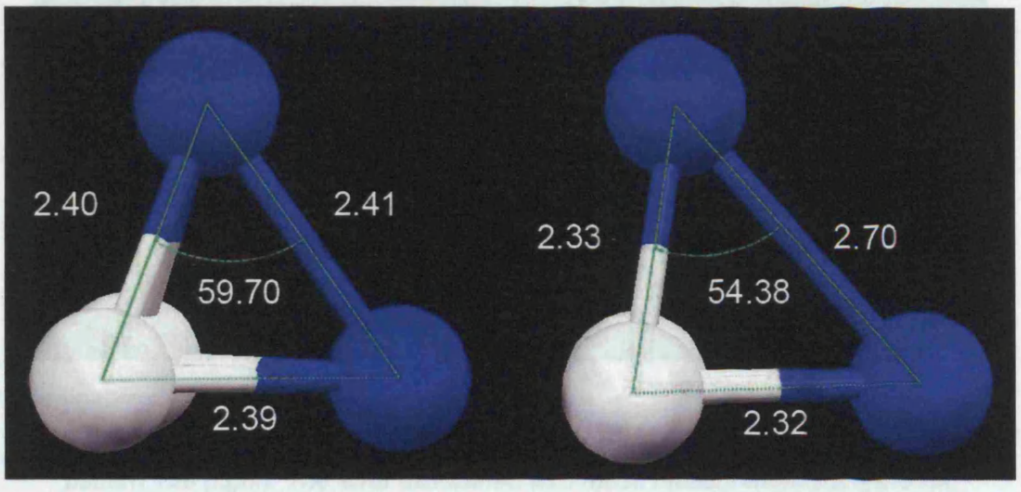

Figure 5.4.1.7a: Comparison of the tetrahedra for NaSi at room temperature (left) and for pattern 130 (right). The error associated with these measurements is ±0.1 Å.

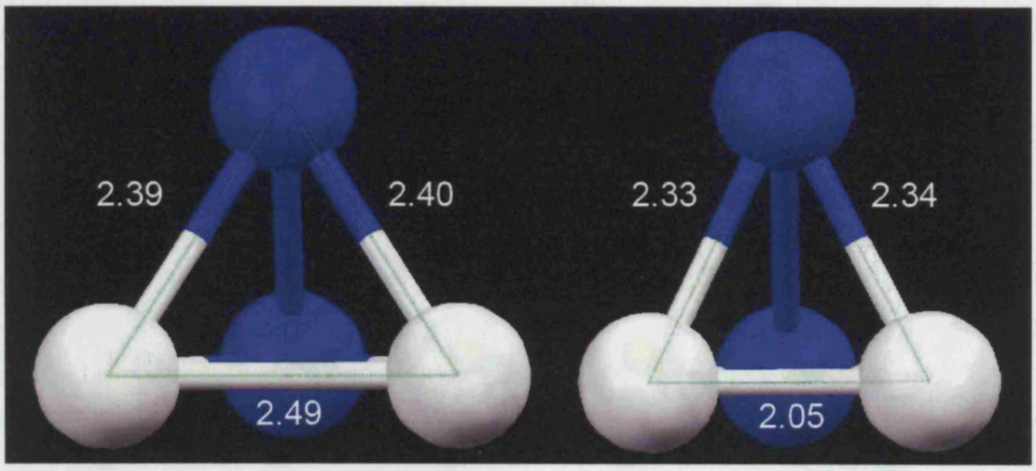

Figure 5.4.1.7b: Comparison of the tetrahedra for NaSi at room temperature (left) and for pattern 130 (right). The error associated with these measurements is ±0.01 Å.

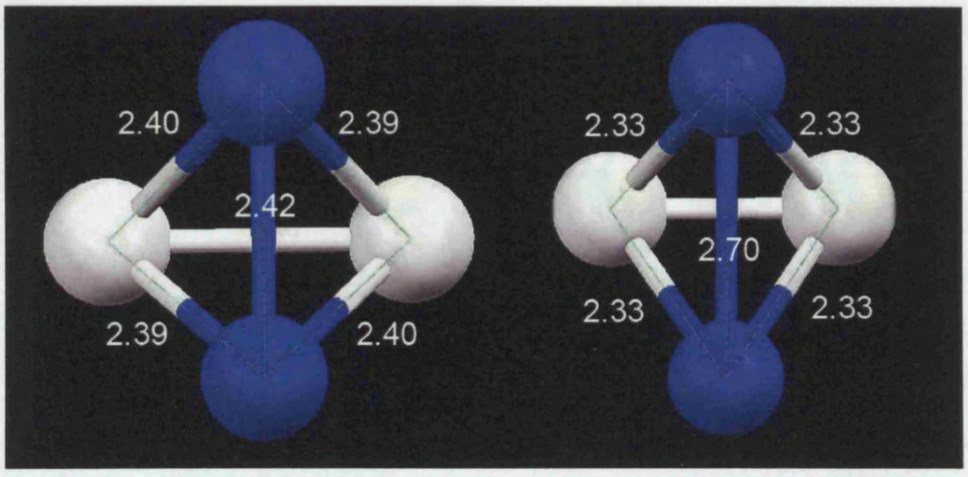

Figure 5.4.1.7c: Comparison of the tetrahedra for NaSi at room temperature (left) and for pattern 130 (right). The error associated with these measurements is ±0.01 Å.

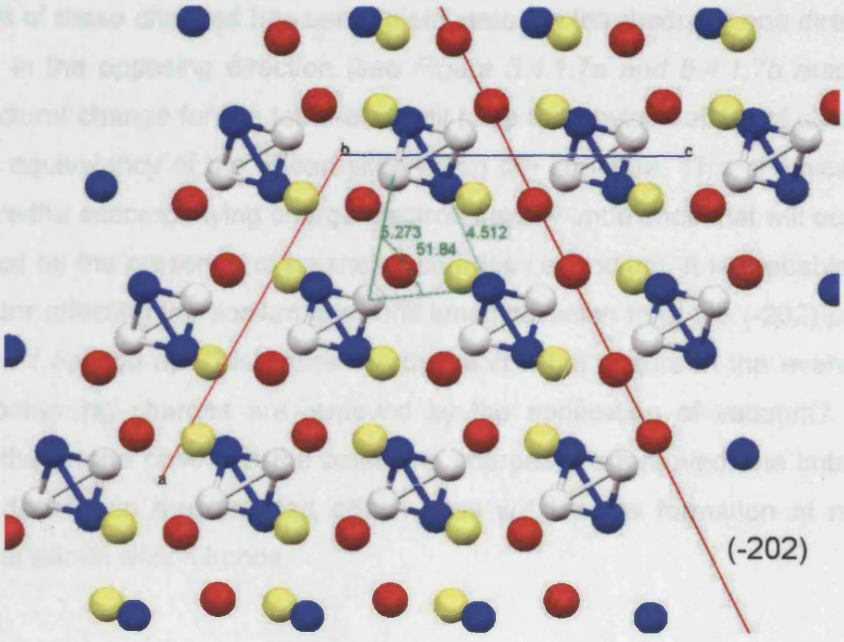

Figure 5.4.1.8a: Diagram shows the distance and angle relationships between tetrahedra situated close to the (-202) plane for NaSi at room temperature, viewed along the b axis. (Note: Compare the tilt of the tetrahedra from figure 5.4.1.8.a against b, also compare Na deviation from the (-202) plane).

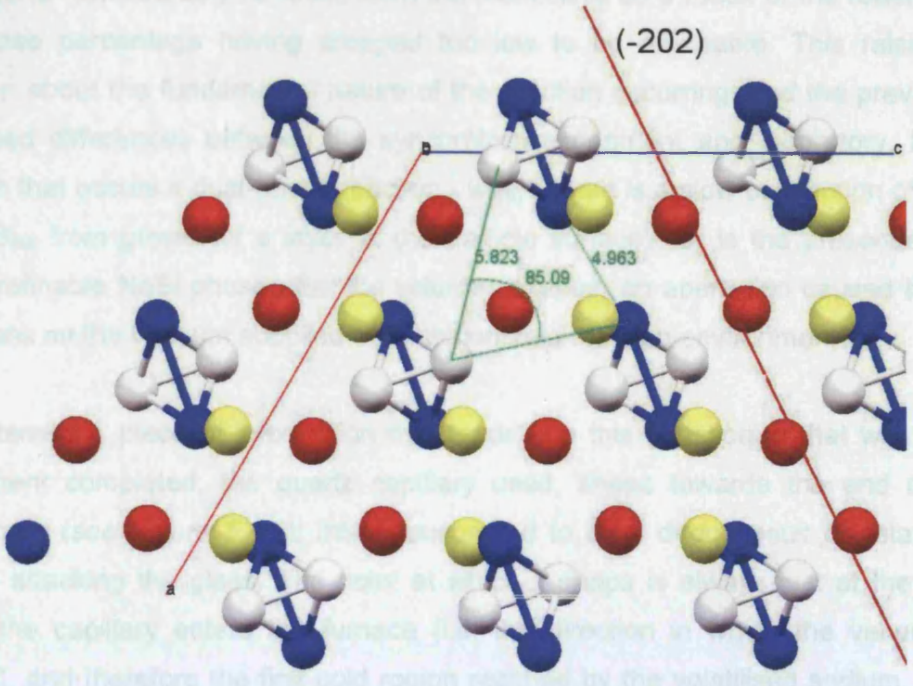

Figure 5.4.1.8b: Diagram shows the distance and angle relationships between tetrahedra situated close to the (-202) plane for NaSi at room temperature, viewed along the b axis. (Note: Compare the tilt of the tetrahedra from figure 5.4.1.8.a against b, also compare Na deviation from the (-202) plane).

The result of these changes has been to elongate the tetrahedra in one direction and narrow it in the opposing direction (*see Figure 5.4.1.7a and 5.4.1.7b respectively*). This structural change for the tetrahedra will have the obvious effect of changing the chemical equivalency of the silicon sites within the structure. This chemical change will require the accompanying charge/electron density imbalance that will occur, to be rebalanced by the presence of balancing charges i.e. sodium. It is probable that this is the factor affecting the sodium positions small deviation from the (-202) plane (*see Figure 5.4.1.8a and b*). This poses the question: what occurs in the event that the sodium balancing charges are removed by the application of vacuum? It seems possible that in the case that the balancing charges are removed, the imbalance of electron density on the distorted silicon sites will lead to formation of new inter-tetrahedral silicon silicon bonds.

For the remainder of the experiment, it is possible to refine NaSi up until pattern 170 at around 97.5 minutes. Between patterns 130 and 165 it is still possible to achieve a reasonable fit with the same refinement methodology used for the early refinements. However, at point 170 only 3 parameters are refineable and the patterns following 170 are essentially impossible to refine in terms of sodium silicide, the structure being either considerably removed from the monoclinic as a result of the reaction or the phase percentage having dropped too low to be refineable. This raises an question about the fundamental nature of the reaction occurring, and the previously discussed differences between the synchrotron experiment and laboratory. Is the reaction that occurs a dual-phase reaction - where there is a slow conversion of NaSi to Na_8Si_{46} from growth of a layer at the particle surface? Or is the presence of a poorly refinable NaSi phase after the volume collapse, an aberration caused by the limitations on the vacuum supplied and the confined reaction environment?

One interesting piece of information that feeds into this question is that with each experiment completed, the quartz capillary used, snaps towards the end of the experiment (*see Figure 5.4.2*); this is suspected to be a direct result of volatilised sodium attacking the glass. The point at which it snaps is always just at the point where the capillary enters the furnace (i.e. the direction in which the vacuum is applied), and therefore the first cold region reached by the volatilised sodium. If the formation of the clathrate is strongly dependant on the rate of loss of sodium, and the rate of sodium removal from the system is impeded by poor vacuum delivery; is this artificially inducing the presence of a poorly crystalline and poorly resolved NaSi phase, after the first appearance of Na_8Si_{46}?

5.4.2: Na_8Si_{46}

Formation of Na_8Si_{46} is first observed in the experiment at around pattern 125; 75 minutes into the reaction after around 10 minutes at the full reaction temperature (*see Figure 5.4.2.1*). For the Na_8Si_{46} phase refinement was completed using an identical methodology to that described in the NaSi data analysis. However, there was some variation in that it was possible to refine several parameters for the NaSi phase successfully during the early stages of the clathrate formation. There are a number of reasons for this that will be discussed in detail later on in this chapter.

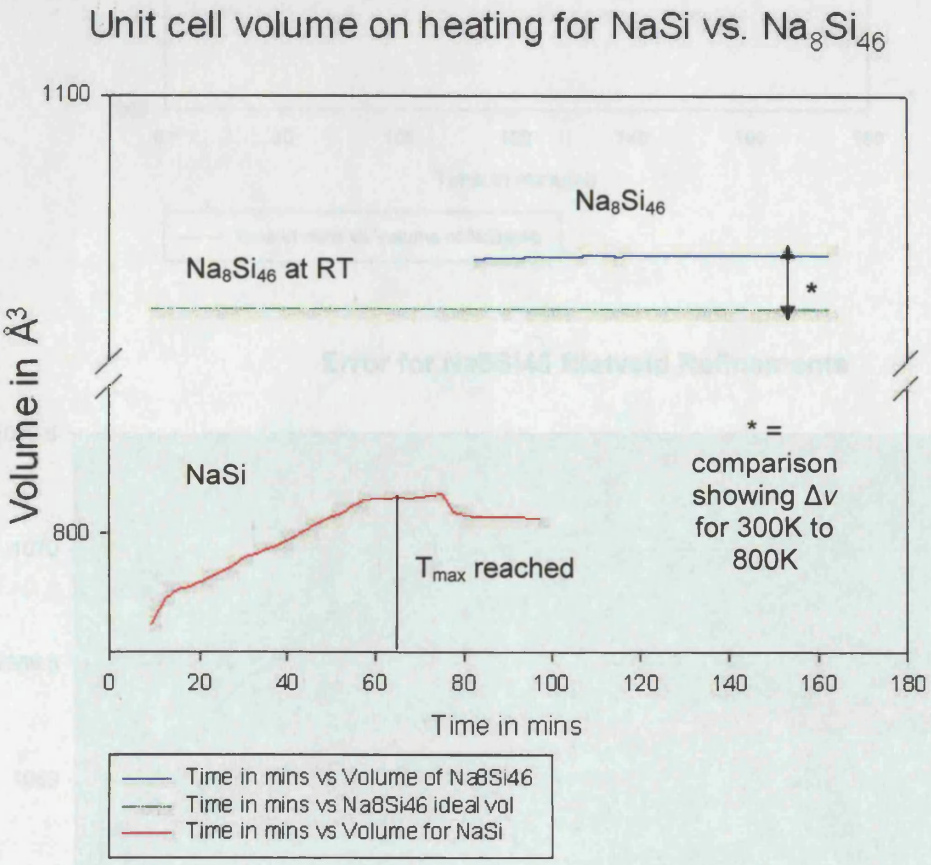

Figure 5.4.2.1: Diagram shows comparison of unit cell volumes for the NaSi (red) and Na_8Si_{46} (blue) in the reaction. The green line represents Na_8Si_{46} at room temperature in the laboratory and is shown for comparison.

On plotting and examination of the trends of the clathrates unit cell volume against time, a rather interesting trend is seen (*see Figure 5.4.2.2*).

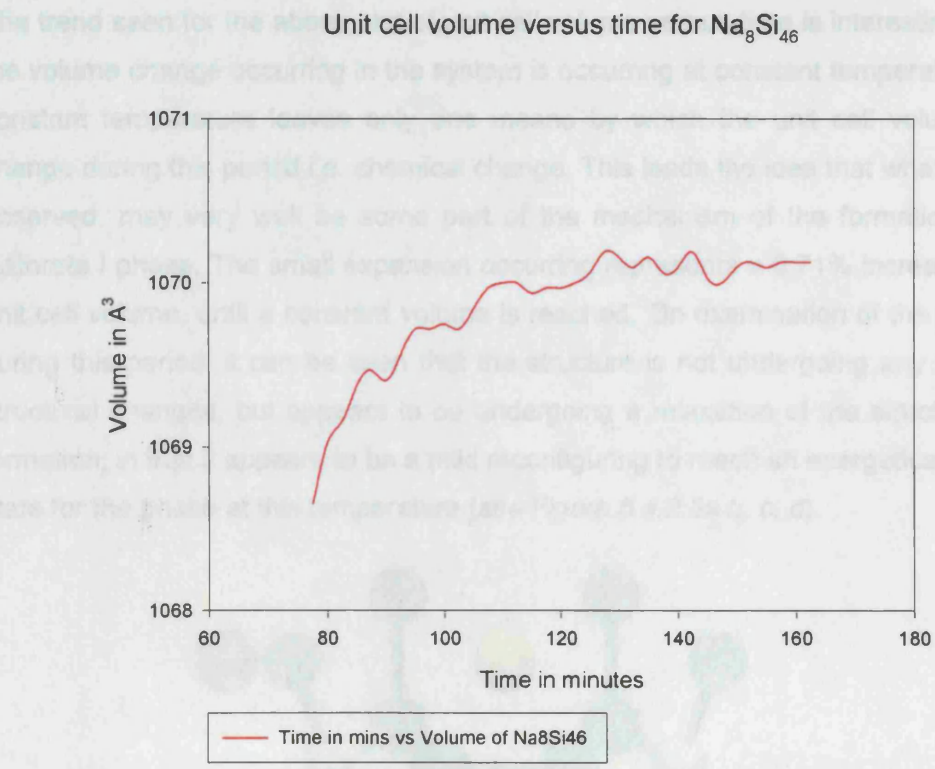

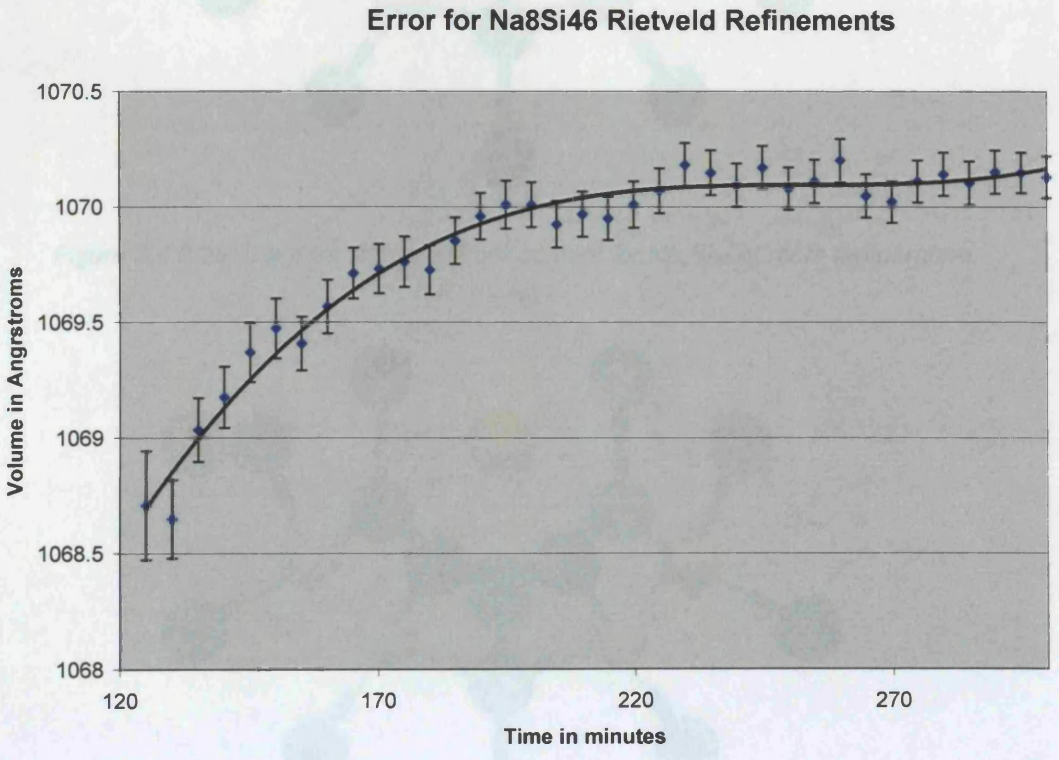

Figure 5.4.2.2: (top) Diagram shows unit cell volume for Na_8Si_{46} versus time during the experiment. The temperature is constant at 500°C for the entirety of the above range. (bottom) Shows the error in Rietveld refinement of the Na_8Si_{46} data.

The trend seen for the above plot of unit cell volume versus time is interesting in that the volume change occurring in the system is occurring at constant temperature. The constant temperature leaves only one means by which the unit cell volume may change during this period i.e. chemical change. This leads the idea that what is being observed, may very well be some part of the mechanism of the formation of the clathrate I phase. The small expansion occurring represents a 0.71% increase in the unit cell volume, until a constant volume is reached. On examination of the structure during this period, it can be seen that the structure is not undergoing any profound structural changes, but appears to be undergoing a relaxation of the structure after formation, in that it appears to be a mild reconfiguring to reach an energetically stable state for the phase at this temperature (*see Figure 5.4.2.3a b, c, d*).

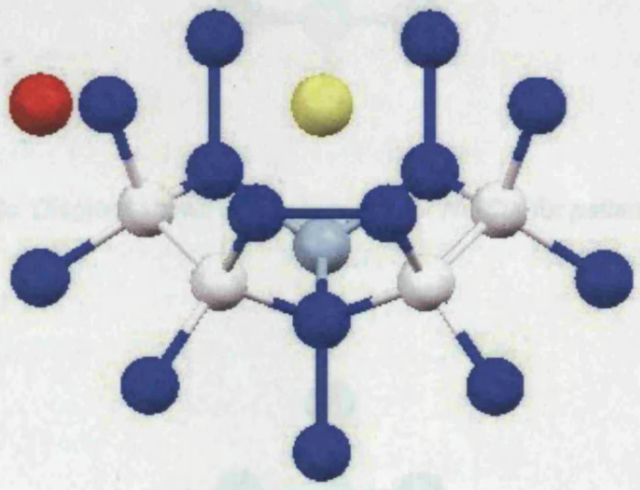

Figure 5.4.2.3a: Diagram shows unit cell content for Na_8Si_{46} at room temperature.

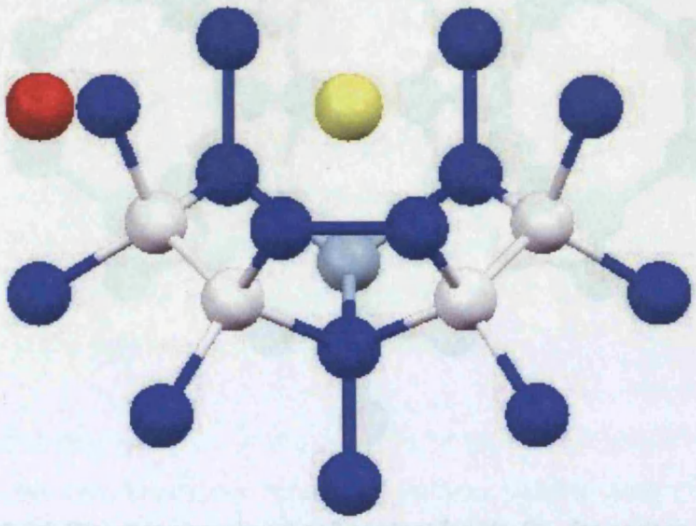

Figure 5.4.2.3b: Diagram shows unit cell content for Na_8Si_{46} for pattern 130 at 500 °C.

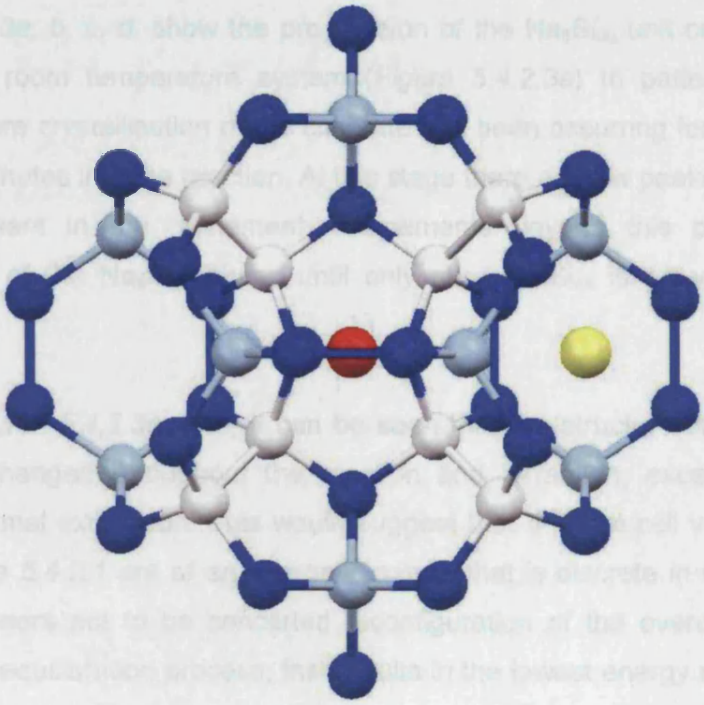

Figure 5.4.2.3c: Diagram shows unit cell content for Na_8Si_{46} for pattern 145 at 500 °C.

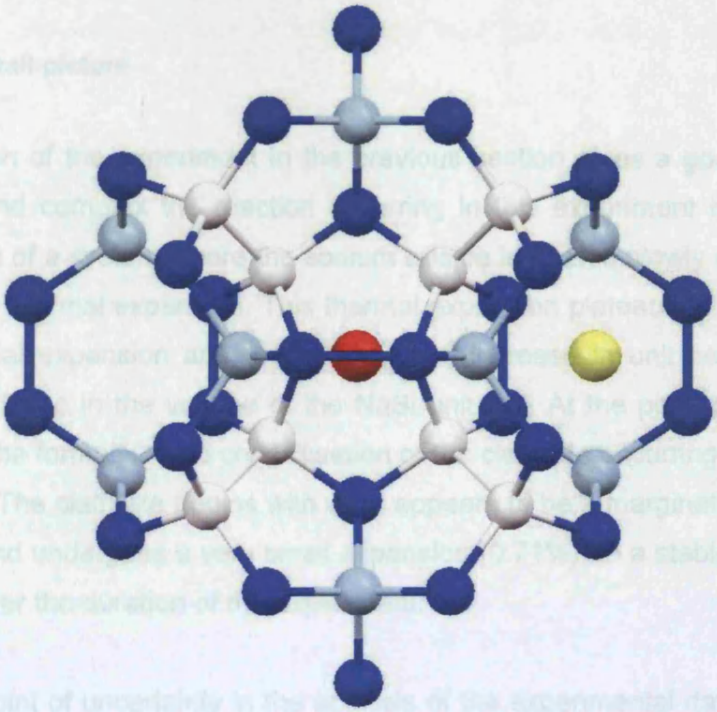

Figure 5.4.2.3d: Diagram shows unit cell content for Na_8Si_{46} for pattern 300 at 500 °C.

Figures 5.4.2.3a, b, c, d, show the progression of the Na_8Si_{46} unit cell content from the literature room temperature system (*Figure 5.4.2.3a*) to pattern 300 (*Figure 5.4.2.3d*), where crystallisation of the clathrate has been occurring for sometime and we are 150 minutes into the reaction. At this stage there are few peaks other than the clathrate present in the refinement. Refinements beyond this point show the crystallisation of the Na_8Si_{46} phase until only pure Na_8Si_{46} is present in the data collected.

From the *Figures 5.4.2.3a, b, c,* it can be seen that the structure of the clathrate I phase is unchanged throughout the reaction and formation, except the obvious effects of thermal expansion. This would suggest that the unit cell volume changes seen in *Figure 5.4.2.1* are of an energetic nature that is discrete in structural terms i.e. there appears not to be concerted reconfiguration of the overall structure but seemingly an equilibration process, that results in the lowest energy structure for the given temperature. The cause of this effect may be related to the possible mechanism of formation (which will be discussed in detail later) in that the clathrate is formed by templating around the guest species and thus on formation may exist with an artificially confined closest approach of neighbouring tetrahedra, as a result of formation of new silcon silcon bonds.

5.4.3: The overall picture

The discussion of the experiment in the previous section gives a good overview of how subtle and complex the reaction occurring in this experiment is. We gain an overall picture of a system where the sodium silicide is heated slowly and undergoes a pronounced thermal expansion. This thermal expansion plateaus to a considerably weaker thermal expansion and a finally a small increase in unit cell volume, that leads to a collapse in the volume of the NaSi unit cell. At the point of collapse, we begin to see the formation and crystallisation of the clathrate occurring in the reaction environment. The clathrate begins with what appears to be a marginally confined unit cell volume and undergoes a very small expansion (0.71%), to a stable structure that crystallises over the duration of the experiment.

The largest point of uncertainty in the analysis of the experimental data, comes from the nature of the two structures reflection profiles. Examination of the phases tick marks in Fullprof, shows this problem (*see Figure 5.4.3.1*).

Figure 5.4.3.1: Diagram shows the calculated reflection profile for NaSi (top) versus Na_8Si_{46} (bottom). It is evident from the diagram that the phases have some very similar reflection positions.

The result of the very close reflection positions is that at high expansion of the NaSi where Na_8Si_{46} is also present, it is prudent to be careful when assigning peak intensity to one phase or the other. The approach chosen to deal with such a problem is to carefully examine the data and scrutinise where the refinement is choosing to assign the peak intensity in terms of phase. Used in conjunction with careful judgement and the balance of the phase for which the majority of peaks can be visually assigned, a good fit can be achieved. It is important to note however, the nature of this very close similarity of reflections for the two phases makes the issue of accurate elucidation of structure, after the first appearance of clathrate in the reaction, considerably more complex than the refinement of the single phase stages for both NaSi and Na_8Si_{46} (*see Figure 5.4.3.2*). It is also important to note that some peaks are deviating more than others, in addition to the two phases undergoing different rates and magnitudes of expansion, resulting in reflections crossing over with those of the other phase in expansion and thus making the picture more complex.

The data region shown in *Figure 5.4.3.2* demonstrates the area of the refinement affected by peak overlap. It is important to note that the refinement of data anti and post this region, are unaffected by this issue and as such the structural information based on the changes occurring in NaSi, which form the basis of the study of formation, are entirely unaffected. The problems associated with accurate refinement in these regions may also, to some extent, be a contributing factor in the fluctuating nature of the trends for unit cell volume for Na_8Si_{46} (*see Figure 5.4.2.2*) though the effect is exacerbated by the use of 5 pattern gaps in the analysis.

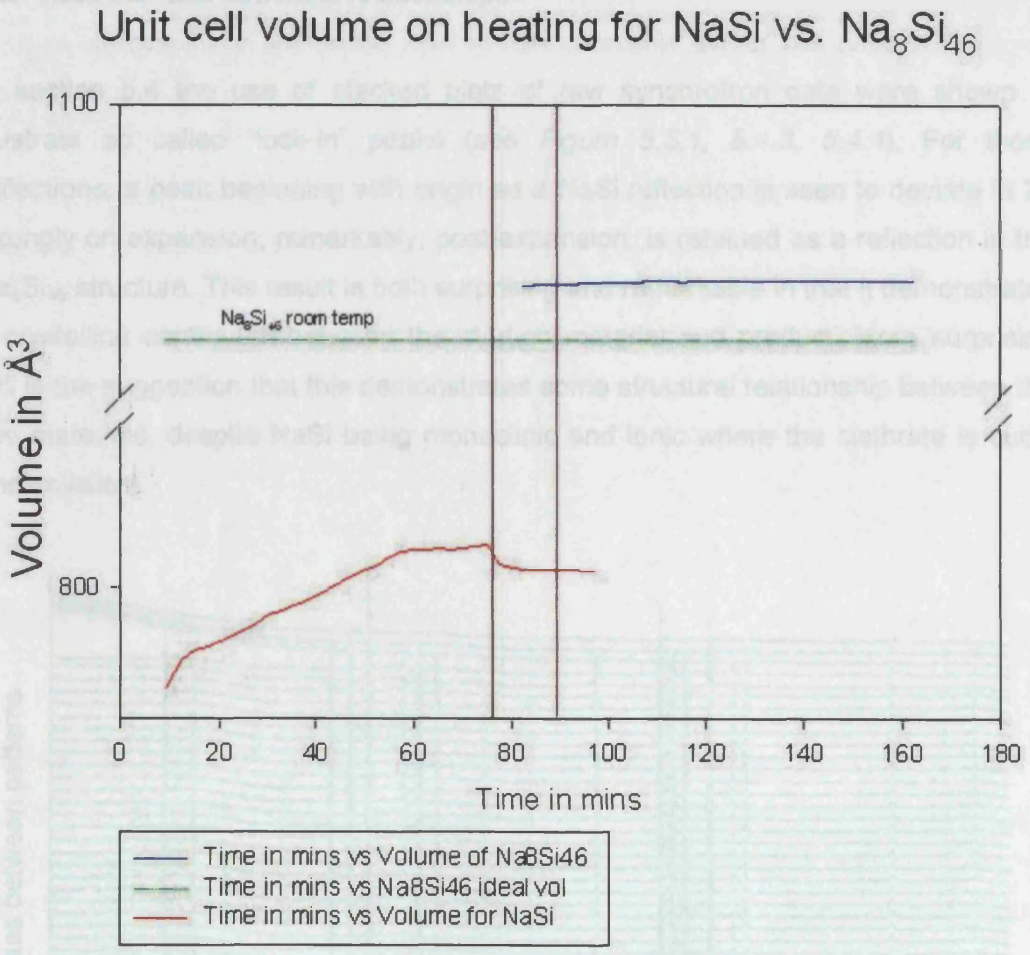

Figure 5.4.3.2: Diagram shows the region of refinement for which complexity and assurity of fit are affected by overlap of NaSi and Na_8Si_{46} reflections.

5.5: "Lock-ins" and structural relationships

In section 5.4 the use of stacked plots of raw synchrotron data were shown to illustrate so called "lock-in" peaks (*see Figure 5.5.1, 5.4.3, 5.4.4*). For these reflections, a peak beginning with origin as a NaSi reflection is seen to deviate in 2θ strongly on expansion; remarkably, post-expansion, is retained as a reflection in the Na_8Si_{46} structure. This result is both surprising and remarkable in that it demonstrates a crystalline continuum between the starting material and product. More surprising still is the suggestion that this demonstrates some structural relationship between the two materials, despite NaSi being monoclinic and ionic where the clathrate is cubic and covalent.

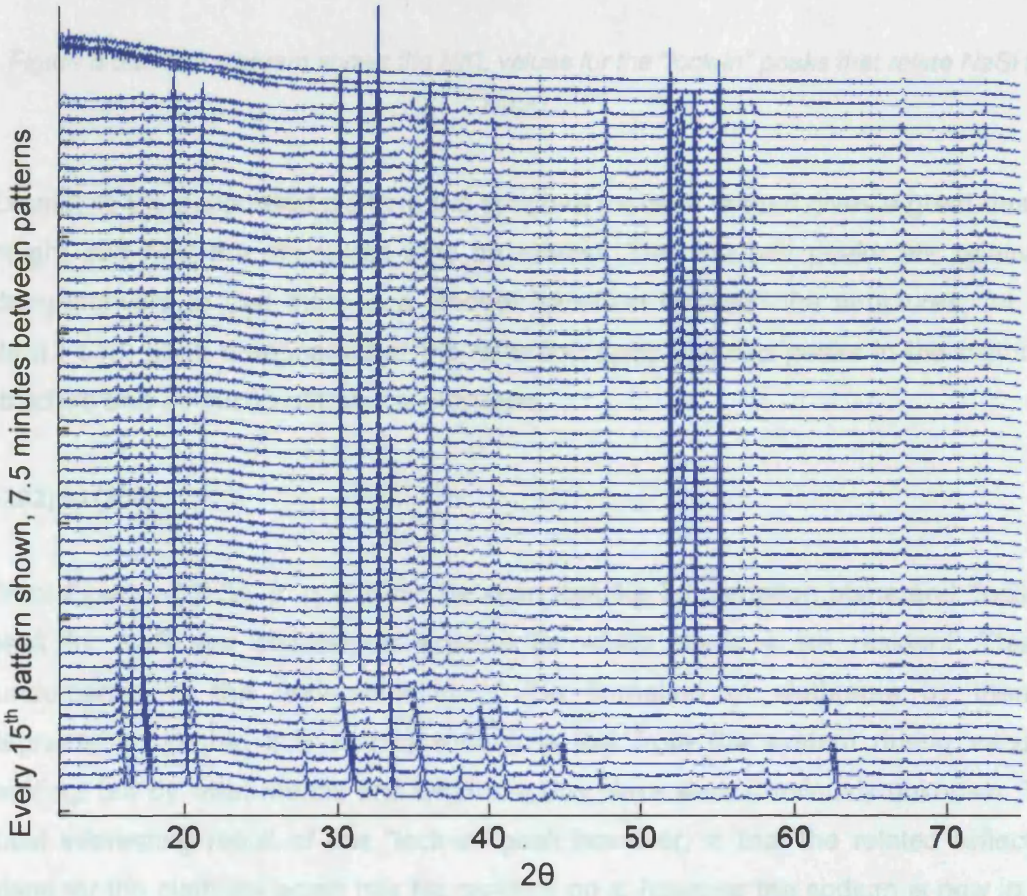

Figure 5.5.1: The diagram shows every 15th pattern in a stacked plot for NaSi to Na_8Si_{46} at 500°C, 8°Cmin^{-1} and 10^{-4} bar vacuum. Spacing between patterns represents 7.5 minutes.

To ascertain the nature of the relationship between these structures, and indeed discover if such a relationship exists, the specific reflection planes can be analysed in structural terms by carefully following the associated peaks through the experiment.

When the specific planes are identified, they can be plotted onto structural diagrams in three dimensions such that the structural changes throughout the reaction can be viewed in relation to the associated plane for both structures.

Though there are a number of peaks that show strong deviation in 2θ, there are three that are unarguably connected between the two structures:

	hkl
NaSi	**Na_8Si_{46}**
-202	200
311	321
-513	422
-513	430

Figure 5.5.2: The diagram shows the HKL values for the "lock-in" peaks that relate NaSi to Na_8Si_{46}.

Examining the associated plane in the structure for each related gives a great deal of insight into how the structures may be related. The first two peaks are relatively straightforward in that there is a smooth transition between the structures; for the NaSi (-513) peak it appears that the reflection splits into two peaks in the clathrate structure and as such both will be examined.

(-202) to (200):

From *Figures 5.5.3a, b, c, d* it can be seen that the 2θ deviation plane and "lock-in" peak for NaSi are centred on a plane for which Na ions are resident. This is fundamental to the understanding of the formation of clathrates by thermal degradation, in that it is known sodium is lost from the system during vacuum heating, but by what means and what role this plays were previously unknown. The most interesting result of this "lock-in" peak however, is that the related reflection plane for the clathrate again has Na resident on it; however the sodium is now in the form of Na atoms and resides directly at the cage centres of the large polyhedral cages of the clathrate. Crucially, the plane lies through the centre of both the pentagonal dodecahedral cages and the tetrakaidecahedral cages linking the sodium sites in the NaSi structure to the cages centres of the clathrate. This may be the first evidence of the growth of type I silicon clathrate as a result of templating of the structure, by the guest species present in the reaction.

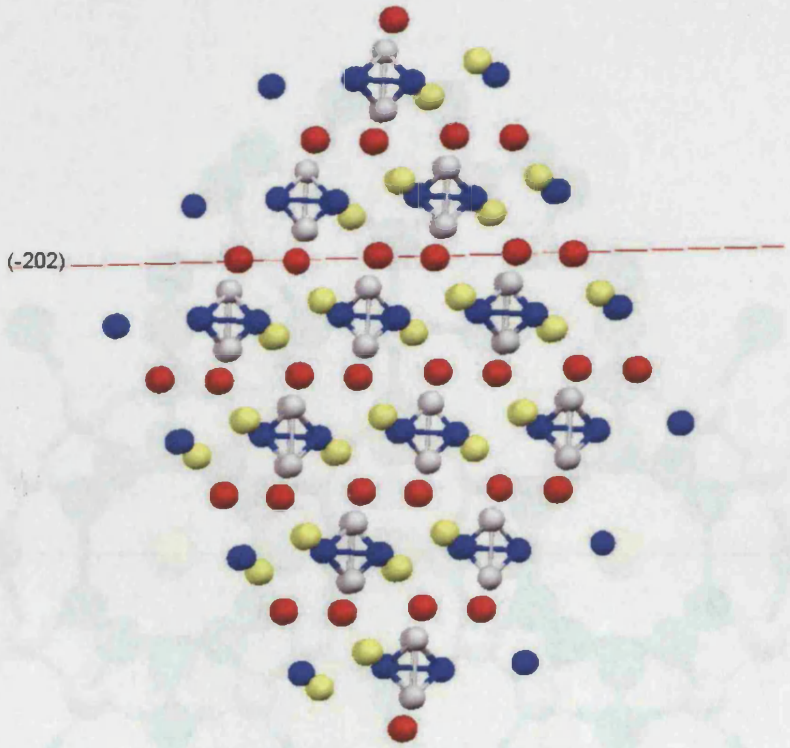

Figure 5.5.3a: The diagram shows the (-202) plane for NaSi at room temperature.

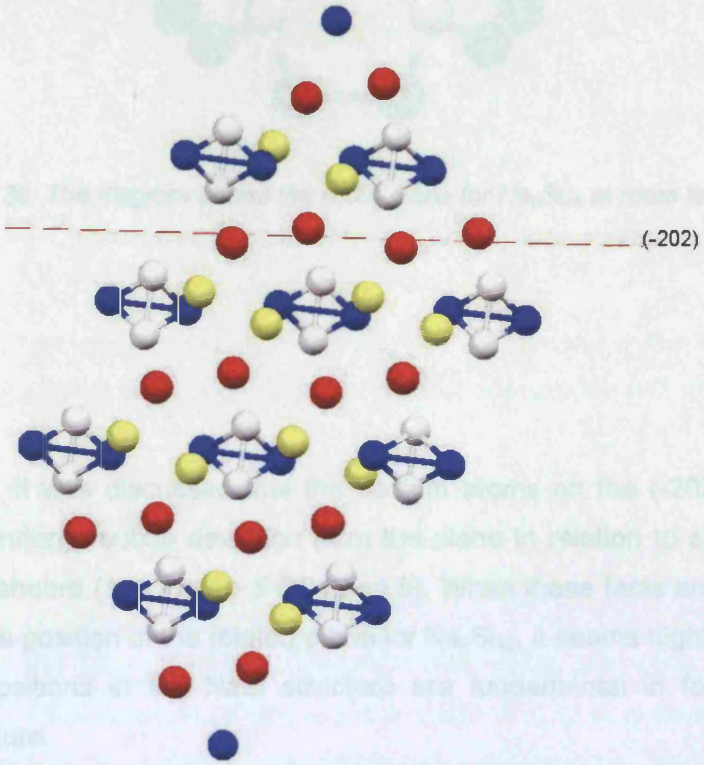

Figure 5.5.3b: The diagram shows the (-202) plane for NaSi for pattern 130 at 500°C.

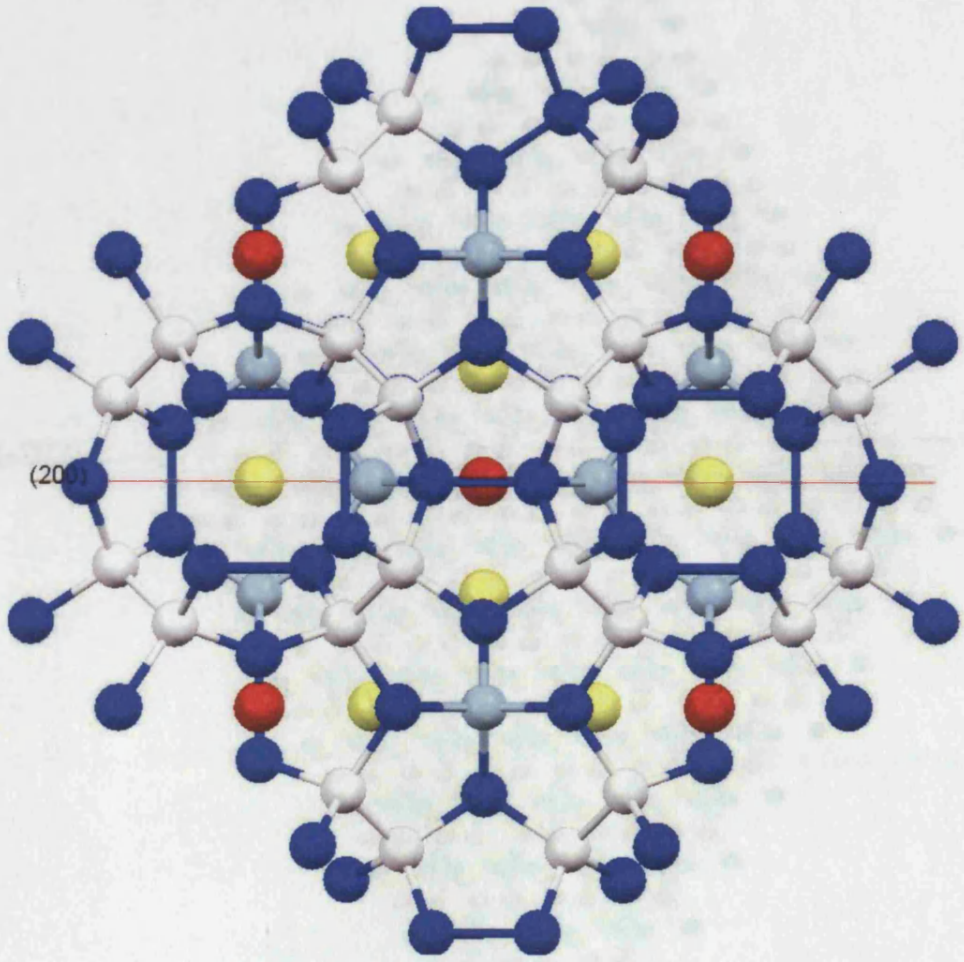

Figure 5.5.3c: The diagram shows the (200) plane for Na_8Si_{46} at room temperature.

In section 5.4, it was discussed that the sodium atoms on the (-202) plane of the silicide, also undergo subtle deviation from the plane in relation to slight rotation of the silicon tetrahedra (*see Figure 5.5.3a and b*). When these facts are considered in context with the position of the related plane for Na_8Si_{46}, it seems highly probable that the sodium positions in the NaSi structure are fundamental in formation of the clathrate structure.

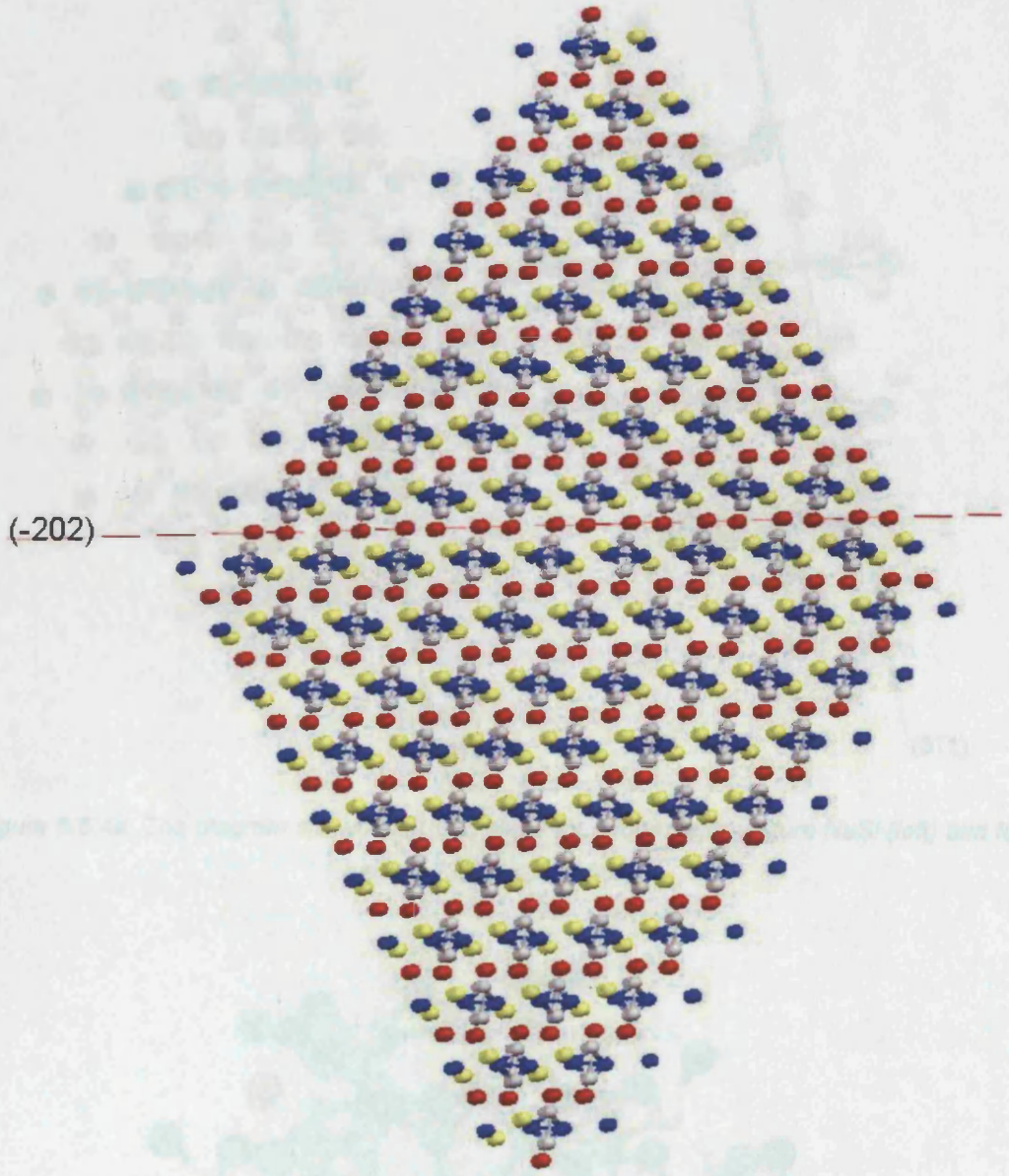

Figure 5.5.3d: The diagram shows the (-202) plane for a room temperature NaSi supercell. The diagram clearly shows the reflection passing through only sodium centres.

(311) to (321):

The picture for the (311) silicide reflection is somewhat less clear. From *Figures 5.5.4a, b, c* it is clear however, that the plane again is host to sodium positions and that these positions are linked to the clathrate by a reflection that resides through cage centres that contain sodium atoms. This again provides more evidence that the sodium positions in NaSi are complicit in the mechanism of formation of the clathrate.

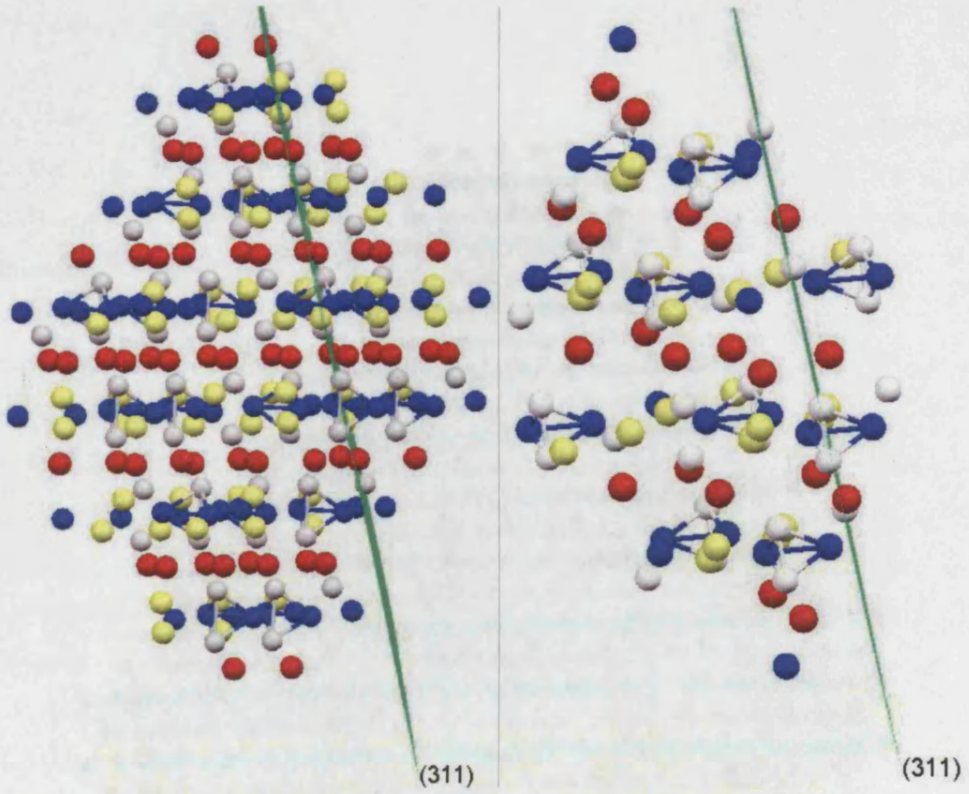

Figure 5.5.4a: The diagram shows the (311) plane for a room temperature NaSi (left) and for pattern 130 at 500°C (right).

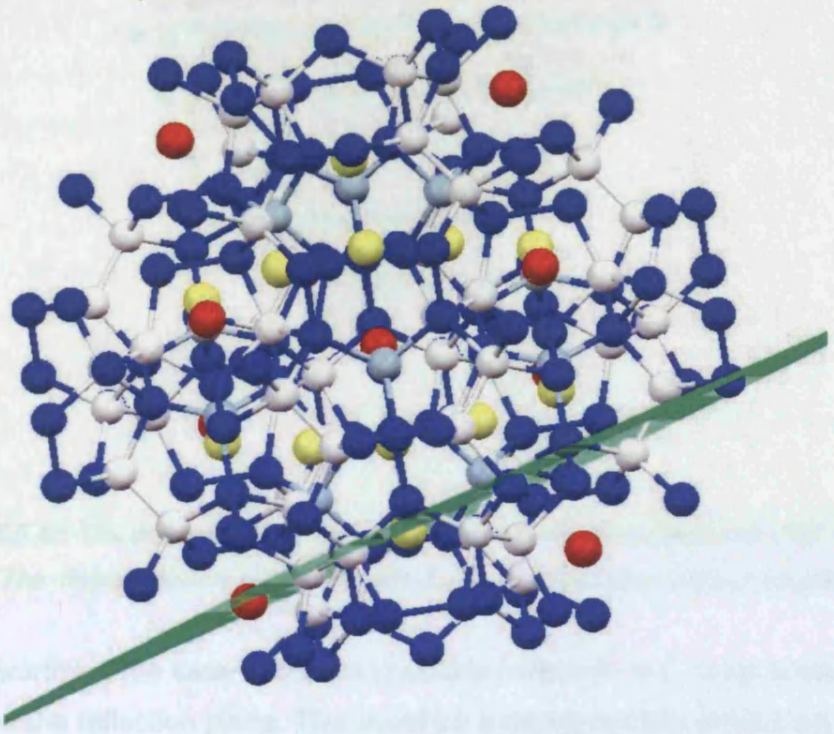

Figure 5.5.4b: The diagram shows the (321) plane Na_8Si_{46} at room temperature.

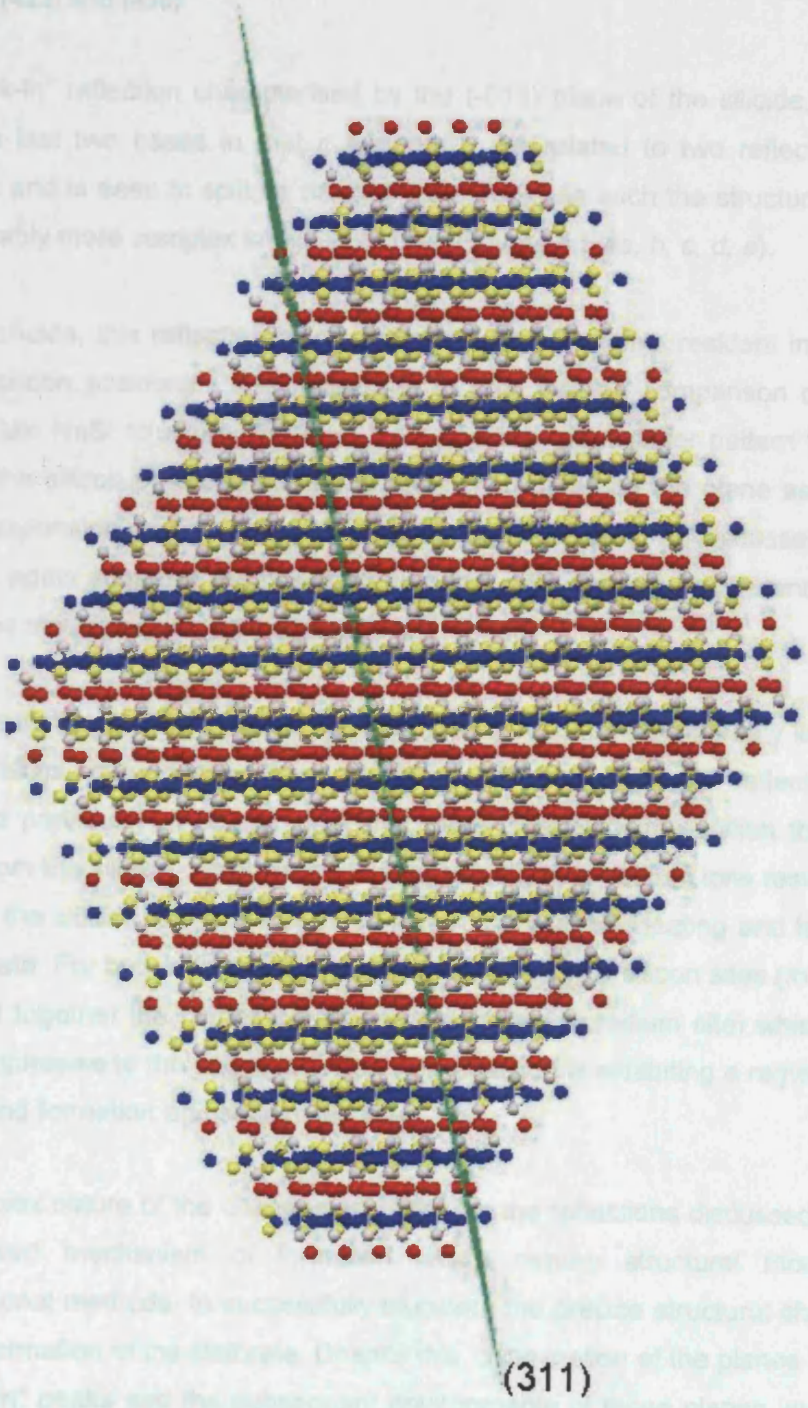

Figure 5.5.4c: The diagram shows the (311) plane for a room temperature NaSi supercell. The diagram clearly shows the reflection passing through sodium centres.

It is noteworthy in the case of the (311) silicide reflection, that some silicon positions also lie on the reflection plane. This could be a demonstration of sites around which mechanistic activity occurs i.e. cage and silicon silicon bond formation at these points.

(-513) to (422) and (430):

The "lock-in" reflection characterised by the (-513) plane of the silicide, is different from the last two cases in that it appears to be related to two reflections in the clathrate and is seen to split as the clathrate forms. As such the structural picture is considerably more complex in this case (*see Figures 5.5.5a, b, c, d, e*).

For the silicide, this reflection plane again has sodium atoms resident in addition to several silicon positions. It is interesting to note that on comparison of the room temperature NaSi structure (*Figure 5.5.5a*) and the structure for pattern 130 (*Figure 5.5.5b*), the silicon positions appear to have lined up along the plane as a result of thermal expansion, in the subtle structural changes occurring as discussed in section 5.4. This again suggests the possibility that this reflection may represent one of the initial sites at which silicon silicon bonds are formed.

When the clathrate is considered, the two reflections have considerably less obvious characteristics, carried over from the initial silicide versus the reflection planes discussed previously. It seems clear that there is no sodium position that remains related from the silicide, which perhaps suggests that the sodium ions residing on the plane for the silicide are some of those lost in the vacuum heating and formation of the clathrate. For both reflections, the clathrate shows only silicon sites (though when examined together the planes do appear to intersect a sodium site) which provides strong emphasise to the suggestion that this reflection is exhibiting a region of silicon silicon bond formation and sodium ion loss.

The complex nature of the changes occurring for the reflections discussed, suggests the detailed mechanism of formation would require structural modelling via computational methods, to successfully elucidate the precise structural changes that result in formation of the clathrate. Despite this, examination of the planes involved in the "lock-in" peaks and the subsequent environments of those planes, suggest that the sodium sites are strongly involved in the mechanism of formation for the clathrate.

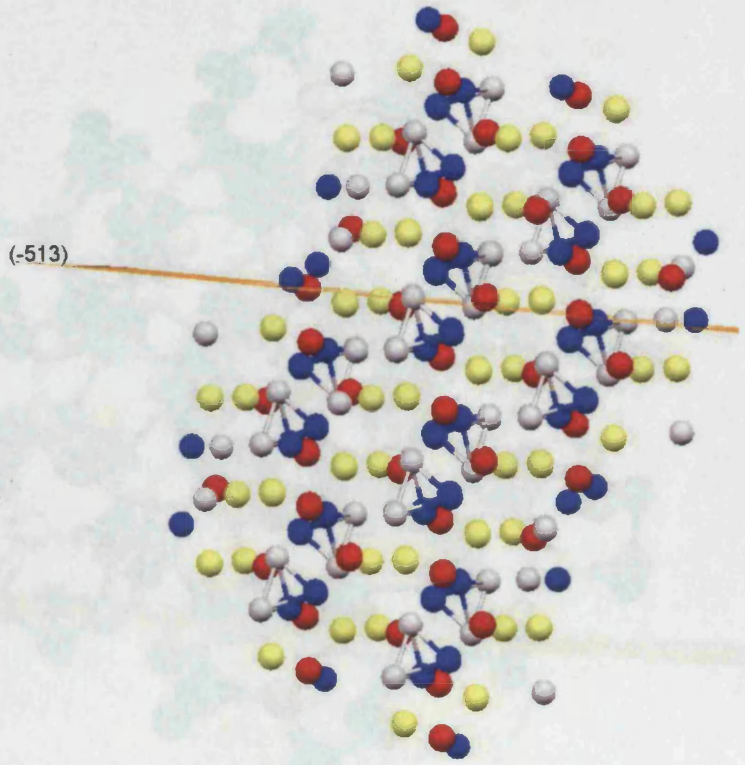

Figure 5.5.5a: The diagram shows the (-513) plane for NaSi at room temperature.

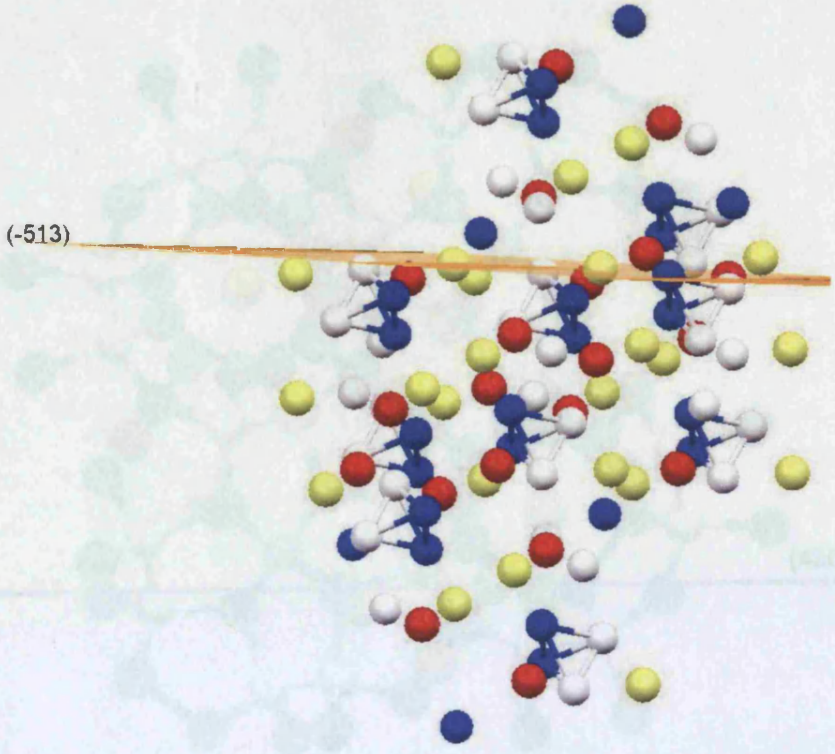

Figure 5.5.5b: The diagram shows the (-513) plane for NaSi for pattern 130 at 500 °C.

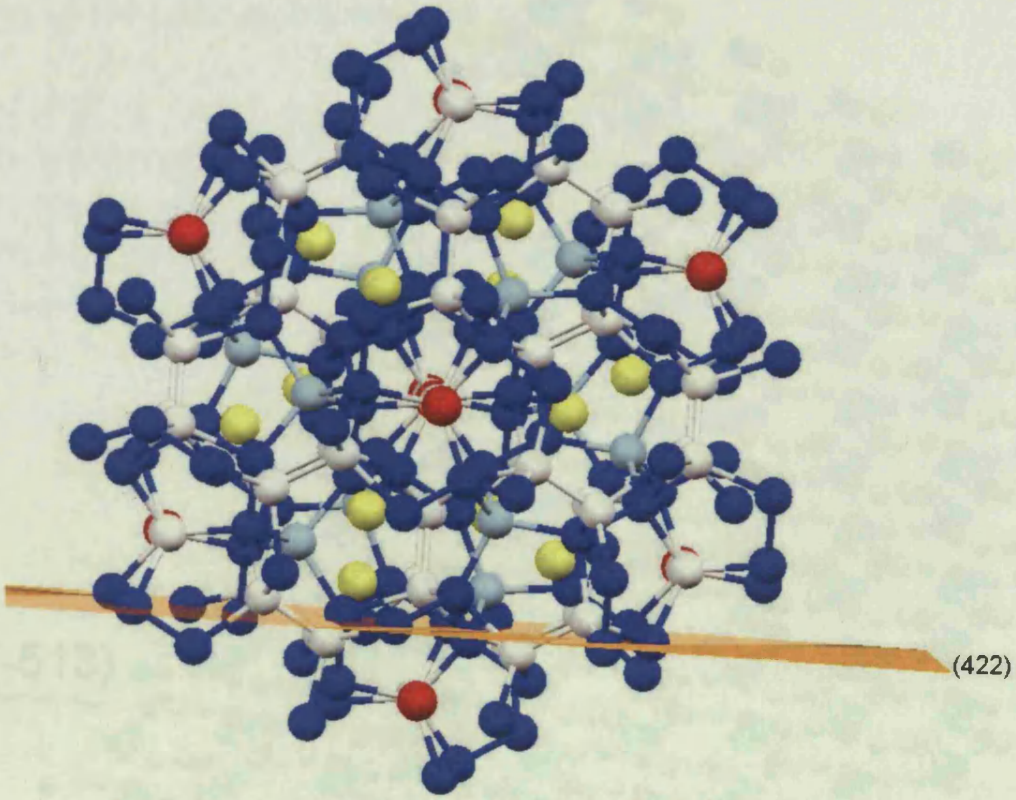

Figure 5.5.5c: The diagram shows the (422) plane for Na_8Si_{46} at room temperature.

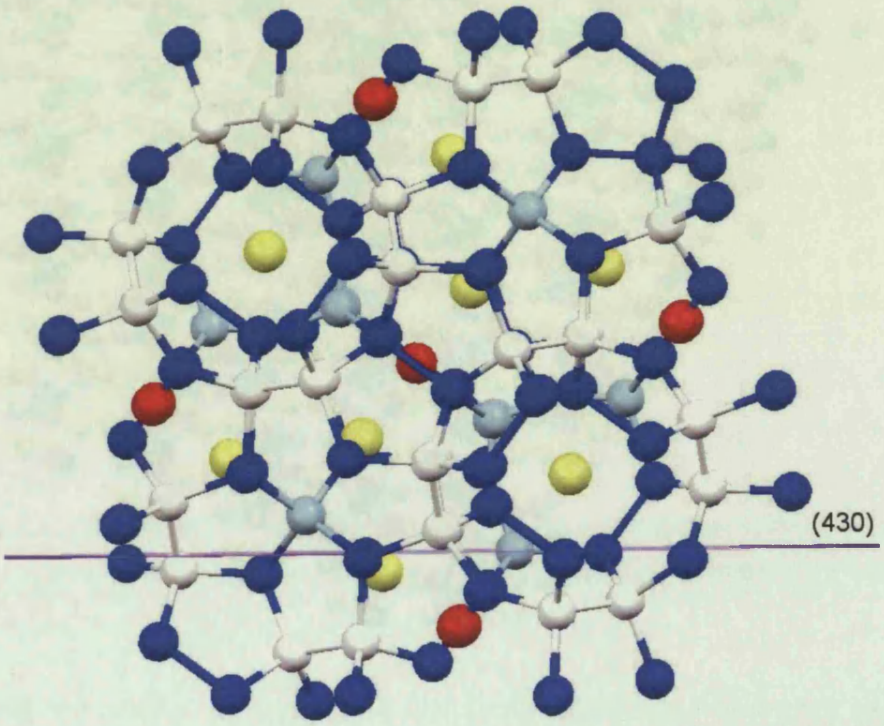

Figure 5.5.5d: The diagram shows the (430) plane for Na_8Si_{46} at room temperature.

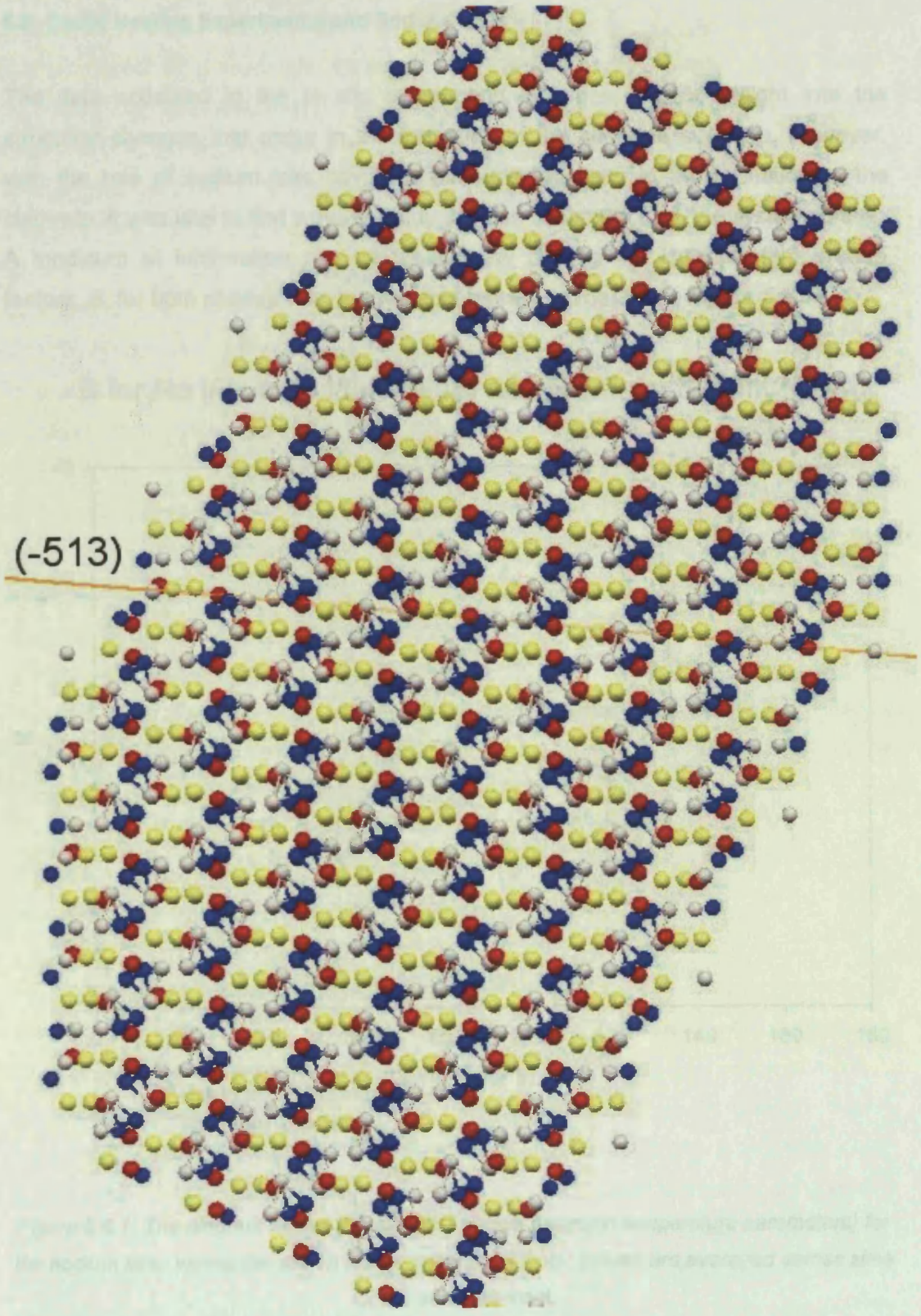

Figure 5.5.5e: The diagram shows the (-513) plane for a room temperature NaSi supercell. The diagram clearly shows the reflection passing through sodium centres.

5.6: Cyclic Heating Experiments and Sodium Loss

The data collected in the *in situ* experiments provides a good insight into the structural changes that occur in the formation of the clathrate structure. However, with the role of sodium loss having a fundamental place in the formation of the clathrate, it was vital to find ways to study the loss of sodium from the system further. A modicum of information can be gleaned by plotting the isotropic temperature factors, *B*, for both phases from the Rietveld refinement data (*see Figure 5.6.1*).

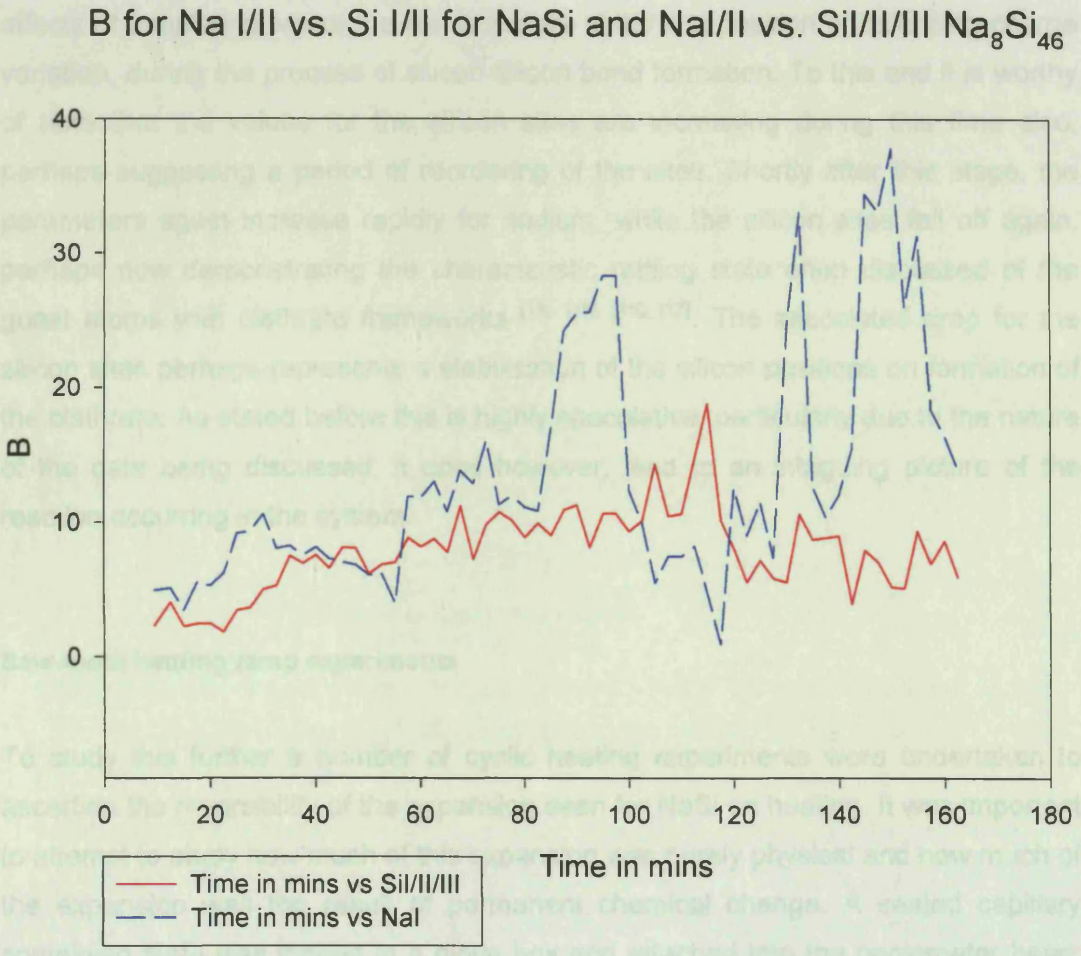

Figure 5.6.1: The diagram shows the refined B values (isotropic temperature parameters) for the sodium sites versus the silicon sites against time. Note: Values are averaged across sites for the same element.

Given that the reaction is occurring at high temperature and that a great deal of the data is thus subject to this, the effect of "smearing" will be prominent in refinements of these parameters. However, when they are plotted against time, the trend shown

is interesting enough such that it is worthy of note. The trend throughout is generally not consistent or smooth and thus can only be considered in very general terms. However, the interesting region considers the period from 80 minutes to around 130 minutes. This corresponds closely to the region in which NaSi is loosing sodium and forming the clathrate. It is interesting then, that the temperature parameters for Na begin to jump very rapidly as this period begins, perhaps suggesting that this region demonstrates a high level of activity, motion or disorder at the sodium sites. The parameters then drop rapidly to a lower level than that of the silicon parameters; though highly speculative it is possible that this represents, to some extent, the affects of templating where the Na atoms are static in a position of balancing charge variation, during the process of silicon silicon bond formation. To this end it is worthy of note that the values for the silicon sites are increasing during this time also, perhaps suggesting a period of reordering of the sites. Shortly after this stage, the parameters again increase rapidly for sodium, while the silicon sites fall off again, perhaps now demonstrating the characteristic rattling state often discussed of the guest atoms with clathrate frameworks [14], [15], [16], [17]. The associated drop for the silicon sites perhaps represents a stabilisation of the silicon positions on formation of the clathrate. As stated before this is highly speculative, particularly due to the nature of the data being discussed; it does however, lead to an intriguing picture of the reaction occurring in the system.

Saw-tooth heating ramp experiments

To study this further a number of cyclic heating experiments were undertaken to ascertain the reversibility of the expansion seen for NaSi on heating. It was important to attempt to study how much of this expansion was purely physical and how much of the expansion was the result of permanent chemical change. A sealed capillary containing NaSi was loaded in a glove box and attached into the goniometer head; no vacuum was used such that the sample could be rotated to improve data quality (In further studies it was observed that the clathrate I can be formed in the absence of a vacuum system, if temperatures slightly above the norm are used). The same techniques were used as for the synthesis experiments but this time with a cyclic temperature profile, characterised by successive heating and cooling of the sample at a moderate ramp rate of 25°Cmin^{-1} (*see Figure 5.6.2*). Data were collected for 59 seconds with a 1 second pause. The data range from 5 to 70° 2θ was again chosen for this experiment, such that the entire range of clathrate reflections was covered.

The objective of the experiment was not gain full structural refinement of the system, but to attempt to ascertain where changes were occurring and to which reflection planes and positions they relate. Most importantly of all, was to attempt to find reversible or irreversible changes with in the system, which denote the beginning of chemical reaction.

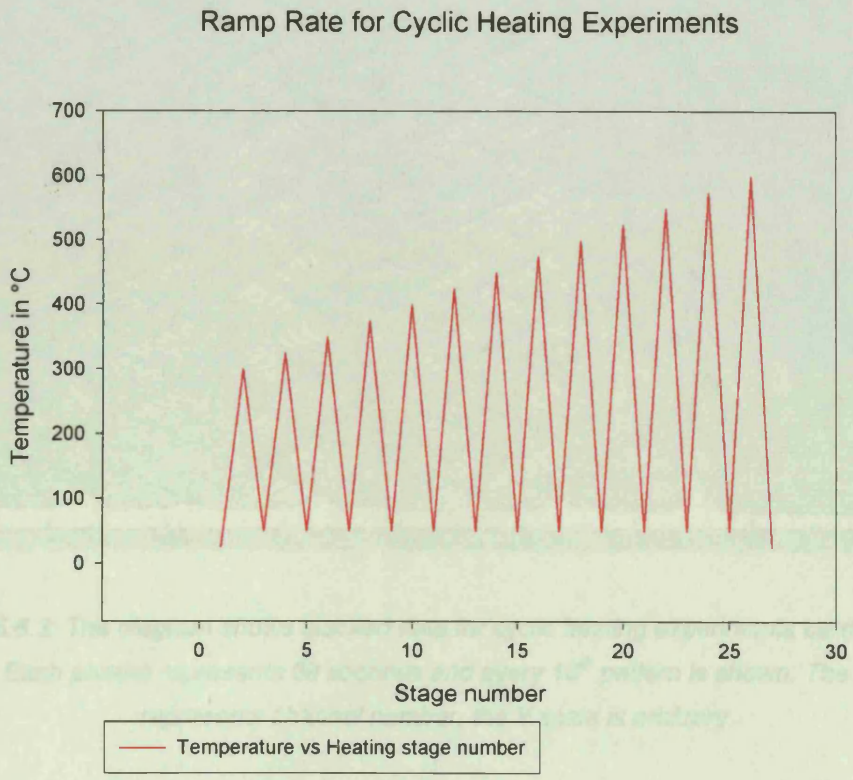

Figure 5.6.2: The diagram shows the cyclic heating profile for reversibility studies on the thermal expansion seen for sodium silicide using synchrotron techniques.

On completion of the experiment, data was viewed as a stacked plot in Matlab, this being visually one of the most effective ways of identifying changes within the system (*see Figure 5.6.3*). A first look at the data shows immediately that strong changes have been occurring during the cyclic heating stages. The first point of note is for the area situated slightly above 1300 on the channel scale; these peaks correspond to the silicide peaks at 19.03° 2θ which represent the plane (-112), which runs central to the NaSi unit cell and is host several to sodium ion positions. The high intensity seen here, may be the result of either further crystallisation of the silicide on heating from a poorly crystalline form or alternatively the result of loss of non-stoichiometric sodium by degassing from the system, as initial heating begins[5].

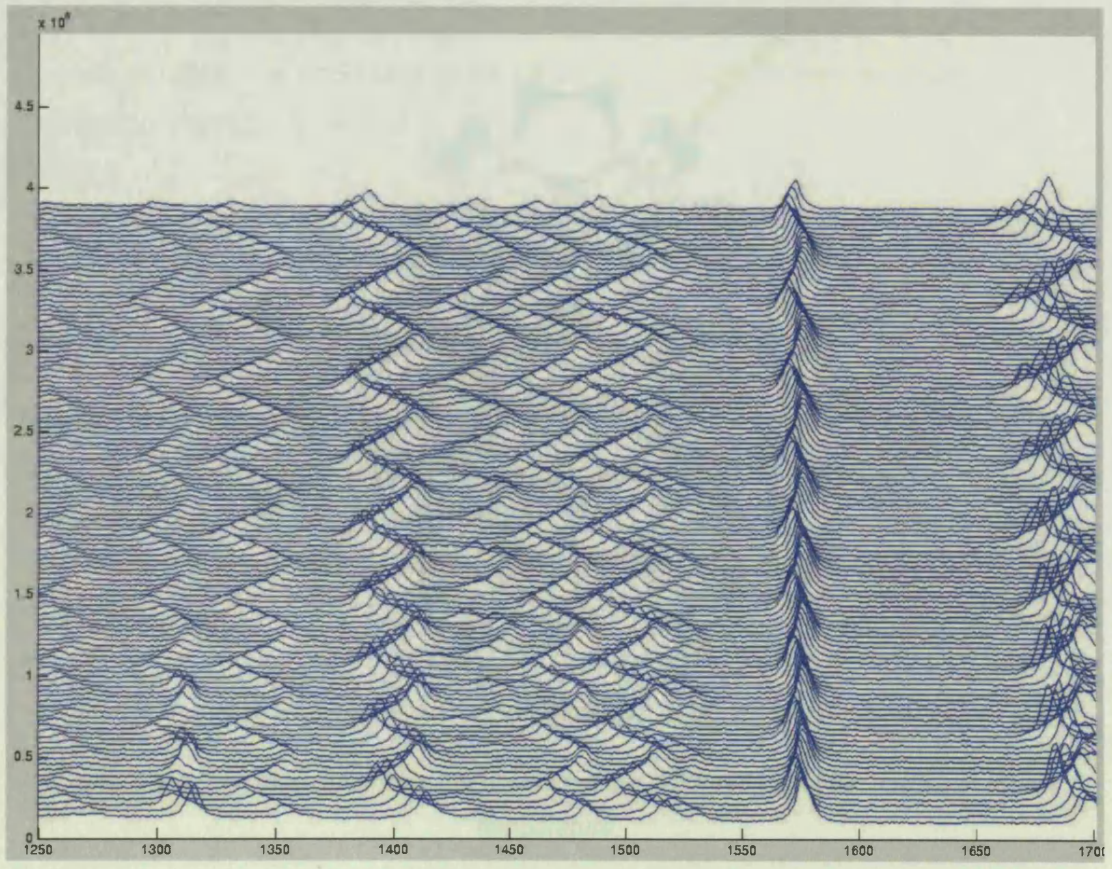

Figure 5.6.3: The diagram shows stacked data for cyclic heating experiments carried out on NaSi. Each pattern represents 59 seconds and every 10th pattern is shown. The X scale represents channel number, the Y scale is arbitrary.

The next important change occurring in the system is incredibly unexpected; this is the peak appearing after two heating cycles around 1430-1450. The transient appearance of peaks at this point is highly unexpected, and suggests some reversibility in the formation. This peak represents the (220) clathrate reflection at around 23.07° 2θ; this reflection is usually a weak, low intensity reflection whose reflection plane runs through a sodium atom at centre of the tetrakaidecahedral cage in the clathrate (*see Figure 5.6.4*). This information suggests again the importance of the guest atom in the formation of the clathrate structure. The interesting point to note also, is the close proximity to the NaSi (-311) peak at 23.26° 2θ (*see Figure 5.6.5*); the (-311) peak runs centrally through several sodium positions.

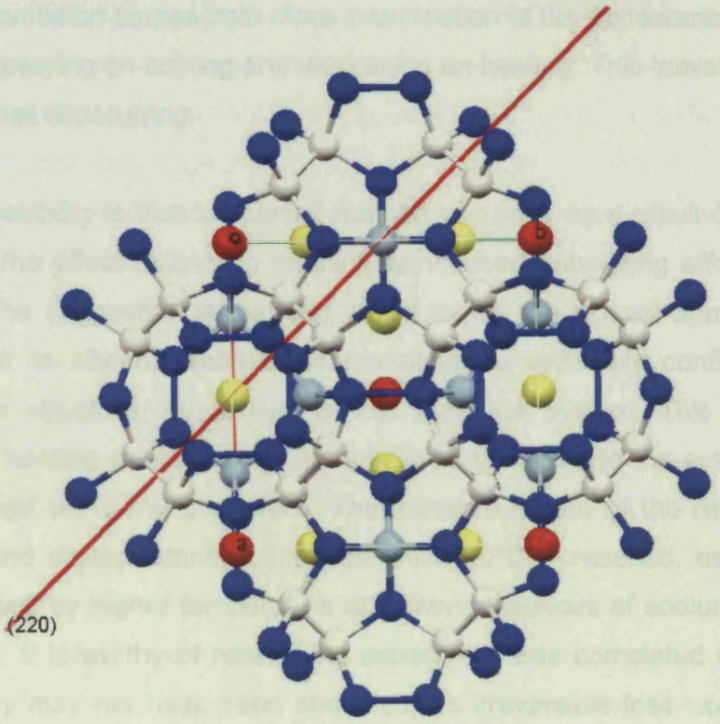

Figure 5.6.4: The diagram shows the position of the (220) reflection for Na_8Si_{46} at room temperature.

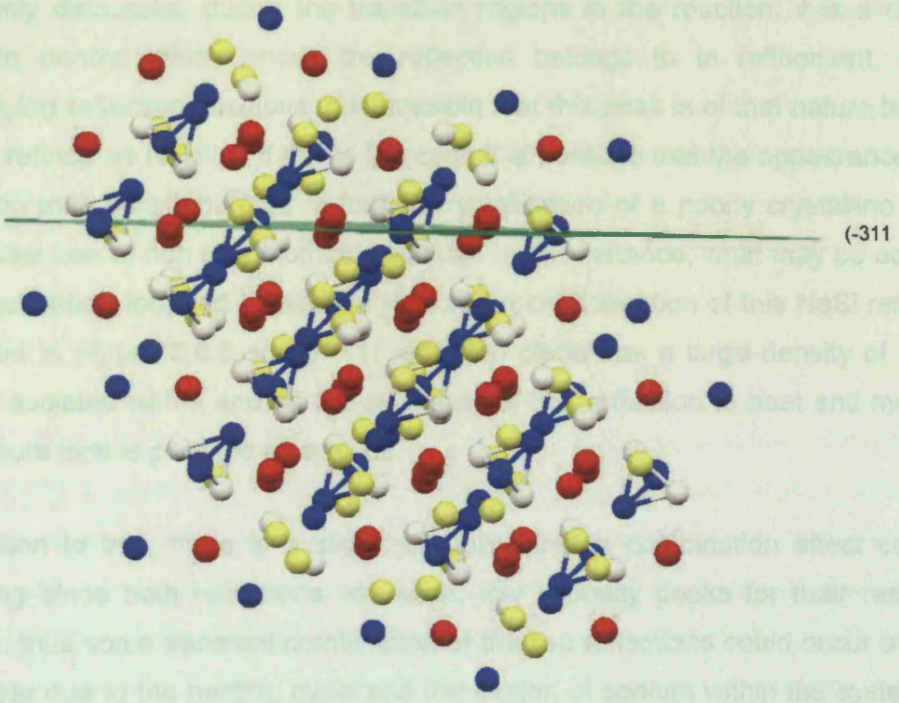

Figure 5.6.5: The diagram shows the position of the (-311) reflection for NaSi at room temperature.

A surprising revelation comes from close examination of the appearance of this peak; the peak is appearing on cooling and dissipating on heating. This leaves two possible solutions to what is occurring:

1: The first possibility is that templating may be occurring as a result of temperature reduction i.e. the effect of cooling creating an induced templating effect by thermal contraction. The suggestion is that this would cause the closest approach of sites that will result in silicon silicon bond formation, to artificially configure into the clathrate cage structure, as sodium is lost from the system. This state is then dissipated by heating reintroducing the volatilised sodium into the system that may have condensed on to the glassware. The transient nature of the reflection i.e. its appearance and disappearance continues until 450°C is reached, as the clathrate form is stabilised by higher temperature and irreversible loss of sodium by attacking the glassware. It is worthy of note, if the experiment was completed under vacuum the reversibility may not have been observed, as irreversible loss would seemingly have been forced by the vacuum system.

2: The second possibility is that the reflection is purely attributable to NaSi. As previously discussed, during the transition regions in the reaction, it is a complex issue to denote which phase the reflection belongs to in refinement, due to overlapping reflection positions. It is possible that this peak is of that nature though it can be refined as Na_8Si_{46}. If this is the case it is possible that the appearance of the reflection may be attributable to further crystallisation of a poorly crystalline phase, after initial loss of non stoichiometric sodium. In this instance, what may be occurring is crystallisation followed by sodium loss and recrystallisation of this NaSi reflection. As noted in *Figure 5.6.5*, the (-311) reflection plane has a large density of sodium sites associated with it and so the sensitivity of this reflection to heat and motion of the sodium ions is possible as a result.

In addition to this, there is a slight possibility that a combination affect could be occurring since both reflections are weak, low intensity peaks for their respective phases, thus some transient combination of the two reflections could occur and thus disappear due to the heating cycle and the motion of sodium within the system as a result. Given the relatively low intensity, it is possible that the areas that appear to show disappearance of the peak, are regions of low intensity for which the peak is lost into the background signal.

It is important to note the possibilities within the system, as a result of the difficulty of refining two phases with overlapping reflections. The above two suggestions are both possible in terms of the limitations of the Rietveld fit. However, the fact that the peak persists as temperatures around 450°C and higher are reached – the ideal temperature for the synthesis of clathrate I in this environment - does lend weight to the peak belonging to the clathrate phase.

In conclusion, the experiment gives an interesting insight into the nature of the sodium loss during the reaction. The picture portrayed here suggests that the question of physical versus chemical expansion and the effect of sodium loss is not simple. It is clear from this particular experiment that there is physical thermal expansion, reversible chemical change and irreversible chemical change occurring during the reaction. It is important to note, that this experiment was not conducted under vacuum as result of the desire to improve data quality; had vacuum been used the result would seemingly have been to lower the temperature at which the formation is irreversible and potentially remove possibility of reversible formation for the reflection. This experiment then, results in information that not only illuminates the physical versus chemical expansion question but additionally feeds speculation on the mechanism of formation of the clathrate. These experiments were the last to be completed towards the end of the study and so it would be of considerable value to repeat them under more controlled conditions in the future; such experiments would undoubtedly provide further insight into both the original question and the mechanism of formation for the clathrate.

5.7: Discussion of the Possible Mechanisms of Formation

The initial aim of this study was to attempt to explain the mechanism of formation of the clathrates, when synthesised by thermal degradation from Zintl phases. After extensive study of the reaction by synchrotron methods and ^{23}Na NMR (*see Chapter 7*), it is possible to pass conjecture on a possible mechanism associated with this chemical change. Consideration of the data discussed in sections 5.4 through 5.6 leads a good outline mechanism at work in this process. Details of these mechanisms are now presented:

Templating by Sodium Atoms

The first mechanism that logically presents itself is the role of sodium atoms as a template for formation of the structure by presenting a nucleation site, of sorts, for the cages to form.

- On heating, the sodium silicide undergoes a large expansion of its unit cell volume. This plateaus off as full temperature is reached and the structure reaches some energetic expansion limit.
- At the absolute limit of expansion the tetrahedra are strongly distorted and thus silicon sites become chemically inequivalent, such that reconfiguring of sodium ions is required to subtly move position to provide electronic balance in the system (as can be seen for the (-202) plane of NaSi at high temperature).
- During the expansion period, a number of reflection planes for sodium silicide undergo strong deviations in 2θ; these reflections are in most cases associated with planes that are heavily populated by sodium ions. These strongly deviating reflections are in some cases directly "locked-in" to reflection planes in the clathrate, by a crystalline continuum between the structures. The associated reflections in the clathrate structure - in at least two cases - represent sodium atoms residing at cages centres.
- After a period of time at full temperature, the silicide unit cell undergoes a rapid drop in volume. This affect may be due to a rapid loss of sodium from the structure or may be an artificial consequences of poor vacuum provided to the confined reaction environment, impeding the reaction; thus a dual phase reaction is suggested but is not the true nature of the reaction, as is supported by the difficult refinement issues associated with the region post pattern 130.
- The period of high expansion at constant temperature for NaSi ends for unknown reasons but it is sensible to suggest that this occurs to due to slow loss of the sodium atoms from the system. As the stoichiometry of the silicide becomes increasingly imbalanced, the overall charge in the system becomes imbalanced in turn. In specific terms, certain silicon sites will retain balancing sodium charge where others loose the closest associated charge and are left with a free loan pair. The result of this would be to provide imbalanced silicon sites for which the formation of silicon silicon bonds is becoming more favourable with increasing time.

- As the loss of sodium continues, the remaining sodium stoichiometry would become low enough such that the silicon tetrahedra per sodium charge would have increased markedly. It is conceivable that, as a result of building charge and tetrahedral distortion, the most highly charged silicon sites would begin to crowd the remaining sodium sites, as predicted by Landau theory and observed in other systems by Dove *et al*[8, 9]. This would of course continue until it is energetically more favourable to form silicon silicon bonds than continue to crowd the remaining sodium sites.
- For such a mechanism to occur, sodium must be reduced in order to leave the system. In addition, formation of silicon silicon bonds may in some cases occur via atypical silicon coordination geometries - via routes involving the interaction of vacant silicon *d*-orbitals - to facilitate such a mechanism.
- In essence, the reality would be that the initial templating sites would be provided by sodium but as a result of the facilitation of the reaction, via flexible chemistry at silicon sites, silicon sites of high coordination geometry would provide scattered sub-nucleation sites around which Si-Si bonding occurs. It is likely that this process is occurring on femto- or atto-second timescales and thus would not be observable using conventional synchrotron techniques.

A schematic representation of the steps associated with the mechanism in this process, is illustrated in Figures 5.7.1 through 5.74.

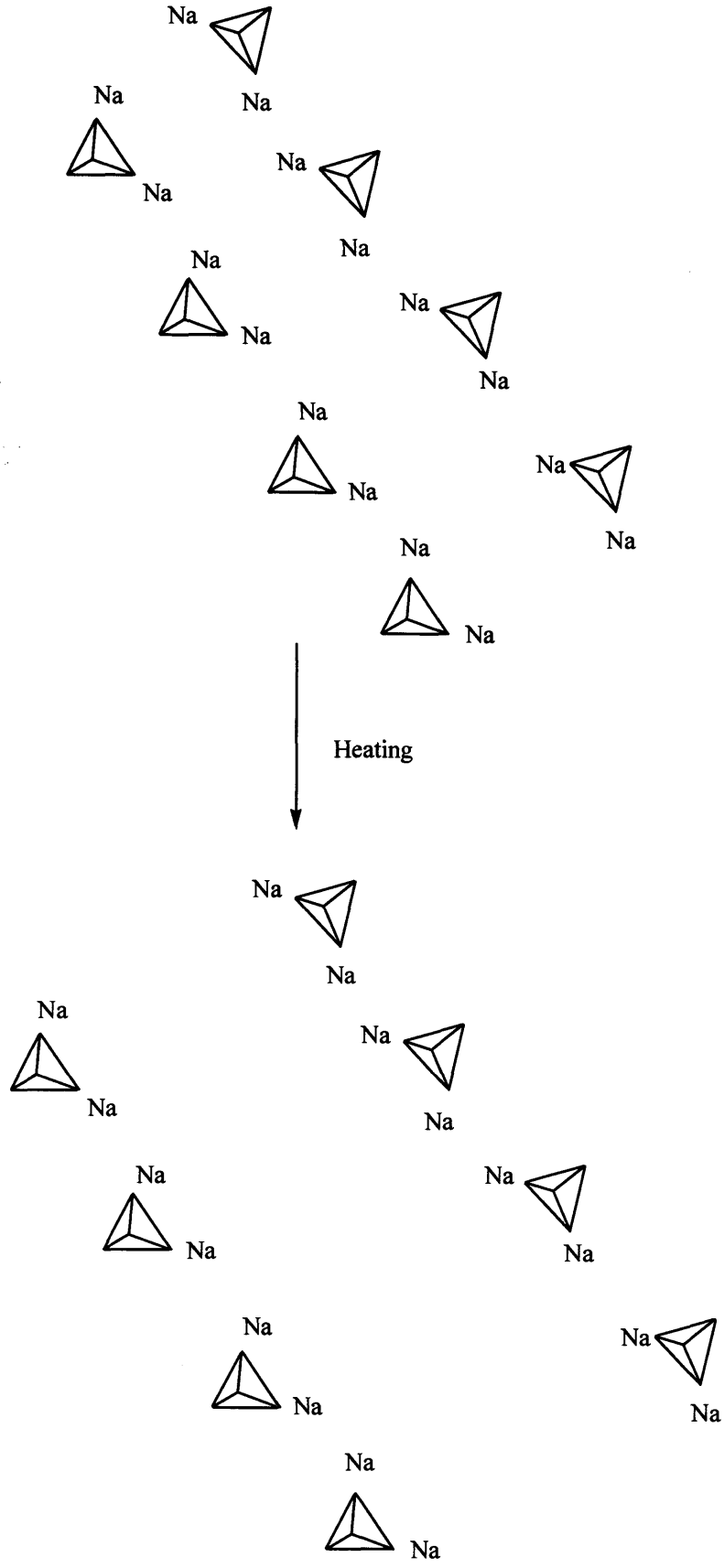

Figure 5.7.1: Schematic representation of the mechanism of formation of clathrate I. The diagram represents NaSi undergoing string thermal expansion.

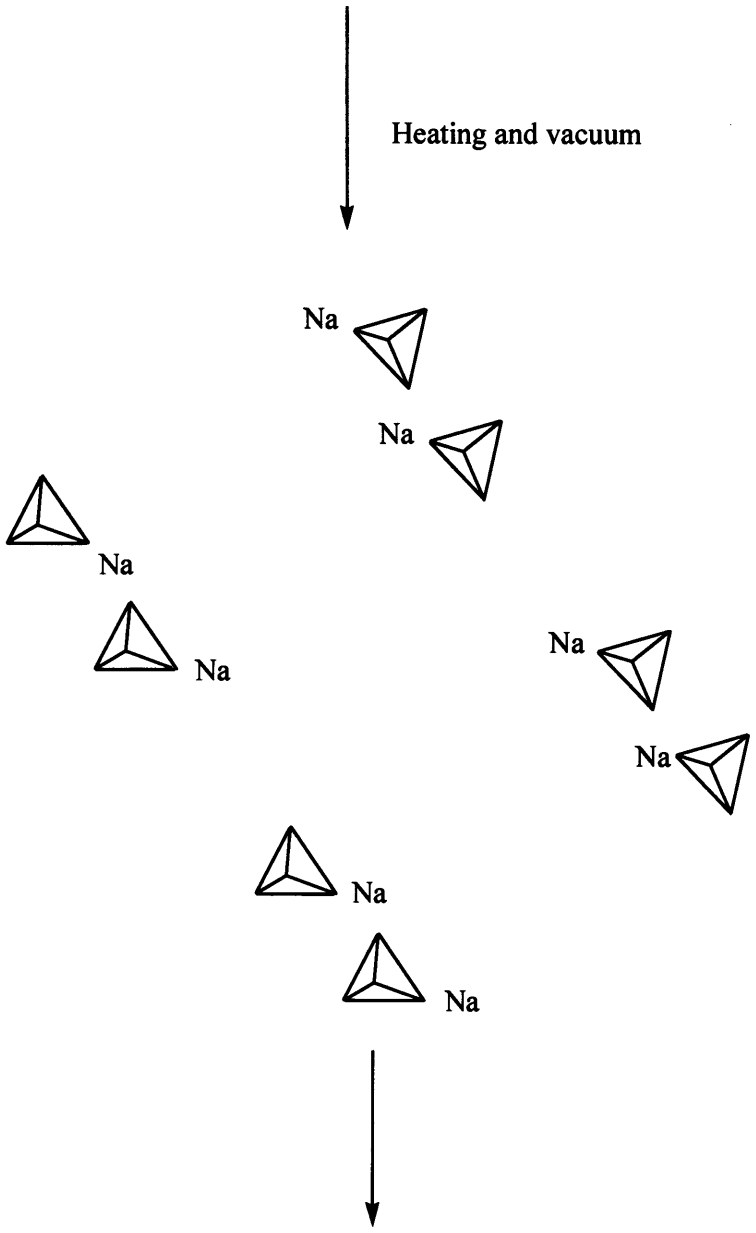

Figure 5.7.2: Schematic representation of the mechanism of formation of clathrate I. The diagram represents NaSi beginning to loose sodium and the structure begins discrete reordering.

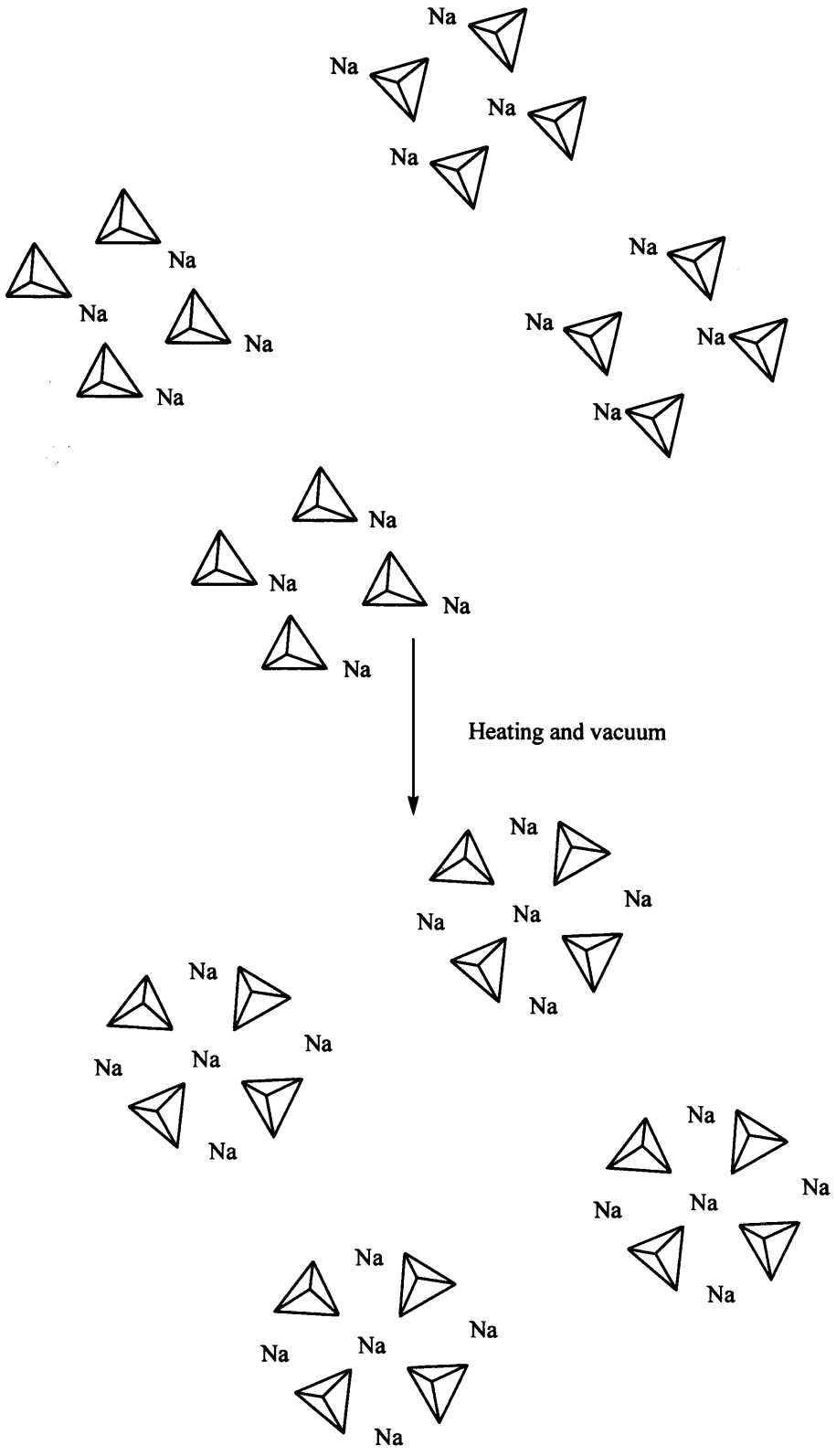

Figure 5.7.3: Schematic representation of the mechanism of formation of clathrate I. Diagram shows the reordering of silicon tetrahedra occurring around the remaining sodium sites as charge imbalance increases in the system due to continuing sodium loss.

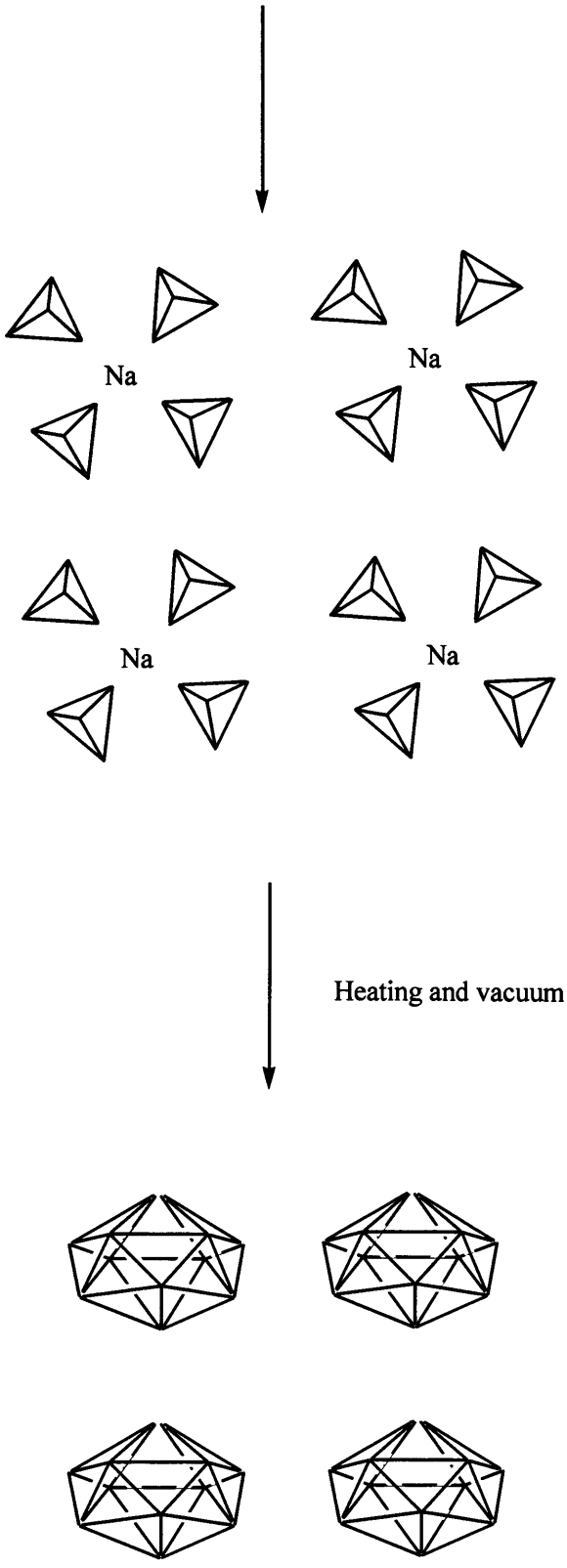

Figure 5.7.4: Schematic representation of the mechanism of formation of clathrate I. Diagram shows the formation of clathrate cages as a result of nucleation by sodium sites, facilitated by further sodium loss and charge imbalance in the system.

The Possibility of a Transient Rhombohedral Phase:

The space groups of the zintl phase and clathrate present in this reaction system are markedly different being *C2/c* and $Pm\bar{3}n$, respectively. As discussed previously, there is seemingly no obvious link between these structures, particularly in terms of the chemistry of each phase. However, on examination of the crystallographic space group tables, it becomes apparent that the two may share a relationship through a subgroup, supergroup relationship. The rhombhedral space group $R\bar{3}c$ represents a space group that is a subgroup to the clathrate I, $Pm\bar{3}n$, phase and a supergroup to the zintl phases, *C2/c*. This information leads to the suggestion that the area of the transition region that is not currently refineable by Rietveld methods may, in fact, represent a phase transition to a rhombohedral phase.

Given this information, refinements were attempted on the transition region using an $R\bar{3}c$ space group. However, the reaction is characterised by the loss of sodium atoms from the system such that the reaction can proceed. This loss of sodium cannot be quantified by the methods used in this study and so it if for these reasons that a full Rietveld refinement is not possible in this instance. As such a Lebail refinement was attempted but did not yield conclusive results as a consequence of the complexity of the reaction system. The inability to fit a rhombohedral phase for these regions does not however, rule it out of hand completely. For this system the loss of sodium and high temperature results in the associated phases existing under both expansion and compositional flux, as sodium is lost and the reaction system continues to form the clathrate. Its is then almost impossible with the techniques used in this experiment to determine if such a phase does, in fact, exist as a transient between the zintl and clathrate phases. These issues may be countered by the use of neutron diffraction techniques due to a higher spatial resolution and the ability to follow the motion of sodium nuclei in the system.

The limitations in the refinement and experiment to deal with the change in stoichiometric composition, proved to make the possibility of a transient phase in this system a currently unanswerable question. However, examination of the literature shows a number of interesting materials that crystallise in the $R\bar{3}c$ space group, that bear some visual structural resemblance to the NaSi structures in the late transition region as well as the clathrate I phase (*see Figures 5.7.5 and 5.7.6*).

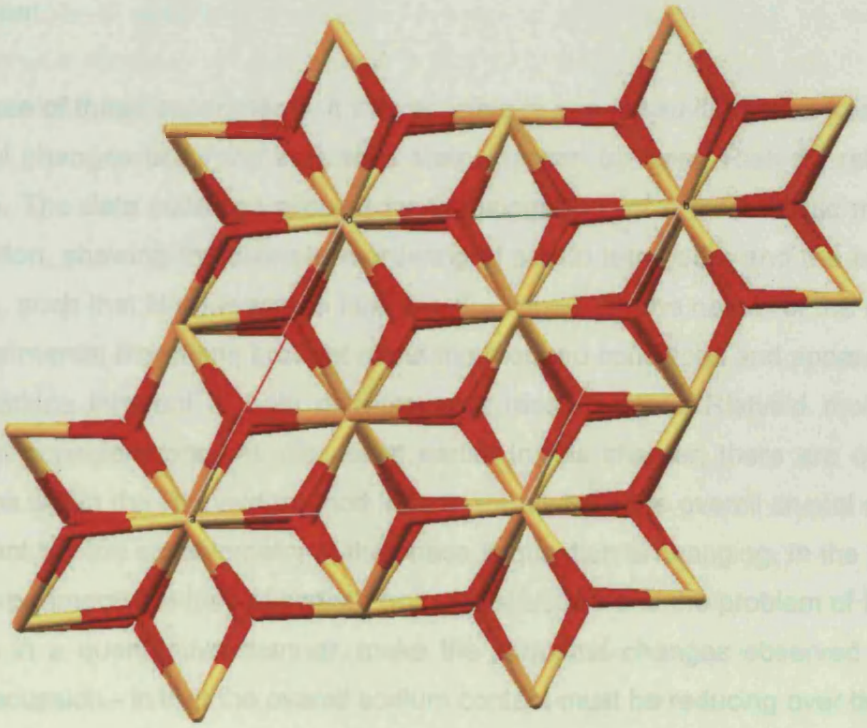

Figure 5.7.5: Structure of α-Al_2O_3 shown along the c axis.

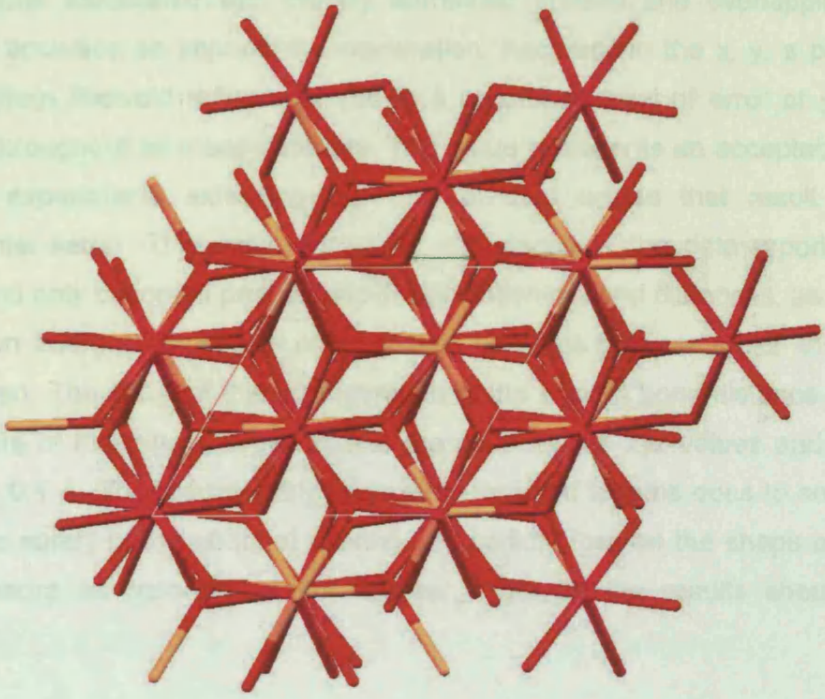

Figure 5.7.6: Structure of $LiNbO_3$ shown along the c axis.

Discussion:

In the case of these experiments, it was possible to use *in situ* diffraction to study the structural changes occurring in a solid state reaction by using Rietveld refinement methods. The data collected allowed for the suggestion of a mechanistic model for the reaction, showing the discrete reordering of silicon tetrahedra and the balancing Na^+ ions, such that NaSi reacts to form Na_8Si_{46}. However, the nature of the reaction, the experimental limitations brought about the required conditions and apparatus and the limitations inherent in both diffractometer resolution and Rietveld method are important considerations. As discussed earlier in this chapter, there are of course limitations within the Rietveld method for a system where the overall crystal structure is constant but the stoichiometry of the phase in question is changing. In the instance of this experiment, the loss of sodium from the structure and the problem of following this loss in a quantitative manner, make the structural changes observed open to some discussion - in that the overall sodium content must be reducing over time.

Where the resolution of the diffractometer is concerned the issue is complex. The challenging nature of the experiment i.e. the necessity to have a static sample and the problems associated with closely correlated phases and overlapping peaks, make the accuracy an important consideration. Accuracy in the x, y, z parameters collected from Rietveld refinement shows a consistent level of error of $\pm$ 0.005 Å routinely throughout all measurements. This value represents an acceptable level of error for experiments exhibiting the kind of data issues that result from the experimental setup. This value allows for confidence in the data reported in this chapter and only becomes problematic in calculation of bond distances, as a result of contribution from xyz directional error, at both positions between which the distance is measured. The result of this consideration of the error in bond distance makes for error orders of magnitude larger than is the case for the xyz values and fall in the order of $\pm$ 0.1 Å. The considerably large error for bond lengths does to some extent reduce the surety of the affect of heating and sodium loss on the shape and size of the tetrahedra as reported in this chapter – though the results should not be dismissed.

The mechanistic detail associated with the formation of the clathrates under these circumstances, has been suggested in this chapter. The experiments have clear disadvantages versus what is possible in an environment without the restrictions seen in the synchrotron beam line environment, but have been successful in

collecting data of excellent quality and margin of error, considering the limitations inherent here. However, in formulating a suggested mechanism the great wealth of literature, collaborator interaction and laboratory/synchrotron observation lends considerable insight and weight to the mechanism expounded here. It is important then, that such considerations are discussed for the reader to view more clearly all of the information associated with the mechanism.

From the earliest experiments by Klemm[1] it was noted that heating of the Zintl phases resulted in sample weight loss (as seen using thermogravimetric analysis) and the formation of a cubic product. The work of Cros[18-22] elaborated on this and showed that the clathrates resulted as a product of this preparation. As time moved on it was found that of the two forms of the clathrate, the type II phase could be selectively deintercalated[3, 7, 23], by the application of vacuum and temperature and with excessive treatment in this manner or with reaction with iodine[24], a totally guest free structure could be achieved. It was also found during this period that the type I phase could not be deintercalated by these methods.

In the ensuing years, research in this area attempted to gain composition control of the clathrate phases to synthesise materials with favourable properties[2, 25]. This work lead to a considerably greater understanding of the conditions associated with the formation of the clathrates. It was found that the type I material was readily prepared using NaSi and slow temperature ramp rates and a range of temperatures assuming a constant vacuum could be achieved within acceptable levels. The formation of the type II clathrate was more difficult to induce from the NaSi Starting material, unless very rapid heating rates were used, often in excess of $50°Cmin^{-1}$. These results suggested that the type I phase is the thermodynamic product, forming under controlled and relatively mild conditions. The type II clathrate appears then as the kinetic product, in its requirement to be subjected to rapid reactions and essentially forcing conditions to promote synthesis with any phase purity. It was also often observed that a mixed product, containing both phases and elemental or amorphous silicon could result[2, 3, 7, 23], suggesting that the reaction system was in fact complex and finely balanced and comprising metastable phases.

A great deal of simulation and theoretical work predicted and studied many structural properties within the known clathrate family and the yet to be synthesised, theoretically predicted materials. The work of Bridges[4] suggested that the guest species may undergo interactions with the polyhedral cage structures within the

clathrate phases, further inferring that the guest atoms may appear off-centre with respect to the cages as a result. This prediction and the propensity for clathrate II to deintercalate under vacuum heating and the total absence of the same behaviour for the clathrate I phase, posed interesting questions about the nature of the interaction of the clathrate phases and their guest atoms not only after formation but during the formation of the phases from the Zintl phase intermediates. Further more, the metastable nature of the phases concerned and the often finely balanced reaction systems added weight to the questions being raised about the guest atoms role in the clathrate formation; was there, in fact, some vital energetic structural role played by the guest atoms in these materials?

In the late 90's and beginning of the new millennium the work of Gryko[5, 6] on the affects of variation of the Zintl starting material, such that the stoichiometric amounts of sodium varied from 1 to as much as 4, presented some surprising results. It seemed that the use of an amorphous alloy of NaSi (approximately $Na_{3-4}Si$, or perhaps more appropriately $Na_x(NaSi)$, where x = 1-3), makes it possible to produce the clathrate II phase using low ramp rates and low reaction temperatures, as the pure, majority product; this result is entirely juxtaposed versus the result seen where NaSi is used. Further more, on using temperatures higher than 400°C, the product began to exhibit a mixture of clathrate I and II, again the exact opposite of the reaction using the NaSi crystalline starting material where increasing the reaction temperature increased the phase percentage of clathrate II in a mixed product.

So in the original reaction using NaSi as the starting reagent, the clathrate II phase is only formed when loss of sodium is very rapid i.e. where high ramp is used; however, in the instance where the amorphous, sodium rich alloy is the starting reagent, where a vast excess of sodium is presnt in the system, the formation of the clathrate II phase appears to be stabilised and has now become the thermodynamic product. The clathrate I phase under these circumstances is only produced by using high temperature and forcing conditions and can be seen as the kinetic product when using a large excess of sodium. Under these circumstances it appears a large excess of sodium stabilises the reactively unstable product, where a 1:1 stoichiometry of sodium requires very rapid degassing of the NaSi sodium to form the clathrate. This also suggests that the clathrate II phase with its larger polyhedra is by some measure stabilised by a large excess of balancing positive charge in its formation. As an aside but relevant to this is the fact that the type I system cannot be deintercalated; what is the nature of the guest to framework interactions in this

phases such that deintercalation is not possible? This then must pose very pertinent questions about the true nature of the relationship between formation of the clathrate and the guest species.

A fortuitous event was to shed further light upon the reaction conditions within the system. Upon modification of the reaction system and applying a number of new apparatus iterations to the system, Gryko[5, 6], observed phase purity change with the diameter of the glassware apparatus, such that narrow diameter glass apparatus resulted in mixed phase products, where wide diameter resulted in phase pure products, assuming the appropriate conditions were chosen for such a reaction. This was, of course, in fact a consequence of the affect on the vacuum of the variation of glassware bore and so indirectly the affect on the rate of loss of sodium from the system. This suggested that the local vapour pressure of sodium in the reaction system may in fact, limit the formation of one or other phase and thus rate limit the reaction and result in a system that undergoes partial equilibration and thus exhibits partial phase impurity as a resulted of equilibration of the desired kinetic product to the undesirable thermodynamic product. These results again suggest that the fundamental factor in control of which phase is formed under what conditions, is inexorably tied to the rate of loss of the guest species.

So now a picture begins to appear in which the rate of loss of guest species is fundamental in phase denomination but also the use of extremes of guest species in the starting material, can profoundly affect the nature of the products with respect to the conditions used, effectively reversing the kinetics associated with the two phases.

On completion of the earliest *in situ* synthesis experiments, signs of a structural link between the Zintl phase and clathrate I phase began to suggest the mechanism that has been expounded in this chapter. Strong support for the mechanism comes in the refinement data showing that the "lock-in" structural relationships in the x-ray data centre around the sodium positions for both the NaSi phase and the clathrate I – importantly for the clathrate, often at the cages centres. Thought it has never formally been expressed in the literature, its was long suspect that the guest species may by some means template the formation of the clathrate, by performing some role in a capacity as a centre of balancing charge for transition states occurring at the silicon sites in the formation of silicon silicon bonds. Though it has not been proven conclusively in this study, the methods employed and the experiments developed have gone some way to add wait to these suppositions.

5.8: References

1. Klemm, W., *Metalloids and their compounds with the alkali metals.* Proc. Chem. Soc. London, 1958: p. 329-341
2. Ramachandran, G., et al., J. Solid State Chem, 1999. **145**.
3. Gryko, J., P. McMillan, F, and O. Sankey, F, Phys. Rev. B, 1996. **54**.
4. Bridge, F. and L. Downward, Phys. Rev. B, 2004. **70**.
5. Gryko, J., *Personal Communication.* Jacksonbille State University, 2006.
6. Gryko, J., P. Hutchins, T, and P. McMillan, F, Unpublished Results, 2006.
7. Gryko, J., et al., *Low-density framework form of crystalline silicon with a wide optical band gap.* Phys. Rev. B, 2000. **62**.
8. Dove, M., T, *Theory of displacive phase transitions in minerals.* American Mineralogist, 1997. **82**: p. 213-244.
9. Swainson, I., P, M. Dove, T, and M. Harris, J, *Neutron Powder Diffraction Study of the Ferroelastic Phase Transition in Sodium Carbonite.* Condensed Matter Physics, 1995. **7**: p. 4395-4417.
10. Evans, J.S. and I.R. Evans, *Beyond Classical Applications of Powder Diffraction.* Royal Society of Chemistry: Tutorial Review, 2004. **33**: p. 539-547.
11. Walton, R., I and D. O'Hare, *Watching solids crystallise using in situ powder diffraction.* Chem. Commun, 2000. **2000**: p. 2283-2291.
12. Witte, J. and H. Von Schnering, G, Z. Anorg. Allg. Chem., 1964. **327**.
13. GMBH, K.K. *Sodium Chloride Data.* 2007 [cited; Available from: http://www.korth.de/eng/503728952d091450d/503728952d0b6863b.htm.
14. Slack, G., A, Mater. Res. Symp. Proc, 1997. **478**.
15. Nolas, G., S, et al., Appl. Phys. Lett, 1999. **73**.
16. Paschen, S., et al., Phys. Rev. B, 2001. **64**.
17. Uher, C., J. Yang, and S. Hu, Mater. Res. Soc. Symp. Proc., 1999. **545**.
18. Cros, C., *Phd Thesis No. 229.* University of Bordeaux, 1970.
19. Cros, C., M. Pouchard, and P. Hagenmuller, Compt. Rend, 1965. **260**.
20. Cros, C., M. Pouchard, and P. Hagenmuller, *Sur deux nouvelles phases du système silicium-sodium.* C.R. Acad. Sc, 1965. **260**.
21. Cros, C., M. Pouchard, and P. Hagenmuller, *Sur une nouvelle famille de clathrates minéraux isotypes des hydrates de gaz et de liquides. interprétation des résultats obtenus.* J. Solid State Chem, 1970. **2**.
22. Cros, C., et al., *Sur deux composés du potassium isotypes de l'hydrate de krypton.* Bull. Soc. Chim. fr, 1968. **7**.

23. Gryko, J., P. McMillan, F, and O. Sankey, F, J. Solid State Chem, 1996. **145**.
24. Ammar, A., et al., *On the clathrate form of elemental silcon, Si136 : Preparation and characaterisation of NaxSi136 (X->0). .* Science, 2004. **6**.
25. Ramachandran, G., *PhD Thesis.* Arizona State University, 2003.

Chapter 6

Studying rapid degassing of NaSi using x-ray in situ synchrotron x-ray diffraction: Attempted synthesis of clathrate II

6.1: Further Experiments:

Included in the original goal of this study was the desire to synthesise both the clathrate I and clathrate II materials and to do this under a variety of conditions. Multiple experiments were completed using various target synthesis temperatures, heating durations and ramp rates. As has been mentioned earlier, many of the data sets were lost as a result of the formation of *d*-Si as a by product of the reaction to such an extent that the data were virtually unusable.

However, a certain number of datasets using variable conditions were viable and are reported here. The least significant of these in terms of new information, were those of variable heating duration and variable synthesis temperature. In the case of variable heating time, the reactions show either, poorly crystalline products in the case of shorter heating, or increasingly well crystallised and phase pure products for increasingly longer reactions. For variable synthesis dwell temperatures the issue is again relatively simple; for low temperatures the reaction is slower in beginning and generally requires considerably longer reaction time for high purity and crystallinity to be reached. In the case of higher dwell temperatures, i.e. those above 500°C, it is generally observed that the reaction begins before the heating stage has ended and thus the data provides a more difficult picture to analyse, since the structural changes are occurring at variable temperature.

Among these data sets for both variation of temperature and variation of heating duration, there are two common features in the data. The first common feature is the complex nature of the transition region, in which very close similarity of reflection positions results in the refinement issues discussed throughout chapter 5. The second feature is the presence of "locked-in" reflections, between the two phases. The prevalence of these two features as common to all datasets provides encouraging qualitative comparison versus the data that was susceptible to Rietveld refinement.

Variation of the temperature ramp at which the synthesis dwell temperature is reached, was to be amongst the most intriguing experiments but least valuable in terms of Rietveld refinement. It has been known since the earliest work of Ramachandran *et al* [1], [2] that "flash degassing" - the use of rapid heating under vacuum - can be used to induce selective formation of the clathrate II phase versus the clathrate I phase. Such synthetic procedures require precise control of the

reaction environment and rely firmly on the ability to provide high vacuum (10^{-5} bar). However, despite the confined reaction environment and a vacuum of an order of magnitude lower than is used for the laboratory synthesis, it was possible to use the same basic assembly to run very high ramp rate experiments. Using the furnace described in Chapter 4 with precise control and monitoring, using a eurotherm controller and software interface, it was possible to use ramp rates between 50°Cmin^{-1} and 250°Cmin^{-1} (it was also possible to preheat the furnace and drive it precisely onto the sample from the control room, essentially providing a near instant flash heat). Calibration of the system using boron nitride showed very rapid heat exchange with little or not noticeable lag in temperature delivery to the sample. The use of such high temperature delivery rates adds somewhat to the difficulty of the experiment, in that thermal shock becomes a considerable issue that must be overcome for successful completion of the synthesis. The problems of thermal shock can be alleviated to some extent by very careful loading of the sample, such as to ensure good packing of the sample and utilise the affects of the silicides strong electrostatic adhesion affects, in association with the quartz surface of the capillary. The problem may also be reduced by means of a period of vacuum degassing, to remove nitrogen gas present in the sample from the glove box preparation; during rapid heating it is probably that expansion of any residual gas will cause the sample to be dislodged into the vacuum system. In addition, careful stabilisation of the vacuum before heating goes some way to reducing the instance of thermal shock unloading of the sample into the vacuum line. Though these means reduce this issue in the experiment, it does not entirely remove such possibilities occurring and indeed thermal shock unloading of the sample was relatively common. This occurred regularly enough such that it prompted the use of seal capillaries with no associated vacuum, for some of the experiments.

Though challenging, the experiments gave rise to a number of complex data sets for which refinement with full parameter variation was near impossible. Some of these datasets were subjected to analysis by careful variation of the parameters of triple and dual phase refinement environments, by careful manipulation of the refinement parameters in Rietveld analysis by hand. It was in this manner possible to identify the presence of clathrate II reflections occurring in a number of reactions, using the flash degassing methodology. *Figures 6.1.1 - 6.1.9* show one such experiment. The experiment in question shows a sealed capillary, flash heated by driving the furnace onto the sample at full temperature and then retain at 500°C for several hours, while data is collected every 30 seconds.

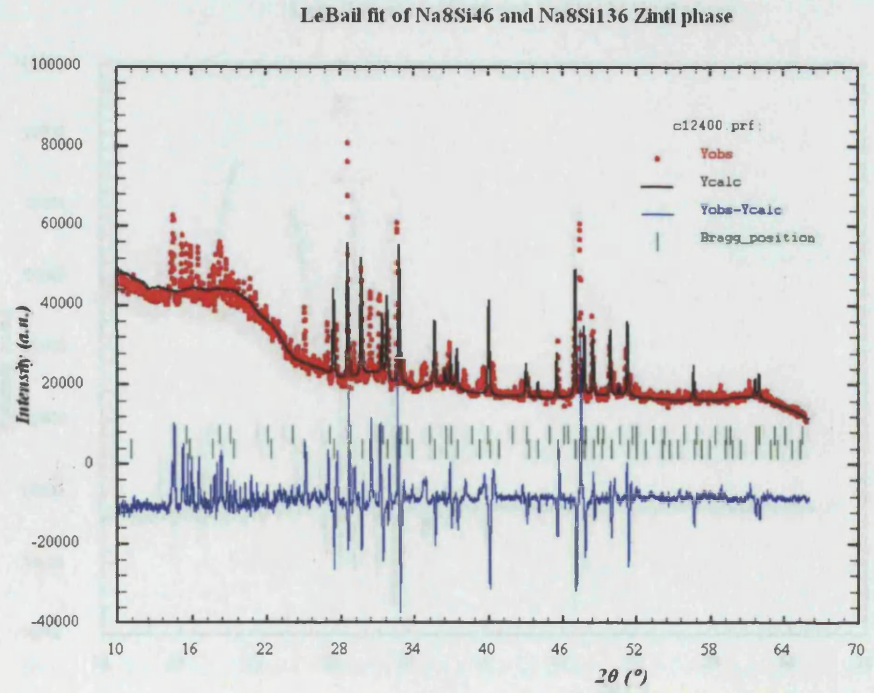

Figure 6.1.1: The diagram shows the dual phase refinement of Na_8Si_{46} and $Na_{24}Si_{136}$ during flash degassing at 500°C at 200 minutes into the reaction.

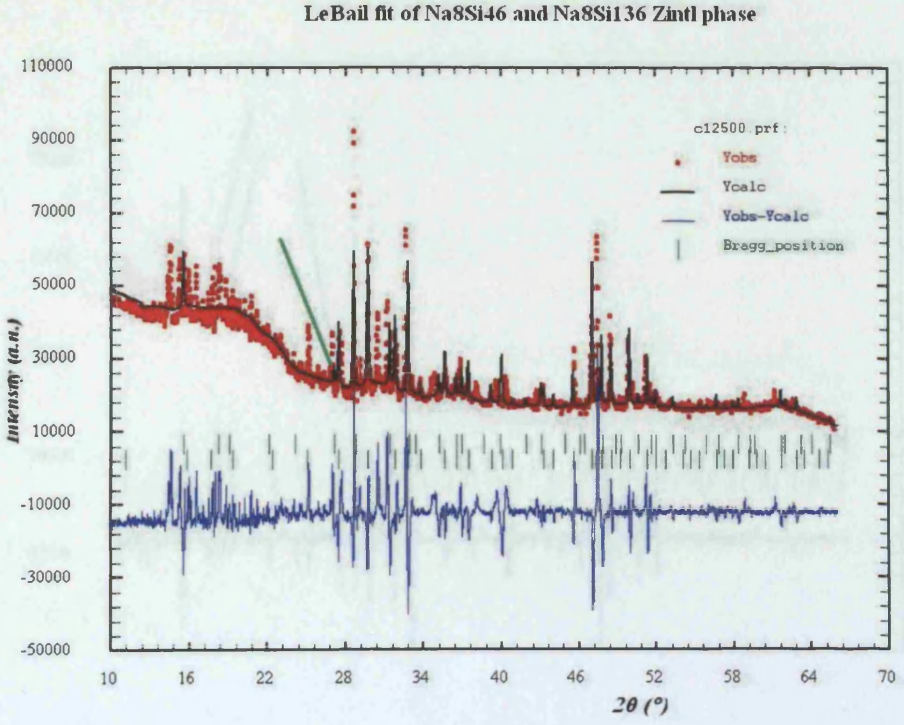

Figure 6.1.2: The diagram shows the dual phase refinement of Na_8Si_{46} and $Na_{24}Si_{136}$ during flash degassing at 500°C at 250 minutes into the reaction.

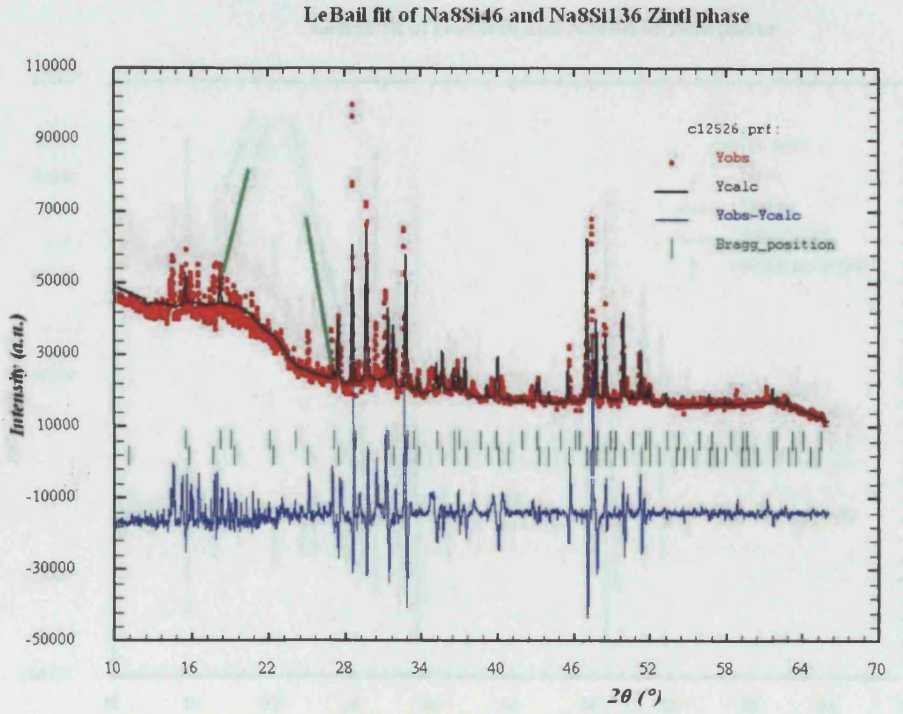

Figure 6.1.3: The diagram shows the dual phase refinement of Na_8Si_{46} and $Na_{24}Si_{136}$ during flash degassing at 500°C at 263 minutes into the reaction.

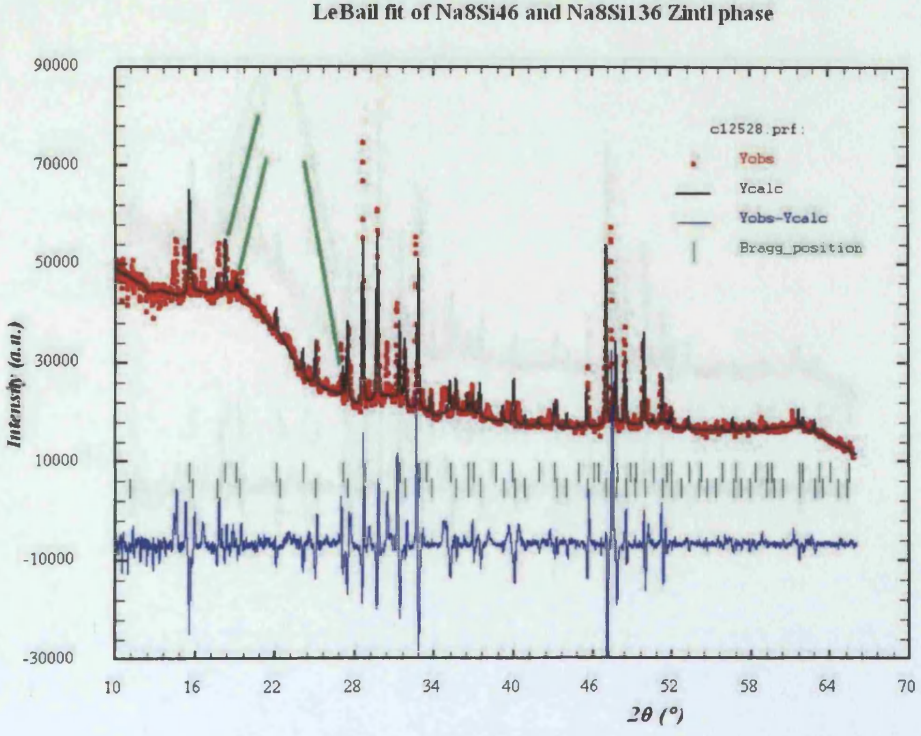

Figure 6.1.4: The diagram shows the dual phase refinement of Na_8Si_{46} and $Na_{24}Si_{136}$ during flash degassing at 500°C at 264 minutes into the reaction.

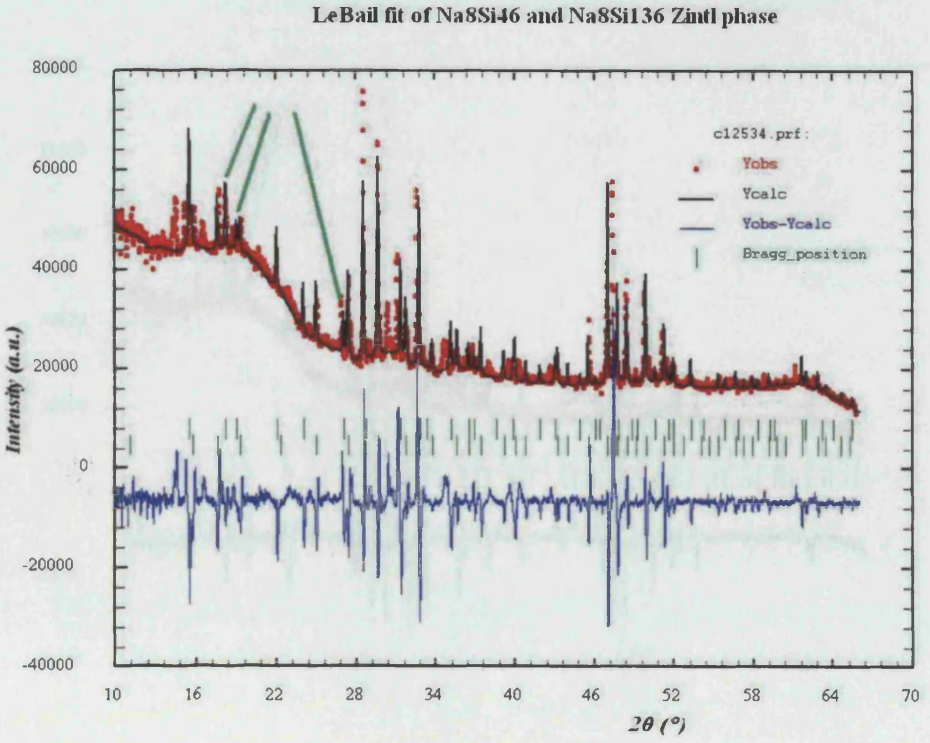

Figure 6.1.5: The diagram shows the dual phase refinement of Na_8Si_{46} and $Na_{24}Si_{136}$ during flash degassing at 500°C at 267 minutes into the reaction.

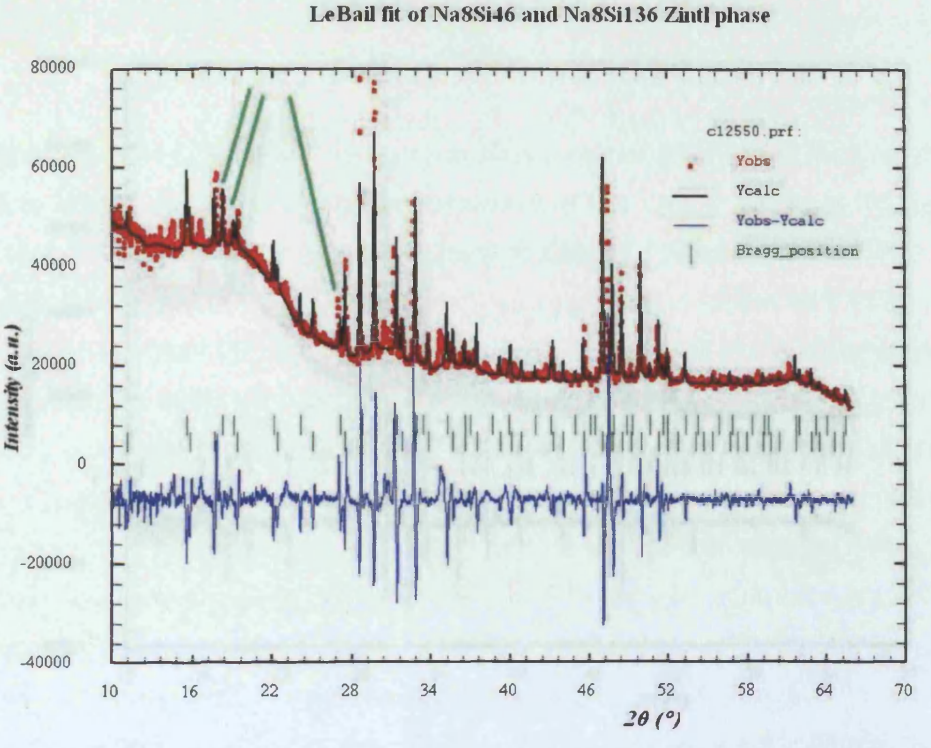

Figure 6.1.6: The diagram shows the dual phase refinement of Na_8Si_{46} and $Na_{24}Si_{136}$ during flash degassing at 500°C at 275 minutes into the reaction.

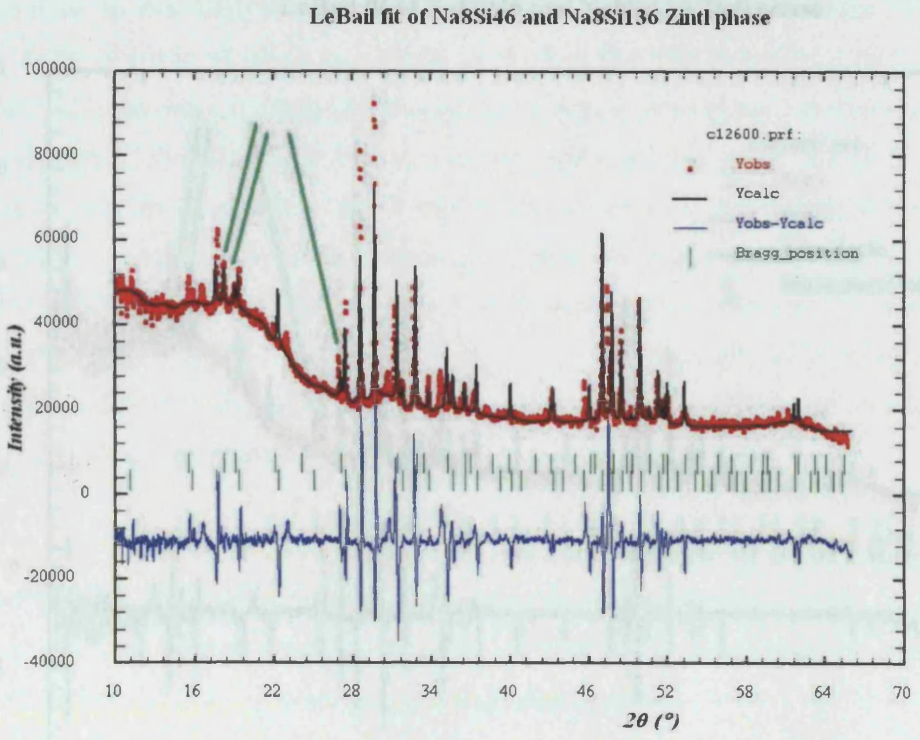

Figure 6.1.7: The diagram shows the dual phase refinement of Na_8Si_{46} and $Na_{24}Si_{136}$ during flash degassing at 500°C at 300 minutes into the reaction.

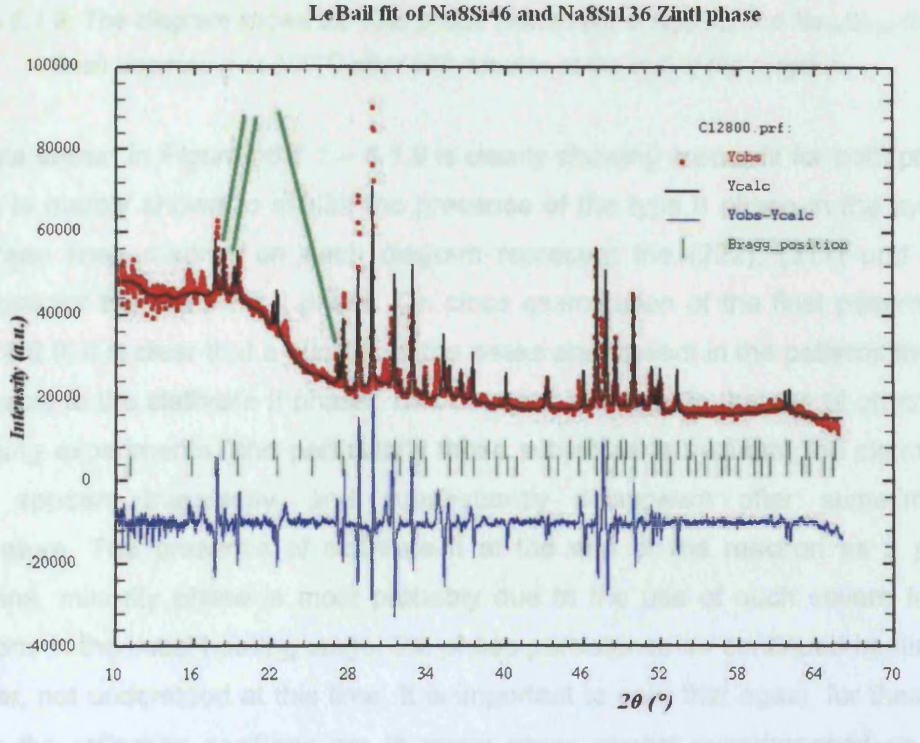

Figure 6.1.8: The diagram shows the dual phase refinement of Na_8Si_{46} and $Na_{24}Si_{136}$ during flash degassing at 500°C at 400 minutes into the reaction.

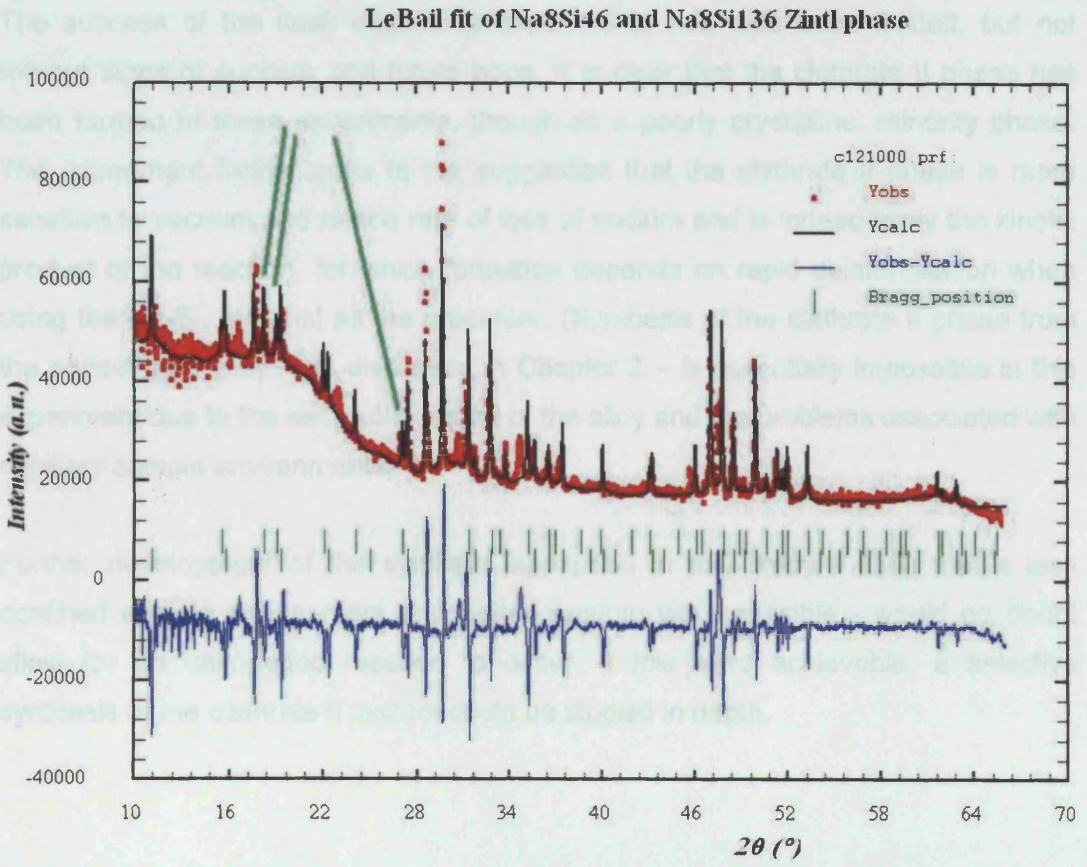

Figure 6.1.9: The diagram shows the dual phase refinement of Na_8Si_{46} and $Na_{24}Si_{136}$ during flash degassing at 500°C after 500 minutes at the end of the reaction.

The data shown in *Figures 6.1.1 – 6.1.9* is clearly showing a poor fit for both phases and so is merely shown to exhibit the presence of the type II phase in the system. The green lines marked on each diagram represent the (222), (311) and (422) reflections for the clathrate II phase. On close examination of the final pattern (*see Figure 6.8.9)* it is clear that a number of the peaks are present in the patterns that are attributable to the clathrate II phase. This data set is unique in that for all other flash degassing experiments (and particularly those subjected to vacuum) the clathrate II phase appears transiently, and subsequently disappears after sometime at temperature. The presence of clathrate II at the end of the reaction as a poorly crystalline, minority phase is most probably due to the use of such severe forcing conditions in the initial heating stage; the phase persistence on continued heating, is, however, not understood at this time. It is important to note that again, for these two phases the reflection positions are in many cases almost superimposed on each other, this again compounds the issue of phase identification.

The success of the flash degassing experiments has thus been limited, but not without signs of success and future hope. It is clear that the clathrate II phase has been formed in these experiments, though as a poorly crystalline, minority phase. The experiment further adds to the suggestion that the clathrate II phase is more sensitive to vacuum and hence rate of loss of sodium and is indeed likely the kinetic product of the reaction, for which formation depends on rapid deintercalation when using the Na_1Si_1 material as the precursor. (Synthesis of the clathrate II phase from the sodium rich alloy – as discussed in Chapter 2 – is essentially impossible in this experiment due to the semi solid nature of the alloy and the problems associated with capillary sample environments).

Further development of the synthetic apparatus in this study - such that a less confined sample environment and better vacuum were possible - would no doubt allow for an unimpeded reaction to occur. If this were achievable, a selective synthesis of the clathrate II system could be studied in depth.

6.2: References

1. Ramachandran, G., et al., J. Solid State Chem, 1999. **145**.
2. Ramachandran, G., *PhD Thesis.* Arizona State University, 2003.

Chapter 7

Studying Synthesis of Solid State Clathrates *in situ* using ^{23}Na NMR

7.1 Introduction:

The *in situ* x-ray diffraction studies showed that on heating NaSi exhibits a large thermal expansion, which combined with the loss of sodium from system to drive the reaction, brings into question the nature and activity at the sodium sites during heating, at high temperature and during clathrate formation. Realisation of experiments *in situ* using synchrotron techniques, made clear that it was indeed possible to study the nature of the reaction where NaSi is induced to form clathrate I. However, as more information became available from the experimental runs, more and more questions were raised about the nature of sodium during the reaction and the role it plays in formation of the clathrate. As has been discussed in Chapter 5, it is a fundamental limitation of the Rietveld method that it cannot account for loss of sodium from the system, which must occur for the reaction to proceed. There are several small experimental observations that result from the *in situ* synchrotron experiments, which feed further into speculation on the sodium atoms state and role in the process:

1. In stoichiometrically imbalanced silicides, sodium sensitive reflections often show large intensity drops as heating begins and 100°C is reached and the excess sodium is lost into the vacuum system. This poses the question, what is the nature of the sodium in the system at full temperature and during the reaction? Is the sodium closer to liquid on heating or does it remain in the solid state and essentially sublime out of the system, when vacuum is applied? If the sodium is closer to the liquid state what does that imply about the mechanism of formation of the clathrate; can the sodium exist almost as a liquid metal solvent in which the reaction occurs?
2. The cyclic heating experiments shown in Chapter 5, section 6 demonstrate that the formation of clathrate appears to be reversible under certain circumstances. The question then is, what is the nature of the sodium such that it may initially be lost and then reintroduced into the system to reform the silicide structure? Is this suggesting that the sodium is sitting in the system as vapor and may be reintroduced on cooling? Is the sodium resident as a liquid and may be reintroduced on cooling?
3. It is clear that sodium must be lost from the system but some amount must also remain for the clathrate to be formed. As details of the suggested mechanism became clear (as discussed in Chapter 5), it was obvious that

there was the possibility of more than one state in which sodium may reside during the transformation.

These questions obviously could not be answered by using *in situ* synchrotron techniques and so it was to solid state nuclear magnetic resonance imaging (NMR) the study turned. ^{23}Na NMR has been employed in the field of clathrates research previously[1], [2], and has been shown to provide clear denomination of sodium sites within the differing polyhedral clathrate cages. Given successful use in previous studies, ^{23}Na NMR would seem to be perfect for consideration of the sodium sites in the reaction, if a high temperature congener of the *in situ* experiment could be completed. The experiments were completed in collaboration with the University of Warwick, department of physics, using a custom designed probe capable of temperatures in excess of 1000°C.

Though a high temperature ^{23}Na NMR experiment was feasible there were a number of considerations that make such an experiment technically more problematic. As such it is important to consider the differences between this experiment and the *in situ* x-ray diffraction experiments.

1. The first issue is that the chosen sample holder cannot contain any sodium and must be able to be filled under inert conditions and sealed without exposure to atmosphere.
2. The nature of the NMR magnet and probe are such that provision of vacuum is essentially impossible. This limitation meant experiments were to be completed without any vacuum applied to the sample.
3. The temperature control used in the experiments was not capable of controlled ramps and therefore, rapid collection. As such temperatures were set manually and the system allowed to equilibrate before data collection was completed.
4. Data collection was on the minutes timescale and could require as long as 30 minutes for good data to be collected.

So a ^{23}Na NMR experiment was possible for studying the sodium sites in the system during the reaction. The limitations however, make the experiment not an exact copy of the *in situ* study. These limitations and the complicated experimental considerations aside, it was beneficial to attempt to study the sodium sites in more detail to determine their nature during heating and the transformation.

7.2 Experimental Detail:

The high temperature NMR probe used in these experiments was developed by Smith *et al*[3] at the University of Warwick department of physics (*see Figure 7.2.1*). The probe is composed of ceramic tube around which the nichrome heating coil is wound. The copper radio-frequency (RF) coil is placed through a ceramic tube, mounted onto a brass base that seals the system into place. The system is designed for static high temperature NMR; though rotors may be used as serviceable sample containers they are not however, ideal for high temperature work.

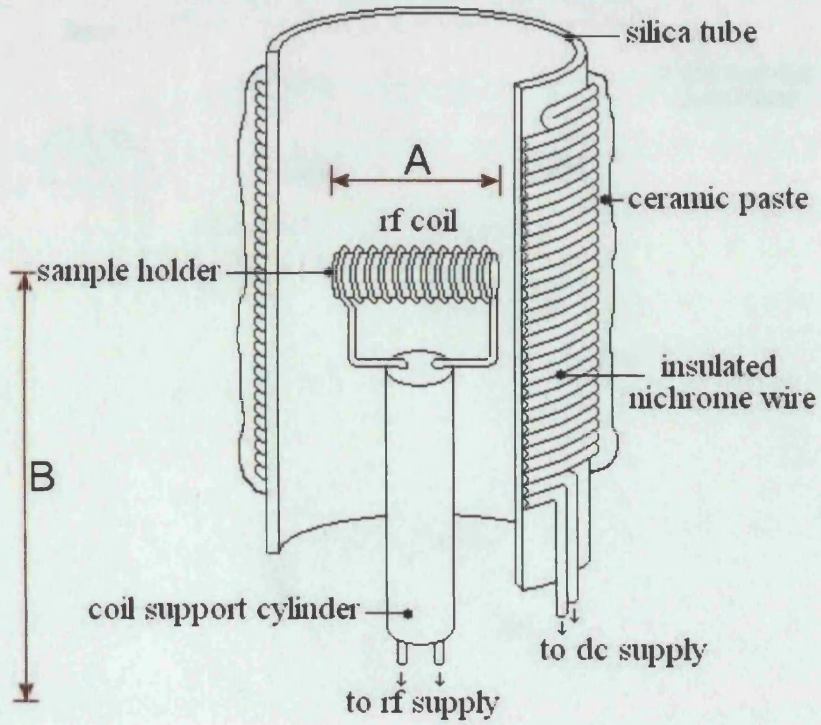

Figure 7.2.1: High temperature NMR probe capable of operation up to and exceeding 1000°C. A = 2.5 cm, represents the maximum size of any sample container, horizontally across the probe. B = 7.5 cm, distance from the bottom of the radio frequency coil to the base of the probe. This represents the maximum vertical size of any sample holder[3].

A sample holder was designed that could be loaded in the inert atmosphere of the dry-box and sealed off for the duration of the experiment. Additionally, the container was required to contain no sodium in its composition and be operable up to 600°C or greater. The arrangement of the probes inner compartment allows for 2.5 cm horizontally and 7.5 cm vertically (*see Figure 7.2.1*), when considering apparatus

used inside the probe environment. These restrictions suggested the best possible candidate was SiO_2 glass tubing, which was hand blown and sealed using a glass torch. The obvious solution would be to make a pill shaped sample holder within the 2.5 cm limitation – essentially a mimic of standard NMR rotors – but this was unsuitable, requiring heating and sealing of the glass very close to the NaSi, which reacts rapidly at glass-torch temperatures. The solution was to make an "L-shaped" glass tube which can be sealed at one end, loaded inside a glove-box and placed into a sealed vacuum assembly for evacuation, the sample is then evacuated and sealed using a high temperature glass-torch (*see Figure 7.2.2*).

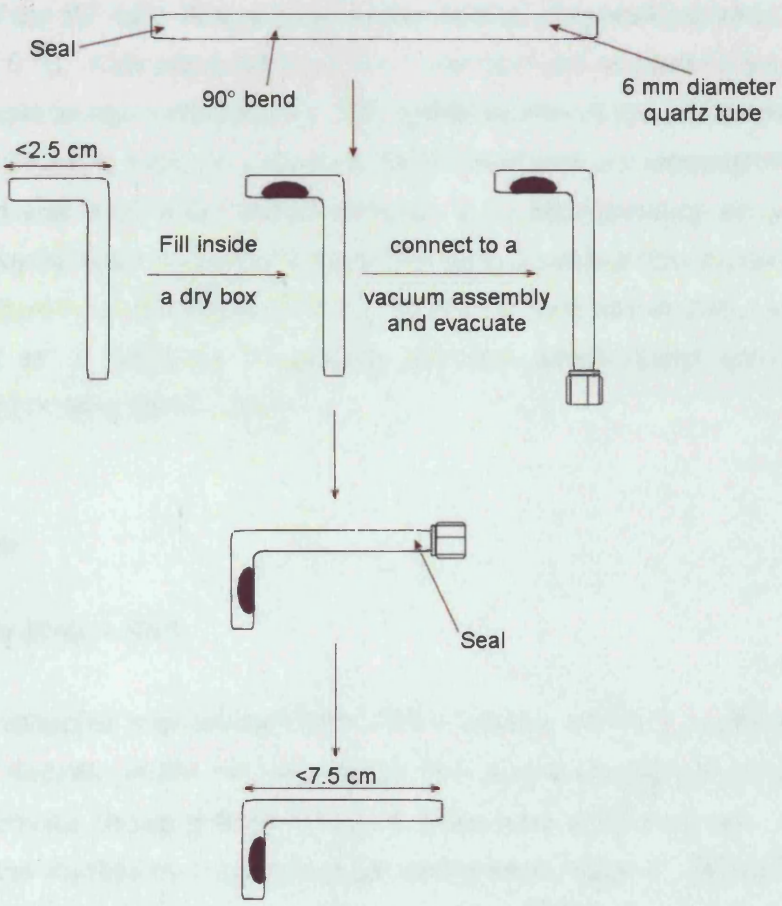

Figure 7.2.2: Procedure for making high temperature NMR sample holders from SiO_2 glass tubing.

The SiO_2 glass sample holder was then placed into the RF coil and is held in place using non-flammable tape, which melts on heating - this serves to keep the sample situated correctly during insertion of the probe.

Static ^{23}Na NMR spectra were recorded using the custom-built probe (*see Figure 7.2.1*) in a 7.05 T magnetic field, corresponding to a ^{23}Na Larmor frequency of 79.3 MHz. Heating of the sample was achieved via a resistive nickel/chromium coil wound in a bifilar way with its axis parallel to the magnetic field and the RF coil at the centre. This coil was held in place by a SiO_2 glass tube and ceramic cement, and insulated with silica fibre material. The coil had a resistance of approximately 22 Ω, and sample temperatures of up to 1000 °C were easily possible using a 100 W DC power supply.

Calibration of the probe was previously conducted with a thermocouple placed at the position of the RF coil. At any given power setting, temperatures were reproducible to within ± 5 °C. After adjusting the power, one hour was allowed for the temperature of the sample to reach equilibrium. The heated section of the probe was surrounded by a water jacket to keep the outside of the probe at ambient temperature. The pulse width used was 3 μs which was determined to be approximately equal to a 90° tip angle. Recycle delay was set at 1 second to allow an acceptable signal to noise ratio to be obtained in a relatively short space of time (around 30 minutes). Aqueous NaCl was used as a reference compound, with the single sharp line from this at 79.385751211 MHz set to 0 ppm.

7.3 Results:

Site activity of Na in NaSi:

The data collected was phased such that a positive intensity profile was seen for NaSi and clathrate peaks, where present. The data were normalised and the 0ppm position defined versus a NaCl standard. Data were plotted as ppm versus signal intensity and stacked by temperature for comparative reasons. Several experiments were completed with a range of temperature conditions, to encompass a good spread across the possible synthesis temperatures, from both the lower end of the spectrum, around 400°C to the upper end at 600°C. Utilising temperatures above 550°C would not normally be considered for the clathrate synthesis due to the tendency for mixed phases to form at such high synthesis temperatures, however, in this experiment the absence of vacuum due to experimental restraints caused by the NMR apparatus, suggested the use of slight forcing conditions may prove fruitful. The use of forcing conditions was also suggested by preliminary runs completed at 375°C

using traditional NMR rotors; despite long heating, repeated runs failed to produce clathrate at 375°C, again due most probably to the absence of vacuum in the system. The first experiment completed in the SiO_2 glass sample holders, was a 405°C slow heat designed to retest the results previously seen at lower temperatures in the preliminary study; as previously seen the clathrate did not form. However, the state of the sodium sites for NaSi on heating was demonstrated (*see Figure 7.3.1*). At room temperature the sodium signal at 0ppm is characteristic of the sodium sites in NaSi. Na is a spin I=3/2 nuclei and therefore quadrapolar in nature. This gives rise to the characteristic asymmetric peak shape, seen at ambient temperatures. This peak shape represents spherical asymmetry of the sodium site in its specific chemical environment.

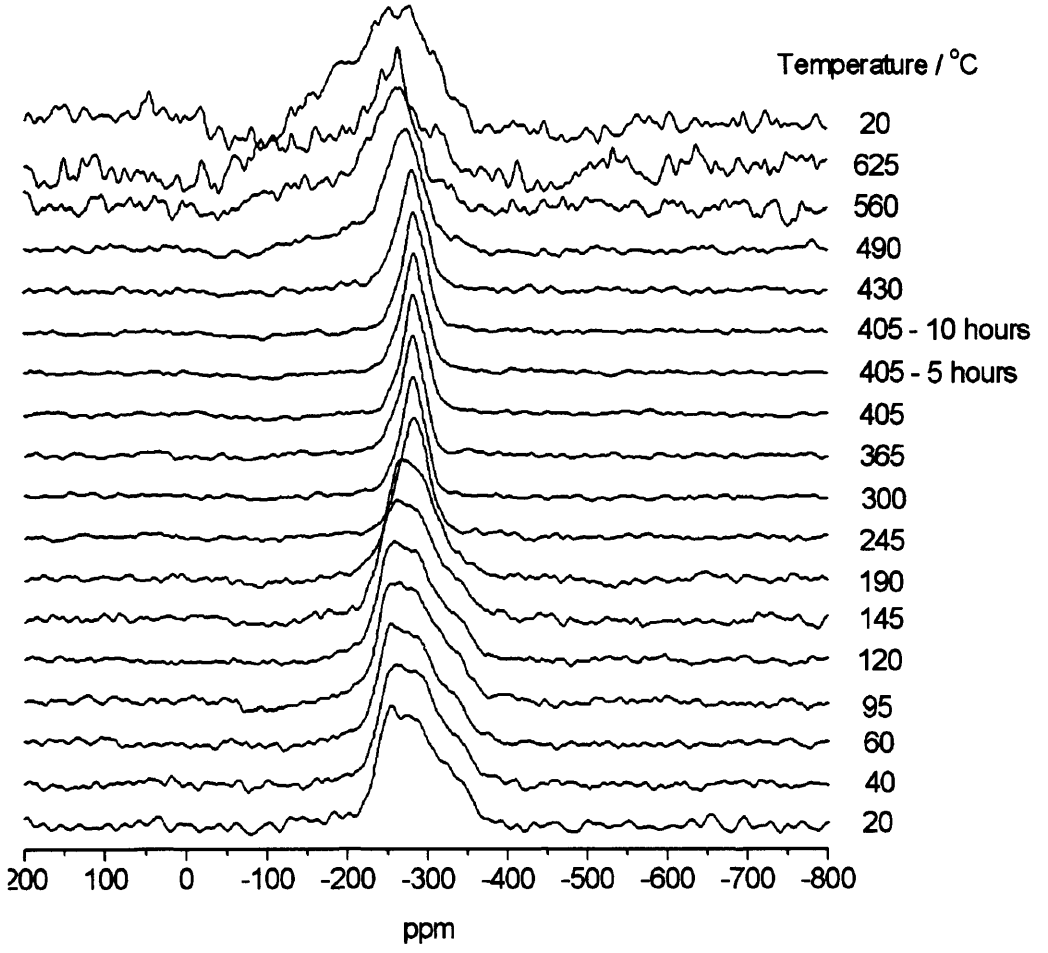

Figure 7.3.1: Stacked data for heating of NaSi from ambient to 405°C for the formation of clathrate. Data are stacked and arbitrarily separated by temperature for comparison. Note: -300ppm should be taken as 0ppm and is the result of incorrect calibration. Note RF coil destruction degrading data quality at high temperature.

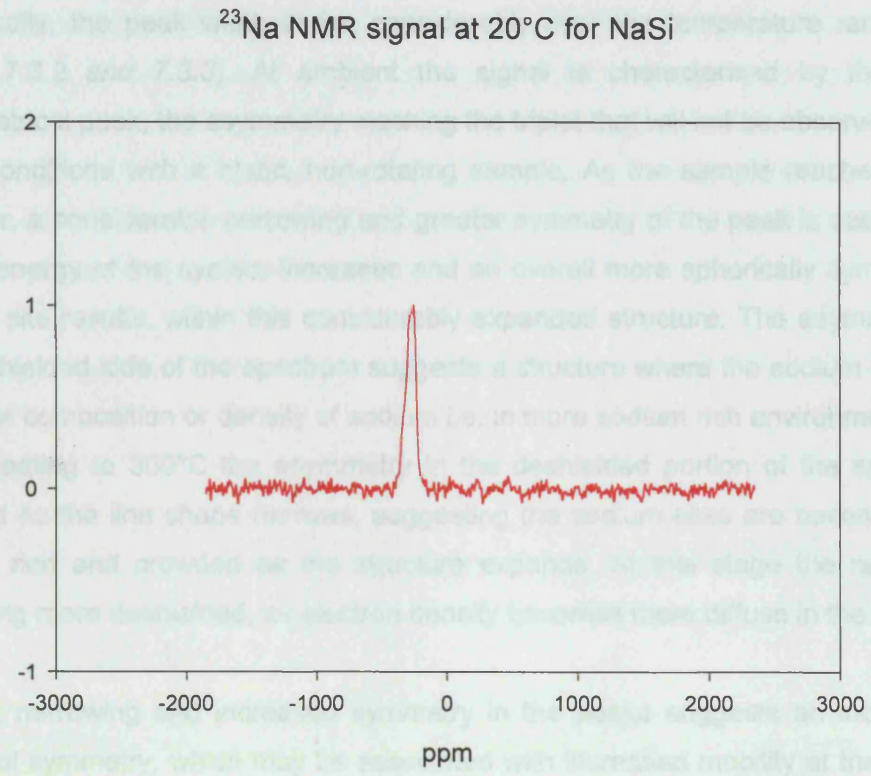

Figure 7.3.2: ^{23}Na NMR data at 20°C for NaSi showing peak shape and width.

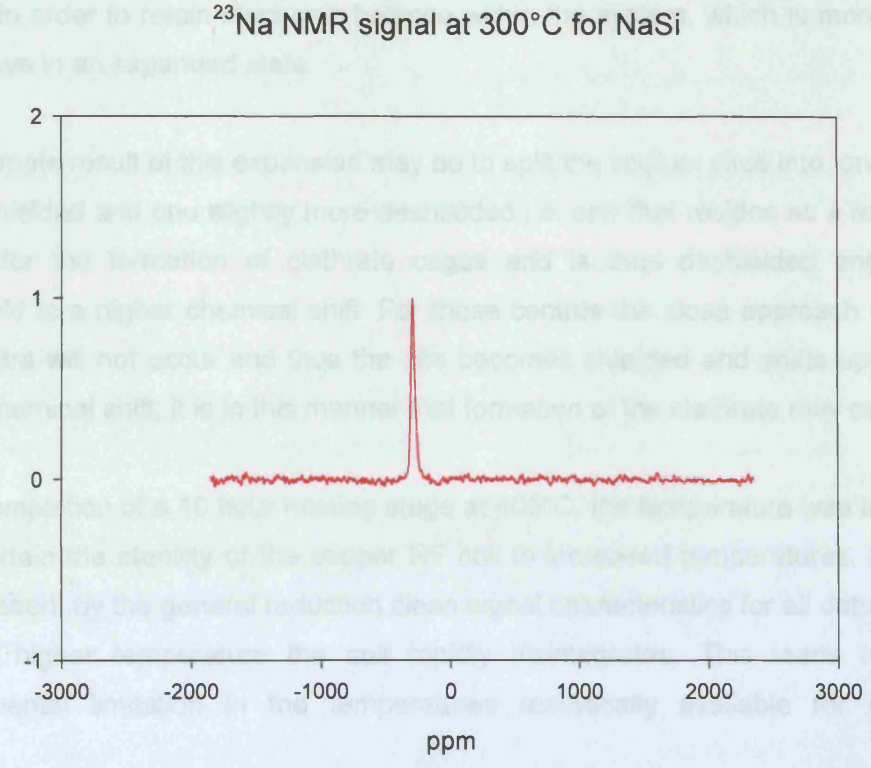

Figure 7.3.3: ^{23}Na NMR data at 300°C for NaSi showing peak shape and width.

Additionally, the peak width varies considerably over the temperature range (*see Figure 7.3.2 and 7.3.3*). At ambient the signal is characterised by the broad asymmetrical peak, the asymmetry masking the triplet that will not be observed under these conditions with a static, non-rotating sample. As the sample reaches 300°C however, a considerable narrowing and greater symmetry of the peak is seen as the kinetic energy of the system increases and an overall more spherically symmetrical sodium site results, within this considerably expanded structure. The asymmetry on the deshielded side of the spectrum suggests a structure where the sodium sites are of higher composition or density of sodium i.e. in more sodium rich environments[4], [5]. Upon heating to 300°C the asymmetry in the deshielded portion of the spectra is reduced as the line shape narrows, suggesting the sodium sites are becoming less sodium rich and crowded as the structure expands. At this stage the nuclei are becoming more deshielded, as electron density becomes more diffuse in the system.

Overall, narrowing and increased symmetry in the peaks suggests an increase in spherical symmetry, which may be associated with increased mobility at the sodium sites as heating leads to more expanded structure. The apparent deshielding would suggest possible reduction in the electron density of the sodium sites as the expansion within the system forces electron density to become more diffuse. This occurs in order to retain electronic balance within the system, which is more difficult to achieve in an expanded state.

The ultimate result of this expansion may be to split the sodium sites into, one slightly more shielded and one slightly more deshielded i.e. one that resides as a templating region for the formation of clathrate cages and is thus deshielded and shifted downfield to a higher chemical shift. For these centres the close approach of silicon tetrahedra will not occur and thus the site becomes shielded and shifts upfield to a lower chemical shift; it is in this manner that formation of the clathrate may occur.

After completion of a 10 hour heating stage at 405°C, the temperature was increased to ascertain the stability of the copper RF coil to increased temperatures. It can be clearly seen, by the general reduction clean signal characteristics for all data regions, that at higher temperature the coil rapidly disintegrates. This leads to further experimental limitation in the temperatures realistically available for extended periods.

The trends seen in this experiment were again observed in further experiments at 400°C with a 10 hour heating stage (*see Figure 7.3.4*). In this experiment however, the sample was cooled to ambient after the heating stage instead of further heating to test the RF coil, as in the first experiment. The data collected shows better a signal to noise ratio on the whole and clearly demonstrates the same peak narrowing and increase in peak symmetry on heating.

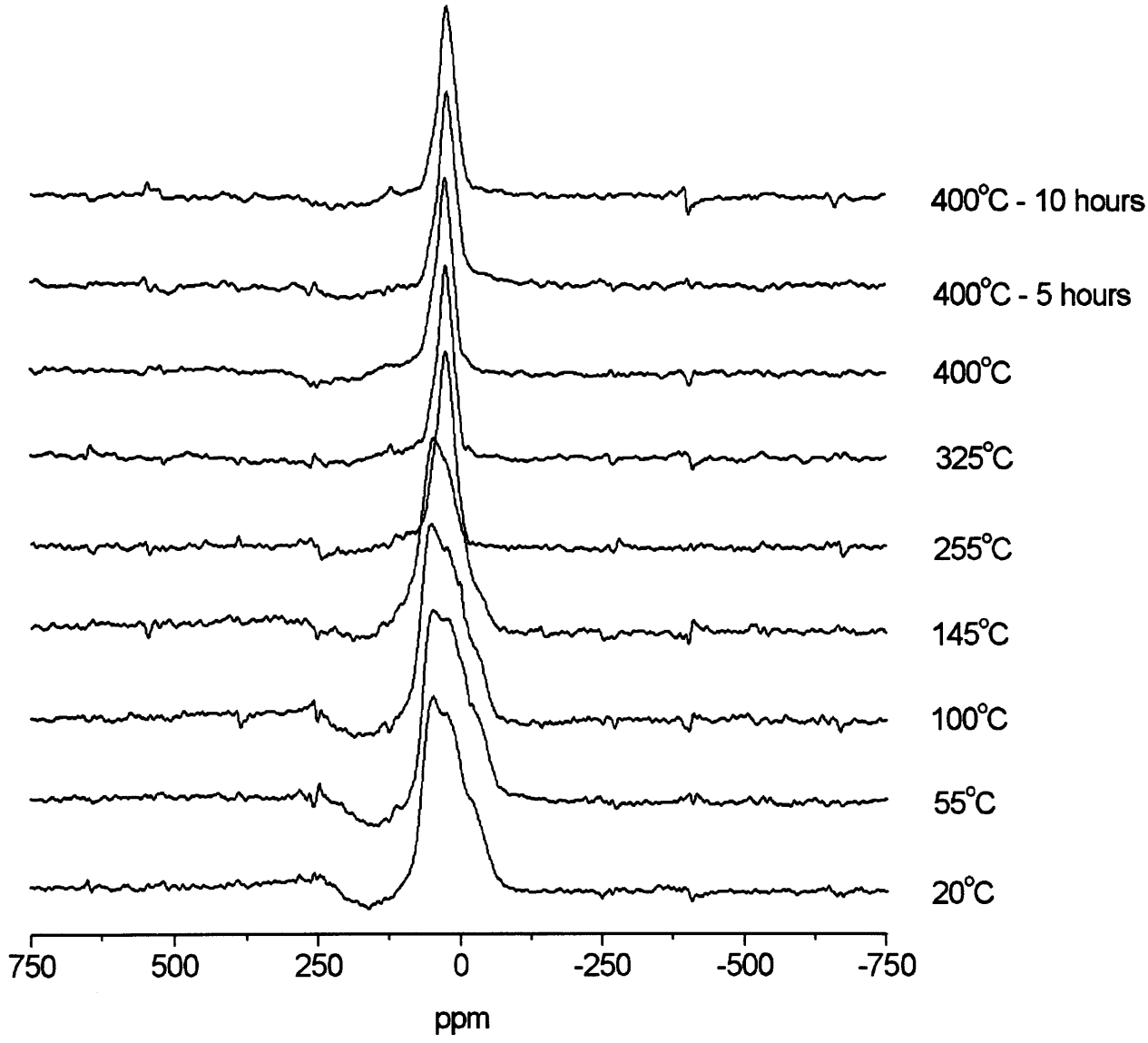

Figure 7.3.4: Stacked data for heating of NaSi from ambient to 400°C for the formation of clathrate. Data are stacked and arbitrarily separated by temperature for comparison.

Activity of Na sites during the formation of clathrate from NaSi:

As discussed previously, prolonged use of temperatures in the 500-650°C temperature range results in rapid degradation in data quality, as destruction of the copper RF coil begins. However, earlier experiments also show that the absence of vacuum, results in the usual formation temperatures for the clathrate being insufficient to induce the reaction. The problem then, is how to successfully observe the formation of clathrate without destruction of the RF coil and which and its effect on data quality. In practice, this is a considerable experimental challenge, which can in reality be solved by the use of a more temperature resistant metal for the RF coil, which in itself is a complex problem to solve. The solution then was to attempt shorter heating experiments at higher temperatures, to try and observe the state of the Na sites in NaSi as clathrate forms, but crucially, before the RF coil is destroyed or data quality becomes too poor.

The final experiment completed was to attempt to heat to 600°C for a reduced heating period, to observe clathrate formation. Realistically, the experiment was to observe both clathrate formation and the destruction of the rf coil; the question being which would occur first.

The experiment showed the characteristic trends seen for NaSi in the previous experiments (*see Figure 7.3.5*). However, in this experiment, examination and comparison of the individual datasets and particularly 20°C (*see Figure 7.3.6*) versus 600°C (*see Figure 7.3.7*) after 1 hour and 2 hours (*see Figure 7.3.8*) of heating, seems to show clathrate I formation has occurred[1], [2]. In the data collected at 2 hours at 600°C, two peaks appear to have formed around the 2000ppm region. Though the RF coil has indeed begun to degrade at this stage, the peaks persist within the data until 4 hours at 600°C (*see Figure 7.3.9*), where the rf coil has become too degraded for useable to be collected. As the experiment continues on to 6 hours of heating (*see Figure 7.3.10*), it is clear the RF coil is essentially completely degraded in terms of data collection capability.

The important conclusion to note from this data is comparison of the sodium site peak shape, before degradation of the coil, against that for 1 and 2 hours of heating at 600°C. Though the signal to noise ratio is problematic in this region, it is clear that the site is of the more symmetrical nature seen during heating for NaSi. This again suggests a degree of mobility and increased spherical symmetry at the sodium sites.

So by using increased synthesis temperatures in the absence of vacuum, it was indeed possible to form clathrate in this experiment. Though degradation of the RF coil is problematic, it is surmountable with the use of these increased temperatures and reduced reaction times. From the data, it appears that clathrate begins to form with prolonged heating of NaSi, after the site symmetry of the sodium positions in the NaSi structure have changed and moved into less sodium rich environments i.e. undergone the large thermal expansion observed in the *in situ* experiments and discussed in Chapter 5.

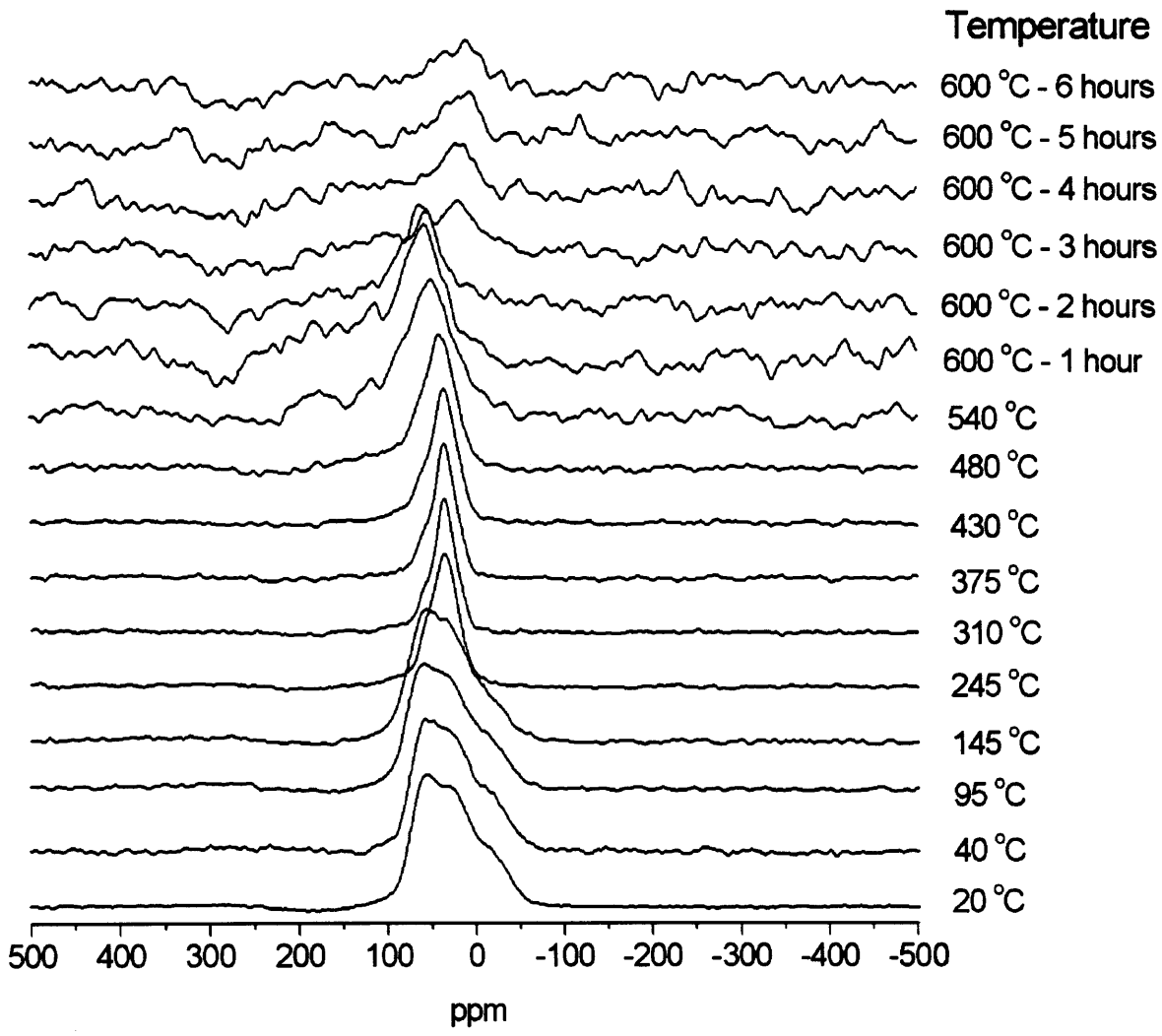

Figure 7.3.5: Stacked data for heating of NaSi from ambient to 600°C for the formation of clathrate. Data are stacked and arbitrarily separated by temperature for comparison. Note RF coil destruction degrading data quality at high temperature.

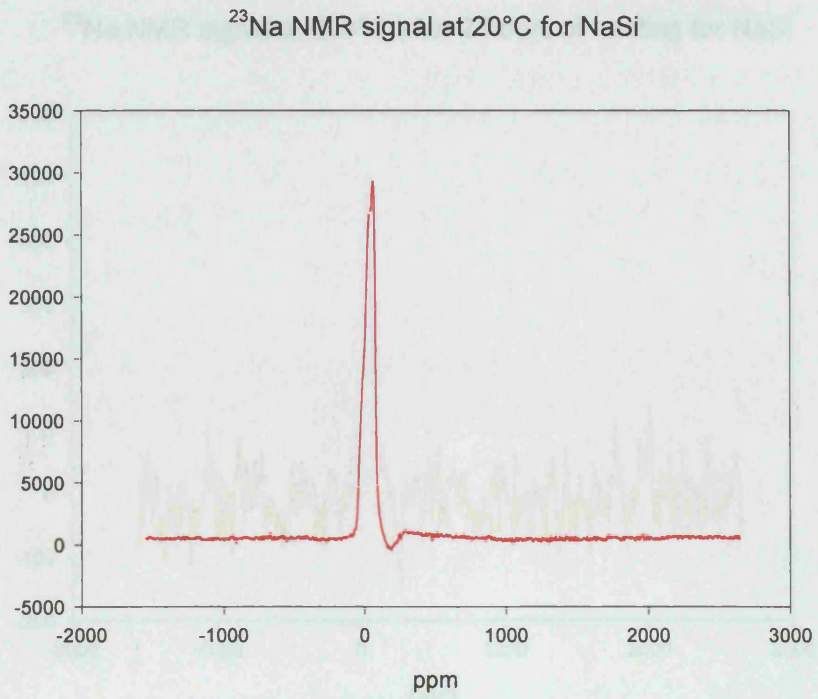

Figure 7.3.6: ^{23}Na NMR data at 20°C for NaSi showing peak shape and width.

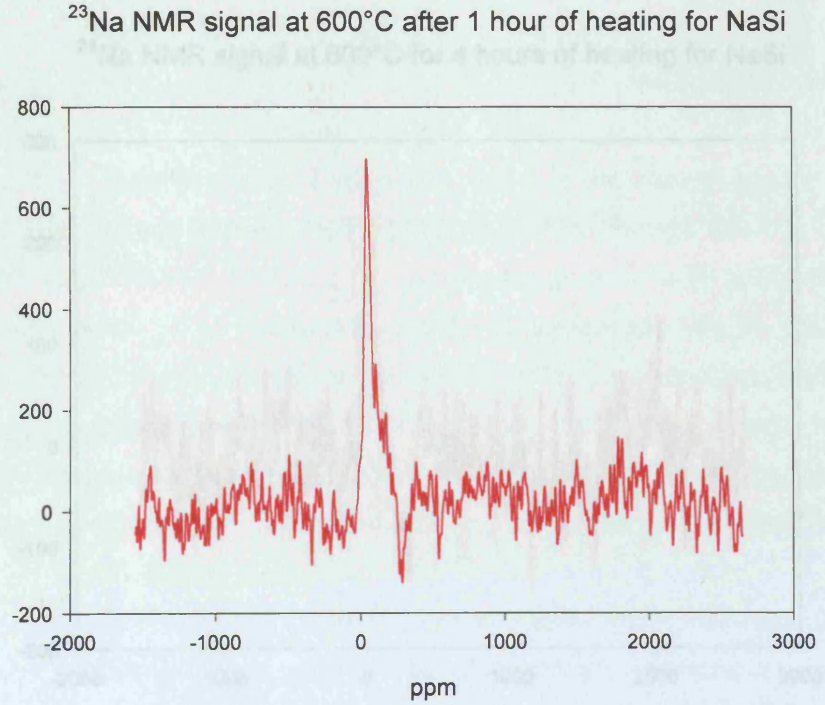

Figure 7.3.7: ^{23}Na NMR data at 600°C for NaSi showing peak shape and width after 1 hour of heating.

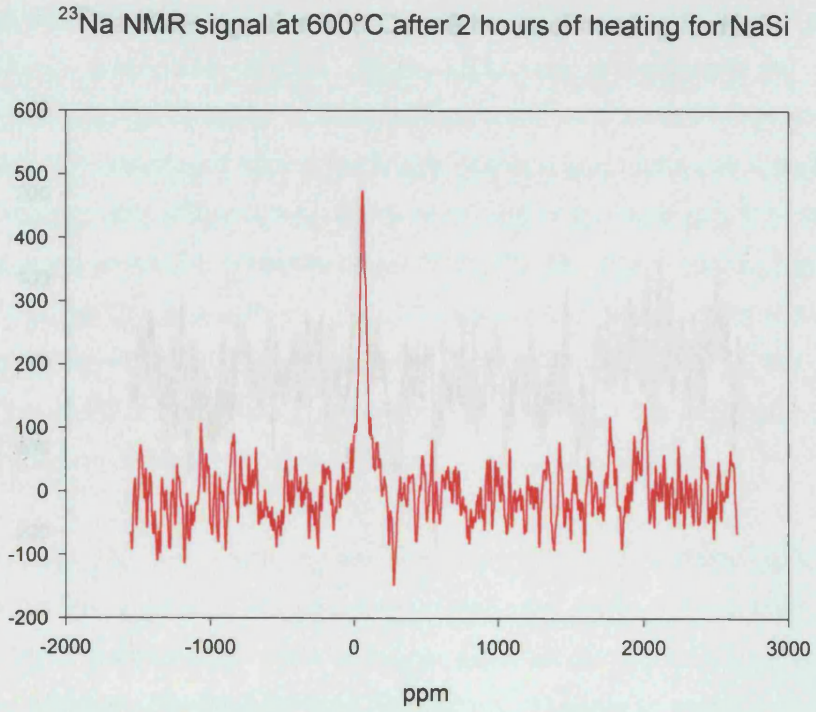

Figure 7.3.8: ^{23}Na NMR data at 600°C for NaSi showing peak shape and width after 2 hours of heating.

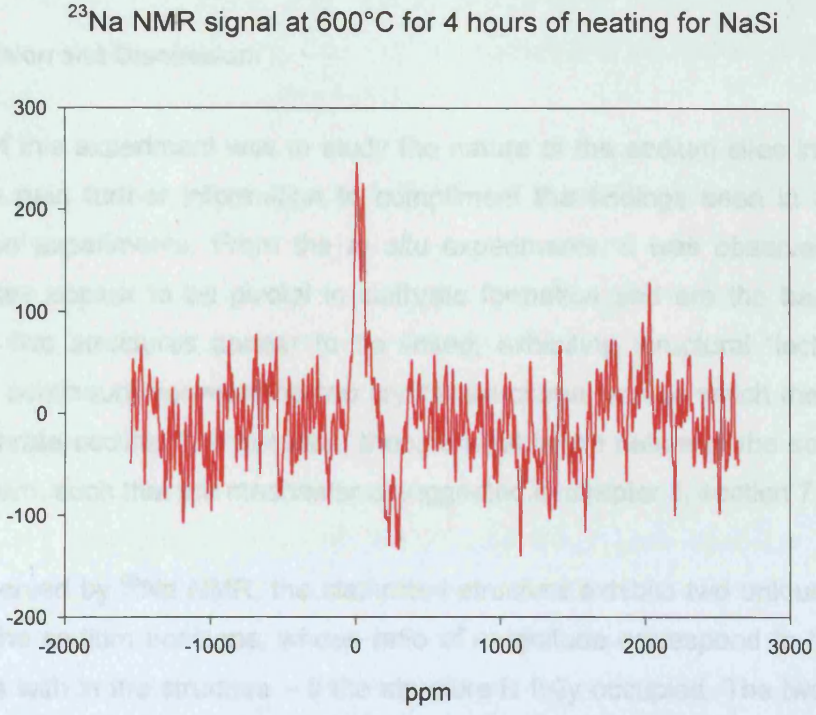

Figure 7.3.9: ^{23}Na NMR data at 600°C for NaSi showing peak shape and width after 4 hours of heating. Note RF coil destruction degrading data quality at high temperature.

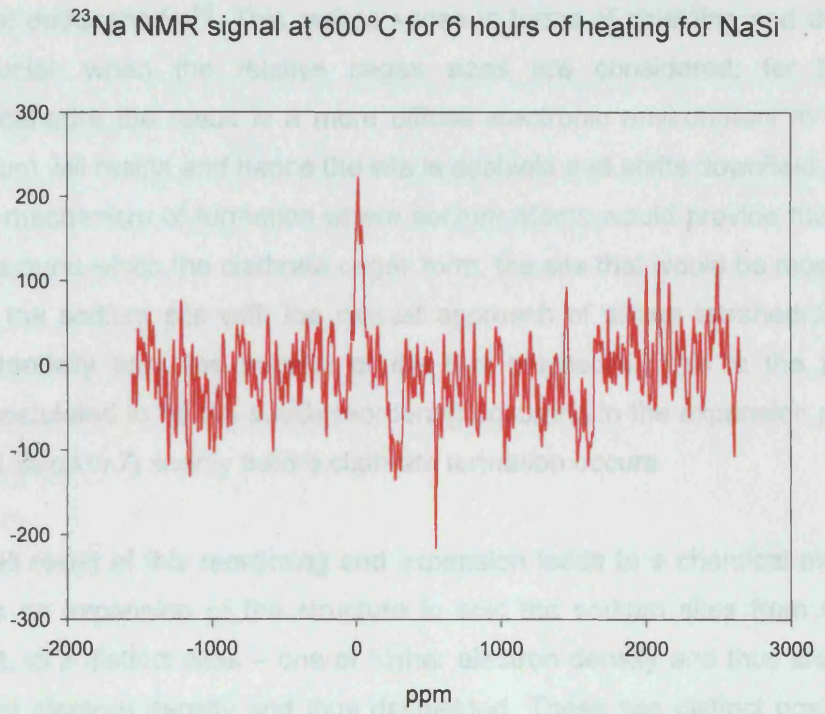

Figure 7.3.10: ^{23}Na NMR data at 600°C for NaSi showing peak shape and width after 6 hours of heating where the rf coil has completely degraded. Note RF coil destruction degrading data quality at high temperature.

7.4 Conclusion and Discussion:

The aim of this experiment was to study the nature of the sodium sites in NaSi and attempt to gain further information to compliment the findings seen in the *in situ* synchrotron experiments. From the *in situ* experiments, it was observed that the sodium sites appear to be pivotal in clathrate formation and are the basis around which the two structures appear to be linked, exhibiting structural "lock-ins" in a crystalline continuum between the two crystal structures, across which the formation of the clathrate occurs. The question, then, is what is the nature of the sodium sites in the system, such that the mechanisms suggested in chapter 5, section 7.

When observed by ^{23}Na NMR, the clathrate I structure exhibits two unique chemical shifts for the sodium positions, whose ratio of magnitude correspond to the ratio of cage types with in the structure – if the structure is fully occupied. The two chemical shifts represent the sodium atoms residence inside these two different polyhedral sites[1], [2]; the chemical shift that appears downfield represents the sodium sites for the tetrakaidecahedral cages and the chemical shift upfield the sodium site for the

pentagonal dodecahedra[1]. This makes sense in terms of shielding and deshielding of the nuclei, when the relative cages sizes are considered; for the larger tetrakaidecahedra the result is a more diffuse electronic environment in which the sodium atom will reside and hence the site is deshield and shifts downfield. It follows then, in s mechanism of formation where sodium atoms would provide the chemical template around which the clathrate cages form, the site that would be most shielded would be the sodium site with the closest approach of silicon tetrahedra and thus would potentially form the smaller of the two polyhedra. This is the templating process postulated to be the subtle reordering occurring in the expansion stage (*see Chapter 5, section 7*) shortly before clathrate formation occurs.

The overall result of this reordering and expansion leads to a chemical mechanism, that relies on expansion of the structure to split the sodium sites from chemically equivalent, to 2 distinct sites – one of higher electron density and thus shielded, the other lower electron density and thus deshielded. These two distinct positions then seemingly facilitate the mechanism further, as chemical and electronic imbalance grows in the system. This suggestion is supported by the findings of Chapter 5, section 4, where the distortion of the silicon tetrahedra is considered. It would not then be unsuitable to hypothesise that these shielded and deshield sodium positions, will be specifically associated with one crystallographic position or other for the distorted silicon tetrahedral, such that electronic balance is maintained and an overall "electronic symmetry" of structure is reached.

This conjecture of course cannot be verified by current solid state NMR techniques, given the timescales upon which the splitting of sites would presumably occur. These experiments however, do demonstrate the changes at the sodium sites in NaSi as it is heated and as formation of the clathrate occurs. The experiment demonstrates the increase in symmetry of the sodium sites on heating and the shift from a sodium rich environment, to and expanded more electronically diffuse environment as expansion proceeds. This gives good agreement with the model supported by Rietveld analysis of the *in situ* x-ray data and the suggested mechanism of formation from Chapter 5. These results further add to the idea of the role of the large thermal expansion of NaSi and raise conjecture about rapid hopping of Na^+ under expansion and hence Na^+ motion, which facilitates sodium loss and drives the reaction.

7.5: References

1. Reny, E., et al., Journal of Solid State Chemistry and Crystal Chemistry, 1998. **Serie II**.
2. Gryko, J., P. McMillan, F, and O. Sankey, F, Phys. Rev. B, 1996. **54**.
3. O'Dell, L., *PhD Thesis.* University of Warwick, 2007.
4. James Kirkpatick, R., *MAS NMR Spectroscopy of minerals and glasses.* Reviews of Mineralogy, 1988. **18**.
5. Philips, B., L, R. James Kirkpatick, and G. Hovis, L, *^{23}Na, ^{27}Al and ^{29}Si MAS NMR Study of an Al/Si ordered alkali feldspar solid in solution.* Phys. Chem. Mineral, 1988. **16**.

Chapter 8

Conclusions and Future Work

8.1 Conclusion and Discussion:

Though the compositions, structures and properties of the solid state clathrates have been studied both experimentally and theoretically in great depth, the mechanism of formation of these materials has scarcely been mentioned in the literature. The main aim of this study was to attempt to address this problem and understand the mechanism of formation of these materials. The lack of discussion or study of this reaction within the literature perhaps reflects the complex experimental nature of attempting to study the subject, as was found during this project.

In the earliest work on clathrates by Klemm *et al*[1], [2], thermogravimetric analysis experiments showed a distinct weight loss for metalloids on heating, and the resultant compounds possessed structures of a cubic nature. The work of Cros *et al*[3], [4], [5], [6], built on these observations and it was found that the cubic structures were iso-structural with clathrate hydrate structures. Since the original work, it has been assumed that loss of the alkali cations from the Zintl phase and accompanying Si-Si bond formation is key to formation of the clathrate. There are currently no proposed mechanisms of formation for the clathrates in the literature, but the use of *in situ* x-ray diffraction in this study, has allowed us to begin to propose a model for the mechanism of formation.

In order to complete studies of the mechanism of formation of the clathrates, a custom experiment was designed and engineered specifically for the purposes of high vacuum, thermal degradation reactions, *in situ* at station 6.2 at the SRS Daresbury. These custom experiments were the first of their kind to be completed using time-resolved *in situ* diffraction and high vacuum synthesis methods together. The technique developed has potential applications in larger scale WAXS studies, as well as white beam experimental set-ups, for high vacuum environments. Development of the novel apparatus for this study was the sole facilitator of the *in situ* experiments, which would have been impossible without such efforts.

The time-resolved *in situ* diffraction results displayed in this thesis, suggest an unexpected structural link between the monoclinic sodium silicide structure and the cubic silicon clathrate I structure. This structural link centres on related planes in both materials for which sodium cations are resident. In multiple cases, throughout the diffraction profiles collected in these experiments, *d*-spacings appear to "lock-in" and relate the structures in a crystalline continuum. For the silicide structure the relevant

planes are host to rows of sodium positions, where for the clathrate I structure the associated planes that exhibit the "lock-in" phenomena, are for sodium atoms residing at the centres of polyhedral cages. This result is strong evidence for the role of the sodium atoms as templating sites in the formation of the clathrate cages.

In situ synchrotron cyclic heating experiments on sodium silicide have shown some degree of reversibility in the formation of the clathrate I structure which was hither to, unsuspected. This observation is particularly interesting in the light of the fact that the fully formed clathrate I structure has not yet been reported to have a variable stoichiometry and thus, only occurs in the fully occupied Na_8Si_{46} form.

The effect of rapid degassing of sodium silicide was studied using *in situ* synchrotron diffraction techniques. It was shown that formation of clathrate II from NaSi is strongly dependant on the rate of loss of sodium. The rate of loss of sodium was controlled in these experiments by the use of flash heating with ramp rates up to $200°Cmin^{-1}$ and the application of vacuum. It was found that formation of the clathrate II structure is considerably impeded in a confined reaction environment and where high vacuum is not achieved.

^{23}Na NMR provided insight into the chemical environment in which the sodium atoms reside, during the formation of the clathrate. Heating of the silicide produces sodium sites that are less crowded and vary in electronic nature considerably on heating. This large expansion and electronic variation is conceivably the result of the subtle reordering occurring in the structure before clathrate I is formed. Though the challenging nature of the experiments makes assurity of conclusion speculative, the data does indeed suggests strongly that changes in site symmetry and thus electronic state, as well increased mobility and spherical symmetry of the sodium sites within the structure, are complicit in formation of the clathrate.

8.2 Future Work:

Throughout the course of this study, the considerably challenging experimental nature of many of the experiments produced several instances for which greater development may produce interesting further studies or experiments. Some of the most interesting and intriguing of these are detailed below:

***In situ* preparation of Clathrate II and ID15:**

The in situ experiments routinely showed that formation of the clathrate II structure could not be achieved with the experimental set-up developed for station 6.2 at the SRS Daresbury. The main problem causing this experimental limitation was the poor beam penetration with respect to the sample, of around 1.5 mm of quartz tubing. This limitation is profound when consideration of the application of high vacuum is considered. From laboratory experiments and the literature[7], [8], [9], [10], in it well know that in using Na_1Si_1 as the precursor phase in formation of clathrates, a rapid heating stage is required to produce the clathrate II phase under vacuum heating conditions.

As is discussed in chapters 3 and 4, the small bore of the capillary required for beam penetration at station 6.2 daresbury results in high vacuum being applied, most probably, as a gradient across the neck of the capillary and not directly into the sample. The result is that even with very rapid heating, clathrate II cannot be made as a pure or majority phase using this technique. The solution then, is to utilise a higher energy beam with considerably high sample penetration but that retains the same or better time resolution as is present with station 6.2's rapid2 detector.

Station ID15 at the ESRF Grenoble provide time-resolved data in the order of 300 milliseconds in addition to 30-1000KeV. The beam penetration of sample is easily possible through as much as an inch of glass. Use of such a station could then provide the means to use considerably larger sample assemblies that would facilitate high vacuum delivery direct to the sample. The apparatus used in this study could be relatively simple modified to study the formation of type II clathrates using this station, should suitable high ramp heating methods also be available. An experiment of this kind would be incredible interesting in terms of a comparison of the difference in mechanism of formation for the clathrate I versus clathrate II structure. Such an experiment would also be capable of utilising various starting material

stoichiometries, such that the reactions of sodium rich alloy preparations could be examined.

Stabilisation of the Clathrate II structure by synthesis using sodium rich alloy:

Chapter 2, section 3 discusses the interesting result of thermal degradation methods when used on sodium rich alloys of the form, $Na_{3/4}Si_1$. In these experiments the amorphous sodium rich alloy is treated using typical synthesis condition for the formation of the type I clathrate. However, in this case, the type II clathrate structure predominates as single phase product until temperatures in excess of 400°C are used. This result is very intriguing in that with the 1:1 starting silicide, Na_1Si_1, essentially all conditions except flash heating and high vacuum, produce the type I structure. The result of the synthesis using the alloy is totally contrary to the observation in the *in situ* experiments and laboratory in that the clathrate I structure under all conditions using the 1:1 precursor, appears to be the thermodynamic product.

It would seem then that the introduction of a large excess of sodium in the starting material, in some way stabilises the mechanism of formation for the clathrate II, which appears to be the kinetic product in the 1:1 reaction. So, in total contrast, the system that previously required very rapid thermal degradation for formation to occur, appears to become the thermodynamic product in the presence of excess sodium. This suggests that the mechanism of formation of the type II clathrate is not identical to that of clathrate I detailed in this study.

The work of Tse *et al*[11], provide interesting insight into the electronic nature of silicon sites in the various associated systems in this study:

d-Si – $4e^-$/Si
Na_8Si_{46} – $4.17e^-$/Si
$Na_{24}Si_{46}$ – $4.18e^-$/Si

Thus, assuming the full occupied clathrate II is formed in the first instance in the reaction, it requires a higher average electron density per silicon in the structure for stability. Is this an indication that a templating mechanism for the clathrate II structure may occur with the presence of several cations per forming cage, such that the higher electron density required for the silicon centers of the type II may balanced?

Further study of this problem and the discrete mechanistic differences occurring in the formation of clathrate II from both starting materials, would be an interesting and challenging experimental undertaking.

^{23}Na NMR with high vacuum and improved temperature control:

Chapter 5, section 2 discusses the limitation of the high temperature ^{23}Na NMR experiments, completed in this study. It is of no doubt that a great deal more information could be gleaned from such experiments if further strides could be made in terms of the experimental challenges posed in the study. Fundamentally, the use of vacuum would provide a great deal more information and give access to lower temperature syntheses. In practise applying vacuum would be a considerable experimental design task.

The other limitation of the experiment is the lack of accurate temperature control or controlled and monitored ramping. Completing the experiment with the use of eurotherm like control and monitoring of temperature would create an experiment considerably closer in nature to those completed at the SRS Daresbury.

Mixed Phase Si-Ge clathrates:

The work of Ramachandran *et al*[10], touched on attempts to synthesise phases of mixed silicon and germanium nature, but retaining the clathrate structure. The work was based around attempts using NaGe and NaSi in direct heating experiments to produce the mixed phase. The results were studied using x-ray diffraction methodologies but the resultant product was not formally characterised.

The mechanism of formation hypothesised in this study, provides new speculation into possible methods of achieving such phases. One possibility is to use thermal degradation methodologies but use zintl precursors containing different cations relative to silicon and germanium. The logic behind this approach centres on the idea of cage templating by the cations. The probable outcome in a successful mixing would not be to form mixed Si/Ge tetrahedra but instead to form bonds between isolated Si pure and Ge pure tetrahedra. In such an eventuality, the electronic

requirements at the Si versus Ge centres would seemingly not be identically in electronic, geometrical or steric terms. It would therefore seem prudent, to provide a different templating cation for each species. The drawback to this approach is of course, that the resultant mixed phase would not be cation pure for one cation, but would also be of mixed denomination.

Other obvious approaches would be to use the zintl phase of one species and the pure powder of the other, ground together and subjected to prolonged heating over several days.

***In situ* neutron scattering experiments:**

One of the major issues associated with the in situ experiments associated in this thesis, is the inherent resolution of the associated spectrometer. As is discussed in chapter 5 section 7, the resolution associated with these experiments, though good under these conditions, doesn't allow for the mechanism to be conclusively proved. Its is then desirable to complete experiments that have increased spatial resolution such that further conclusive evidence may be collected to support this mechanism.

Neutron experiments offer exceptional spatial resolution as a consequence of the means by which the experiments are carried out. The reality of scattering originating from the nuclei of the atom allows for excellent spatial resolution as well as a means by which the motions and quantities of sodium with in the NaSi and Na_8Si_{46} structures can be quantified. It is for these reasons that a study utilising neutron scattering and applying the same reaction conditions utilised in the *in situ* experiments would be so desirable. Realising an neutron congener of the synchrotron in situ experiment may be the answer to following sodium loss in the system such that conclusive data may be collected for the mechanism in this reaction system.

8.3: References

1. Schafer, R. and W. Klemm, *Wietere beitrage zur kenntnis der silicide und germanide der alkalimetalle.* Z. Anorg. Allg. Chem., 1961. **312**: p. 214-220.
2. Klemm, W., *Metalloids and their compounds with the alkali metals.* Proc. Chem. Soc. London, 1958: p. 329-341
3. Kasper, J., S, et al., *Clathrate structure of silicon Na_8Si_{46} and Na_xSi_{136} (x < 11).* . Science, 1965. **150**.
4. Cros, C., et al., *Sur deux composés du potassium isotypes de l'hydrate de krypton.* Bull. Soc. Chim. fr, 1968. **7**.
5. Cros, C., M. Pouchard, and P. Hagenmuller, *Sur deux nouvelles phases du système silicium-sodium.* C.R. Acad. Sc, 1965. **260**.
6. Cros, C., M. Pouchard, and P. Hagenmuller, *Sur une nouvelle famille de clathrates minéraux isotypes des hydrates de gaz et de liquides. interprétation des résultats obtenus.* J. Solid State Chem, 1970. **2**.
7. Ramachandran, G., et al., J. Solid State Chem, 1999. **145**.
8. Gryko, J., P. Hutchins, T, and P. McMillan, F, Unpublished Results, 2006.
9. Gryko, J., *Personal Communication.* Jacksonbille State University, 2006.
10. Ramachandran, G., *PhD Thesis.* Arizona State University, 2003.
11. Tse, J., S, et al., Phys. Rev. Lett, 2000. **85**.

Appendices

Appendix 1: Data for low temperature x-ray diffraction studies on guest-free silicon clathrates (see Chapter 3). Data for the three high angle peaks studied in the low temperature experiments for one temperature cycle

Temp in K	Peak 1	Err 1	Peak 2	Err 2	Peak 3	Err 3	Refined a value	Err in refined a
5.9	51.0170	0.0046	53.0170	0.0021	54.1886	0.0045	14.6570	0.0047
16.0	50.9979	0.0045	53.0185	0.0021	54.2003	0.0043	14.6558	0.0021
20.5	51.0072	0.0059	53.0162	0.0029	54.2065	0.0061	14.6543	0.0020
25.5	51.0092	0.0062	53.0142	0.0029	54.1968	0.0055	14.6559	0.0013
30.1	51.0138	0.0058	53.0157	0.0030	54.2062	0.0064	14.6540	0.0022
31.5	51.0316	0.0049	53.0319	0.0023	54.2141	0.0045	14.6513	0.0027
34.4	51.0208	0.0064	53.0182	0.0030	54.1971	0.0059	14.6551	0.0036
40.0	51.0040	0.0065	53.0161	0.0027	54.2065	0.0061	14.6545	0.0024
45.7	51.0097	0.0059	53.0169	0.0030	54.2027	0.0065	14.6548	0.0010
50.5	51.0109	0.0062	53.0213	0.0030	54.2052	0.0062	14.6542	0.0005
55.5	51.0133	0.0054	53.0162	0.0028	54.1958	0.0055	14.6558	0.0023
59.8	51.0191	0.0068	53.0155	0.0031	54.2135	0.0056	14.6523	0.0040
61.3	51.0130	0.0049	53.0251	0.0025	54.1896	0.0046	14.6570	0.0049
70.2	51.0187	0.0049	53.0273	0.0026	54.2020	0.0053	14.6542	0.0024
75.0	51.0239	0.0059	53.0262	0.0024	54.2182	0.0054	14.6511	0.0024
80.0	51.0231	0.0059	53.0193	0.0026	54.1967	0.0051	14.6552	0.0038
85.0	51.0166	0.0051	53.0220	0.0024	54.1993	0.0051	14.6549	0.0023
90.4	51.0188	0.0054	53.0233	0.0031	54.1951	0.0052	14.6556	0.0039
95.6	51.0129	0.0057	53.0223	0.0027	54.2006	0.0053	14.6549	0.0013
100.0	51.0030	0.0047	53.0159	0.0028	54.1969	0.0051	14.6562	0.0003
104.3	51.0193	0.0058	53.0201	0.0027	54.2000	0.0050	14.6547	0.0028
110.6	51.0080	0.0055	53.0278	0.0024	54.1985	0.0049	14.6554	0.0025
114.9	51.0021	0.0056	53.0225	0.0024	54.2064	0.0054	14.6544	0.0023
118.9	50.9918	0.0049	53.0028	0.0025	54.1828	0.0048	14.6596	0.0003
120.4	51.0214	0.0068	53.0198	0.0031	54.2152	0.0066	14.6518	0.0033
125.2	51.0138	0.0064	53.0240	0.0028	54.2017	0.0070	14.6546	0.0013
130.1	51.0121	0.0070	53.0201	0.0032	54.2074	0.0081	14.6538	0.0012
135.0	51.0206	0.0068	53.0109	0.0030	54.1943	0.0074	14.6559	0.0045
140.5	51.0227	0.0065	53.0269	0.0030	54.2056	0.0067	14.6533	0.0023
145.1	51.0103	0.0063	53.0219	0.0031	54.2082	0.0063	14.6537	0.0012
149.5	51.0019	0.0068	53.0146	0.0034	54.1923	0.0075	14.6571	0.0009
154.7	51.0175	0.0062	53.0197	0.0030	54.1994	0.0064	14.6549	0.0025
160.0	51.0187	0.0061	53.0145	0.0027	54.1964	0.0057	14.6555	0.0035
165.0	51.0127	0.0059	53.0118	0.0029	54.1824	0.0060	14.6585	0.0051
181.9	51.0039	0.0054	53.0142	0.0030	54.1972	0.0057	14.6561	0.0003
192.2	51.0048	0.0062	53.0129	0.0032	54.1900	0.0065	14.6574	0.0017
199.5	50.9977	0.0060	53.0120	0.0031	54.1802	0.0068	14.6595	0.0032
212.1	50.9990	0.0064	53.0110	0.0032	54.1894	0.0066	14.6578	0.0007
222.1	50.9865	0.0065	52.9924	0.0028	54.1705	0.0058	14.6623	0.0016
229.7	51.0021	0.0056	53.0011	0.0026	54.1817	0.0049	14.6593	0.0028
275.0	50.9827	0.0062	52.9996	0.0029	54.1830	0.0064	14.6601	0.0018
294.5	50.9848	0.0052	53.9949	0.0031	54.1769	0.0054	14.6612	0.0002

Appendix 2: Methods of calculation used in chapter 5.

Forumlae:

Calculation of the coefficient of thermal expansion:

Thermal expansion is calculated using the formula:

$$\alpha = \frac{1}{L}\frac{\delta L}{\delta T}$$

α = Coefficient of thermal expansion

L = Unit cell volume

δL = Change in the unit cell volume

δT = Change in temperature

Units = k^{-1}

Calculation of the unit cell volume for monoclinic structure:

The formula used to calculate the unit cell for volume for monoclinic systems is:

$$V = abc \sin(\beta)$$

V = Unit cell volume

a = Unit cell length along the a axis

b = Unit cell length along the b axis

c = Unit cell length along the c axis

β = The angle separating the a and c axes

Units = $Å^3$

Appendix 3: *In situ* diffraction data patterns discussed in Chapter 5, sections 4 and 5

NaSi:

Pattern 19:

Time: 9.5 minutes

Temperature: 76°C

RWP: 40.7

Refinement cycles: 25

Parameters refined: 24

a: 12.16036 (0.0013)

b: 6.54800 (0.0006)

c: 11.14369 (0.0012)

β: 119.08507 (0.0053)

Unit cell volume: 796.3519 (0.015)

	x	sx	y	sy	z	sz	B	sB	occ.	socc.
Na1	0.36154(	193)	0.65956(	277)	0.37907(	205)	5.005(502)		0.737(	17)
Na2	0.63232(	86)	0.89468(	139)	0.45159(	98)	5.005(502)		1.518(	26)
Si1	0.45014(	120)	0.24843(	148)	0.31380(	109)	2.388(260)		1.000(	0)
Si2	0.61007(	101)	0.43816(	148)	0.36510(	105)	2.388(260)		1.000(	0)

Rietveld fit of NaSi phase

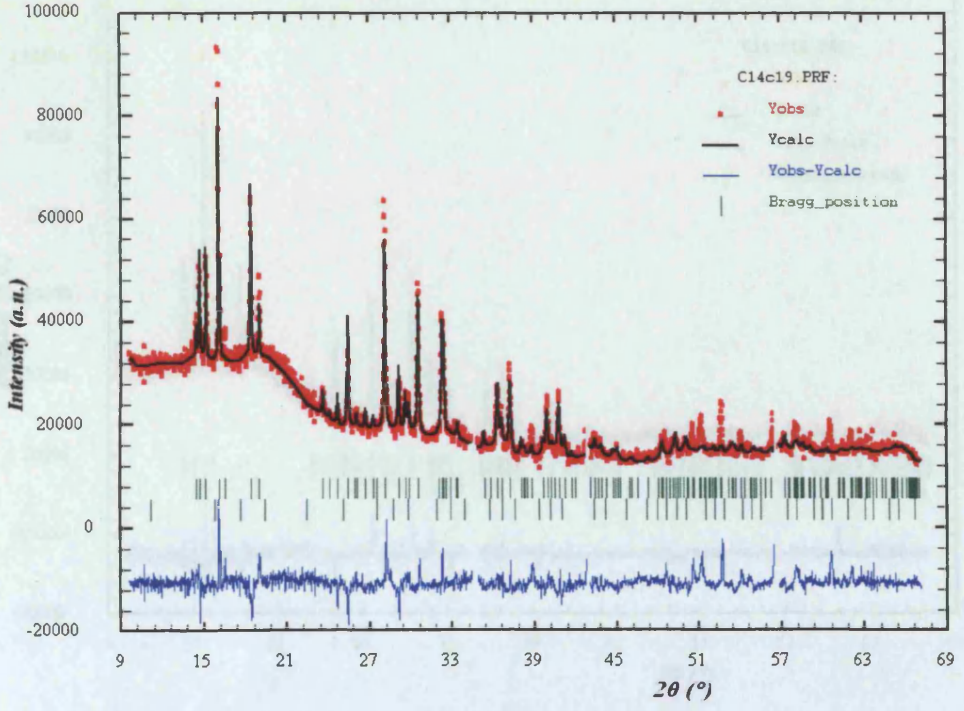

Pattern 115:

Time: 57.5 minutes

Temperature: 456°C

RWP: 45.4

Refinement cycles: 25

Parameters refined: 23

a: 12.3309 (0.001)

b: 6.6864 (0.0004)

c: 11.3738 (0.0009)

β: 120.0787 (0.004)

Unit cell volume: 811.4409 (0.26)

	x	sx	y	sy	z	sz	B	sB	occ.	socc.
Na1	0.34139(	185)	0.65498(	284)	0.35470(	188)	11.900(938)		0.745(	22)
Na2	0.62315(	99)	0.89011(	187)	0.42369(	103)	11.900(938)		1.171(	24)
Si1	0.46031(	117)	0.23875(	158)	0.31605(	112)	8.790(349)		1.000(	0)
Si2	0.61150(	109)	0.45167(	151)	0.35287(	115)	8.790(349)		1.000(	0)

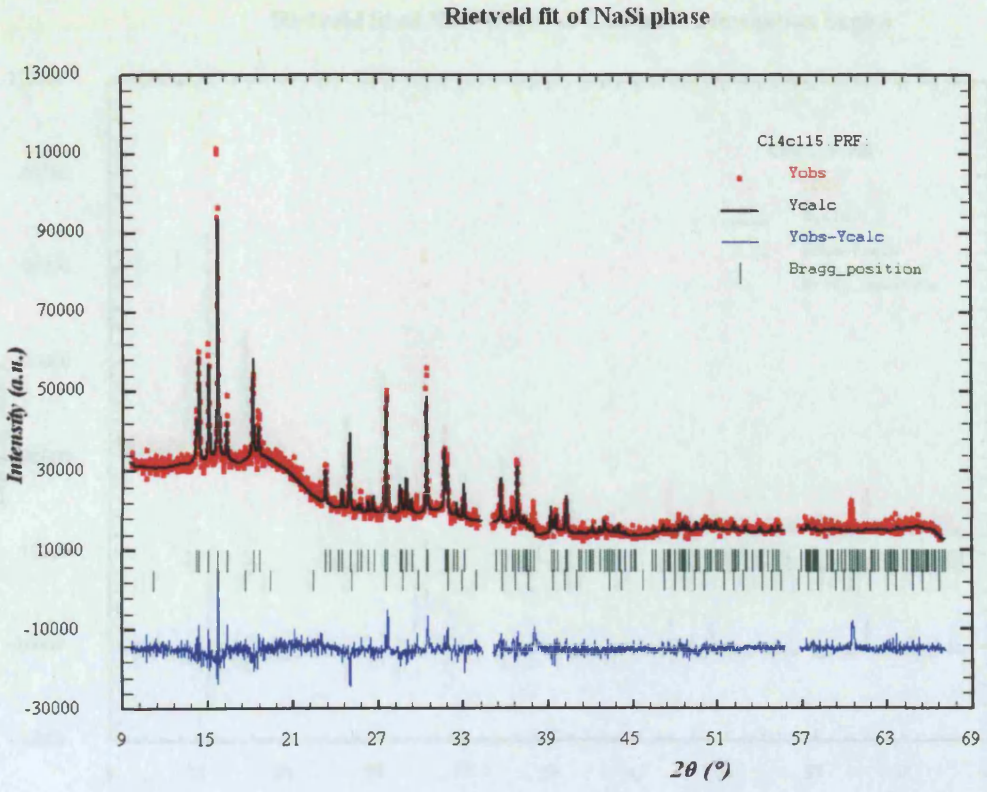

Pattern 125:

Time: 75.0 minutes

Temperature: 500°C

RWP: 50.6

Refinement cycles: 25

Parameters refined: 24

a: 12.3385 (0.001)

b: 6.6961 (0.001)

c: 11.3886 (0.001)

β: 120.1440 (0.004)

Unit cell volume: 813.7809 (0.007)

	x	sx	y	sy	z	sz	B	sB	occ.	socc.
Na1	0.34591	(196)	0.63678	(269)	0.35732	(189)	11.301	(977)	0.805	(24)
Na2	0.62477	(115)	0.88782	(213)	0.43018	(125)	11.301	(977)	1.131	(27)
Si1	0.45525	(141)	0.23742	(193)	0.31724	(127)	10.730	(476)	1.000	(0)
Si2	0.61843	(128)	0.46602	(193)	0.35943	(130)	10.730	(476)	1.000	(0)

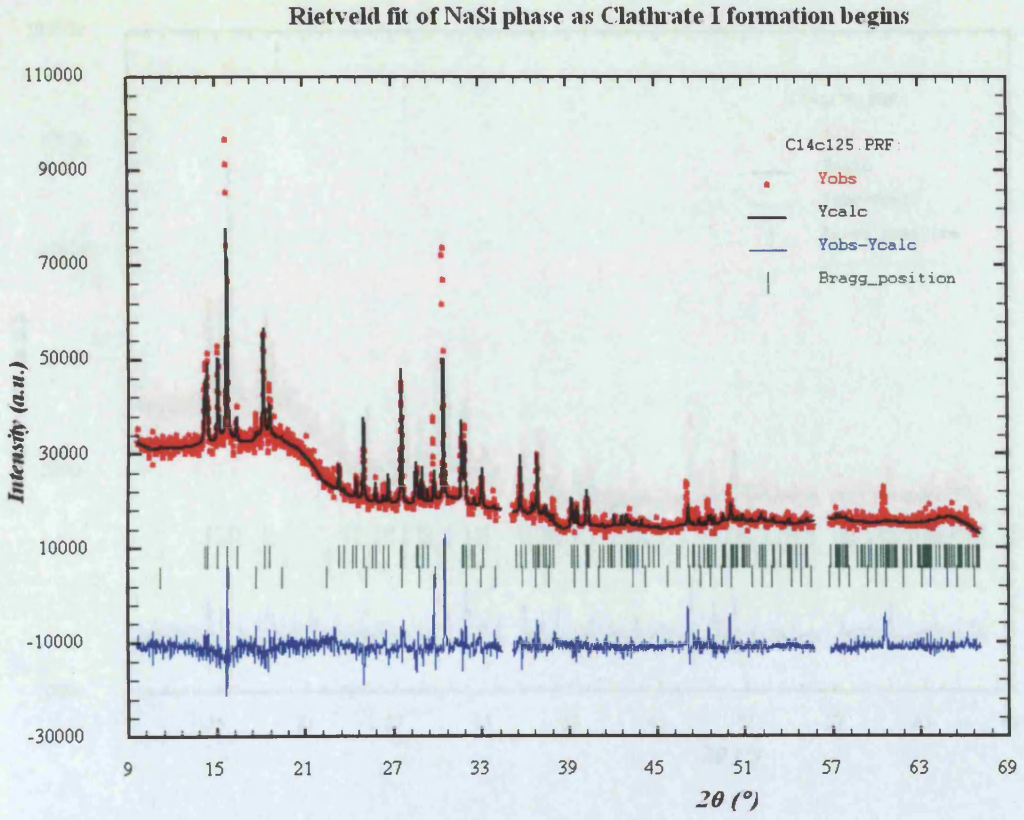

Pattern 130:

Time: 77.50 minutes

Temperature: 500°C

RWP: 57.1

Refinement cycles: 25

Parameters refined: 24

a: 12.2973 (0.001)

b: 6.6857 (0.0007)

c: 11.3527 (0.001)

β: 120.0413 (0.006)

Unit cell volume: 807.9465 (0.42)

	x	sx	y	sy	z	sz	B	sB	occ.	socc.
Na1	0.35065	(291)	0.65164	(476)	0.37917	(389)	12.029	(999)	0.725	(37)
Na2	0.62708	(158)	0.88477	(356)	0.42776	(206)	12.029	(999)	1.114	(42)
Si1	0.46737	(194)	0.23008	(272)	0.31745	(188)	10.086	(679)	1.000	(0)
Si2	0.61888	(189)	0.46923	(286)	0.35593	(238)	10.086	(679)	1.000	(0)

Rietveld fit of NaSi phase as Clathrate I formation begins

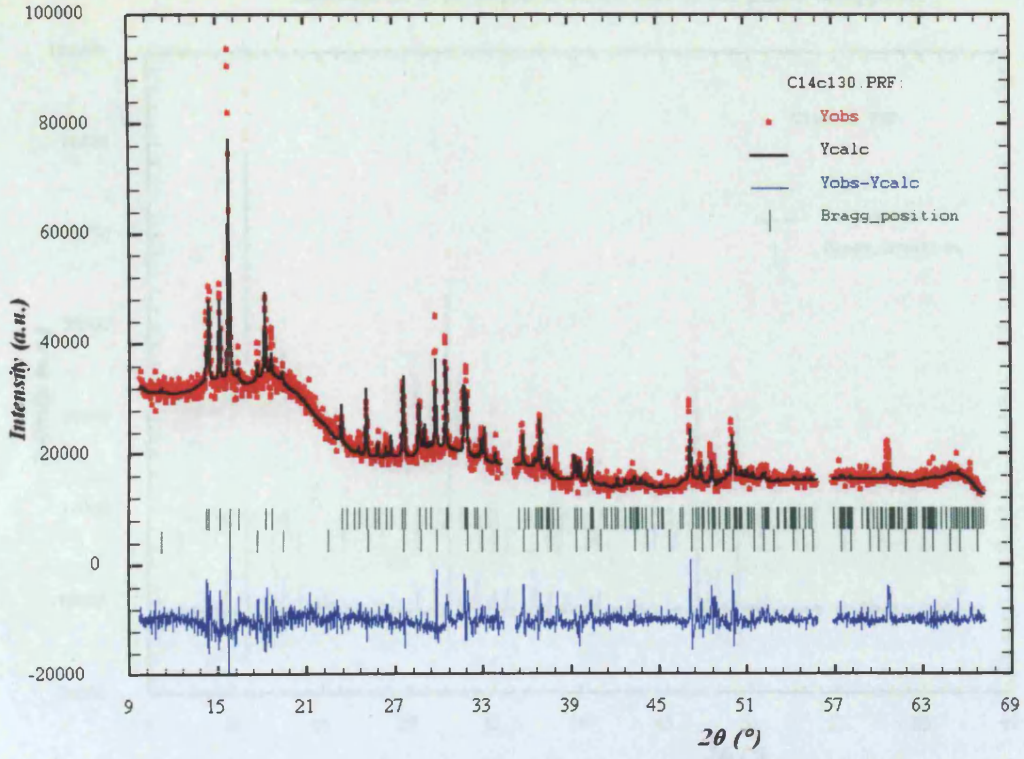

Pattern 170:

Time: 97.5 minutes

Temperature: 500°C

RWP: 57.2

Refinement cycles: 25

Parameters refined: 3

a: 12.2697 (0.001)

b: 6.6875 (0)

c: 11.3329 (0.0003)

β: 120.0022 (0)

Unit cell volume: 805.3161 (0.11)

	x	sx	y	sy	z	sz	B	sB	occ.	socc.
Na1	0.29002(	0)	0.66577(	0)	0.42019(	0)	28.304(	0)	1.210(	0)
Na2	0.60137(	0)	0.85656(	0)	0.44252(	0)	28.304(	0)	1.891(	0)
Si1	0.45409(	0)	0.24558(	0)	0.31819(	0)	10.659(	0)	1.000(	0)
Si2	0.60884(	0)	0.48762(	0)	0.35849(	0)	10.659(	0)	1.000(	0)

Rietveld fit of NaSi phase as the last of the phase disappears

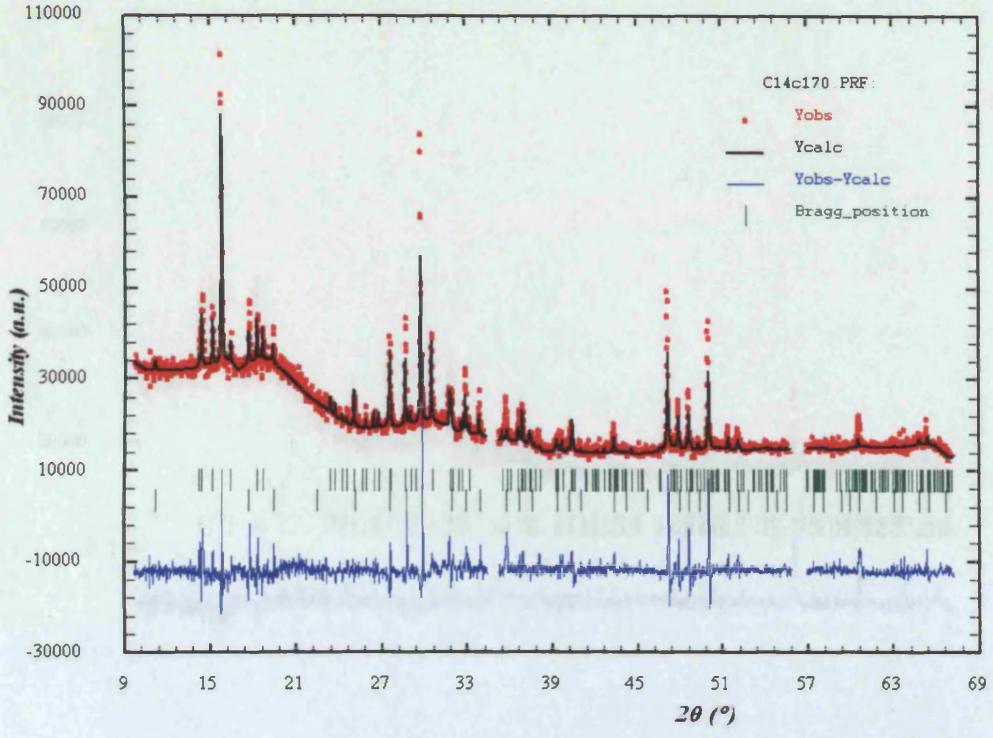

Na_8Si_{46} Phase:

Pattern 130:

Time: 65 minutes

Temperature: 500°C

RWP: 46.4

Refinement cycles: 25

Parameters refined: 37

a: 10.2238 (0.00054)

Unit cell volume: 1060.10 (0.169332)

Dual phase refining for Na_8Si_{46} then NaSi in order

	x	sx	y	sy	z	sz	B	sB	occ.	socc.	Mult
Na1	0.00000(0)		0.00000(0)		0.00000(0)		-5.004(999)		0.033(6)		2
Na2	0.25000(0)		0.50000(0)		0.00000(0)		-4.428(999)		0.104(10)		6
Si1	0.00000(0)		0.30512(177)		0.11914(182)		-1.727(650)		0.500(0)		24
Si2	0.17950(157)		0.17950(157)		0.17950(157)		-0.203(818)		0.333(0)		16
Si3	0.25000(0)		0.00000(0)		0.50000(0)		-4.302(999)		0.125(0)		6

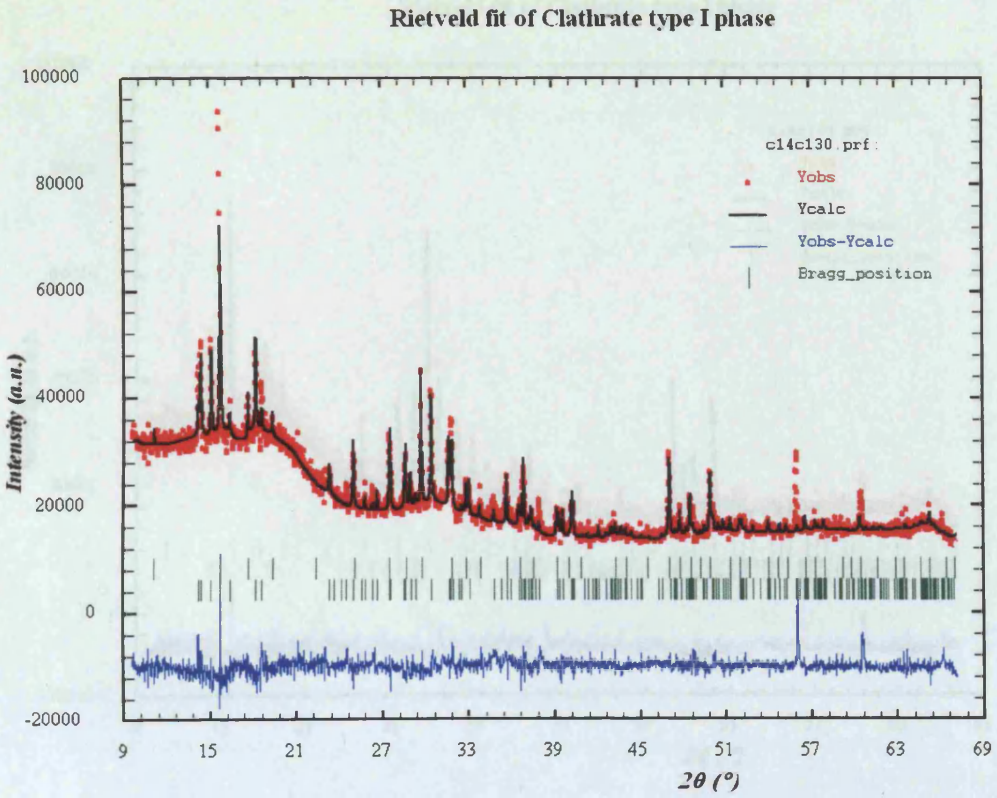

Pattern 145:

Time: 72.5 minutes

Temperature: 500°C

RWP: 41.7

Refinement cycles: 25

Parameters refined: 37

a: 10.2261 (0.00041)

Unit cell volume: 1069.38 (0.128624)

Dual phase refining for Na_8Si_{46} then NaSi in order

	x	sx	y	sy	z	sz	B	sB	occ.	socc.	Mult
Na1	0.00000(	0)	0.00000(	0)	0.00000(	0)	-2.971(999)		0.042(	3)	2
Na2	0.25000(	0)	0.50000(	0)	0.00000(	0)	-0.750(999)		0.096(	6)	6
Si1	0.00000(	0)	0.30688(111)		0.11810(	108)	0.407(428)		0.500(	0)	24
Si2	0.18005(	94)	0.18005(	94)	0.18005(	94)	0.596(519)		0.333(	0)	16
Si3	0.25000(	0)	0.00000(	0)	0.50000(	0)	1.498(950)		0.125(	0)	6

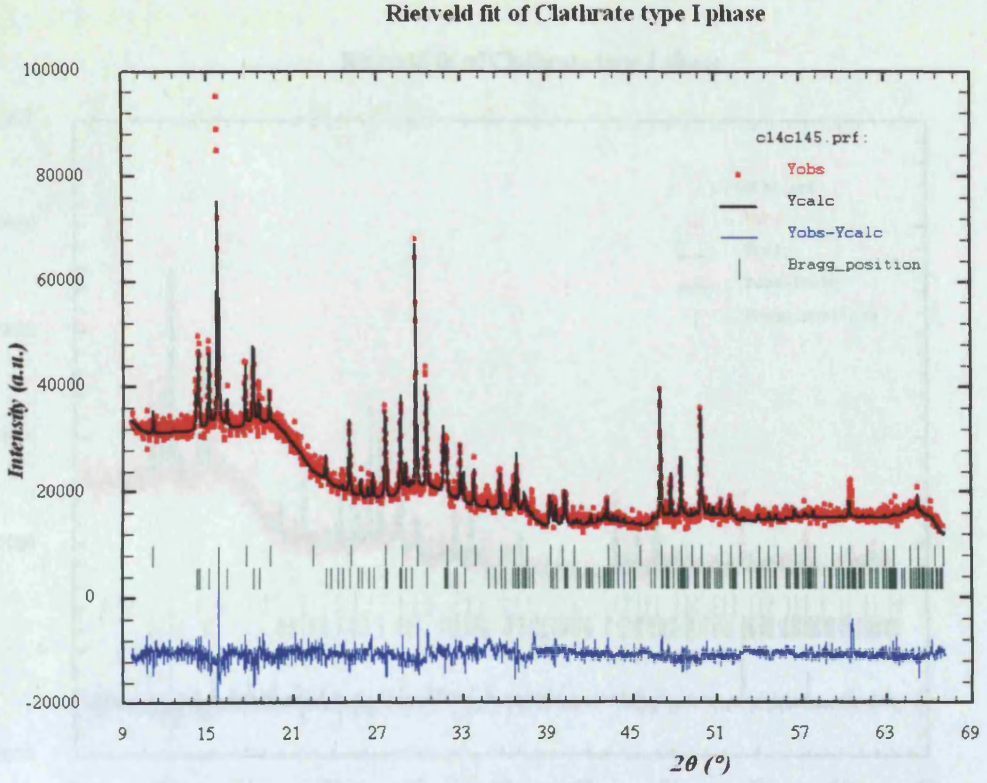

Pattern 300:

Time: 72.5 minutes

Temperature: 500°C

RWP: 35.4

Refinement cycles: 25

Parameters refined: 38

a: 10.2285 (0.00029)

Unit cell volume: 1070.01 (0.091)

Dual phase refining for Na_8Si_{46} then NaSi in order

	x	sx	y	sy	z	sz	B	sB	occ.	socc.	Mult
Na1	0.00000(0)		0.00000(0)		0.00000(0)		-1.274(983)		0.035(2)		2
Na2	0.25000(0)		0.50000(0)		0.00000(0)		4.727(999)		0.114(4)		6
Si1	0.00000(0)		0.30661(55)		0.11928(55)		0.430(220)		0.500(0)		24
Si2	0.18113(48)		0.18113(48)		0.18113(48)		0.678(260)		0.333(0)		16
Si3	0.25000(0)		0.00000(0)		0.50000(0)		1.062(453)		0.125(0)		6

Rietveld fit of Clathrate type I phase

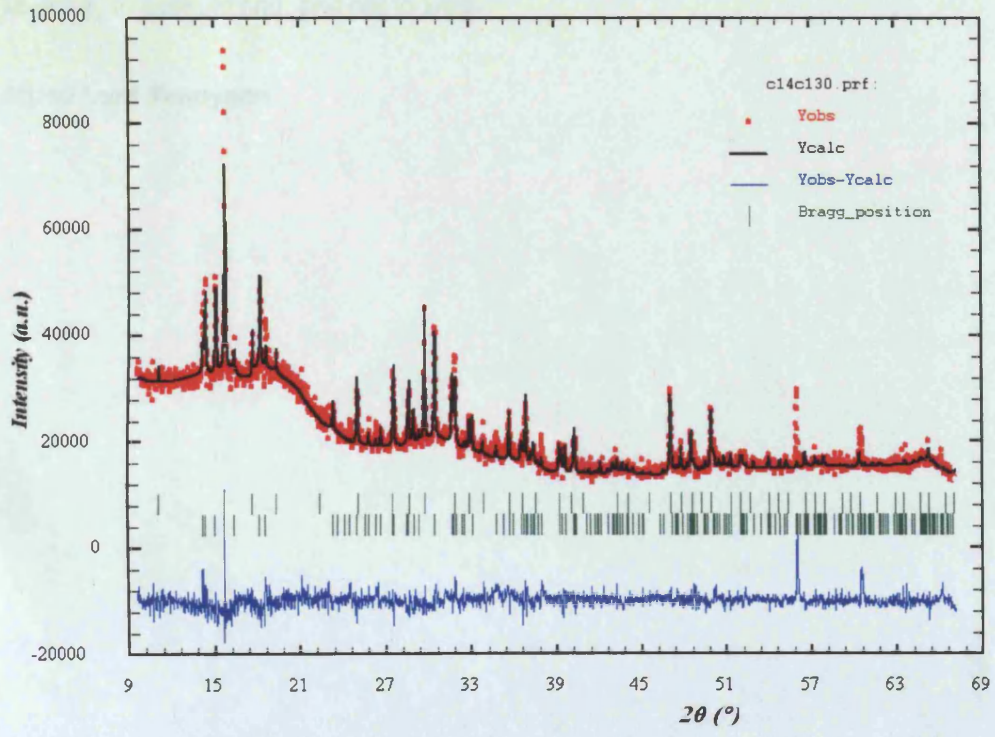

It may be that the gulfs will wash us down:
It may be we shall touch the Happy Isles,
And see the great Achilles, whom we knew.
Tho' much is taken, much abides; and tho'
We are not now that strength which in old days
Moved earth and heaven; that which we are, we are;
One equal temper of heroic hearts,
Made weak by time and fate, but strong in will
To strive, to seek, to find, and not to yield.

Alfred Lord Tennyson

UNIVERSITY OF LONDON

SENATE HOUSE. MALET STREET, LONDON, WCIE 7HU

REPRODUCTION OF THESES

A thesis which is accepted by the University for the award of a Research Degree is placed in the Library of the College and in the University of London Library. The copyright of the thesis is retained by the author.

As you are about to submit a thesis for a Research Degree, you are required to sign the declaration below. This declaration is separate from any which may be made under arrangements with the College at which you have *pursued* your course (for internal candidates only). The declaration will be destroyed if your thesis is not approved by the examiners, being either rejected or referred for revision.

Academic Registrar

To be completed by the candidate

NAME IN FULL (please type surname in BLOCK CAPITALS)

PhD Peter Thomas HUTCHINS

THESIS TITLE In situ Synthesis studies of Silicon Clathrates

DEGREE FOR WHICH THESIS IS PRESENTED Doctor of Philosophy (Ph.D.)

DATE OF AWARD OF DEGREE *(To be completed by the University):* _____

DECLARATION

1. I authorise that the thesis presented by me in *[18-09-2007] for examination for the MPhil/PhD Degree of the University of London shall, if a degree is awarded, be deposited in the library of the appropriate College and in the University of London Library and that, subject to the conditions set out below, my thesis be made available for public reference, inter-library loan and copying.

2. I authorise the College or University authorities as appropriate to supply a copy of the abstract of my thesis for inclusion in any published list of theses offered for higher degrees in British universities or in any supplement thereto, or for consultation in any central file of abstracts of such theses.

3. I authorise the College and the University of London Libraries, or their designated agents, to make a microform or digital copy of my thesis for the purposes of inter-library loan and the supply of copies.

4. I understand that before my thesis is made available for public reference, inter-library loan and copying, the following statement will have been included at the beginning of my thesis: The copyright of this thesis rests with the author and no quotation from it or information derived from it may be published without the prior written consent of the author.

5. I authorise the College and/or the University of London to make a microform or digital copy of my thesis in due course as the archival copy for permanent retention in substitution for the original copy.

6. I warrant that this authorisation does not, to the best of my belief, infringe the rights of any third party.

7. I understand that in the event of my thesis being not approved by the examiners, this declaration would become void.

***Please state year by hand, using a pen.**

DATE 18·09·2007 SIGNATURE _____

Note: The University's Ordinances make provision for restriction of access to an MPhil/PhD thesis and/or the abstract but only in certain specified circumstances and for a maxiumum period of two years. If you wish to apply for such restriction, please enquire at your College about the conditions and procedures. External Students should enquire at the Research Degree Examinations Office, Room 261, Senate House.

THIS DECLARATION MUST BE COMPLETED AND RETURNED WITH THE EXAMINATION ENTRY FORM